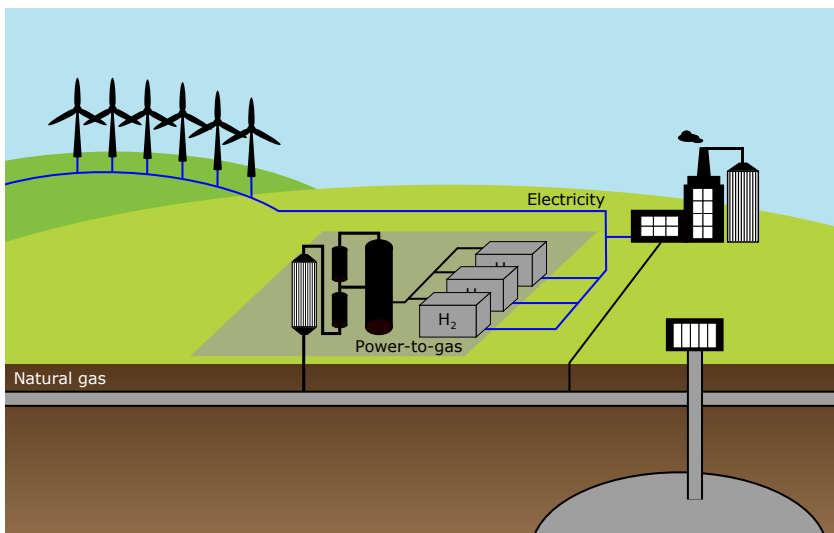


Storage via power-to-gas in future energy systems

The need for synthetic fuel storage in systems with high shares of intermittent renewables



Andreas Belderbos

Supervisors:
Prof. dr. ir. W. D'haeseleer, supervisor
Prof. dr. ir. E. Delarue, co-supervisor

Dissertation presented in partial fulfillment of the requirements for the degree of Doctor of Engineering Science (PhD): Mechanical Engineering

February 2019

Storage via power-to-gas in future energy systems

The need for synthetic fuel storage in systems with high shares of intermittent renewables

Andreas BELDERBOS

Examination committee:

Prof. dr. ir. H. Hens, chair

Prof. dr. ir. W. D'haeseleer, supervisor

Prof. dr. ir. E. Delarue, co-supervisor

Prof. dr. ir. D. Van Hertem

Prof. dr. ir. W. Van Herterijck

Prof. dr. G. Pepermans

Prof. dr. P. Taylor

(Newcastle University)

dr. N. Keyaerts

(ACER)

Dissertation presented in partial fulfillment of the requirements for the degree of Doctor of Engineering Science (PhD):
Mechanical Engineering

February 2019

© 2019 KU Leuven – Faculty of Engineering Science
Uitgegeven in eigen beheer, Andreas Belderbos, Celestijnenlaan 300 box 2421, B-3001 Leuven (Belgium).

Alle rechten voorbehouden. Niets uit deze uitgave mag worden vermenigvuldigd en/of openbaar gemaakt worden door middel van druk, fotokopie, microfilm, elektronisch of op welke andere wijze ook zonder voorafgaande schriftelijke toestemming van de uitgever.

All rights reserved. No part of the publication may be reproduced in any form by print, photoprint, microfilm, electronic or any other means without written permission from the publisher.

Preface - Dankwoord

“Ontdek jezelf. Begin bij de wereld.” is de slogan van de KU Leuven, de universiteit die ik met trots mijn alma mater mag noemen. Deze tekst is de synthese van iets meer dan vier jaar waarin ik de vrijheid heb gekregen om zowel de wereld als mezelf te ontdekken. Deze vier jaar van doctoraatsonderzoek waren niet mogelijk geweest zonder een aantal mensen, die ik hiervoor wil bedanken.

Vooreerst wil ik graag mijn promotoren, William D’haeseleer en Erik Delarue, bedanken voor de mogelijkheid die ze me boden om dit doctoraat te starten. William, bedankt dat ik onder uw supervisie dit onderzoek mocht voeren. Bedankt om richting te geven aan het onderzoek, om me aan te moedigen in mijn werk en altijd waardevolle feedback te geven op mijn teksten. Bedankt ook om me de kans te geven op conferentie te gaan in binnen- en buitenland, om zo ook buiten de literatuur de wereld te kunnen ontdekken. Erik, bedankt om steeds beschikbaar te zijn voor grotere en kleinere vragen, om mee na te denken over de verschillende modellen en hun formuleringen en voor de film quotes die ten gepaste tijden de vergaderingen luchtig hielden.

VITO (Vlaamse Instelling voor Technologisch Onderzoek) wil ik bedanken voor de financiering van mijn doctoraat en voor de samenwerking doorheen het onderzoek. Ana en Kris, bedankt voor jullie begeleiding doorheen mijn doctoraat. Bedankt ook om mijn onderzoek geregeld in een niet-academische context te plaatsen en om me in contact te brengen met de industrie.

I would also like to thank all members of the examination committee for their valuable feedback, which significantly improved the quality of this dissertation. Prof. Hens, thank you for chairing my examination committee. Dirk and Wilfried, thank you for supervising the progress of this research as a member of the supervisory committee and for all valuable suggestions and comments provided along the way. Phil, Guido and Nico, thank you for the discussions we had during this research, for reading this dissertation and for the comments

during the preliminary defense.

Ik bedank graag alle collega's om van TME een leuke werkplek te maken, voor de wekelijkse happy hours, het jaarlijkse TME weekend en de BBQs. Daniël, Roel, Stefan, Juliana, Maarten, Mats, Sarah, Bart, Sander, Reinart en Javier, bedankt voor de fijne sfeer in het kantoor en de kotentocht/etentjes op geregelde tijdstippen. Dank aan Dieter, Bram en Tim voor de organisatie van wekelijkse Alma-lunches en de memorabele uitnodigingen die hier steeds mee gepaard gaan. Bedankt ook aan Valérie, Marina en Cindy voor de vriendelijke administratieve ondersteuning. Verder wil ik een speciaal woord van dank richten aan enkele collega's die hebben bijgedragen tot dit werk. Kenneth, Kenneth en Kris, bedankt voor de discussies over modellen, resultaten en de energieproblematiek in zijn geheel. Wim, bedankt voor de ondersteuning tijdens het modelleren van gasstromingen en het werken met de Vlaamse supercomputer. Hanspeter, bedankt voor de Latex en Python scripts die het werk aanzienlijk vergemakkelijkten.

Mijn vrienden wil ik bedanken om tijdens deze vier jaren de nodige afwisseling te voorzien naast het onderzoek met etentjes en weekends in Oostende. In het bijzonder wil ik Pieter-Jan, Julien en Bertold bedanken om samen project Mahi op te zetten en soms late avonden of vroege ochtenden door te werken, maar ook om begrip op te brengen voor mijn periodes van afwezigheid om bijvoorbeeld dit onderzoek neer te schrijven. Verder wil ik Joeri en Liesbet bedanken voor het leuke samen wonen wanneer ons eigen huis verbouwd werd.

Tenslotte wil ik ook mijn ouders, broers en Viktor bedanken, voor jullie interesse in mijn onderzoek en het aanbieden van een rustige schrijf-plek, voor de steun tijdens lastige momenten die onlosmakelijk gepaard gaan aan het ontdekken van de wereld, voor de fijne feestjes, broersweekends en vakanties en voor het ongetemperde enthousiasme bij het zien van getallen en grafieken op een computerscherm.

Gladys, een laatste woord van dank gaat naar jou. Ik wil jou niet enkel bedanken voor de steun tijdens de voorbije vier jaren maar voor alle acht jaren die we ondertussen samen door het leven gaan. Ik wil jou bedanken voor alles wat we samen al ondernomen hebben, voor de ambiance die je in huis brengt en voor je zoete glimlach, kortom om te zijn wie je bent en om mij tegelijkertijd de ruimte te geven om mijn dromen na te jagen. Gladys, ik kijk er naar uit om samen met jou aan het volgende avontuur te beginnen!

Andreas
Leuven, februari 2019

Abstract

Rising global temperature concerns drive unprecedented changes in the electrical power system like the massive deployment of intermittent renewable energy sources. Such large-scale renewables deployment requires a variety of flexibility options for the electrical power system to be operated reliably. One of the possibly important flexibility options is storage. Next to battery storage and pumped hydro storage, which have a comparably small storage capacity, indirect energy storage via power-to-gas (P2G) might be interesting for long-term (seasonal) storage due to its large scale energy storage potential.

This dissertation studies the need for such energy storage via power-to-gas in future energy systems dominated by intermittent renewable energy sources, together with the operational impact of power-to-gas on the integrated electric power and natural gas systems. This overall goal is split in different sub-objectives: (i) Assessment of the value of electricity storage for an investor in a given electricity market. (ii) Identification of the circumstances which require electricity storage via P2G to justify the need for investing in P2G conversion. (iii) Once P2G would be installed, evaluation of the impact of such P2G units on the operation of both the electrical power and natural gas systems.

Several tools are developed to study each of the above mentioned research questions. (i) Three novel cost metrics, similar to the traditional levelized cost of electricity are presented to express the value of storage in an electricity market. (ii) An energy system investment model is presented to assess the cost optimal amount of installed storage capacity, and in particular P2G, in future energy systems under different environmental constraints. (iii) A novel integrated operational energy system model comprising the electrical power and natural gas sectors has been developed to analyze the impact of P2G on the operation of the natural gas network.

Applying the different cost metrics to storage technologies showed how those metrics can be used to assess the economic viability of different storage

technologies. However, different examples also showed that it is not useful to apply such levelized cost metrics to storage units with small energy storage reservoirs like conventional batteries. For such technologies, a market price analysis with full temporal detail is recommended.

Portfolio optimization studies showed that investments in P2G are triggered by a requirement for large energy storage capacities which is typically related to long-term seasonal storage of surplus renewable generation. High shares of renewable generation could be installed as a consequence of an imposed renewable target (above 70%), or when high CO₂ emission prices would occur (1000€/ton and above) in combination with an absence of CO₂ sequestration possibility. Once P2G is installed, it can also be used for short-term storage cycles and deliver auxiliary services to the electrical power grid.

Short-term operational results indicate that the current Belgian gas network contains ample amounts of inherent flexibility to accommodate P2G integration in high renewable settings. The network can deal with possibly volatile gas injections from P2G without impacting the normal operation of conventional natural gas producers.

Beknopte samenvatting

De toenemende bezorgdheid over de opwarming van de aarde leidt tot drastische veranderingen in het elektriciteitssysteem, zoals de toenemende hoeveelheid intermitterende hernieuwbare bronnen (zon en wind). De installatie van zulke hernieuwbare energiebronnen op grote schaal vereist een toenemende hoeveelheid flexibiliteitsopties om een veilige uitbating van het elektriciteitsnet te garanderen. Een mogelijks belangrijke flexibiliteitsoptie is energieopslag. Naast batterijen en pompcentrales, die een relatief lage energiec capaciteit hebben, kan indirecte energieopslag via "power-to-gas (P2G)" interessant zijn voor lange-termijn (seizoens) opslag omwille van zijn groot opslagpotentieel.

Dit proefschrift onderzoekt de nood aan energieopslag via power-to-gas in toekomstige energiesystemen die gedomineerd worden door intermitterende hernieuwbare bronnen en de operationele impact van power-to-gas op het geïntegreerde elektriciteits- en aardgasnetwerk. Dit onderzoek is opgesplitst in drie delen: (i) Onderzoek van de waarde van elektriciteitsopslag voor een investeerder in een gegeven elektriciteitsmarkt. (ii) Identificeren van de omstandigheden die elektriciteitsopslag via P2G noodzakelijk maken. (iii) Indien P2G geïnstalleerd is, evaluatie van de impact van P2G eenheden op de uitbating van zowel het elektriciteitsnetwerk als het aardgasnetwerk.

Verskillende mathematische modellen werden ontwikkeld om ieder van de bovengenoemde onderzoeksvragen te bestuderen. (i) Drie nieuwe genormaliseerde kosteenheden (levelized cost metrics) zijn voorgesteld om de waarde van opslageenheden in een elektriciteitsmarkt uit te drukken. (ii) Een investeringsmodel is ontwikkeld om de hoeveelheid geïnstalleerde opslagcapaciteit, en P2G in het bijzonder, te analyseren in een kost-optimaal elektriciteitssysteem dat onderworpen werd aan verschillende duurzaamheidsdoelstellingen. (iii) Een korte-termijn operationeel model bestaande uit de elektriciteitssector en de gasector werd ontwikkeld om de invloed van P2G op de dagelijkse uitbating van beide systemen te analyseren.

Het toepassen van de verschillende genormaliseerde kosteenheden op opslagtechnologieën toont aan dat de kosteenheden kunnen gebruikt worden om de economische rendabiliteit van de opslagtechnologieën in een gegeven elektriciteitsmarkt te analyseren. Twee voorbeelden tonen echter aan dat het gebruik van zulke kosteenheden niet nuttig is voor opslagtechnologieën met kleine energiereservoirs, zoals conventionele batterijen. Voor zulke technologieën is het aangeraden om een analyse te maken van het volledige prijsprofiel doorheen de tijd.

Verschiedende investeringsanalyses tonen aan dat investeringen in P2G economisch optimaal zijn wanneer er een noodzaak is aan lange-termijn energieopslag. Deze noodzaak ontstaat typisch wanneer er een grote hoeveelheid intermitterende hernieuwbare bronnen geïnstalleerd zijn. Grote hoeveelheden hernieuwbare bronnen worden geïnstalleerd wanneer exogeen een hoge hernieuwbare doelstelling wordt opgelegd of wanneer er een hoge CO₂ emissieprijs is in combinatie met het gebrek aan de mogelijkheid tot CO₂ berging. Eens P2G geïnstalleerd is, kan het natuurlijk ook worden aangewend voor korte-termijn opslag en het leveren van diensten aan het elektriciteitsnetwerk.

Korte-termijn operationele resultaten tonen aan dat het Belgische aardgasnetwerk voldoende inherente flexibiliteit bezit om de installatie van P2G toe te laten. Het netwerk kan, mogelijks volatiele, gasinjecties van P2G opvangen zonder dat de normale uitbating van traditionele gasleveranciers beïnvloed wordt.

List of Abbreviations

AADP	available average discharge price
AAOP	available average operational profit
AAPS	available average price spread
ACC	average charging cost
AEL	alkaline electrolyzer
BOP	balance of plant
CC	carbon capture
CCGT	combined cycle gas turbine
EAC	equivalent annual cost
GFPP	gas-fired power plant
GHG	greenhouse gas
HHV	higher heating value
iRES	intermittent renewable energy sources
LCOE	levelized cost of electricity
LCOS	levelized cost of storage
MES	multi-carrier energy system
MIP	mixed integer program
OCC	overnight construction cost
OCGT	open cycle gas turbine

O&M operation and maintenance

P2G power-to-gas

PEM polymer electrolyte membrane

PHS pumped hydro storage

PV photovoltaic

RADP required average discharge price

RAOP required average operational profit

RAPS required average price spread

RES renewable energy sources

rWGS reverse water-gas shift

SM synthetic methane

SMR steam methane reformer

SOEC solid oxide electrolysis cell

TCC total charging cost

TSO transmission system operator

WGS water-gas shift

Nomenclature

Sets

$c \in \mathcal{C}$	set of compressors c
$e \in \mathcal{E}$	set of power-to-gas units e
$ng \in \mathcal{NG}$	set of gas nodes ng
$pl \in \mathcal{PL}$	set of pipelines pl
$gs \in \mathcal{GS}$	set of gas storages gs
$t \in \mathcal{T}$	set of time steps t
$v \in \mathcal{V}$	set of valves v
$gw \in \mathcal{GW}$	set of gas shippers gw
$x \in \mathcal{X}$	set of piecewise linear pressure intervals x
$x2 \in \mathcal{X}2$	set of piecewise linear flow intervals $x2$
$zg \in \mathcal{ZG}$	set of gas zones zg

Parameters

$A_{n,e}^{ely}$	location matrix, linking electrolyzers e to electricity nodes n	$\{0,1\}$
$A_{ng,e}^{met}$	location matrix, linking methanizers e to gas nodes ng	$\{0,1\}$
$A_{ng,i}^{gfpp}$	location matrix, linking gas fired power plants i to gas nodes ng	$\{0,1\}$
C_{gs}	gas storage cost per storage gs	$[\text{€}/\text{Nm}^3]$
C_{gw}	gas production cost per gaswell gw	$[\text{€}/\text{Nm}^3]$
C_c	gas compressor cost	$[\text{€}/\text{Nm}^3]$
D_x^p	piece-wise linear pressure intervals	$[\text{bar}]$
D_{x2}^q	piece-wise linear flow intervals	$[\text{Nm}^6/\text{h}^2]$
ζ	energy content per volume natural gas	$[\text{MWh}/\text{Nm}^3]$

η_e^{ely}	electrolyzer e efficiency	$[-]$
η_e^{met}	methanizer e efficiency	$[-]$
η_i^{pp}	power plant efficiency	$[-]$
\overline{F}_e^{met}	maximum synthetic methane production of methanizer e	$[MW_{CH_4}/\Delta t]$
\underline{F}_e^{met}	minimum synthetic methane production of methanizer e	$[MW_{CH_4}/\Delta t]$
G_c	compressor pressure increase ratio	$[-]$
\overline{p}_{ng}	maximum nodal pressure	$[bar]$
\underline{p}_{ng}	minimum nodal pressure	$[bar]$
G_v	valve pressure reduction ratio	$[-]$
\overline{S}_e^h	maximum hydrogen buffer level of power-to-gas unit e	$[MWh_{H_2}]$
\underline{S}_e^h	minimum hydrogen buffer level of power-to-gas unit e	$[MWh_{H_2}]$
H_{x2}^q	quadratic piece-wise linear flow intervals	$[Nm^3/h]$
H_x^p	quadratic piece-wise linear pressure intervals	$[bar^2]$
$Ia_{pl,ng}^{in}$	location matrix, linking each pipeline pl to its entry node ng	$\{0,1\}$
$Ia_{pl,ng}^{out}$	location matrix, linking each pipeline pl to its exit node ng	$\{0,1\}$
$Ic_{c,ng}^{in}$	location matrix, linking each compressor c to its entry node ng	$\{0,1\}$
$Ic_{c,ng}^{out}$	location matrix, linking each compressor c to its exit node ng	$\{0,1\}$
IR_{gs}	minimum gas storage injection rate	$[Nm^3/h]$
$Iv_{v,ng}^{in}$	location matrix, linking each valve v to its entry node ng	$\{0,1\}$
$Iv_{v,ng}^{out}$	location matrix, linking each valve v to its exit node ng	$\{0,1\}$
$Iz_{zg,ng}$	location matrix, linking each gas node ng to a gas zone zg	$\{0,1\}$
K_{pl}^q	pipeline characteristic linking flow and pressure drop	$[bar^2/Nm^6]$
K_{pl}^m	pipeline characteristic linking pressure and line-pack	$[bar/Nm^3]$
$L_{ng,t}^g$	gas load at node ng	$[Nm^3/h]$

$L_{zg,t}^g$	gas load at zone zg	$[Nm^3/h]$
C_e^{ely}	operations and maintenance cost of electrolyzer e	$[\text{€}/MW \Delta t]$
C_e^{met}	operations and maintenance cost of methanizer e	$[\text{€}/MW_{CH_4} \Delta t]$
MDT_e^{met}	minimum down time of methanizer e	$[\Delta t]$
MUT_e^{met}	minimum up time of methanizer e	$[\Delta t]$
\overline{G}_e^{ely}	maximum electric power consumption of electrolyzer e	$[MW]$
RD_{gs}	maximum ramp-down rate of gas storage gs	$[MW_{CH_4}/\Delta t]$
RD_e^{met}	maximum ramp-down rate of methanizer e	$[MW_{CH_4}/\Delta t]$
RD_{gw}	maximum ramp-down rate of gas well gw	$[MW_{CH_4}/\Delta t]$
RU_{gs}	maximum ramp-up rate of gas storage gs	$[MW_{CH_4}/\Delta t]$
RU_e^{met}	maximum ramp-up rate of methanizer e	$[MW_{CH_4}/\Delta t]$
RU_{gw}	maximum ramp-up rate of gas well gw	$[MW_{CH_4}/\Delta t]$
SD_e^{met}	maximum shut-down rate of methanizer e	$[MW_{CH_4}/\Delta t]$
SU_e^{met}	maximum start-up rate of methanizer e	$[MW_{CH_4}/\Delta t]$
\overline{S}_{gs}	maximum gas storage level	$[Nm^3]$
\underline{S}_{gs}	minimum gas storage level	$[Nm^3]$
WR_{gs}	maximum gas storage withdrawal rate	$[Nm^3/h]$
\overline{W}_{gw}	maximum gas well production rate	$[Nm^3/h]$
\underline{W}_{gw}	minimum gas well production rate	$[Nm^3/h]$
Δt	length of one time step in hours	$[h]$

Decision Variables

$cost_{c,t}^{comp}$	operation cost of compressor c at time step t	$[\text{€}/\Delta t]$
$cost^{gas}$	total operational cost of gas system	$[\text{€}]$
$cost_{gs,t}^{stor}$	operation cost of gas storage gs at time step t	$[\text{€}/\Delta t]$
$cost_{gw,t}^{well}$	operation cost of gas well gw at time step t	$[\text{€}/\Delta t]$
$cost_{e,t}^{ptg}$	operation cost of power-to-gas unit e at time step t	$[\text{€}/\Delta t]$
$\delta_{ng,t,x}^p$	auxiliary variable assuring piece-wise linear pressure intervals are used in logical order	$[0,1]$

$\delta_{pl,t,x2}^q$	auxiliary variable assuring piece-wise linear flow intervals are used in logical order	$\{0,1\}$
$f_{e,t}^{met}$	methanizer e synthetic methane production at time step t	$[MW_{CH_4}]$
$\gamma_{ng,t,x}^p$	auxiliary variable assuring piece-wise linear pressure intervals are used in logical order	$\{0,1\}$
$\gamma_{pl,t,x2}^q$	auxiliary variable assuring piece-wise linear flow intervals are used in logical order	$\{0,1\}$
$g_{e,t}^{ely}$	electric power consumption of electrolyzer e during time step t	$[MW]$
$q_{ng,t}^{gfpp}$	gas consumption by gas fired power plant at node ng at time step t	$[Nm^3/h]$
$h_{e,t}^{ely}$	hydrogen production of electrolyzer e during time step t	$[MW_{H_2}]$
$h_{e,t}^{met}$	hydrogen consumption of methanizer e during time step t	$[MW_{H_2}]$
$m_{pl,t}$	average line-pack level in pipeline pl during time step t	$[Nm^3]$
$p_{ng,t}$	pressure at node ng during time step t	$[bar]$
$\tilde{p}_{pl,t}$	average pressure in pipeline pl during time step t	$[bar]$
$q_{c,t}$	gas flow through compressor c at time step t	$[Nm^3/h]$
$q_{gs,t}$	gas flow to or from storage gs at time step t	$[Nm^3/h]$
$q_{gw,t}$	gas production rate at well gw at time step t	$[Nm^3/h]$
$q_{v,t}$	gas flow through valve v at time step t	$[Nm^3/h]$
$\tilde{q}_{pl,t}$	average gas flow through pipeline pl at time step t	$[Nm^3/h]$
$q_{pl,t}^{in}$	entry flow of pipeline pl at time step t	$[Nm^3/h]$
$q_{ng,t}^{met}$	methanizer e synthetic methane production at time step t	$[Nm^3/h]$
$q_{pl,t}^{out}$	exit flow of pipeline pl at time step t	$[Nm^3/h]$
$s_{e,t}^h$	hydrogen buffer level of power-to-gas unit e at time step t	$[MW_{h_{H_2}}]$
$s_{gs,t}^l$	level of gas storage gs at time step t	$[Nm^3]$
$v_{e,t}^{met}$	start-up status of methanizer e at time step t	$\{0,1\}$
$w_{e,t}^{met}$	shut-down status of methanizer e at time step t	$\{0,1\}$
$z_{e,t}^{met}$	on/off-status of methanizer e at time step t	$\{0,1\}$

Contents

Abstract	iii
Beknopte samenvatting	v
List of Abbreviations	viii
Nomenclature	ix
Contents	xiii
1 Introduction	1
1.1 Context	2
1.2 Motivation	3
1.3 Objectives	5
1.4 Outline	6
2 Overview of different synthetic fuel production processes	9
2.1 General overview of the power-to-gas process	10
2.2 Electrolyzer	10
2.3 Methanizer	17
2.4 Other synthetic fuels	20

2.5	Summary and conclusions	24
3	Cost evaluation of storage	27
3.1	Introduction	28
3.2	Levelized cost of electricity formulation and explanation of its meaning	32
3.3	Storage cost terminology	33
3.4	Parameter variations	39
3.5	'Available' prices compared to 'required' prices	44
3.6	Discussion of the results	52
3.7	Summary and conclusions	57
4	Identification of the need for long-term electricity storage	59
4.1	Introduction	60
4.2	Sustainability of synthetic fuels	61
4.3	Methodology	62
4.4	Case data	65
4.5	Results and discussion	69
4.6	Results considering the hydrogen sector	105
4.7	Summary and conclusions	109
5	Generalization of energy storage sizing: power versus energy requirements	113
5.1	Introduction	114
5.2	Input data, assumptions and general principles	116
5.3	Methodological case: block profiles	120
5.4	Sinusoidal profile	127
5.5	Real profiles	130
5.6	Summary and conclusions	137

6	Unit commitment model for a combined electricity and gas system	139
6.1	Introduction	140
6.2	Model description	143
6.3	Model verification	156
6.4	Illustrative case studies	163
6.5	Summary and conclusions	175
7	Operational impact of P2G on the energy system	177
7.1	Introduction	178
7.2	Methodology	179
7.3	Input parameters	180
7.4	Case studies	194
7.5	Results and discussion	196
7.6	Summary and conclusions	202
8	Summary, conclusions and suggestions for further research	205
8.1	Summary and conclusions	206
8.2	Suggestions for further research	210
A	Levelized cost metrics including income tax	213
B	Arbitrage model formulation	217
C	Investment model	219
D	Leuven University System Model (LUSYM)	229
	References	241
	Short curriculum	253

List of publications	255
-----------------------------	------------

Chapter 1

Introduction

Rising climate change concerns drive unprecedented changes in the electrical power system, like the massive deployment of intermittent renewable energy sources (iRES). Such large-scale iRES deployment requires a variety of flexibility options for the electrical power system to be operated reliably. One of the important flexibility options is storage.

This dissertation studies the need for indirect energy storage via power-to-gas in future energy systems dominated by intermittent renewable energy sources, together with the operational impact of power-to-gas on the integrated electrical power and natural gas systems.

This chapter introduces the research presented in this dissertation. Section 1.1 first provides the context in which this research is embedded. Next, the motivation for this research is explained in Section 1.2 followed by a discussion of the objectives and scope in Section 1.3. To end, Section 1.4 outlines the main chapters of this document.

1.1 Context

The rise of global average temperature levels and their suspected cause from a rise of greenhouse gasses (GHGs) in the atmosphere has driven governments worldwide to take actions. On a global level, many countries have expressed the intention to peak their GHG emissions as soon as possible to hold the increase in global average temperature below 2°C [1]. On a European level, the European Union has agreed in their 2020 climate and energy package [2] to reduce their GHG emission by 20% compared to 1990 levels, to obtain 20% of the EU end energy from renewable energy sources (RES) and to improve the energy efficiency by 20% compared to a set baseline by 2020. A more recent climate and energy framework as proposed by the EU Commission specifies targets with respect to 2030 [3, 4]. Aiming to obtain at least 32% of EU end energy from RES and to improve energy efficiency by at least 32.5% compared to a set baseline, which are expected to lead to a reduction of GHG emissions by around 45% compared to 1990 levels. On a country level, Belgium has agreed to contribute to the European 2020 targets by obtaining 13% of its end energy from RES [5]. Many different pathways have been analyzed to reach these energy and climate targets. In all of them, the electrical power system plays a crucial role in decreasing GHG emissions. In addition, the required reduction of GHG emission in heating and transportation is likely to cause a shift from conventional fossil fueled heating and transport to electrical heat pumps and electrical vehicles, making the electrical power system even more important in the transition towards a sustainable energy provision. Depending on the transition pathway, RES shares in the European electrical power sector are projected to increase up to 64-97% by 2050¹ [6, 7].

The global paradigm shift towards low carbon energy systems triggers a massive installation of intermittent renewable energy sources (iRES) capacity², such as solar photovoltaic (PV) and wind power generation. Globally, installed solar PV capacity increased from 176 GW_e in 2014 to 300 GW_e in 2016 [8, 9] and wind capacity increased from 350 GW_e in 2014 to 467 GW_e in 2016 [8, 9]. A characteristic of this iRES generation capacity is that its output depends on variable and often uncertain weather conditions. Since intermittent renewable energy sources generate electrical power depending on the instantaneous weather conditions rather than the instantaneous electrical power demand, substantial local overproduction is expected in regions with large generation over-capacities. In contrast, during nights and during wind-deficient-cold-spell periods, installed PV and/or wind capacity may be idle leading to a lack of generation. To

¹RES shares in terms of a fraction of the annual electrical energy

²The term ‘intermittent’ renewables is used to denote both the variable character and the limited predictability of the electricity generation from these renewable sources.

deal with both the lack and the surplus of iRES generation and to assure the required balance between instantaneous electrical power generation and demand, flexibility tools are necessary. Five options are usually considered: (1) thermal power plant cycling; (2) the presence of strong electrical grids to exchange electrical power with other regions; (3) storage of electrical energy; (4) active electricity demand response (load shifting); (5) curtailment of superfluous renewable electricity generation³. These flexibility options are already in use today and will become much more important in future electricity-generation systems [10, 11, 12]. All flexibility options differ with regard to their power rating, ramp rates, energy rating, investment costs and operational costs. Electricity storage could be an interesting source of flexibility as it can both absorb excess electrical power and generate electrical power when other generation capacity is unable to deliver.

1.2 Motivation

Given the global paradigm shift towards a low carbon energy system dominated by renewables on the long-term horizon, comprehensive system-integration studies of the technical and economic concepts are necessary to guarantee a sustainable and reliable energy system at acceptable cost. Although some electricity storage is already installed and successfully operated, additional research must be done with regard to its effective technical and economic integration in electricity systems [13]. Especially the possible use of long-term (indirect) electricity storage requires more study.

Many different types of storage exist, both for short and long time periods (i.e., having different energy reservoir characteristics) and with different charge and discharge power capacity ratings [14, 15, 16]. In electrical power systems, storage is historically dominated by pumped hydro [17, 18], although the amount of installed battery capacity has been growing in recent years [19]. In future energy systems in the NW-European region, storage being able to cover periods of one to two weeks at peak demand may be necessary to cover a possible cold spell [20]. Since pumped hydro and batteries are incapable of covering such long duration efficiently, the conversion of superfluous electrical power to hydrogen and preferentially synthetic methane to further increase the energy density (usually referred to as “power-to-gas”) whereby that synthetic methane is then fed into gas turbines, might become an important option [21, 22, 23]. Of all possible synthetic fuels, this dissertation focuses on methane since it can

³Often a sixth flexibility measure is mentioned, being the so-called sector-coupling (between the electricity system and the heating and transportation systems). But this type of coupling actually resorts under demand response and real or virtual storage.

take advantage of the existing natural gas network and its energy density is higher than that of hydrogen, which is a key parameter for large-scale storage.

While the importance of long-term electricity storage is recognized and the concept of indirect electricity storage via power-to-gas (P2G) is known, the actual implementation of storage through the P2G-option is rather novel. This dissertation intends to provide insights concerning the use of P2G for energy storage on two key points.

First, the use of synthetic methane for long-term storage in a cost-optimal energy system is investigated, depending on the characteristics of the electricity system, the cost of CO₂ emissions (under the European Emission Trading System) and the techno-economic characteristic of power-to-gas units. In addition to the economic efficiency of synthetic methane in the transition towards a sustainable electrical power sector, attention is given to the sustainable character of this synthetic methane. After all, synthetic methane still relies on carbon to form chemical bonds resulting in CO₂ formation when the methane is actually used.

Second, once power-to-gas (P2G) units are installed, they create an additional connection between the electrical power and natural gas systems, besides the already existing connection from gas-fired power plants (GFPPs) as shown in Figure 1.1. The impact of such stronger interlinkage of both systems on the operation of the gas network will be investigated. Special consideration will be given to the transfer of flexibility requirements from the electrical power system to the gas system and its effect on pressure levels and gas flows.

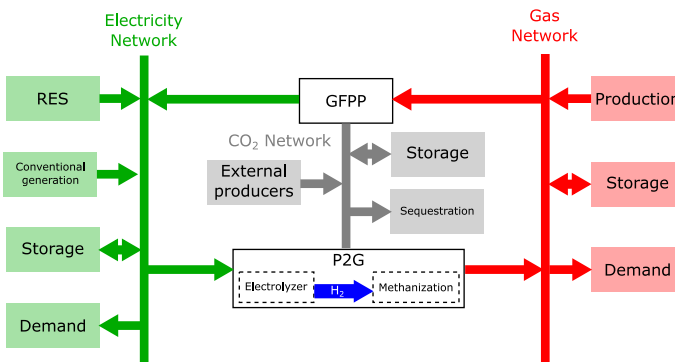


Figure 1.1: Overview of the energy system, whereby both gas-fired power plants (GFPPs) and power-to-gas (P2G) create a coupling between the electrical power and natural gas systems. (H_2 = hydrogen gas.)

1.3 Objectives

Given the flexibility challenges facing the electrical power system as outlined before, **the main objective of this PhD research is to investigate the opportunities and/or need for indirect electricity storage via power-to-gas in future energy systems under different constraints.** This overall goal can be further split in different sub-objectives:

- Assessing the cost/value of electricity storage for an investor in a given electricity market;
- Identification of the circumstances (and specification of the crucial parameters) which require electricity storage via P2G in energy systems dominated by intermittent renewable energy sources, to justify the need for investing in P2G conversion;
- Once P2G would be installed, evaluate the impact of such P2G units on the operation of both the electrical power and gas systems.

Several tools are developed to answer the above research questions, which will be presented in this dissertation.

- Three novel cost metrics, similar to the traditional levelized cost of electricity (LCOE) are presented to express the value of storage in an electricity market;
- An energy system investment model is presented and implemented to assess the amount of installed storage capacity, and in particular P2G, in future cost-optimal energy systems under different environmental constraints;
- A novel integrated operational energy system model comprising the electrical power and gas sectors has been developed to analyze the impact of P2G on the operation of the gas network.

1.3.1 Scope and main assumptions

The research presented in this dissertation only considers the energy system, its technical, economic and some environmental aspects, like CO₂ emissions. Although social aspects and environmental concerns like land and water use are also important, they are not within the scope of this research. Investigating whether there is at all a need for electricity storage via P2G in future

energy systems is a logical first step before investigating the social and entire environmental impact of it.

In line with this focus on the techno-economic aspects of energy systems, a perfect competitive energy market is assumed in all studies presented in this work. No strategic behavior of market players is considered. Furthermore, no technology support mechanisms, like feed-in tariffs or subsidies are accounted for.

During this research, deterministic optimization models are often used to provide answers for the objectives outlined before. In these optimizations, perfect foresight of future events, like the magnitude of hourly iRES generation, is assumed, neglecting uncertainty. Although there is no perfect foresight in reality, using such methodology has the advantage of providing clear results which allow for an unambiguous interpretation.

Two different optimization models are used during this research, an investment model and an operational model. Due to the low technical detail of the investment model, an optimization horizon of 1 year (Chapter 4) and up to 3 years (Chapter 5) is used with hourly time steps. The operational model, which contains more technical detail, is used with an optimization horizon of 24 hourly time steps (Chapters 6 and 7).

1.4 Outline

The outline of this dissertation is as follows:

Chapter 2 presents a description of the P2G process and a review of the main technical components required to produce synthetic gas. The technical state-of-the-art and economic characteristics are discussed in the context of energy systems with high shares of RES capacity. Chapter 2 ends with an overview of other synthetic fuels and their advantages and disadvantages compared to synthetic methane.

Chapter 3 considers the cost of storage and how it can be expressed by means of different metrics. The traditional levelized cost of electricity (LCOE) is translated to a levelized cost of storage (LCOS), of which the advantages and disadvantages are investigated. This leads to the introduction of three novel metrics to express the cost of storage, the required average discharge price (RADP), the required average price spread (RAPS) and the required average operational profit (RAOP). Examples are presented to illustrate the effectiveness and limitations of these metrics. Chapter 3 concludes with some

real-life examples of the different novel storage metrics. This chapter is based on:

Belderbos, A., Delarue, E., Kessels, K. and D'haeseleer, W. *Levelized cost of storage - Introducing novel metrics*. Energy Economics 67 (2017), 287–299.

Chapter 4 evaluates the use of P2G in future cost-optimal energy systems. First, an analysis is made of the conditions which have to be met in order to use P2G as renewable energy storage technology. Next, an energy system investment model is presented which determines the cost optimal electricity generation and storage portfolio to serve a given electrical power demand under different environmental constraints. A last analysis extends the optimization of the electricity generation and storage portfolio by considering both the electrical power demand and a hydrogen demand from industry, which allows to investigate the need for P2G if it can be used both as storage technology and to provide chemical feedstock to the industry. This chapter includes elements from:

Belderbos, A., Delarue, E. and D'haeseleer, W. *Possible role of Power-to-Gas in future energy systems*. European Energy Markets Conference (EEM), May 2015, Lisbon.

Belderbos, A., Delarue, E. and D'haeseleer, W. *Critical factors shaping the need for long-term energy storage via power-to-gas*. TME working paper.

Chapter 5 aims to generalize the optimization analysis presented in chapter 4 by investigating the link between optimally installed P2G capacity and variations in both the electrical power demand and renewable generation profiles. The share of P2G capacity in the total storage capacity is compared to the duration and magnitude of renewable surplus generation and shortage. This method is first applied to methodological demand and renewable generation profiles, after which it is applied to real profiles. This chapter is based on:

Belderbos, A., Virag, A., D'haeseleer, W. and Delarue, E. *Considerations on the need for electricity storage requirements: Power versus energy*. Energy Conversion and Management 143 (2017), 137-149.

Chapter 6 introduces a novel integrated operational model comprising the electrical power and gas systems, which is used in chapter 7 to analyze the impact of P2G on the gas system operation. The model objective and formulation are

presented first, followed by a verification of the gas flow representation. Chapter 6 concludes with five case studies to illustrate the value of the novel model aspects compared to existing models in the literature. This chapter includes elements from:

Belderbos, A., Bruninx K., Valkaert, T., Delarue, E. and D'haeseleer, W. *Facilitating renewables and power-to-gas via integrated electric power-gas system scheduling*, TME working paper.

Valkaert, T., Belderbos, A. and D'haeseleer, W. *Modeling transient gas flows through uniform pipelines with a focus on line pack and line pack flexibility.*, TME working paper.

Chapter 7 analyzes the impact of P2G on the daily operation of the gas network. The gas network flexibility used by P2G and its effect on the operation of conventional gas production facilities, storage and GFPPs is discussed. This chapter includes elements from:

Belderbos, A., Valkaert, T., Bruninx K., Delarue, E. and D'haeseleer, W. *Facilitating renewables and power-to-gas via integrated electric power-gas system scheduling*, TME working paper.

Chapter 8 summarizes and concludes the research presented in this dissertation and provides recommendations for future research.

Chapter 2

Overview of different synthetic fuel production processes

This chapter presents an overview of the principles to produce synthetic fuels. The production of synthetic methane is elaborated most extensively since it will be the main focus of this work.

First a general overview of the entire power-to-gas process is given in Section 2.1, after which the technical details, operational limits and economic characteristics of individual electrolyzer and methanation units are presented and discussed in Section 2.2 and 2.3, respectively. Section 2.4 provides high-level information of other synthetic fuels which could be produced starting from electrical energy. Section 2.5 concludes this chapter by summarizing the main findings.

The technical and economic characteristics presented in this chapter will be used to select model parameters in all subsequent chapters.

2.1 General overview of the power-to-gas process

The term "power-to-gas" (P2G) is in the literature used to denote the process of converting electrical energy to hydrogen or methane, depending on the different process steps considered. The first process step is always the decomposition of water in hydrogen and oxygen using electrical power. A possible consecutive step is the synthesis of the electrically produced hydrogen and CO₂ to produce methane. Unless otherwise specified, the term power-to-gas (P2G) is used in this dissertation to denote the entire process to produce synthetic methane from electrical power. A schematic overview of the different process steps is given in Figure 2.1.

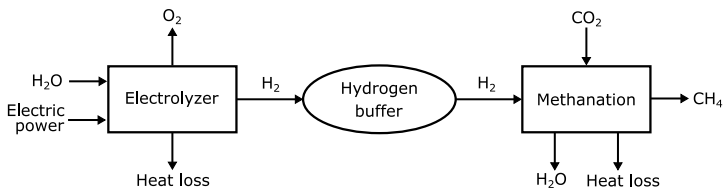


Figure 2.1: Overview of the power-to-gas process steps, including an intermediate hydrogen buffer.

2.2 Electrolyzer

2.2.1 Operating principles

In the electrolysis step, a direct current is applied to pure water decomposing the water molecules in hydrogen and oxygen following the reaction given in Eq. (2.1) [24].

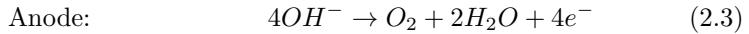
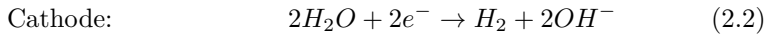


The overall reaction presented in Eq. (2.1) occurs in two phases, a reduction reaction at the cathode and an oxidation reaction at the anode. The exact shape of both reactions depends on the charge carrier, which in turn depends on the electrolyzer technology used.

There exist three different types of electrolyzer technologies, in decreasing order of maturity: alkaline electrolyzer (AEL), polymer electrolyte membrane (PEM) electrolyzers and solid oxide electrolysis cell (SOEC). All three types will be discussed next.

Alkaline electrolyzer

An alkaline electrolyzer cell is composed of two electrodes immersed in electrolyte, a 20-40% aqueous potassium hydroxide (KOH) solution. Both electrodes are separated using a microporous diaphragm which allows the movement of ions. When a direct current is applied to the AEL cell, a reduction reaction occurs at the cathode, producing hydrogen and hydroxide ions as shown in Eq. 2.2. The hydroxide ions can migrate through the diaphragm to be oxidized at the anode to produce oxygen and water as given in Eq. (2.3) [24].



A schematic representation of water decomposition in an AEL is given in Figure 2.2.

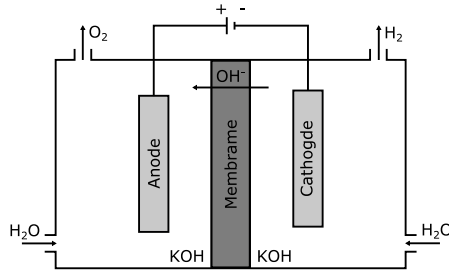


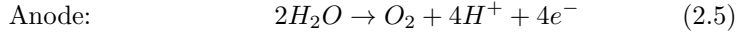
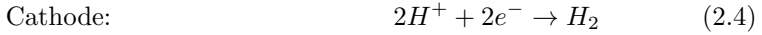
Figure 2.2: Schematic representation of the alkaline electrolyzer operating principle. Figure based on [24].

Alkaline electrolyzers are the most mature type of electrolysis technology. Although they were predominantly used for steady state processes, many manufactures can now produce alkaline electrolyzers capable of following the volatile production profile of intermittent renewables [12]. Detailed technical specifications are provided in section 2.2.2.

Polymer electrolyte membrane electrolyzer

Instead of liquid electrolytes used in AEL, a proton conducting membrane is used as solid polymer electrolyte in a polymer electrolyte membrane (PEM) electrolyzer. When a direct current is applied to the PEM cell, pure water is oxidized at the anode following Eq. (2.5). After the oxidation, hydrogen ions are transported through the proton exchange membrane towards the cathode

where hydrogen is produced during the reduction reaction as shown in Eq. (2.4) [24].



A schematic representation of water decomposition in a PEM electrolyser is given in Figure 2.3.

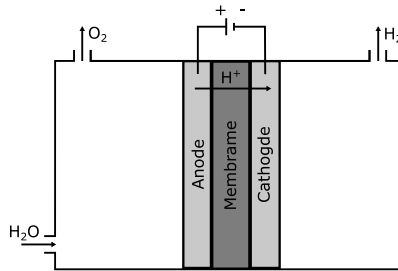
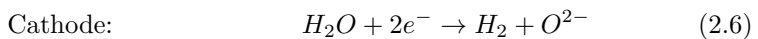


Figure 2.3: Schematic representation of the polymer electrolyte membrane electrolyzer operating principle. Figure based on [24].

A detailed description of the technical characteristics is also provided in the following section 2.2.2.

Solid oxide electrolysis cell

In a solid oxide electrolysis cell (SOEC) a thin solid oxide layer is used as the electrolyte. Water vapor fed to the SOEC is reduced at the cathode forming hydrogen and oxygen ions as shown in Eq. (2.6). At high temperatures, the thin solid oxide layer becomes conductive for these oxygen ions to migrate to the anode side for oxidation to oxygen molecules as follows from Eq. (2.7) [24].



A schematic representation of water decomposition in a SOEC is given in Figure 2.4.

Although reported SOEC efficiencies ($\sim 90\%$) are much higher than those of AEL and PEM electrolyzers [15], the high temperatures at which they operate

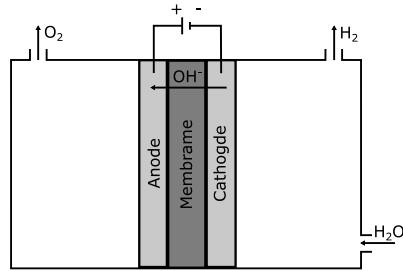


Figure 2.4: Schematic representation of the solid oxide electrolysis cell operating principle. Figure based on [24].

could lead to thermal inertia and result in limited dynamic operation. Therefore and due to the limited maturity of the electrolyzer technology, SOEC will not be further considered in this thesis.

2.2.2 Technical characteristics of electrolyzers

To allow for correct interpretation of the technical aspects (and economic aspects in the following sub-section), a few remarks need to be made. First, no industry standard yet exists on the nominal capacity and the overload capacity of an electrolyzer unit; hence the nominal capacity is entirely defined by the individual vendor [25]. The cost of an electrolyzer unit is, however, often expressed in €/kWe with the ‘kWe’ referring to the nominal electrical capacity. Furthermore, the efficiency varies with the load level of the electrolyzer and hence the efficiency at nominal capacity depends on how the nominal capacity is defined. The lack of such industry standard on the definition of nominal capacity makes it hard to compare technical and economic characteristics reported in the literature.

A second reason why comparing data reported in the literature is not straightforward, is due to the ambiguous definition of an electrolyzer ‘unit’ as stipulated by Frank et al. [26]. Depending on the author, an electrolyzer ‘unit’ comprehends at least the electrolyzer cell stack, but could also include the entire balance of plant (BOP). The BOP is a term used to denote all peripheral systems used for electrical power conversion, treatment, compression and storage of the hydrogen gas, treatment of feed-in water and thermal balancing of the unit. Technical and economic characteristics of the electrolyzer cell stack will clearly differ from the characteristics of the entire unit, including BOP; however, it is not always clear from the literature whether reported figures apply to the cell stack or the entire unit including BOP.

In the remainder of this thesis, all technical and economic characteristics will be referring to the entire electrolyzer unit, including the BOP.

Efficiency

The energy efficiency of an electrolyzer unit is defined as the energy contained in the produced hydrogen divided by the electrical energy consumed by the unit to produce that amount of hydrogen. The efficiency of the cell stack is reported to decrease for an increasing hydrogen production rate [27]. This decrease is, however, counteracted by an increasingly efficient use of the BOP. Although the entire energy consumption of the BOP will increase for higher hydrogen production rates, the BOP energy consumption per unit of produced hydrogen will decrease.

The range of electrolyzer efficiencies reported in the literature is given in Table 2.1. All efficiencies are expressed in the higher heating value (HHV) of hydrogen.

Table 2.1: Efficiencies of AEL and PEM electrolyzers, including the BOP.

AEL	PEM	Source
67-82%	74-87%	[28]
65-80%	60-80%	[29]
	72.8%	[26]
60.2-70.8%	54.3-70.8%	[25]

Start-up times

Electrolyzer start-up times depend on the temperature of the electrolyzer cell stack as described by Buttler and Spliethoff [25]. Start-ups from warm and pressurized stand-by mode can occur within 1-5 minutes for AEL and within seconds for PEM electrolyzers. The time required for a cold start-up depends on the maximum possible rate at which the cell stack can be heated, which is limited by the maximum current and voltage of the rectifier in relation to the cell-stack size and by the allowable corrosion at maximum current and voltage levels. For AEL, cold start-ups in the order of one to several hours are reported while for the PEM electrolyzers, a cold start in the range of several minutes is reported. An overview of start-up times is given in Table 2.2.

Table 2.2: Warm and cold start-up times for AEL and PEM electrolyzers, including the BOP.

	AEL	PEM
Warm start	1-5 minutes	seconds
Cold start	1-2 hours	5-10 minutes

Operating range

During electrolyzer operation, a continuous hydrogen contamination in the oxygen stream occurs due to diffusion of hydrogen gas through the electrolyzer membrane and due to electrolyte circulation (in case of AEL) [30]. The hydrogen diffusion through the membrane is nearly independent of the operating point of the electrolyzer, hence lowering the operating point results in a relative increase of hydrogen contamination, possibly leading to flammable mixtures. The minimum operating point of an electrolyzer is hence determined by the maximum allowable hydrogen contamination in the oxygen stream, which is typically 1-2% [25]. The resulting minimum operating point of AEL is 10-40%; for PEM electrolyzers, the minimum load is lower due to the low gas permeability of the polymer membrane (most suppliers even state no technical limit of minimum load) [25].

Note that individual electrolyzer unit sizes range from several kilowatts to megawatts [31]. Large-scale electrolyzer plants consist of multiple individual electrolyzer units which can be switched on and off individually. The minimum operating load of the entire plant is hence equal to the minimum load of one individual unit which can be very low compared to the overall plants' nominal operating point, resulting in a very wide operating range at plant-level.

The maximum operating point is defined by the maximum overloading capacity which depends on the defined nominal operating point as mentioned before. For clarity, a maximum operating point of 100% of nominal capacity will be used in the remainder of this thesis. Hence no overload capacity is considered.

Ramp rates

NREL performed tests showing very dynamic operating capabilities of both AEL and PEM electrolyzers allowing them to be used for frequency regulation [32]. Buttler and Spliethoff [25] report that once the electrolyzer is at nominal temperature, it can vary its full operating range in the order of seconds.

2.2.3 Economic characteristics of electrolyzers

Overnight construction cost

The overnight construction cost (OCC) is composed of the equipment cost and the installation cost, the latter typically in the order of 5-15% of the equipment cost [25]. Although AEL is a mature technology, a wide range of OCC figures are reported in the literature, as shown in Table 2.3. This could partly result from a different definition of the electrolyzer unit, which may or may not include the BOP depending on the author [26]. All the figures reported in Table 2.3 are assumed to include the BOP, although it is not always clear which components are exactly included in the BOP.

The range of reported costs for PEM electrolyzers is bigger than for AEL, probably since the technology is less mature and hence a wider range of cost estimations is made for the PEM technology. Note that the costs in Table 2.3 stem from literature published in different years and that it is often unclear on which year the cost figures are based. Therefore, the reported OCC should be interpreted with caution.

Table 2.3: Cost characteristics of AEL and PEM electrolyzers.

AEL	PEM	Source	Year of publication
900-1125 €/kW _e ^a	400-600 €/kW _e ^a	[28]	2013
	1460-2390 €/kW _e ^b	[33]	2017
800-1500 €/kW _e	1400-2100 €/kW _e	[25]	2018

^a Using 75% efficiency to convert expression in kW_{H₂} to kW_e.

^b Using a 2017 average exchange rate of 1.13 \$/€.

Operation and maintenance cost

The fixed operation and maintenance cost is often provided as a percentage of the initial construction cost per year. For AEL figures between 2-3% are reported [25] and for PEM electrolyzers they could range from 1.5% [33] to 5% [25].

The variable operation and maintenance cost is predominantly determined by the price of electricity and water, which depends on electrolyzer location and time of operation.

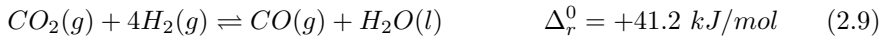
2.3 Methanizer

2.3.1 Operating principles

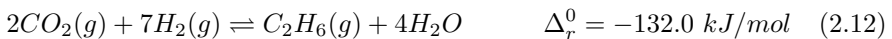
In the methanation step, hydrogen and CO_2 are converted to methane and water. This process is called the Sabatier process, named after Paul Sabatier who discovered the process in 1902 [24]. The overall chemical equation goes as follows:



A two-step reaction mechanism is assumed, first a reverse water-gas shift (rWGS) reaction to convert hydrogen and carbon dioxide to carbon monoxide and water, as shown in Eq. (2.9). Second, a hydrogenation reaction occurs to convert the carbon monoxide and hydrogen to methane and water, Eq. (2.10).



The reaction equilibrium and process speed are determined by the pressure and temperature at which the reaction takes place. Depending on the exact process conditions, carbon precipitation can occur following the Boudouard reaction (Eq. (2.11)) [34] and higher hydrocarbons can be produced, of which ethane is the most stable and is formed according to Eq. (2.12) [35].



The methanation reaction can occur in two ways: catalytic or biological, depending on whether a chemical catalyst or biological micro-organisms are used to facilitate the conversion from hydrogen and CO_2 to methane. Each of these methanation methods has its advantages and disadvantages, however, it seems that catalytic reactors are more suitable for larger industrial methanation plants. This is mainly due to the low gas velocity through the biological reactors, which would require very high reactor volumes to reach high methane production rates [31]. For this reason and since the focus of this thesis is large-scale energy storage via power-to-gas, the remainder of this section will discuss catalytic methanation.

2.3.2 Technical characteristics of methanizers

Before diving in the technical characteristics of methanation reactors, a few remarks should be made concerning the interpretation of the presented data. First, many different types of catalytic reactors exist, which distinguish themselves by their design. Fixed-bed and fluidized-bed reactors are the most well-known, although three-phase and structured-bed reactors have gained a lot of research attention lately [24]. Second, irrespective of the reactor design, different catalysts can be used, the most well-known is a nickel-based catalyst, although many variations exist [36]. Third and lastly, similar to electrolyzers, a difference should be made between characteristics referring to the reaction column only and characteristics referring to the entire methanation plant, including the balance of plant (BOP) [26].

The technical characteristics provided in this section, and economic characteristics in the next section, refer to the entire methanation plant, including the BOP. Nonetheless, due to the presence of such wide variety in reactor design and catalyst types, the characteristics found in the literature and discussed next, span a wide range of values. Since the interest of this thesis is mainly in determining the relevance of P2G in a larger system context, averaged methanation plant characteristics will be used later in the different studies.

Efficiency

The energy efficiency of the methanation process is defined as the energy contained in the produced methane divided by the energy consumed in the form of hydrogen. This energy efficiency should not be confused with the chemical conversion efficiency which refers to the yield of reaction products (methane). Since this thesis is focused on the energy aspects of the methanation process, the term efficiency will always refer to the energy efficiency while a chemical conversion efficiency of 100% is assumed.

A theoretical upper limit for the energy efficiency can be calculated by considering a stoichiometric methanation reaction and using the higher heating value (HHV) of reagents and reaction products. Taking a methane HHV of 887.18 kJ/mol and a hydrogen HHV of 284.26 kJ/mol, a maximum efficiency of 78% can be found following Eq. (2.13):

$$\eta^{met} = \frac{\text{HHV}_{\text{CH}_4} \cdot \text{mol}_{\text{CH}_4}}{\text{HHV}_{\text{H}_2} \cdot \text{mol}_{\text{H}_2}} = \frac{887.18 \text{ kJ/mol} \cdot 1}{284.26 \text{ kJ/mol} \cdot 4} = 78\% \quad (2.13)$$

The energy contained in the hydrogen feed-in which is not converted to methane appears in the form of heat since the methanation reaction is exothermic.

Although this maximum energy efficiency applies only to the reaction process and hence does not account for any energy consumption in the BOP, still higher efficiencies are reported in the literature for the entire plant, up to 85% [28]. This is explained as often heat recovery is incorporated in the efficiency calculation. Frank et al. [26] presents a clear distinction between the efficiency without heat recovery (72.7%) and with heat recovery (up to 89.2%), depending on the temperature at which the recovered heat is used.

Start-up and shut-down times

The methanation reaction occurs at high temperature (200-750°C [28]). In order to start up the reactor, it should first be heated to a temperature of at least 200°C while the reactor is simultaneously purged with hydrogen or an inert gas to prevent catalyst poisoning [31]. The limiting factor during start-up is the time required to heat up the reactor, which depends on the reactor design, catalyst volume and peripheral systems [35, 31]. Cold-start times in the range of hours are reported in the literature [28].

To shut down a reactor, a process of purging the reactor at temperatures above 200°C and gradually cooling down the catalyst has to be followed, opposite to the start-up procedure [31].

Minimum operating point

The operating point of a methanation reactor depends on the specific reactor design. Although there is no minimum production rate required for the reaction process, the energy contained in the produced methane should exceed the energy consumption by the peripheral systems for the process to be useful. In addition, some reactor designs require a minimum operating point for the heat management system to work adequately. Götz et al. report a minimum load between 10-40% of nominal load, depending on the reactor design [31].

Ramp rates

Dynamic operation of the methanation plant poses a risk to the catalyst due to temperature swings which may cause catalyst cracking or sintering. However, using adequate temperature control would allow the methanation plant to operate dynamically [31]. The ramp rates thus depend partly on the temperature control and the thermal inertia of the catalyst bed, which increases with the catalyst volume and hence the reactor size. Although Lefebvre et al. present

ramp rates of over 40% of nominal capacity in 10-20 minutes without temperature control issues [34], the experiment was only demonstrated on a lab-scale reactor and results might possibly not hold for industry-scale reactors. No specific ramp rates have yet been reported in the literature for such industrial scale reactors.

2.3.3 Economic characteristics of the methanizers

Overnight construction cost

A wide range of overnight construction cost (OCC) figures between 130 and 1500 €/kW_{CH₄} is reported in the literature, as is also mentioned by Götz et al. [31]. This can be explained by the many different reactor designs available and by the relative low maturity of methanation technology in the context of P2G, which requires a more dynamically operated reactor compared to the traditionally steady-state operated chemical processes.

Operation and maintenance cost

A fixed operation and maintenance cost of 5-7.5% of the OCC per year is reported by Parra et al. [33]. A report by DNV-Kema reports a figure as high as 10% of the OCC per year [28]. This fixed operation and maintenance cost includes the peripheral systems but excludes the production of hydrogen, i.e. the electrolysis step is not accounted for in these figures.

The technical and economic characteristics discussed in the two previous sections will be used in all following chapters as input parameters for the different case studies.

2.4 Other synthetic fuels

Although electrically produced hydrogen and synthetic methane are the focus of this dissertation, many different synthetic fuels exist, which will be discussed briefly in this section. A list of the most common fuels is provided below:

- Syngas
- Methanol
- Ethanol
- Dimethyl ether

- Heavy hydrocarbons

Note that, since the interest of this dissertation is in storage of electrical energy, only synthetic fuels which can be produced starting from electrical energy are discussed. Fuels and production processes starting from fossil fuels, biomass or other sources [21] will hence not be considered as they fall outside the scope of this work.

Each of the fuels listed before can be made starting from electrically produced hydrogen or syngas. In addition, many of the synthetic fuels can be converted into another fuel, as shown in Figure 2.5.

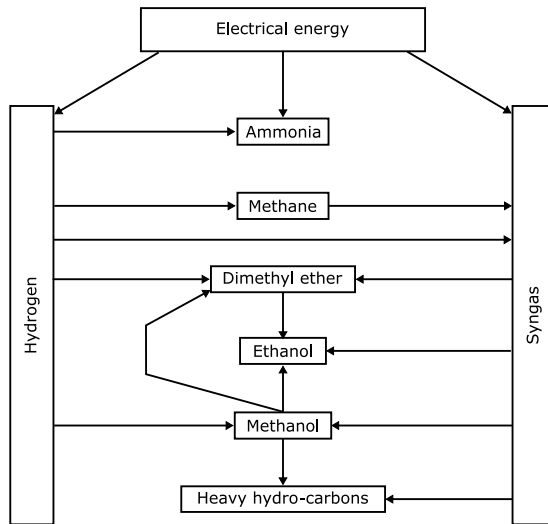


Figure 2.5: Most important production-paths for synthetic fuels starting from electrical energy.

An overview of different production processes for each of the synthetic fuels is discussed next.

2.4.1 Syngas

Syngas is a mixture of hydrogen, CO and, sometimes, CO₂. It can be produced by co-electrolysis of water and CO₂ using electrical power [37], by reacting captured CO₂ with hydrogen in a reverse water-gas shift (rWGS) reaction or by dry-reforming (synthetic) methane. During the production of syngas by co-electrolysis of water and CO₂, a reduction of both water and CO₂ occurs at

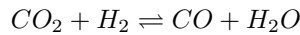
the cathode as follows:



The liberated oxygen ions can then travel through the membrane to the anode where the oxidation reaction occurs as follows:

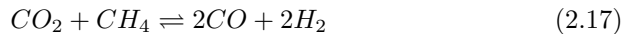


Syngas can be produced by mixing CO_2 with hydrogen and sparking a reverse water-gas shift (rWGS) reaction as given in Eq. (2.9) and repeated here:



Removing water from the reaction products and adding additional hydrogen results in the required syngas.

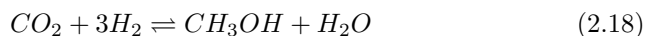
When syngas is obtained by dry-reforming synthetic methane, a reaction occurs as follows [37]:



The production of syngas from methane is currently the most used production path in industry. However, in a low-carbon future where methane is produced synthetically starting from electrically produced hydrogen, it is expected that syngas will be produced directly from hydrogen or by co-electrolysis of water and CO_2 . In addition, many liquid fuels can be produced from methane, with syngas as an intermediate product in the reaction process. Although this process occurs quite frequently in industry when starting from fossil methane as feedstock, it is likely not the most economically and energetically efficient route to produce synthetic liquid fuels when starting from electrical energy. Hence, synthetic fuel production paths starting from synthetic methane are not explicitly shown in Figure 2.5.

2.4.2 Methanol

Methanol can be produced by direct hydrogenation of CO_2 or by the syngas-to-methanol process [37]. When methanol is produced by direct hydrogenation, the reaction occurs as follows [38]:

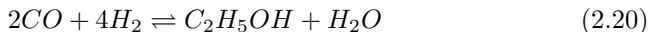


When starting from syngas, methanol is produced as follows [39]:



2.4.3 Ethanol

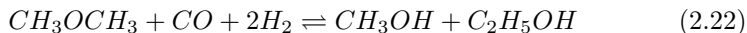
Ethanol can be produced from syngas. Depending on the catalyst used, a direct synthesis from syngas occurs as follows [40]:



Alternatively, the production of ethanol from syngas can occur via an intermediate product, which can be either methanol or dimethyl ether. When methanol is used as intermediate product, a homologation of methanol occurs [41]:

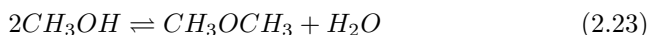


When dimethyl ether is used as intermediate product, the overall reaction becomes [40]:



2.4.4 Dimethyl ether

The most conventional way to produce dimethyl ether is directly from methanol by de-hydration of the methanol molecule, according to the following reaction [42, 43]:



This method is also known as the indirect synthesis method and differs from the direct synthesis method, which starts from syngas. In the direct synthesis method, methanol is also formed as an intermediate product (Eq. (2.19)), which is in a simultaneous reaction de-hydrated to dimethyl ether (Eq. (2.23)) [44]. A difference with the indirect synthesis method is that the direct synthesis method occurs in one process.

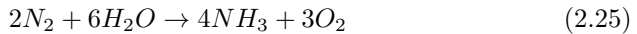
A third option to produce dimethyl ether is the direct hydrogenation of CO_2 . A hybrid catalyst is used which causes both a synthesis of methanol (Eq. (2.18)) and de-hydration of this methanol to dimethyl ether according to Eq. (2.23). Both reactions occur simultaneously, without the need for an intermediate water-gas shift (WGS) reaction to convert CO_2 to CO [39].

2.4.5 Ammonia

The most common process for production of ammonia is the Haber–Bosch process which synthesizes ammonia from hydrogen and nitrogen, according to the following reaction [45]:

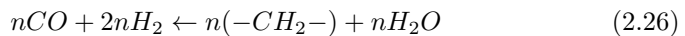


Alternatively when starting from surplus electrical energy, ammonia can be synthesized electrochemically starting from nitrogen and pure water, thereby avoiding the hydrogen production step, as follows [46]:



2.4.6 Heavy hydrocarbons

The most popular hydrocarbons like gasoline, diesel and kerosene, can also be produced synthetically starting from syngas or methanol [47]. When hydrocarbons are produced from syngas, the well-known Fischer-Tropsch process is used. Depending on the process conditions, a wide range of hydrocarbons are produced which can further be upgraded to liquid fuels in conventional petroleum refineries. The Fischer-Tropsch reaction is given in Eq. (2.26) with n a positive integer



To produce hydrocarbons from methanol, the Methanol-to-Gasoline process is used, developed by Exxon Mobil. In this process, methanol is first de-hydrated to form dimethyl ether (Eq. (2.23)), which is then converted to olefins, which are in turn converted to gasoline [47].

2.5 Summary and conclusions

Starting from a surplus of renewable electrical energy, many different synthetic fuels can be produced. Hydrogen and syngas can be used directly or as feedstock to produce other synthetic fuels such as methane, methanol, ethanol, dimethyl ether, ammonia and heavier hydrocarbons. The production process of each of these synthetic fuels is discussed in this chapter. Although each of the fuels

have different advantages concerning energy density, carbon content, toxicity etc., special attention is given to synthetic methane since it can use the existing natural gas grid for transport and storage and its energy density is sufficient to allow for large-scale storage.

The production of synthetic methane occurs in two phases. First, hydrogen is produced from water using electrical power in an electrolyzer, after which this hydrogen is made to react with CO_2 to form methane in the so-called Sabatier reaction.

Three different types of electrolyzers have been considered: alkaline electrolyzers (AELs), polymer electrolyte membrane (PEM) and solid oxide electrolysis cells (SOECs). Although alkaline electrolyzers were predominantly used for steady state processes, many manufactures can now produce alkaline electrolyzers capable of following the volatile production profile of intermittent renewables. PEM electrolyzers are having a slightly faster start-up time due to their compactness and have a bigger operating range. SOEC are still in the research phase. Although their reported efficiencies are much higher than those of alkaline and PEM electrolyzers, it is yet unclear whether SOEC can handle dynamic operation due to the high temperatures at which they operate, which lead to high thermal inertia.

The methanation reaction can take place in a catalytic or biochemical manner. The catalytic process is more controllable, but highly sensitive to impurities in the reactant stream. Impurities form a lesser problem for biological methanation but their methane production rate per reactor volume is significantly lower compared to catalytic methanation reactors. Biological methanation is hence less suitable for large-scale units. Many reactor designs exist for catalytic methanation, this and the relative low maturity of methanation technology in a renewable context leads to wide range of technical and economic parameters found in the literature.

The technical and economic characteristics presented in this chapter will be used as input parameters for the case studies in all subsequent chapters.

Chapter 3

Cost evaluation of storage

This chapter is mainly based on:

Belderbos, A., Delarue, E., Kessels, K. and D'haeseleer, W. *Levelized cost of storage - Introducing novel metrics*. Energy Economics 67 (2017), 287–299.

Before investigating the possible role of power-to-gas (P2G) in future energy systems, this chapter first presents different cost metrics to express the economic viability of storage units in a given electricity market. For conventional electricity generation technologies, the levelized cost of electricity (LCOE) is a well-known metric. In the context of electricity storage however, such LCOE-like metrics are only limitedly applicable as the finite energy storage capacity can limit the charge and discharge scheduling decisions of the storage operator. In addition, the “fuel”, i.e., charged electricity, and “generated electricity”, i.e., discharged electricity, is one and the same commodity which requires to use an adapted levelized cost metric. This chapter analyzes three different levelized cost metrics and their application to electricity storage units used for electrical energy arbitrage. In addition, the strengths and shortcomings of these storage cost metrics are analyzed in order to determine how they can be applied correctly.

This chapter starts with an introduction of cost metrics and an overview of the literature in Section 3.1. Next, a short review of the traditional LCOE metric is given in Section 3.2, which is followed in Sections 3.3 and 3.4 by an introduction and analysis of three levelized cost metrics applicable to storage. The use of these cost metrics together with historical price profiles is shown in Section 3.5 and discussed in Section 3.6. Section 3.7 concludes this chapter.

3.1 Introduction

To analyze the economic potential of different storage technologies and determine which technology could store the necessary electrical energy in the most economically efficient way, investors¹ and policy makers can use a set of tools ranging from the calculation of a summary cost metric to a simulation of the entire electricity system or market. One of the most well-known summary cost metrics to analyze the economic potential of a conventional generation technology is the levelized cost of electricity (LCOE) [48]. This cost metric is well established for conventional generation technologies but Joskow has shown that applying the metric to generation technologies which are not fully dispatchable (e.g. intermittent renewable energy sources (iRES)) should be done with caution as it could easily lead to flawed conclusions [49]. An adapted formulation of the LCOE metric was presented by Reichelstein and Sahoo [50] to make it applicable to iRES. Inspired by the reflections by Joskow on applying the levelized cost methodology to iRES, the aim of this chapter is to analyze the levelized cost metric applied to storage technologies and to outline how it can be used correctly.

Specifically for storage, there are several studies which use a range of cost metrics to compare different technologies. The US DOE and EPRI [51] list 5 costs metrics which can be used to analyze the economic potential of different storage technologies: the installed cost, the levelized cost of capacity, the levelized cost of energy and the present value of life-cycle costs both expressed in cost per installed power capacity and cost per installed energy storage capacity. They apply the different metrics to different technologies, but do not elaborate on the metrics themselves. In a similar way, Jülch [52] applies the LCOE metric, termed the levelized cost of storage (LCOS), to different storage technologies in order to compare them. Zakeri and Syri [53] distinguish between a levelized cost of electricity and a levelized cost of storage, where the latter excludes the cost of charging electricity. This metric is then used to compare the life cycle cost of different storage technologies. Compared to the aforementioned studies, the present chapter analyzes the levelized cost metrics for storage technologies themselves and how to use such metrics in general rather than applying them to specific storage technologies.

Few studies exist which analyze the levelized cost metrics applied to storage in a general way, rather than applied to specific situations. The existing studies are discussed below and although the cost metrics proposed in each study have their specific merits, they all couple storage to a specific generation technology,

¹Although the investor, owner and operator of a storage unit can be three different entities, in this work we assume they are all one and the same and will use the terms investor, owner and operator as synonyms.

thereby assuming a fixed cost for input energy. Pawel [54] has presented a method to calculate the levelized cost of stored electricity in a similar way as the traditional LCOE and has extended the formulation to analyze hybrid iRES-storage plants. The World Energy Council (WEC) [19] proposed a formulation for the LCOS in their report on electricity storage. In this formulation, the cost for input energy, or the charging cost, is left out of the calculation to avoid obscuring the results with too many assumptions. However, during further analysis in the report, storage is coupled with iRES and thus implicitly taking the levelized cost of this iRES as cost of input energy, as Pawel [54] did. Lai and McCulloch [55] use the LCOS formulation as provided by the WEC to analyze the cost component of storage in a hybrid iRES-storage plant. Together with the levelized cost component of the iRES capacity, they come to a metric termed the Levelized Cost of Delivery, which, although analyzed in a different manner, sums up to a similar metric as Pawel [54] introduced. Poonpun and Jewell [56] calculate a storage cost as a cost added to each kWh of stored energy. In this chapter we show that this methodology neglects the cost due to efficiency losses, which in turn depends on the cost of input energy.

This chapter adds to the existing literature as we extend the analyses made by Pawel, the WEC and Lai and McCulloch. The presented work aims at giving a more comprehensive analysis as it studies the impact of each parameter of the levelized cost metric. Rather than looking at hybrid iRES-storage plants, we focus our analysis solely on storage which acts upon a given price profile (i.e., which arbitrages in the electricity market). This facilitates interpretation of the results and makes the outcome more broadly applicable. The objective of this work is two-fold: first, three cost metrics are presented and analyzed in depth to gain insights on the cost of storage in general. Second, the strengths and shortcomings of these cost metrics are analyzed to outline when and how a levelized cost metric can be applied correctly to storage.

The perspective taken in this chapter is that of an actor who sees a varying electricity price profile on which he can act to arbitrage between moments with high prices and moments with low prices. In contrast to the traditional terminology of naming the cost metrics from a cost perspective, the cost metrics in this chapter are named from a price perspective to make a clearer distinction between the different metrics. For typical generation units (both of the conventional and intermittent/variable type), the LCOE is traditionally referred to as the levelized "cost" of electricity although it is defined in terms of the electricity price that breaks even the costs. In this chapter, we will focus more on the required average electricity price for reaching that break-even point for the investor/owner/operator².

²The origin of this price related name will be explained in the next section.

Three storage cost metrics are presented and analyzed which differ in the part of the variable cost that is accounted for:³

1. the “required average discharge price”, should cover the full cost of the stored electricity: it allows the investor/owner/operator to break-even the investment cost, including payments on capital (interest for debt financing and a certain rate of return for equity), and other fixed and variable costs, incorporating the cost for the input electricity (that is effectively “bought” and is the equivalent of the fuel cost in typical generation units, if any);
2. the “required average price spread”, is equal to the difference between the required average discharge price and the average price (being a cost) at which input electricity is charged;
3. the third metric is the “required average operational profit” which is the average profit an investor should make from arbitrage for recovering the investment cost, including payments on capital.

The three cost metrics are analyzed analytically and illustrated by simple methodological examples. These examples allow to identify specific points of attention when applying a levelized cost metric to storage and to outline how a levelized cost metric can be used correctly in such cases.

Results of this research show that when a levelized cost metric is used, care should be taken when the average charging cost is neglected, or is assumed to be zero, as this implicitly means that the round-trip efficiency of a storage technology is not accounted for. Also, it will be shown that a limited energy storage capacity can limit the storage operator to capture the full possible arbitrage profit of a certain price profile. In fact, the influence of this limited energy capacity is hard to evaluate without extensive calculation as it impedes estimating the total number of operating hours, the average electricity price during charging and the average electricity price during discharging. It will become clear that a 1-on-1 translation of the LCOE to storage is insufficiently precise for storage technologies with limited energy storage reservoir, like batteries, which might lead to poor investment decisions. Instead, it is recommended to use the levelized cost metric in combination with an analysis of an entire representative price profile. In such case, using a levelized cost metric which is independent of the charging cost is most convenient to use as it can be compared to multiple price profiles without having to change the assumption for the average charging cost. This is a similar finding as was mentioned by the World Energy Council [19].

³Note that all cost metrics are a reformulation of the Net Present Value which is equal to 0. The metrics differ in the share of variable costs that is explicitly accounted for.

As IRENA points out in their report on battery storage for renewables [57], the levelized cost metric is not necessarily representative for the value of storage as a storage facility can provide additional (“ancillary”) services to the energy system not accounted for in the levelized cost metric. In the presented research, the value of such services is not included. This could be taken into account by subtracting a value term from the cost calculation but it is opted to leave this for future work as extra complexity might obscure the presented results. A second assumption made in this work is that of full foresight of the price profile for the storage operator. The absence of full foresight in real applications could be taken into account by adapting the method used to calculate a storage operator’s possible arbitrage profit. This does not change, however, the way in which the different cost metrics can be used.

A few other remarks and caveats of this work must be mentioned upfront. The analysis presented should be as widely applicable as possible, meaning that it pertains to storage units/facilities of any size, capacity and application circumstance; the range of applicability stretches from short-time storage (like batteries) with perhaps several cycles per day, to intermediate-term storage (such as pumped hydro and compressed air storage), where cycling may range from days to weeks, up to long-term or seasonal storage (such as power-to-gas), where cycle periods may extend to months. This implies that the expressions must be able to account for various construction duration lengths (and hence the cost for “interest during construction”)⁴ —which may be negligible for e.g., batteries, but not for larger storage units. Furthermore, in the interest of generality⁵, we prefer not to use the concept of number of cycles. If desired, the conversion is easily made, e.g., for units with several cycles per day or per month, the amount of discharged electricity in year t (that we will refer to as MWh_t^d) can be written as $MWh_t^d = P \cdot 365 \cdot \chi_d \cdot \tau = E \cdot 365 \cdot \chi_d$ or $MWh_t^d = P \cdot 12 \cdot \chi_m \cdot \tau = E \cdot 12 \cdot \chi_m$ with P the installed power capacity, E the installed energy capacity, τ the discharge duration per cycle (with $E = P \cdot \tau$), and χ_d or χ_m the number of discharge cycles per day or per month, respectively. Note also that one can write the “produced” (i.e., discharged) electrical energy, using the “load factor”, LF, being the ratio of the “number of discharging hours” NDH divided by 8760 h/a, as follows, $MWh_t^d = P \cdot NDH = P \cdot LF \cdot 8760$.

To keep a sharp focus on the newly introduced metrics for storage, we will keep the formulae as transparent as possible, thereby ignoring taxes (e.g., tax deduction for depreciation) and subsidies. Although these transfer payments could be reasoned away as not being real economic costs, they do indeed impact

⁴For larger facilities, the word “construction” is commonly used; for smaller units, perhaps words like for “installation” or “erection” are more appropriate, whereby it is effectively understood that it does not take much time.

⁵Although we simplify our analysis by always charging and discharging at the rated/nominal power capacity of the storage device.

the profitability for investors/owners and should therefore be considered in the levelized cost of electricity (LCOE) as seen by investors in whatever tax regime or subsidy environment they operate. However, because this is very dependent on the tax/subsidy regimes (of which there is a large variety worldwide) and we do not wish to overload our formulae presented here, we will discuss important tax and subsidy elements in the levelized cost of electricity (LCOE) concept, thereby relying strongly on Reichelstein and Yorston [58], in Appendix A.

3.2 Levelized cost of electricity formulation and explanation of its meaning

The levelized cost of electricity (LCOE) for an electrical power generating unit is defined as *the fictitious average electricity price during its operation hours and needed over the lifetime of the plant to break even the full costs for the investor/operator/owner (including the desired rate of return and interest payment on debt, which are included in the discount rate r , being equal to the “weighted average cost of capital”, $WACC$ ⁶)*. Thus, the LCOE is the fictitious stable electricity price needed to make the present value of the sum of all costs and all revenues over the entire operational life of the unit equal to zero.

It is computed as follows [48]:

$$LCOE = \frac{\sum_t (OCC_t + OM_t + FC_t + CO_{2,t} + D_t) \cdot (1+r)^{-t}}{\sum_t MWh_t (1+r)^{-t}} \quad (3.1)$$

Where:

- OCC_t = The Overnight Capital Cost expended in year t ⁷
- OM_t = Operation & maintenance costs in year t , excluding fuel and possible CO_2 tax
- FC_t = Fuel costs in year t
- $CO_{2,t}$ = CO_2 tax costs in year t
- D_t = Decommissioning and waste management costs in year t

⁶Conventionally, $WACC = r_{debt}(Db/Tot)(1 - tc) + r_{equity}(Eq/Tot)$, with $Db + Eq = Tot$ and whereby Tot is the total volume of capital to be covered, Db the amount of debt financing and Eq the amount of equity; r_{debt} is the interest rate on debt and r_{equity} the expected rate of return for investors on own capital. tc is the corporate tax rate to be used to recover part of the interest paid on the loan. In the simplified philosophy of no taxes, the factor $(1 - tc)$ should be dropped. The user must decide whether to use the real or the nominal discount rate, and thus account for inflation or not.

⁷Note that t usually refers to one year, however, in every expression given in this chapter, t could denote any time interval as long as the discount rate r is adapted accordingly.

- MWh_t = The amount of electricity generated in MWh in year t , being equal to $P \cdot NOH = P \cdot LF \cdot 8760$, with P the installed power capacity, NOH the number of operating hours and LF the average load factor.
- $(1 + r)^{-t}$ = The discount factor for year t , with r being the discount rate

Many of the costs usually take place in a different time period: investments (represented by OCC_t) take place during the construction or installation period, whereas OM_t , FC_t and $CO_{2,t}$ (if any) occur during the plant operation and decommissioning D_t takes place after the plant has stopped, and often even a few years after that. Often the index t is taken to be zero at the onset of operation, so that the construction period runs over a negative index. Through the discount factor $(1 + r)^{-t}$, the expression then automatically computes the 'interest during construction' expenditures.

To introduce a *levelized cost of storage (LCOS)*, a 1-on-1 translation of the LCOE might be considered, thereby adopting its meaning in the sense that "fuel cost" becomes "charging cost" (i.e., the price at which input electrical power is "bought" by the storage facility) and 'MWh generated' becomes the amount of MWh discharged and thus sold in the market. The meaning of LCOS would therefore read:

The LCOS could be defined as *the fictitious average electricity price during discharging needed over the lifetime of the storage plant to break even the full costs for the investor (including payments for capital)*.

By means of the following analysis and the introduction of three cost metrics, it will become clear that the LCOS as defined above is incomplete in the sense that it is insufficiently precise and might therefore lead to poor investment decisions.

3.3 Storage cost terminology

It turns out that a distinction can be made between three cost metrics which, although being related to the LCOS, are more precisely formulated as: the *required average discharge price (RADP)*, the *required average price spread (RAPS)* and the *required average operational profit (RAOP)*. The word "average" is a life-time average and each of these cost metrics is expressed on a per unit energy basis (i.e., per MWh). To improve the readability, often we will distinguish between "per unit of discharged energy" (MWh^d) and "per unit

of charged energy” (MWh^c). Note that all three storage cost metrics must be expressed as ‘required’, to reflect the need for a break even overall cost.

As already mentioned, a levelized cost approach for an investor/owner/operator should include capital-related tax and/or subsidy effects to align these cost metric formulations with the Net Present Value result for such actors, as recommended by Reichelstein and Yorston [58]. However, to keep the focus on storage specific aspects of the cost metrics, the tax effect is neglected in the main text of the chapter. For completeness, an extended formulation of each cost metric, including these tax effects, is given in Appendix A.

In the following part of this section, a mathematical formulation of all three cost metrics is given.

3.3.1 Required average discharge price (RADP)

The *required average discharge price (RADP)* is basically a literal translation of the traditional LCOE formulation as given in Eq. (3.1). For full-cycle P2G storage, CO_2 might be emitted by the electricity producing unit and should thus be taken into account, however, for most storage facilities, there would be no (operational) CO_2 -tax and thus that term could be omitted. To simplify the formulation, the CO_2 -tax and decommissioning costs are omitted and variable operation & maintenance costs are neglected. An extended formulation of the cost metrics, including these costs, is given in appendix A. The formulation for the required average discharge price is thus given in Eq. (3.2).

$$RADP = \frac{\sum_t (OCC_t + FOM_t + TCC_t) \cdot (1 + r)^{-t}}{\sum_t MWh_t^d (1 + r)^{-t}} \quad (3.2)$$

Where:

- OCC_t = The Overnight Capital Cost expended in year t
- FOM_t = Fixed operation & maintenance costs in year t
- TCC_t = Total cost of charged electricity in year t
- MWh_t^d = The amount of electricity discharged in MWh in year t
- $(1 + r)^{-t}$ = The discount factor for year t, with r being the discount rate

Note that as already mentioned, $MWh_t^d = P \cdot 365 \cdot \chi_d \cdot \tau = E \cdot 365 \cdot \chi_d$ or $MWh_t^d = P \cdot 12 \cdot \chi_m \cdot \tau = E \cdot 12 \cdot \chi_m$ with P the installed power capacity, E the installed energy capacity, τ the discharge duration per cycle (with $E = P \cdot \tau$), and χ_d or χ_m the number of discharge cycles per day or per month, respectively. As seen, the energy storage capacity does not explicitly appear in the formula

for RADP although it has an effect via the amount of discharged electricity; it is thus implicitly present in the factor MWh_t^d . This is obvious in the expressions of the previous sentence and it will be discussed more extensively in Section 3.5.

TCC refers to the total charging cost. The reader must observe that only one cost for the charged electricity is defined and used throughout the chapter. This is similar to the LCOE philosophy for conventional generation plants, where there is one fuel cost, conventionally expressed in, €/MWh_e or \$/MWh_e, hence taking into account the conversion efficiency (and thus the efficiency losses) of the plant. In our case for storage devices, the equivalent “fuel cost” is the cost of the charged electricity, whereby this cost also includes the effects of the efficiency losses during both charging and discharging, which are in our definition combined in the round-trip efficiency η_{RT} . There is no need to distinguish between efficiency losses during charging and discharging (similar to the fact that for conventional generation it is not necessary to split up the efficiency in a thermodynamic part of the cycle and an electrical part of the electricity generator, etc.). The only difference from a system’s perspective between a generation plant and a storage device is the time delay between the “fuel” input (i.e., charging) and electrical power output (i.e., discharging) in a storage device.

In general, the ‘required’ average discharge price differs from the average electricity price over the whole year as only prices during the time intervals of discharging are taken into account. Likewise, the charging cost is not equal to the annual average electricity price multiplied with the number of charging hours. Rather, the charging cost is the sum of the actual electricity prices at charging times, or said differently, the relevant ‘average charging cost’ (*average charging cost (ACC)*) is the weighted average cost obtained by averaging only during the charging hours and accounting for the amount of charged energy.

3.3.2 Required average price spread (RAPS)

The price spread is defined as the difference between the discharging price and the charging price. The *required average price spread (RAPS)* is defined as given in Eq. (3.3), where MWh_t^c expresses the amount of electricity charged in MWh in year t .

$$\begin{aligned} RAPS &= \frac{\sum_t (OCC_t + FOM_t + TCC_t) \cdot (1+r)^{-t}}{\sum_t MWh_t^d (1+r)^{-t}} - \frac{\sum_t TCC_t \cdot (1+r)^{-t}}{\sum_t MWh_t^c (1+r)^{-t}} \\ &= RADP - ACC \end{aligned} \quad (3.3)$$

We have defined the *average charging cost (ACC)* as the total charging cost divided by the total amount of charged electricity (MWh^c) as indicated in Eq.

(3.4):

$$ACC = \frac{\sum_t TCC_t \cdot (1+r)^{-t}}{\sum_t MWh_t^c (1+r)^{-t}} \quad (3.4)$$

When exogenous charging, e.g., due to rain in a pumped hydro storage reservoir, and self-discharging are neglected, the amount of energy charged and discharged are linked through the round-trip efficiency η_{RT} , where we have assumed that η_{RT} is constant:

$$\sum_t MWh_t^d (1+r)^{-t} = \eta_{RT} \sum_t MWh_t^c (1+r)^{-t} \quad (3.5)$$

Using Eq. 3.5, the *required average price spread (RAPS)* expression of Eq. 3.3 can be simplified to:

$$RAPS = \frac{\sum_t (OCC_t + FOM_t + (1 - \eta_{RT})TCC_t) \cdot (1+r)^{-t}}{\sum_t MWh_t^d (1+r)^{-t}} \quad (3.6)$$

Eq. (3.6) shows that the *required average price spread (RAPS)* should cover the investment costs, the operation & maintenance costs and the cost due to efficiency losses (given by the term $[1 - \eta_{RT}]TCC_t$).

3.3.3 Required average operational profit (RAOP)

The *total operational profit (OP)* is the total revenue from discharging electricity minus the total cost from charging electricity. The required total OP for breaking even must equal the total costs expended for capital investment and fixed operation & maintenance costs and equals the difference between the required total revenue from discharging and the total charging cost as expressed

in Eq. (3.7):⁸

Required total OP

$$\begin{aligned} &= \sum_t (OCC_t + FOM_t + TCC_t) \cdot (1+r)^{-t} - \sum_t (TCC_t) \cdot (1+r)^{-t} \\ &= \sum_t (OCC_t + FOM_t) \cdot (1+r)^{-t} \end{aligned} \quad (3.7)$$

For the reasons explained underneath Eq. (3.2), there is only one TCC which is canceled out from the first line of Eq. (3.7).

The *required average operational profit (RAOP)* can be defined by expressing the required total OP on a per unit of discharged energy basis, leading to Eq. (3.8):

$$RAOP = \frac{\sum_t (OCC_t + FOM_t) \cdot (1+r)^{-t}}{\sum_t MWh_t^d (1+r)^{-t}} \quad (3.8)$$

3.3.4 Numerical illustration of the different cost metrics

An example is presented to illustrate the *required average discharge price (RADP)*, the *required average price spread (RAPS)* and the *required average operational profit (RAOP)* introduced in the previous subsection. The example looks only at one year of operation for simplicity; the capital costs and fixed operation and maintenance cost are therefore converted in an equivalent annual fixed cost. Table 3.1 shows the assumed fixed cost, the round-trip efficiency, the total number of discharging hours and the average charging cost for the reference case. Parameter values will be varied within the different illustrative cases to follow. The parameter values used are not based on a specific technology but are merely chosen for illustrative purposes. For all examples, the storage unit is assumed to charge and discharge at nominal power. This is not necessarily the case in real situations but results can easily be generalized by expressing them in equivalent full load hours.

⁸Note that, when certain costs, like labor costs, would be accounted for as fixed rather than variable operation & maintenance cost, our definition of operational profit would differ from the traditional definition as the latter excludes labor costs from the FOM when calculating the operational profit; Where in our definition all indirect costs are regarded fixed and remain in the calculation. However, if such labor cost is a direct cost (hourly wage) and as such accounted as variable operation & maintenance cost, both definitions become equal as shown in Appendix A.

Table 3.1: Storage parameters used for the reference case

Installed power capacity (P)	1 MW
Equivalent Annual Fixed cost (OCC + FOM)	30,000 €
Round-trip efficiency (η_{RT})	80 %
Number of discharging hours (NDH)	1000 h
Averaged charging cost (ACC)	20 €/MWh ^c

Recall that no parameter is provided for the energy storage capacity E as there is no need to explicitly take it into account in the different cost metrics.⁹ Also the duration during which no charging or discharging takes place is not needed, although it limits the max time during which electrical power can be discharged.

The RADP, RAPS and RAOP are calculated for the reference case. For 1,000 h of discharging at nominal capacity of 1 MW (and thus discharging 1,000 MWh), a total amount of 1,250 MWh ($= 1,000 \text{ h} \times 1 \text{ MW}/\eta_{RT}$) needs to be charged, costing 25,000 €. Using Eqs. (3.2), (3.6) and (3.8), this leads to the results shown in Table 3.2.

Table 3.2: Different cost metrics for a storage with parameters as provided in Table 3.1

RADP	55 €/MWh ^d
RAPS	35 €/MWh ^d
RAOP	30 €/MWh ^d

As indicated in the previous subsection, the *required average discharge price* (RADP) covers all fixed and variable costs. The sum of all costs per installed MW is in this example equal to 30,000 € fixed cost and 25,000 € charging cost, resulting in a total cost of 55,000 €. Divided by 1000 h of discharging electricity at nominal power results in a *required discharge price* of 55 €/MWh^d. The *required average price spread* (RAPS) is equal to the *required average discharge price*, $RADP = 55 \text{ €/MWh}^d$, minus the *average charging cost* (ACC), 20 €/MWh^c, which is equal to 35 €/MWh^d.¹⁰ Putting it in a different perspective, the *required average price spread* (RAPS) is also equal to the fixed

⁹Indeed, it is implicitly present via $MWh_t^d = P \cdot 365 \cdot \chi_d \cdot \tau = E \cdot 365 \cdot \chi_d$ or $MWh_t^d = P \cdot 12 \cdot \chi_m \cdot \tau = E \cdot 12 \cdot \chi_m$ with $E = P \cdot \tau$ and $NDH = 12 \cdot \chi_m \cdot \tau$ or $NDH = 365 \cdot \chi_d \cdot \tau$, so that $MWh_t^d = P \cdot NDH = P \cdot LF \cdot 8760$. (The symbols were defined near the end of Section 3.1.)

¹⁰Note that the subtraction of €/MWh^c from €/MWh^d is valid as both terms have the same unit (i.e. €/MWh). The superscripts c and d are only added for clarity, but do not change the unit of the cost.

cost and cost due to efficiency losses. Indeed, applied to this example, the efficiency losses per MW capacity amount to $(1,250 \text{ MWh}^c - 1,000 \text{ MWh}^d) \times 20 \text{ €/MWh}^c = 5,000 \text{ €}$. Added to the fixed cost and divided by all discharged electrical energy leads to a *required average price spread (RAPS)* of 35 €/MWh^d . The *required average operational profit (RAOP)* only covers the fixed costs as shown and explained by Eq. (3.8): dividing the capital cost of $30,000 \text{ €}$ by all discharged electricity (being $1,000 \text{ MWh}$) leads to an RAOP of 30 €/MWh^d . Note that the RAOP does not explicitly account for any operational costs as this is implicitly captured in the definition of the *required average operational profit (RAOP)*.

3.4 Parameter variations

To gain deeper insight in the presented cost metrics, different parameters (charging cost, efficiency and amount of discharged electricity) will now be varied to analyze their effect on each metric and on the difference between the metrics.

3.4.1 Varying the average charging cost

To analyze the sensitivity of each cost metric to different average charging costs, a numerical illustration is presented first. For this example, the same fixed cost, number of discharging hours and efficiency are used as given for the reference case in Table 3.1. The *average charging cost (ACC)* is changed from 0 €/MWh^c to 100 €/MWh^c . The resulting cost metrics RADP, RAPS and RAOP are shown in Figure 3.1.

It is clear from Figure 3.1 that the *required average operational profit (RAOP)* is constant for all average charging costs (ACC). This follows from Eq. (3.8) which indicates that the RAOP should only cover the fixed costs. The *required average discharge price (RADP)* and the *required average price spread (RAPS)* increase with an increase in ACC, with a slope as given by Eqs. (3.9) and (3.10):

$$\frac{\partial \text{RADP}}{\partial \text{ACC}} = \frac{\sum_t (1+r)^{-t}}{\eta_{RT}} \quad (3.9)$$

$$\frac{\partial \text{RAPS}}{\partial \text{ACC}} = \frac{(1 - \eta_{RT}) \sum_t (1+r)^{-t}}{\eta_{RT}} \quad (3.10)$$

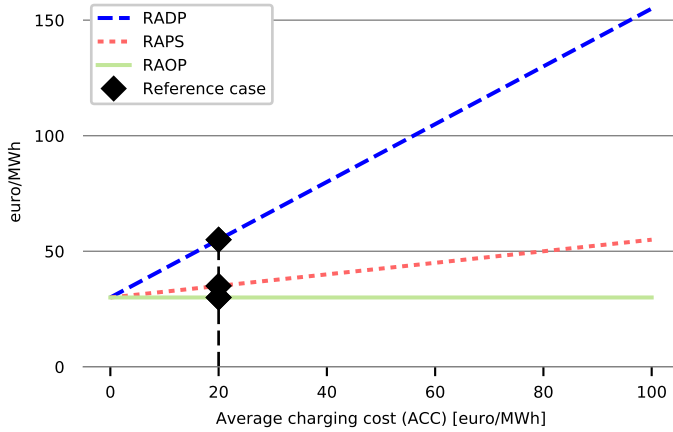


Figure 3.1: *Required average discharge price (RADP), required average price spread (RAPS) and required average operational profit (RAOP) as a function of the average charging cost (ACC) for a storage device with characteristics as given in Table 3.1, with constant round-trip efficiency and constant amount of discharged electricity.*

Figure 3.1 and Eqs. (3.9) and (3.10) show that the RADP increases more steeply than the RAPS for an increasing ACC. This can be explained as the RADP accounts for the full cost of all charged electricity, while the RAPS only account for the cost of energy lost due to efficiency losses. It is clear that the slopes of both sensitivities are not a function of the amount of discharged electricity but they do depend on the round-trip efficiency and the discount rate. This means that a change in ACC will have a bigger effect on the RADP and RAPS of storage units with a lower efficiency and will have no effect on the RAPS when the round-trip efficiency η_{RT} would become 100%.

In the given example, all cost metrics (RADP, RAPS and RAOP) become equal when the ACC is equal to zero. This is easily explained since all three measures only differ in how they account for the cost of energy losses or the full cost of charged electricity, as can be seen from Eqs. (3.2), (3.6) and (3.8). Note that when a variable cost different from the charging cost would be taken into account, the RADP and RAPS would increase with equal magnitude and would thus be different than the RAOP for an ACC equal to zero.

3.4.2 Varying the round-trip efficiency

The round-trip efficiency is varied next. A graphical illustration shown in Figure 3.2 is used to gain some basic insights.

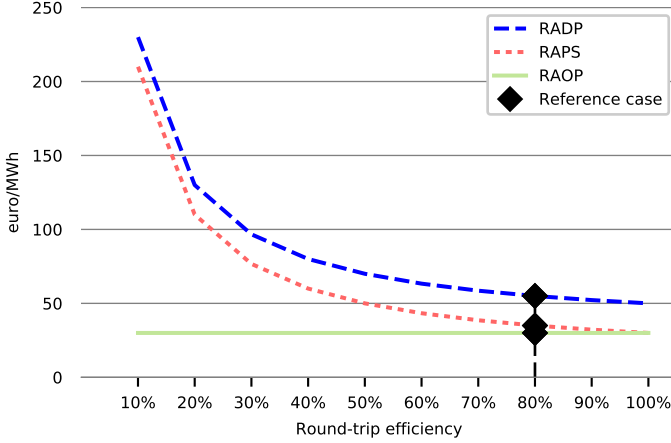


Figure 3.2: *Required average discharge price (RADP), required average price spread (RAPS) and required average operational profit (RAOP) as a function of the round-trip efficiency. For a storage unit with characteristics as given in Table 3.1, with constant average charging cost (ACC) and constant amount of discharged electricity.*

It is clear that the *required average operational profit (RAOP)* is independent of the round-trip efficiency. This can be understood as the operational profit should, by definition, cover only the capital expenditures and fixed operational and maintenance costs. Since the round-trip efficiency impacts only the variable operational costs, it has no effect on the RAOP. This is also shown by Eq. (3.8). The *required average price spread (RAPS)* and the *required average discharge price (RADP)* both decrease with an increasing round-trip efficiency and do so both with the same absolute magnitude. This can be understood by looking at the sensitivity of the RADP and RAPS to a change in round-trip efficiency η_{RT} as given in Eq. (3.11):

$$\frac{\partial RADP}{\partial \eta_{RT}} = \frac{\partial RAPS}{\partial \eta_{RT}} = \frac{-\sum_t ACC \cdot (1+r)^{-t}}{\eta_{RT}^2} \quad (3.11)$$

The sensitivity formulated in Eq. (3.11) is negative since both the RADP and RAPS decrease with an increasing efficiency. This is normal as the RADP

and the RAPS need to cover, besides the fixed costs, the full cost of charged electricity and the cost of efficiency losses, respectively. When the efficiency increases, less electricity needs to be charged per MWh of discharged electricity and hence, *ceteris paribus*, the total charging cost and the cost due to efficiency losses decrease. Eq. (3.11) shows that the slope of this sensitivity is not a function of the amount of discharged electricity but it does depend on the *average charging cost (ACC)*. The magnitude of the slope of this sensitivity decreases with a decreasing *average charging cost (ACC)* (in absolute value), and becomes zero when the ACC is equal to zero.

The difference between the RADP and the RAPS is equal to the *average charging cost (ACC)* as presented in Eq. (3.12). This is obvious from Eq. (3.3), or following Eq. (3.4):

$$RADP - RAPS = ACC = \frac{\sum_t TCC_t \cdot (1+r)^{-t}}{\sum_t MWh_t^c \cdot (1+r)^{-t}} \quad (3.12)$$

As a final note, it is pointed out that the RAPS and RAOP merge when the round-trip efficiency is 100% and no variable costs other than the charging cost are accounted for. This can be understood by looking at the difference between the *required average price spread (RAPS)* and the *required average operational profit (RAOP)* which is obtained by subtracting Eq. (3.8) from Eq. (3.6), with the result shown in Eq. (3.13). This difference is exactly equal to the cost of efficiency losses per MWh of discharged electricity. Clearly, if no cost is incurred due to losses when the round-trip efficiency is 100%, the right hand side of Eq. (3.13) becomes zero and the RAPS is equal to the RAOP:

$$RAPS - RAOP = \frac{(1 - \eta_{RT}) \sum_t TCC_t \cdot (1+r)^{-t}}{\sum_t MWh_t^d \cdot (1+r)^{-t}} \quad (3.13)$$

Rewriting Eq. (3.13) by using the relationship between the amount of charged and discharged electricity as given in Eq. (3.5) and the expression for the ACC in Eq. (3.4), shows that, although suggested differently by the denominator in Eq. (3.13), the difference between RAPS and RAOP is independent of the amount of discharged electricity:

$$\begin{aligned} RAPS - RAOP &= \frac{(1 - \eta_{RT}) \sum_t ACC \cdot (1+r)^{-t}}{\eta_{RT}} \\ &= \left(\frac{1}{\eta_{RT}} - 1 \right) \cdot ACC \cdot \sum_t (1+r)^{-t} \end{aligned} \quad (3.14)$$

3.4.3 Varying the amount of discharged electricity

The *required average discharge price (RADP)*, the *required average price spread (RAPS)* and the *required average operational profit (RAOP)* of a storage unit with characteristics as given in the reference case (Table 3.1) are shown in Figure 3.3 for different numbers of discharge hours. It is clear that the RADP, RAPS and RAOP change with the same difference in absolute magnitude (i.e., they stay kind of 'parallel'). To clarify this, we refer back to Eqs. (3.12) and (3.14) and present Eq. (3.15) which all show that the difference between the RADP, RAPS and RAOP only depends on the *average charging cost (ACC)* and, except for the difference between RADP and RAPS, on the round-trip efficiency but not on the number of discharging hours:

$$\begin{aligned} RADP - RAOP &= \frac{TCC_t \cdot \sum_t (1+r)^{-t}}{\sum_t MWh_t^d (1+r)^{-t}} & (3.15) \\ &= \frac{\sum_t ACC \cdot (1+r)^{-t}}{\eta_{RT} \sum_t (1+r)^{-t}} = \frac{ACC \cdot \sum_t (1+r)^{-t}}{\eta_{RT} \sum_t (1+r)^{-t}} = \frac{ACC}{\eta_{RT}} \end{aligned}$$

The decreasing trend of the RADP, RAPS and RAOP in Figure 3.3 originates from the fixed costs (capital and fixed operation & maintenance), which are divided by an increasing number of discharging hours. Hence the fixed costs decrease per unit of discharged energy.

From Figure 3.3 and Eqs. (3.12), (3.14) and (3.15) above, we can also conclude that the slope of change as a function of the change in number of discharging hours is equal for each cost metric. In Eq. (3.16), this is expressed by differentiating the RADP, RAPS and RAOP with respect to the amount of discharged electricity MWh_t^d :

$$\frac{\partial RADP}{\partial MWh_t^d} = \frac{\partial RAPS}{\partial MWh_t^d} = \frac{\partial RAOP}{\partial MWh_t^d} = \frac{-\sum_t (OCC_t + FOM_t) \cdot (1+r)^{-t}}{\sum_t (MWh_t^d)^2 (1+r)^{-t}} \quad (3.16)$$

The formulation in Eq. (3.16) shows that the sensitivity of each cost metric to a varying amount of discharged electricity is independent of the *average charging cost (ACC)* and the round-trip efficiency.

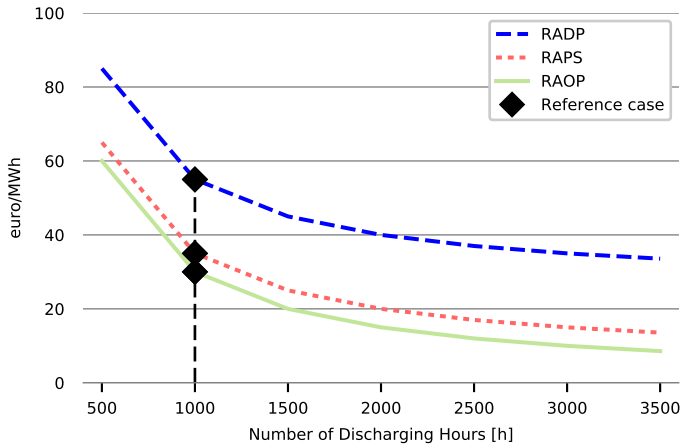


Figure 3.3: *Required average discharge price (RADP), required average price spread (RAPS) and required average operational profit (RAOP) as a function of the number of discharging hours. For a storage unit with characteristics as given in Table 3.1, with constant average charging cost (ACC) and constant round-trip efficiency.*

3.5 ‘Available’ prices compared to ‘required’ prices

In the previous sections, three different *required* average price metrics were introduced, which express the conditions for the storage investor to break even the full investment cost, including the rate of return on investment, and possible operational costs, depending on the metric. To assess whether this storage investor will indeed break even on an investment, these *required* average price metrics could be compared to representative historical *available* average prices, as seen by the storage unit. Using available prices, again three metrics are formulated: the *available average discharge price (AADP)*, the *available average price spread (AAPS)* and the *available average operational profit (AAOP)*. It will be shown that when an available average price metric is higher than the required average price metric, it is worthwhile to invest in storage.

Note that the available, or observed, instantaneous electricity price chronology that prevails in the market and that a certain storage unit ‘sees’ might differ from the occurring electricity price chronology that the unit can take advantage of when the energy storage capacity is limited. Two examples are presented to illustrate this. In a first example, we learn that the number of hours actually available for arbitrage can differ between storage units even if they act upon

the same occurring price profile. Figure 3.4 below shows a day-night price pattern with an alternating 12 hour low-price period and 12 hour high price period. If this pattern would occur for an entire year, there would be 4380 potential discharge hours with high prices and 4380 potential charging hours with low prices. A storage unit with a round-trip efficiency of 100% and an energy storage to power capacity ratio (E/P-ratio) of 12 hours or more, would be able to charge during all hours with low prices and discharge during all hours with high prices. However, a storage unit with an E/P-ratio of e.g. 5 hours would see the same price profile but would only be able to charge for 5 hours and discharge for 5 hours a day due to energy storage limitations. For a storage unit with a limited E/P-ratio of 5 hours, the occurring price pattern is clearly different from the actually 'available' price pattern which the unit is able to capture.

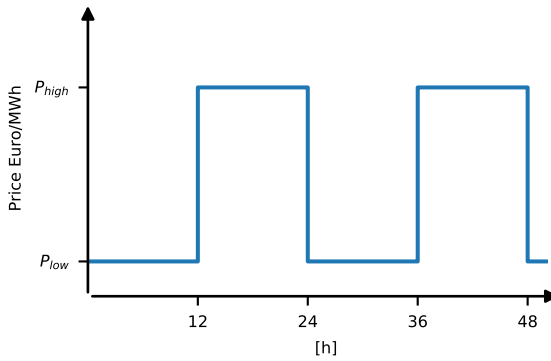


Figure 3.4: Reoccurring price signal with 24h period and alternating prices.

In a second example it is shown that one occurring price profile can lead to different available average charging and discharging prices for different storage units. An illustrative occurring price profile is presented in Figure 3.5. Consider again two storage units with different E/P-ratios, one with an E/P-ratio of 12h and one with an E/P-ratio of 5 hours who act upon the price profile shown in Figure 3.5. It is clear that the first storage unit can charge for 12 hours and then discharge for 12 hours, leading to an actually available average charging price of 15 €/MWh and an actually available average discharging price of 35 €/MWh. The second storage unit with a smaller E/P-ratio can only charge for 5 hours and would in an optimal scenario only charge during the hours with lowest price and discharge during the hours with highest price. Although this would lead to an actually available average charging price of 10 €/MWh and

an actually available average discharge price of 40 €/MWh, the total profit of the storage operator would be lower.

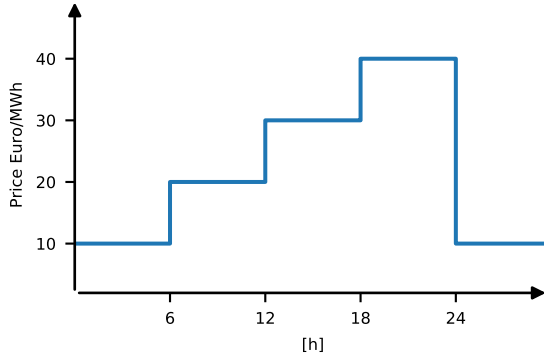


Figure 3.5: Reoccurring price signal with 24h period and increasing prices.

Both examples show the need to carefully analyze the entire occurring price profile when determining the average available cost metrics. The previous examples show furthermore that it is necessary to account for specific storage unit characteristics in this price profile analysis. Specifically when the storage unit is not always freely dispatchable by the storage operator, e.g., due to a limited energy storage capacity, considering only leveled cost metrics without analyzing representative price profiles might lead to erroneous conclusions considering the profitability of storage investments.

In the following sub-sections, the three *available* price metrics are introduced and graphically presented as a function of the number of discharge hours. A sensitivity analysis on the energy-to-power ratio and the round-trip efficiency is performed for each of the available price metrics. Furthermore, a comparison between the *required* price metric and the *available* price metric is presented and discussed.

3.5.1 Available average discharge price (AADP)

The *available average discharged price (AADP)* is equal to the average electricity price during actual discharge hours and is entirely defined by a given price profile and storage operation, as expressed in Eq. 3.17,

$$AADP = \frac{\sum_t DR_t \cdot (1+r)^{-t}}{\sum_t MWh_t^d (1+r)^{-t}} \quad (3.17)$$

Where:

- DR_t = Total revenue of discharged electricity in year t
- MWh_t^d = The amount of electricity discharged in MWh in year t
- $(1 + r)^{-t}$ = The discount factor for year t, with r being the discount rate

The *available average discharge price (AADP)* is calculated based on historical price profiles. In the following examples the Belgian day-ahead electricity prices in 2015 will be used [59]. To calculate the AADP, a small optimization program, presented in Appendix B, has been developed and is used to optimize the charging and discharging decisions of the storage operator, assuming perfect foresight of the prices and taking into account the installed capacity in terms of charging power, discharging power and energy storage. The optimization result is a charging and discharging sequence for the entire year and allows calculating the total charging cost, total discharging revenue, an available average charging price and *available average discharge price (AADP)*. In the following examples, the AADP is calculated as a function of the number of discharging hours (NDH). This NDH is imposed on the storage operator as the maximum number of hours he is allowed to discharge in a year.¹¹

Two examples are presented in Figure 3.6 to gain insight in the AADP concept. On the left hand side of Figure 3.6, the AADP as a function of NDH is calculated for different values of the energy-to-power (E/P) ratio and a round-trip efficiency of 80%. On the right hand side of Figure 3.6, the AADP is calculated for different round-trip efficiencies and an unlimited energy-to-power ratio. Both figures show that the AADP decreases for an increasing number of discharging hours (NDH). This is reasonable as a very limited number of discharging hours (NDH) incentivizes the storage operator to discharge only during hours with very high electricity prices. When more discharging hours are allowed, the storage operator will also discharge during hours with lower electricity price which thus decreases the AADP. The left hand side of Figure 3.6 further shows that a limited E/P ratio both decreases the AADP and the number of hours for which arbitrage is profitable. Indeed, for small E/P ratios, a storage operator might be unable to discharge during a substantial period of consecutive hours with high prices as he can only store a limited amount of energy for small E/P ratios. This can limit the profitable arbitrage hours for the storage operator and force the operator to discharge during hours with lower prices, resulting in a lower AADP. The right hand side of Figure 3.6 shows the AADP for different round-trip efficiencies. If the storage unit were to have an unlimited E/P-ratio, the efficiency clearly

¹¹Note that storage owners are expected to operate their storage for as many hours as economically favorable, hence imposing a maximum number of discharging hours is artificial. It is done here, however, to present the evolution of different metrics as a function of the NDH.

has no influence on the magnitude of the AADP as the storage operator will always discharge during hours with highest prices. However, it has an effect on the number of hours for which arbitrage is profitable and hence the efficiency has an influence on the number of discharging hours that the storage unit is operated. Note that it is sometimes unprofitable to operate the storage unit for the maximum allowed NDH; for such cases, the different figures show only a curve for the NDH that the storage is effectively operated.

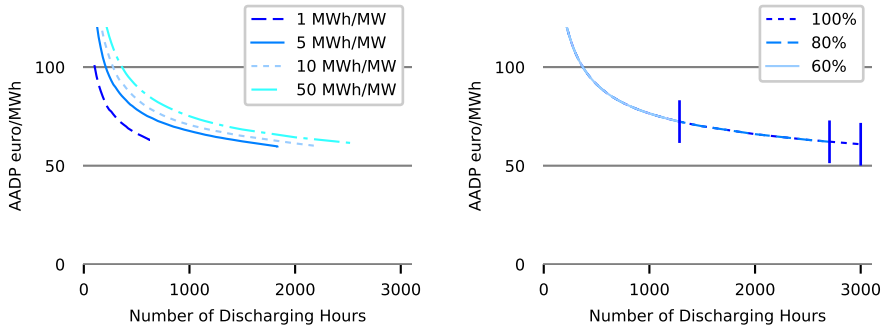


Figure 3.6: The *available average discharge price (AADP)* for a storage unit with parameters as presented in Table 3.1 for occurring prices at the Belgian day-ahead electricity market in 2015. In the left panel, the AADP is presented as a function of the number of discharging hours (NDH) for different energy-to-power (E/P) ratios. In the right panel, the AADP is presented for different round-trip efficiencies and an unlimited E/P ratio.

A comparison of the *available average discharge price (AADP)* and the *required average discharge price (RADP)* is illustrated in Figure 3.7 for different amounts of discharged electricity and for Belgian Day Ahead electricity prices of 2015. In Figure 3.7, the AADP is compared to the RADP whereby the latter is not calculated with a constant and thus average charging cost, but with the available average charging cost obtained from the optimization result which was used to calculate the AADP. The RADP shows a decreasing trend for an increasing number of discharging hours (NDH) which could be anticipated from Figure 3.3 as elaborated before, where a given constant charging price was applied. However, this trend in Figure 3.7 cannot be generalized since an increasing RADP for an increasing NDH could occur as the result of an increasing average charging cost. After all, recall that the *average charging cost (ACC)* used in the RADP calculation was based on the *average charging cost (ACC)* obtained from the AADP calculation and hence increases for increasing NDH. This increase in ACC counters the decrease in fixed costs per unit of discharged electricity.

Depending on which of both effects is strongest, the RADP could show an increasing or decreasing trend for increasing NDH.

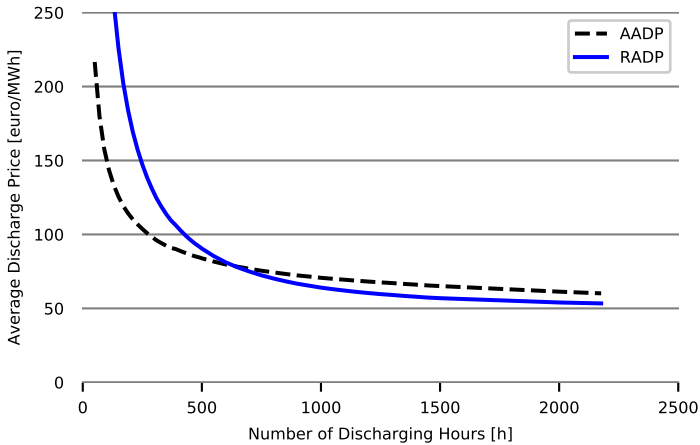


Figure 3.7: Comparison of the *available average discharge price (AADP)* and *required average discharge price (RADP)*. The RADP is calculated with an average charging costs (ACC) obtained from the historical profile used to calculate the AADP. The AADP is calculated for a storage unit with an E/P ratio of 10h.

Note that the intersection between the RADP and the AADP on Figure 3.7 indicates the exact amount of electricity that needs to be discharged, expressed as a number of discharging hours at full power capacity, for the storage owner to break even the full investment cost. However, the same conclusion cannot be drawn if the RADP curve had been calculated using an a priori given, or actually ‘estimated’, ACC. In such case, the intersection point would only give an indication of the break-even point. Therefore an accurate estimation of the ACC, compatible with the optimization procedure for charging and discharging, has to be made in order to compare the RADP to the AADP.

3.5.2 Available average price spread (AAPS)

The *available average price spread (AAPS)* is defined as the difference between the *available average discharge price (AADP)* and the *average charging cost*

(ACC) as expressed in Eq. (3.18):

$$\begin{aligned}
 AAPS &= AADP - ACC \\
 &= \frac{\sum_t DR_t \cdot (1+r)^{-t}}{\sum_t MWh_t^d (1+r)^{-t}} - \frac{\sum_t TCC_t \cdot (1+r)^{-t}}{\sum_t MWh_t^c (1+r)^{-t}} \quad (3.18)
 \end{aligned}$$

Figure 3.8 shows the AAPS for different E/P ratios in the left panel and for different round-trip efficiencies in the right panel. Similar to the AADP, a small E/P-ratio leads to a decrease in the number of hours where arbitrage is profitable and thus a decrease in the AAPS. The decrease of the AAPS with NDH is stronger than the decrease of AADP as not only the average available discharge price decreases, but also the average charging cost increases with increasing NDH. The right panel shows the AAPS for different efficiencies between 60% and 100% while assuming the E/P-ratio to be unlimited. It is clear that the AAPS depends, albeit slightly, on the round-trip efficiency, as opposed to the AADP. This dependency of AAPS on the efficiency is due to an increase in the *average charging cost* (ACC). When the round-trip efficiency decreases, more electricity will have to be charged to maintain a certain amount of discharged electricity. To charge more electricity, the storage operator will be forced to charge also during hours with higher electricity prices, leading to an increase in both the total charging cost and the average charging cost and hence decreasing the AAPS for a decreasing efficiency. Although the hours during which the storage operator will discharge remain the same, and thus the AADP remains equal, the AAPS will decrease as the ACC increases.

A comparison of the *available average price spread* ($AAPS$) and the *required average price spread* ($RAPS$) is illustrated in Figure 3.9. The $RAPS$ curve is monotonically decreasing for an increasing NDH. It was shown before in Figure 3.1 that the $RAPS$ is less sensitive to a change in ACC than the $RADP$ as the $RAPS$ does not account for the full cost of charged electricity but only for the cost of electricity charged to compensate for efficiency losses. Therefore, in this example, the impact of an increasing ACC is lower in magnitude than the decrease in fixed costs per unit of discharged electricity and hence the trend is monotonically decreasing.

Note again that the intersection between $AAPS$ and $RAPS$ on Figure 3.9 indicates the exact break-even point. When an a priori prescribed ACC would be used, the intersection point only indicates the estimated break-even point.

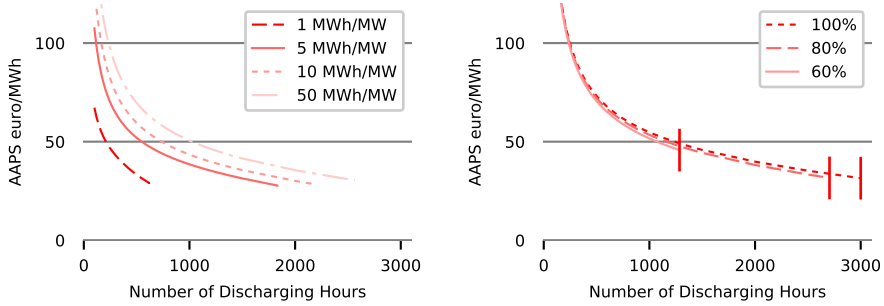


Figure 3.8: The *available average price spread (AAPS)* for a storage unit with parameters as presented in Table 3.1 for occurring prices at the Belgian day-ahead electricity market in 2015. In the left panel, the AAPS is presented as a function of the number of discharging hours (NDH) for different energy-to-power (E/P) ratios. In the right panel, the AAPS is presented as a function of the NDH for different round-trip efficiencies and an unlimited E/P ratio.

3.5.3 Available average operational profit (AAOP)

The *available average operational profit (AAOP)* is expressed in Eq. (3.19). It is equal to the total revenue from discharged electricity minus the total cost of charged electricity, averaged over the total amount of discharged electricity:

$$AAOP = \frac{\sum_t (DR_t - TCC_t) \cdot (1 + r)^{-t}}{\sum_t MWh_t^d (1 + r)^{-t}} \tag{3.19}$$

Figure 3.10 shows the AAOP as a function of the number of discharging hours (NDH) for different E/P-ratios and for different round-trip efficiencies in the left hand side and right hand side panels, respectively. Similar to the analysis in the previous sections, the left panel shows that a decrease in E/P-ratio decreases the AAOP. As before, a small E/P-ratio may cause the storage unit to be empty/full during many consecutive hours with high/low prices and thus prevent the storage operator to capture certain arbitrage opportunities. This in turn leads to a lower *available average operational profit (AAOP)*. The right panel shows that the AAOP decreases for a decreasing round-trip efficiency. A similar trend was observed for the AAPS, where it was already mentioned that a decreasing efficiency leads to increased amount of electricity that needs to be charged in order to discharge a fixed amount of electricity. The electricity needed to compensate for the extra efficiency losses will be charged during hours

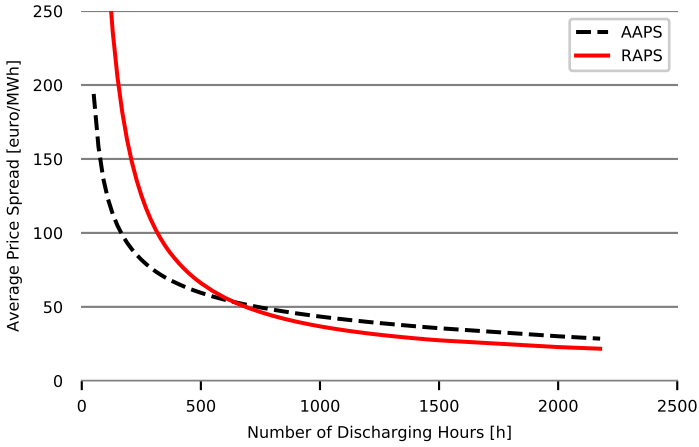


Figure 3.9: Comparison of the *available average price spread (AAPS)* and *required average price spread (RAPS)*. The RAPS is calculated with an average charging costs (ACC) obtained from the historical profile used to calculate the AAPS. The AAPS is calculated for a storage unit with an E/P ratio of 10h.

with higher electricity prices. It thus increases the average charging cost and in turn decreases the *available average operational profit (AAOP)*. Note that a change in round-trip efficiency leads to a change in AAOP which is greater in magnitude than the change in AAPS, which can be understood by comparing Eqs. (3.18) and (3.19).

A comparison of the AAOP and RAOP is shown in Figure 3.11. The intersection between the RAOP and the AAOP indicates the number of discharging hours at full power capacity needed for the storage owner to break even the full investment cost. Note that the RAOP is independent of the *average charging cost (ACC)* and hence the intersection between RAOP and AAOP always indicates the exact break-even point.

3.6 Discussion of the results

By comparing a *required* cost metric to the corresponding *available* cost metric, an investor can assess the profitability of a certain storage unit. When the required cost metric is lower than the available cost metric, it is profitable for the storage owner to invest in the storage unit. The amount of discharged electricity necessary to break-even the investment, is provided by the intersection of the

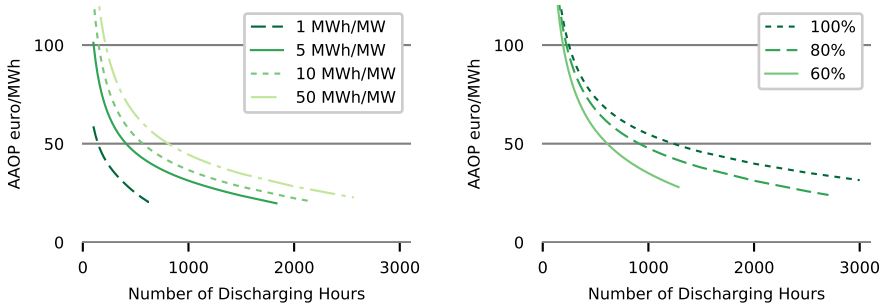


Figure 3.10: The *available average operational profit (AAOP)* for a storage unit with parameters as presented in Table 3.1 for occurring prices at the Belgian day-ahead electricity market in 2015. In the left panel, the AAOP is presented as a function of the number of discharging hours (NDH) for different energy-to-power (E/P) ratios. In the right panel, the AAOP is presented for different round-trip efficiencies with an unlimited E/P ratio.

required and available cost metrics. As noted before, this intersection provides the exact break-even point, when the *average charging cost (ACC)* used to calculate the required cost metric is based on the actually available average charging cost. If a certain given ACC would be used which usually differs from the actually available ACC, the intersection between two metrics provides only an estimation of the break-even point.

Figure 3.12 presents a comparison between the three required cost metrics and their corresponding available cost metrics. The actually available ACC is used for this figure, so the break-even point is equal for all three cost metrics.

As indicated before, the *required average operational profit (RAOP)* is independent of the charging cost. It is therefore not necessary to assume a charging cost ex-ante to calculate the RAOP as a function of the expected number of discharging hours. This way, the profitability of a storage unit for the investor can be estimated without calculating an available average charging cost. It is therefore possible to compare only one RAOP to the AAOP based on different historical price profiles. This is an advantage of the RAOP compared to the RADP and RAPS; it is therefore recommended to use the RAOP. For this reason, the remaining of this section focuses on the operational profits only.

To obtain a better understanding of the effect of changing storage technology parameters on the comparison between the available and required operational

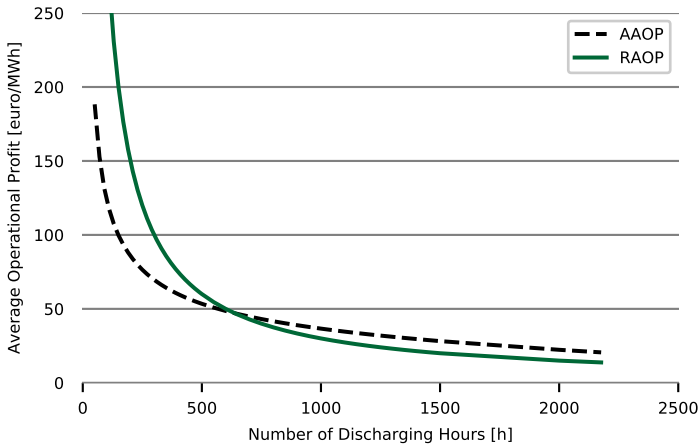


Figure 3.11: Comparison of the *available average operational profit (AAOP)* and *required average operational profit (RAOP)*. The AAOP is calculated for a storage unit with an E/P ratio of 10h.

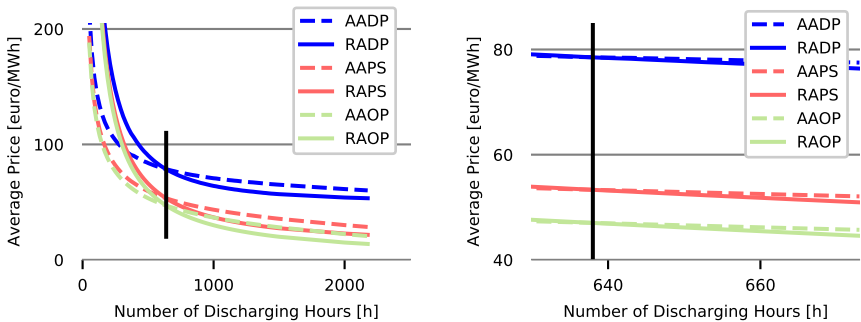


Figure 3.12: Comparison of the three available and the three required cost metrics, with a close-up on the intersection between required and available metrics in the right panel. The required cost metric is calculated using the average charging cost obtained from the calculation of the available cost metric. The available prices are calculated for a storage unit with an E/P ratio of 10h.

profit, some sensitivity analyses are presented next. From previous sections it became clear that the RAOP depends on the total fixed cost and on the number of discharging hours (NDH). The first analysis presented therefore consists of

various RAOP curves as a function of the NDH for different fixed costs. This is shown in Figure 3.13, where the AAOP, calculated based on historical prices from 2015 as before, is compared to different RAOP curves. Depending on the height of the fixed costs, the storage unit becomes profitable above a certain number of discharging hours, in this example for fixed costs of 10,000 euro and for 30,000 euro. However, when the fixed costs are too high, a storage investor will not be able to break even his investment cost by temporal arbitrage on an electricity market with prices similar to those on the Belgian Day Ahead market in 2015, in this example for fixed costs of 50,000 euro and 100,000 euro. Remark that the AAOP and all the RAOP curves stop at 2177 discharging hours since there is no more arbitrage opportunity, and it is hence economically not favorable, to operate the storage for more than this number of discharging hours.

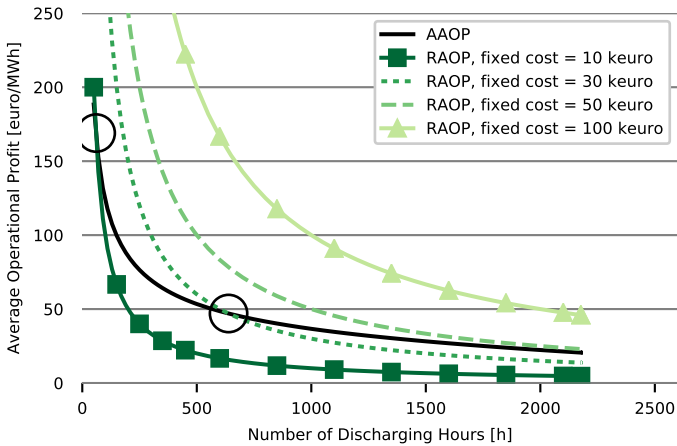


Figure 3.13: Comparison of the *available average operational profit (AAOP)* and *required average operational profit (RAOP)* for different capital cost values. The AAOP is based on Belgian day-ahead electricity prices in 2015 and is calculated for a storage unit with an E/P-ratio of 10h.

Note that current sodium sulfur batteries, for which the E/P-ratio of 10h as used in Figure 3.13 is representative, would have a fixed cost between 3,000,000 and 4,000,000 euro for 1 MW of installed power capacity [19]. A calculated RAOP for this storage technology would thus be so high that it would lay outside Figure 3.13. It is hence not profitable to install such batteries at those prices for energy arbitrage only on the Belgian Day Ahead electricity market in 2015.

In the following sensitivity exercise, the number of discharging hours and energy-to-power ratio is varied, all parameters influencing the AAOP. Figure 3.14 presents a comparison of the RAOP to the AAOP calculated based on the historical prices occurring on the Belgian Day Ahead electricity market from different years. Although all AAOP curves differ slightly, they are of the same order of magnitude, especially for a higher number of discharging hours. In the left panel, the AAOP curves are calculated for a storage technology with an energy-to-power (E/P) ratio of 10 MWh/MW. The AAOP curves on the right figure are calculated for a storage technology with an unlimited E/P ratio. The difference between the left and right panel shows that the E/P ratio has a considerable impact on the AAOP and profitability of a storage unit.

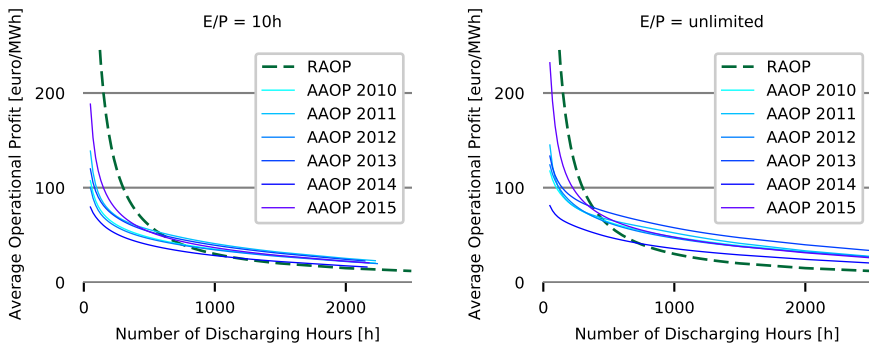


Figure 3.14: In solid lines, the *available average operational profit (AAOP)* for a storage unit with parameters as presented in Table 3.1 for occurring prices at the Belgian day-ahead market in the years 2010-2015. The *required average operational profit (RAOP)* is drawn as a dashed curve. In the left panel, the AAOP is presented as a function of the number of discharging hours (NDH) for an energy-to-power ratio of 10 MWh/MW. In the right panel, the AAOP is presented for an unlimited energy-to-power ratio. The round-trip efficiency equals 80% in both panels.

As a last sensitivity exercise, the AAOP is calculated for different values of the round-trip efficiency. Figure 3.15 presents on the left hand side panel a comparison between the RAOP and the AAOP of different historical price profiles for a storage unit with a round-trip efficiency of 60%. The right hand side panel shows the same curves for a storage technology with a round-trip efficiency of 80%. Recall from section 3.4.2 that the RAOP is independent of the round-trip efficiency but the efficiency does have an influence on both the magnitude of the AAOP and on the amount of electricity for which it is

profitable for the storage investor to arbitrage on the electricity market, as expressed by the attainable NDH and as shown in Figure 3.10 before.

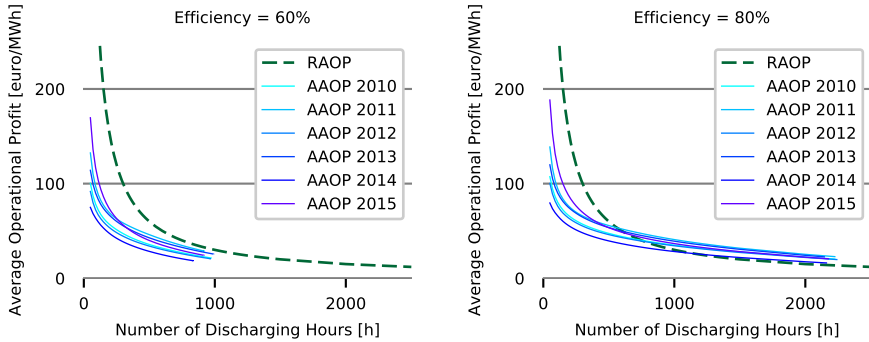


Figure 3.15: In solid lines, the *available average operational profit (AAOP)* for a storage unit with parameters as presented in Table 3.1 for occurring prices at the Belgian day-ahead market in the years 2010-2015. The *required average operational profit (RAOP)* is drawn as a dashed curve. In the left panel, the AAOP is presented as a function of the number of discharging hours (NDH) for an efficiency of 60%. In the right panel, the AAOP is presented for an efficiency of 80%. The E/P ratio used in both panels is 10h. The right panel is identical to the left panel of Figure 3.14.

3.7 Summary and conclusions

Since the increasing share of intermittent renewable energy sources leads to a growing interest in storage capacity, there is a need for simple economic tools which facilitate comparing different storage technologies in order to assess whether an investment in a certain storage unit is worthwhile in a particular market. In this chapter, three new cost metrics have been presented and analyzed which are inspired by the well-known levelized cost of electricity (LCOE). The presented metrics differ in the share of variable costs that is explicitly accounted for. A first metric, the *required average discharge price (RADP)*, covers the full cost of the stored electricity in order for the investor to break-even the investment, including a certain rate of return. The *required average price spread (RAPS)*, a second metric, is equal to the difference between the required average discharge price and the average price at which input electricity is charged. It thus takes into account the fixed costs and the cost due to efficiency losses.

A last metric is the *required average operational profit (RAOP)* which is the average profit an investor should make from arbitrage in order to finance the investment cost and a certain rate of return. This last metric only accounts for recovery of the fixed costs.

Analysis of the three metrics shows that for an increasing *average charging cost (ACC)*, the RADP and RAPS increase, while the RAOP stays constant. Furthermore, when the ACC is exactly zero, or is neglected, care should be taken as this implicitly means that the storage efficiency is not accounted for. All three measures become equal in such case. An increase in the round-trip efficiency leads to a decrease in both the RADP and the RAPS but has again no influence on the RAOP. An increasing number of discharging hours, which is representative for the amount of discharged electricity, leads to a decrease which is equal in magnitude for all three metrics.

Two simple examples show, however, that the energy capacity is not explicitly accounted for in the calculation of the cost metrics. Moreover, it is difficult to evaluate the impact of a small energy capacity on the number of discharging hours and the average price at which electricity can be charged. It is therefore necessary to use the levelized cost metrics in combination with the analysis of entire historical price profiles. Examples were used to show that the RAOP is the most transparent cost metric to use as it is independent of the charging cost and can therefore easily be compared to analyze historical price profiles of different years without having to change the assumption for the average charging cost. Price profile analyses in this work are made under the assumption of perfect foresight for the storage operator. Incorporating uncertainty related to non-perfect price foresight and exploring different operational strategies, by e.g., setting price thresholds for an upper charging price and a lower discharging price, might be examined in future research.

Chapter 4

Identification of the need for long-term electricity storage

This chapter contains elements from:

Belderbos, A., Delarue, E. and D'haeseleer, W. *Possible role of Power-to-Gas in future energy systems*. European Energy Markets Conference (EEM), May 2015, Lisbon.

Belderbos, A., Delarue, E. and D'haeseleer, W. *Critical factors shaping the need for long-term energy storage via power-to-gas*. TME working paper.

This chapter studies the possible role of power-to-gas for electrical energy storage in future energy systems driven by intermittent renewable energy sources. For this reason, an investment model has been built which optimizes the generation and storage portfolio in an electrical energy system while complying with imposed environmental constraints. A broad range of possible cases is studied by varying many technical, economic and environmental parameters.

The chapter starts with an introduction, followed by a discussion on the sustainability of synthetic fuels when used for renewable energy storage in Section 4.2. The research methodology and the developed energy system investment model are presented in Section 4.3. Next, Section 4.4 provides the case study parameters. The results of the different case studies are presented in Sections 4.5 and 4.6, the former considering the electrical energy system while the latter accounts for both the electrical energy and hydrogen system. Section 4.7 finalizes this chapter with a summary and conclusions.

4.1 Introduction

The global awareness of climate change and the corresponding tendency to move towards more sustainable energy systems comprising large shares of iRES generation capacity, drives the need for more flexibility in the electric power system, as discussed in the introduction of this dissertation. The flexibility is required to keep the necessary balance between instantaneous electrical power supply and load and can be provided by different technologies which are currently available: dynamic operation of conventional generation, the electricity grid, energy storage, demand response and curtailment of the intermittent energy sources. Each of these flexibility options has important advantages and disadvantages in terms of cost and efficiency. In this chapter, the amount of cost-optimal installed power-to-gas (P2G) capacity for long-term energy storage in comparison to other flexibility options is studied.

To study the possible role of power-to-gas (P2G) in future high iRES electric energy systems, an electric energy system investment model is developed to optimize the electricity generation and storage portfolio for a given electrical load and iRES generation profile. Some studies investigating the value of P2G already exist. Vandewalle et al. [60] examine the effect of large scale P2G deployment on the interactions between the electric power, gas and CO₂ sectors and its effect on the gas market price. Jentsch et al. [61] study the economic optimal P2G capacity in an 85% iRES scenario. The study presented by van Stiphout [62] uses an elaborate investment model to determine the cost optimal P2G capacity for a limited number of cases in the absence of a CO₂ cost. Blanco et al. [63] use the TIMES model to investigate the optimal P2G capacity in different energy systems on a European scale. They consider energy systems under different CO₂ reduction targets, availability of CCS, biomass, nuclear and coal fired power plants, for different potentials of iRES and geothermal energy, for different P2G characteristics, possible inclusion of the mobility sector and different tax and subsidy schemes. The study presented by Blanco et al. is the most complete study presently available in the literature.

The study presented in this chapter adds to the literature by investigating many different system parameters complementary to the ones investigated by Blanco et al. The amount of cost-optimal installed P2G capacity will be investigated for different imposed shares of RES generation, for different CO₂ emission prices, different iRES mixes and different storage costs. In addition to this, the effect of CO₂ sequestration, P2G, battery and curtailment availability and the possible occurrence of a cold spell on the amount of optimally installed P2G is investigated. Once a thorough understanding of drivers to install P2G in the energy system is obtained, the system is enlarged to incorporate the hydrogen industry where hydrogen is traditionally produced by steam methane

reformer (SMR) and used as a feedstock for the production of chemicals. This way, possible beneficial interactions between the energy and hydrogen sector can be understood. During discussion of the cases, they will be compared to results obtained in the literature. In contrast to the study presented by Blanco et al. [63], the model used here contains less detail and a smaller scope (i.e. only the electricity system and hydrogen load are considered). Before discussing the technical details of the model used in this study, the sustainability of P2G itself is briefly touched upon.

4.2 Sustainability of synthetic fuels

Power-to-gas may be an interesting energy storage technology to cope with the situation of massive iRES injection into the system. In such context, it is instructive to investigate whether the produced methane is carbon neutral or not. To determine whether P2G is a carbon neutral technology, it is necessary to (i) define the notion of carbon neutrality and (ii) look at how the methane is produced.

In this dissertation, energy is regarded as carbon neutral if no carbon is emitted to the environment when the energy is converted from one form to another. Therefore, two conditions should be met. First, the electrical power used in the synthetic methane production process needs to be carbon neutral. Second, the CO₂ produced when using the synthetic methane should be recycled to produce new methane or should be captured and stored.

As an example, two cases are examined and illustrated in Figure 4.1. CO₂ is obtained from a carbon capture plant in both cases. In the first case, the synthetic methane is used in a gas-fired power plant (GFPP) with carbon capture (CC), resulting in a closed carbon loop for the part of CO₂ which is effectively captured.¹ In the second case, the methane is used in a GFPP without CC. As CO₂ is in this second case emitted to the environment, the synthetic methane is not carbon-neutral and hence the stored electrical energy cannot be regarded as renewable.

¹Since capture units do not capture 100% of the CO₂ from flue gases, not all CO₂ is part of a closed carbon loop. To simplify matters we will, however, assume a capture rate of 100% CO₂ from flue gases in the remainder of this thesis.

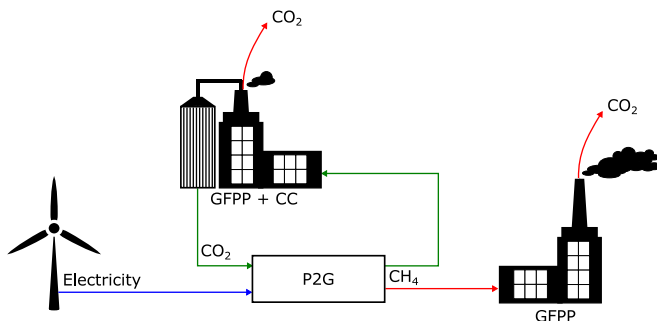


Figure 4.1: A sustainable (closed) carbon cycle and non-sustainable (open) carbon cycle. Note that since capture units do not capture 100% of the CO₂ from flue gases, not all methane used in the GFPP with CC is part of the closed carbon loop

4.3 Methodology

A methodologically oriented energy system investment model is developed to investigate the optimally installed amount of P2G in future energy systems. This model is a linear program which optimizes the electricity generation and storage portfolio to serve a given electrical power demand at lowest cost while meeting imposed environmental constraints (RES target). In principle, the TIMES model used by Blanco et al. [63] or the investment model presented by van Stiphout [62] could be used for this study; however, we have opted to develop a model specifically for this study with the particular aim to be very transparent so as to well understand the behavior of the system in response to parameter changes. In this model only the electric power, gas, carbon and hydrogen sectors are considered and the technical detail is deliberately kept low. In comparison to the other models previously mentioned with larger scope or higher technical detail, the model presented in this chapter considers a higher temporal detail and longer optimization horizon without inflating the computational cost beyond acceptable levels. Such long time horizons are especially useful to study long-term, seasonal, storage. A visual overview of the model is given in 4.2.

The P2G unit is considered as two separate units, electrolyzer and methanizer with intermediate hydrogen buffer. Similarly, the hydrogen system, with hydrogen storage, demand and steam methane reformer, are only incorporated in some cases of this study. This will be clearly indicated for each case throughout the discussion of the results. The most important aspects of the model will be discussed next, while a detailed description and model formulation is provided

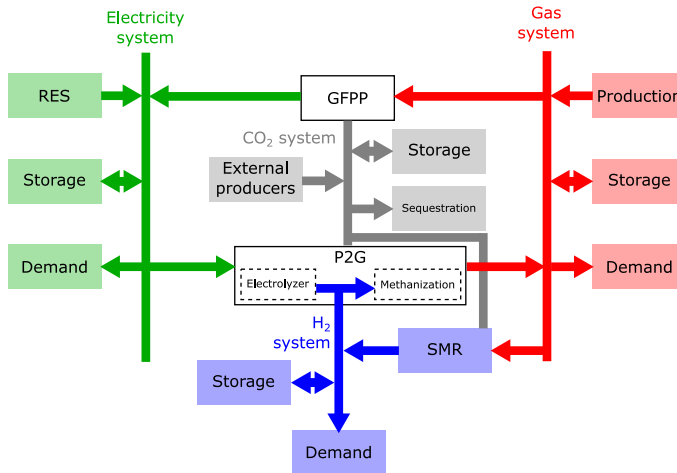


Figure 4.2: overview of the different energy systems accounted for in the investment model. RES = renewable energy source, GFPP = gas-fired power plant, SMR = steam methane reformer.

in Appendix C.

The model objective is to minimize total system cost which is equal to the cost of all installed electricity generation, storage and carbon capture capacity, fixed operation and maintenance (O&M) cost and the variable O&M cost, represented by the cost of consumed natural gas and the cost of emitted and sequestered CO₂. This is formulated in the equation below, with C the cost per unit of capacity for each technology and \bar{p} the installed capacity per technology (both with appropriate sub- and superscripts). “*res*” denotes renewable energy sources with i the type of iRES generation (solar, onshore wind and offshore wind), “*pp*” conventional power plants, “*cc*” carbon capture technology, “*ely*” electrolyzer capacity, “*met*” stands for methanizer, “*smr*” for steam methane reformer, “*bat*” for battery, “*NG*” for natural gas, with q_{NG} the total amount of consumed natural gas, “*SM*” stands for synthetic methane with \bar{e} the installed storage size. “*hs*” stands for hydrogen storage, CO₂ for carbon dioxide, “*em*” for emission and “*seq*” for sequestration with \dot{k} the amount of CO₂ emitted or sequestered per time step t .

$$\begin{aligned}
Cost = & \sum_i C_i^{res} \bar{p}_i^{res} + C_{pp} \bar{p}_{pp} + C_{cc}^{pp} \bar{p}_{cc}^{pp} + C_{ely} \bar{p}_{ely} + C_{met} \bar{p}_{met} + C_{smr} \bar{p}_{smr} \\
& + C_{cc}^{smr} \bar{p}_{cc}^{smr} + C_{bat} \bar{p}_{bat} + C_{NG} q_{NG} + C_{gs} \bar{e}_{SM} + C_{hs} \bar{e}_{hs} \\
& + C_{CO2}^{em} \sum_t \dot{k}_t^{em} + C_{CO2}^{seq} \sum_t \dot{k}_t^{seq} \tag{4.1}
\end{aligned}$$

In this model, three types of constraints are imposed: environmental constraints, technical constraints on the system level and technical constraints on the unit level. The imposed environmental constraint is a minimum share of consumed electrical energy which should originate from renewable sources. For implementation convenience, the environmental constraint is expressed as maximum share of the electricity which may originate from fossil sources as expressed in the following formula, with $\dot{f}_t^{pp,NG}$ the fossil fuel consumption in power plants, η_{pp} the power plant efficiency, $R\%$ the imposed share of renewables and \dot{E}_t^l the instantaneous electrical load per time step t .

$$\sum_t \dot{f}_t^{pp,NG} \eta_{pp} \leq (1 - R\%) \sum_t \dot{E}_t^l \quad \forall t \tag{4.2}$$

When the hydrogen system is accounted for, it is also subject to the same imposed environmental constraint.

Possible revenue from selling the separated oxygen O_2 is not accounted for in the model. That could be an extra income as explained by Vandewalle et al. [60].

In this model, a balancing constraint is imposed on the system level, assuring that the instantaneous electrical load and instantaneous electrical power generation are equal at all times. Electricity is generated by iRES and gas fired power plants (combined cycle gas turbines) fueled with synthetic methane or natural gas. Electricity can be stored indirectly as synthetic methane by P2G with the idea to reconvert the methane to electricity using gas fired power plants, in batteries or by pumped hydro storage. When the hydrogen load from industry is taken into account, this hydrogen can be produced electrically with an electrolyzer or from methane through the steam methane reforming process. When electrolyzer and methanizer are modeled as two separate units, hydrogen can be stored to match the time of production and consumption.

On a unit level, conversion efficiencies are incorporated in the model and, if applicable, CO₂ production and capture rates. For each technology, the maximum production or storage level is bound by the installed capacity.

No dynamic operational constraints, electricity grids, nor gas grids are taken into account. This means that there is no cross-border electrical power exchange with neighboring countries. The electric power system model is thus a point model or, equivalently, a copper plate model. (And similarly, for the natural gas grid/system.)

The most important decision variables are the amount of installed generation or storage capacity and the hourly generation or charging/discharging per technology. The time horizon of the model is 1 year, with hourly resolution.

As said above, the detailed model description is presented in Appendix C. The following section presents the data used in the different case studies.

4.4 Case data

The Belgian electrical load and iRES generation profiles are used as a test case to quantitatively address the opportunities for P2G. Load data of the Belgian electric power system from 2015 are obtained from the Belgian transmission system operator (TSO) [64]. Renewable generation profiles are obtained separately (solar, onshore and offshore wind) from the TSO and are normalized to a maximum magnitude of 1 and scaled according to the installed capacity. Note that only one meteorological year (2015) is used in this chapter. Employing multiple years of meteorological data would alter the results, however, the sensitivity analysis presented in Section 4.5.5 (different iRES mixes) and the results presented in Chapter 5 (using three years of meteorological data) suggest that the results only change slightly. Considering a cold-spell or other extreme weather events would most likely increase the need for flexibility, like installed storage capacities, compared to the results presented here.

In the reference case, no pre-installed generation portfolio (of any kind) is assumed, investments are only allowed for gas fired generation and iRES technologies. For storage, no pre-installed capacity is assumed except for the existing pumped hydro storage (PHS). Further storage investments are only allowed for batteries and P2G, but not for PHS.

The cost characteristics of all conversion, storage and carbon capture technologies are shown in Table 4.1 [65, 28, 66, 67, 68]. The cost data for P2G is based on the review presented in Chapter 2. All cost are assumed to reflect current

(2018) average technology costs. Since pumped hydro storage is assumed to be pre-installed, it has no additional cost.

An equivalent annual cost (EAC) is used to express the annual fixed costs of each technology. This EAC is not related to the levelized cost of electricity (LCOE) or levelized cost of storage (LCOS), which account for all costs, including variable and fuel costs and are expressed on a per energy generated or energy stored basis, as defined in Chapter 3. Rather, this EAC considers only the fixed costs and expresses these costs on an annual basis, independent of the actual operation time. The equivalent annual cost, expression the fixed cost on an annual basis is used since the optimization only has an optimization horizon of 1 year. If the overnight construction cost (OCC) would be used rather than the EAC, the different economic lifetime of each technology would be neglected. In such case, technologies with a long economic lifetime and high OCC would be treated disadvantageously compared to technologies with a shorter economic lifetime and lower OCC.

Table 4.1: Cost characteristics used in the reference case (OCC = Overnight construction cost, DR = Discount rate, EAC = Equivalent annual cost, GFPP = Gas fired power plant characteristics based on combine cycle gas turbines, CC = Carbon capture)

	OCC	Lifetime	DR ^a	O&M ^b	EAC
	€/kW _e	Year	%	%	€/(y · kW _e)
Battery	1500	12	5	1	184.24
CC unit for GFPP ^c	900	20	5	3.5	103.72
GFPP	1000	20	5	3.5	115.24
Onshore wind	1700	20	5	1.5	161.91
Offshore wind	4900	20	7.5	3.5	652.15
Solar PV	1600	20	5	1	144.39
Electrolyzer	550	20	7.5	2	64.95
	€/kW _{CH₄}	Year	%	%	€/(y · kW _{CH₄})
CC unit for SMR	640	25	5	2	55.00
SMR	710	25	5	2	61.03
Methanizer	1800	20	7.5	2	212.57
	€/kWh _{H₂}	Year	%	%	€/(y · kWh _{H₂})
Hydrogen storage	5	20	5	2	0.50

^a Discount rates are risk-adjusted

^b O&M as percentage of overnight construction cost

^c Costs for the carbon capture (CC) unit do not include costs for the GFPP itself, the CC unit should be installed separately

The cost characteristics for natural gas and CO₂ used in the reference case are given in Table 4.2.

Table 4.2: Cost characteristics of natural gas and CO₂ used in the reference case.

Cost	Unit	Value
Natural gas	€/MWh _{CH₄}	30
CO ₂ emission	€/ton	50
CO ₂ sequestration	€/ton	0

The storage and conversion efficiencies of all technologies are given in Table 4.3. The batteries have an energy-to-power ratio of 7.2 kWh/kW, which is typical for grid scale NaS batteries [66]. For pumped hydro storage (PHS), it is assumed that a storage unit with 8000 MWh_e electrical energy and 1000 MW_e electrical power capacity is initially available, inspired on the Belgian PHS in Coe. Note that although most cases are started from a greenfield (i.e. no pre-installed capacity is installed), there is always some pre-installed PHS capacity assumed.

Table 4.3: Storage and conversion efficiencies

	Efficiency	Energy-to-power ratio	Initial energy capacity	Initial power capacity
Battery	90% ^a	7.2 h		
PHS	85% ^a	8.0 h	8000 MWh _e	1000 MW _e
GFPP	55%			
Electrolyzer	75%			
Methanizer	70%			
SMR	80%			

^a Single trip

All carbon related technical characteristics are listed in Table 4.4. The energy cost per captured ton of CO₂ in gas fired power plants corresponds to a drop in GFPP efficiency of 15% or 8.25%pt. The energy cost per captured CO₂ in the steam methane reformer corresponds to a drop in efficiency of 6.25% or 5%pt.

The reference values for each parameter given in Table 4.1 - Table 4.4 will be varied in different cases. An overview of the parameters that will be varied and the possible value range is given in Table 4.5. During discussion of the results, it will be mentioned which parameter values are varied in each case. Note that for the cases which differ in yes-or-no ‘availability’ for certain technologies, the availability of P2G and batteries refers to the availability to

Table 4.4: CO₂-specific technical characteristics

Parameter	Symbol	Unit	Value
Carbon content per MWh methane released in GFPP	$\alpha_{CH_4 \rightarrow CO_2}^{pp}$	ton/ MWh_{CH_4}	0.2
Carbon content per MWh methane released in SMR	$\alpha_{CH_4 \rightarrow CO_2}^{smr}$	ton/ MWh_{CH_4}	0.1828
Electricity “consumed” to capture 1 ton of CO ₂ from GFPP exhaust	χ_{cc}^{pp}	MWh_e /ton	0.4125
Methane “consumed” to capture 1 ton of CO ₂ from SMR	χ_{cc}^{smr}	MWh_{CH_4} /ton	0.3419
Maximum capture rate	\bar{K}	-	1

Table 4.5: Parameter values which will be varied in different cases, reference values emphasized in bold.

Parameter	Unit	Alternative values
RES share	%	30 – 50 – 70 – 80 – 90 – 99 ^a
CO ₂ emission price	€/ton	50 – 100 – 500 – 1000 – 2000
Capacity legacy	-	Yes – No
Battery cost	€/kW _e y	37 – 92 – 184 – 369 – 921
Electrolyzer cost	€/kW _e y	13 – 33 – 65 – 130 – 325
Methanizer cost	€/kW _{CH₄} y	43 – 106 – 213 – 425 – 1063
Sequestration availability	-	Yes – No
P2G availability	-	Yes – No
Battery availability	-	Yes – No
Curtailement availability	-	Yes – No
Cold spell considered	-	No – Every 3 years - Yearly
Hydrogen load considered	-	Yes – No
Minimum SMR share	%	0 – 75
		Onshore Offshore Solar PV
		12 % 22 % 66 %
Share of iRES technology in iRES mix		33.33 % 33.33 % 33.33 %
		No imposed constraints

^a Note that not a 100% RES case is investigated but a 99% RES case. This is done since a 100% RES case often causes numerical problems to compute, which a 99% case does not. Furthermore, the results observed for a 99% RES case are also valid for the 100% RES case, given the limited amount of technical detail accounted for in this study.

install these technologies and, since the cases are started from a greenfield, also the availability to operate these technologies. For curtailment and CO₂ sequestration, ‘availability’ refers to whether it is allowed to curtail iRES and sequester CO₂ (‘available’) or not (‘unavailable’), respectively.

4.5 Results and discussion

The different case studies will be presented and discussed in this section. Before deep-diving in each of the case studies, some main trends of the results are discussed first, to present a general overview.

The results of different case studies show that for ‘standard parameters’, P2G capacity only becomes economic as energy storage technology for high imposed RES shares (expressed as a fraction of the electrical energy consumption per year), above 70%. Only in cases where no other storage technology would be available or the alternative storage technology would be very expensive, P2G becomes cost efficient to install for imposed RES shares starting from 50%. The specific composition of the iRES portfolio has no significant impact on these observations.

A similar, but opposed, observation is made for the battery capacity, which increases significantly when P2G technology is unavailable or very expensive. In cases where iRES curtailment is not allowed, both battery and P2G capacity increase to make sure all peaks of surplus iRES generation are stored.

Since gas-fired power plants are both used to serve the residual (peak) demand with conventional natural gas and as discharge technology for energy stored as synthetic methane, it is observed that a decrease in battery capacity usually leads to an increase of gas-fired power plant capacity and vice versa, while an increase in P2G capacity also leads to an increase in gas-fired power plant capacity and vice versa.

The effect of CO₂ sequestration availability depends on the height of the CO₂ emission price. If a low CO₂ emission price is imposed, the CO₂ sequestration availability has almost no effect on the installed storage and gas fired power plant capacities since otherwise sequestered CO₂ is now simply emitted at an increased (but still ‘tolerable’) cost. If, however, a very high CO₂ emission price is imposed (1000 €/ton and above), it is most economic for the electricity system to avoid the creation of additional CO₂ in the electric energy system through conventional natural gas. Hence, in such very high CO₂ penalty cases, large iRES, P2G and battery capacities are installed, more than required to meet the (minimally) imposed iRES share.

If an external hydrogen industry is taken into account, an exogenous hydrogen load is assumed which is subjected to the same imposed RES target as the electricity system. The hydrogen load can be served by a steam methane reformer (SMR) or an electrolyzer, the former by converting methane to hydrogen, the latter by electrically producing hydrogen from water (denoted as electric hydrogen). Note that fuel cells are not considered in this study. When the hydrogen industry is incorporated in the study boundary, an increase in electrolyzer capacity is observed while the effect on other installed capacities is usually minor. However, in cases where only a limited part of the instantaneous hydrogen load can be served (for whatever reason) directly by electric hydrogen from electrolyzers, then the only way to meet the imposed RES target is to produce electric hydrogen and convert it to synthetic methane, which can be reformed back to hydrogen using a steam methane reformer at a later instant. In such cases, also an increase in methanizer capacity is observed.

4.5.1 Reference case

In the so-called 'reference case', no pre-installed capacity is assumed (i.e., starting from a greenfield for each separate run of imposed RES-share requirement), except for the pre-installed PHS capacity. P2G (electrolyzer and methanizer), batteries, PHS, curtailment and CO₂ sequestration are all available. All reference capacity costs listed in Table 4.1 are used together with a CO₂ emission price of 50 €/ton. A RES share (in terms of electrical energy) of 30%, with a mix of 12% onshore, 22% offshore and 66% solar PV is imposed. No industrial hydrogen load is accounted for in this reference case.

Table 4.6 and Table 4.7 show the installed capacities per technology and the aggregated energy and carbon quantities in the reference case, respectively.

As can be seen from Table 4.6, a total of more than 20 GW_e of iRES capacity is installed to meet the required share of 30% electrical energy originating from RES. The remaining 70% of the electrical energy load is entirely covered by conventional natural gas. The residual electrical power load has a peak load of 13.42 GW_e , covered by 12.42 GW_e GFPP capacity and 1 GW_e PHS which is assumed pre-installed.² Besides the PHS, no additional storage technology is installed. For a RES share of 30%, only a few peaks in RES generation cannot be consumed instantaneously or stored in the existing PHS unit. Given the system under investigation, it is more economic to curtail these few peaks rather than to install additional storage capacity. This leads to a curtailment of 1.35% of the electrical energy originating from iRES, as shown in Table 4.7.

²The model does not install reserve capacities.

Table 4.6: Installed capacities in the reference case.

GFPP	12.42	GW_e
GFPP with carbon capture ^a	6.39	GW_e
Onshore wind	1.57	GW_e
Offshore wind	1.64	GW_e
Solar PV	17.0	GW_e
Battery	0	GW_e
Electrolyzer	0	GW_e
PHS	1	GW_e
Methanizer	0	GW_{CH_4}
Methane storage	0	TWh_{CH_4}
Hydrogen storage	0	TWh_{H_2}

^a 6.39 GW_e of the 12.42 GW_e is equipped with CC capacity. The power rating refers to the nominal output rating of the GFPP, without subtracting any electrical power sacrificed to operate the CC unit.

Table 4.7: Aggregated energy and carbon quantities in the reference case (per year).

Electrical energy load	87.03	TWh_e
GFPP net generation ^a	60.63	TWh_e
Onshore wind	3.22	TWh_e
Offshore wind	5.91	TWh_e
Solar PV	17.73	TWh_e
Curtailement	0.36	TWh_e
	1.35	% of RES
CO ₂ emitted	4.74	Mton
CO ₂ sequestered	17.41	Mton
CO ₂ used	0	Mton

^a the 'net' generation refers to the resulting GFPP generation, after subtracting the electrical power sacrificed to operate the CC unit.

4.5.2 Influence of the imposed RES share

If all hypotheses are kept as in the reference case (i.e., a CO₂ emission price of 50 €/ton, CO₂ sequestration available, battery and P2G storage available and curtailment allowed) and the imposed RES target is increased, it is shown in

Figure 4.3 that electrolyzer and methanizer technology become economic for RES shares higher than 70%. This is comparable with the results presented by Blanco et al. [63] who report P2G investments for RES shares above 60%. In the results presented by van Stiphout [62], investments in P2G technology start only for RES of 90% and higher. This last result could be explained by recognizing that van Stiphout not only considers intermittent renewable energy sources but also controllable RES capacity like biomass.

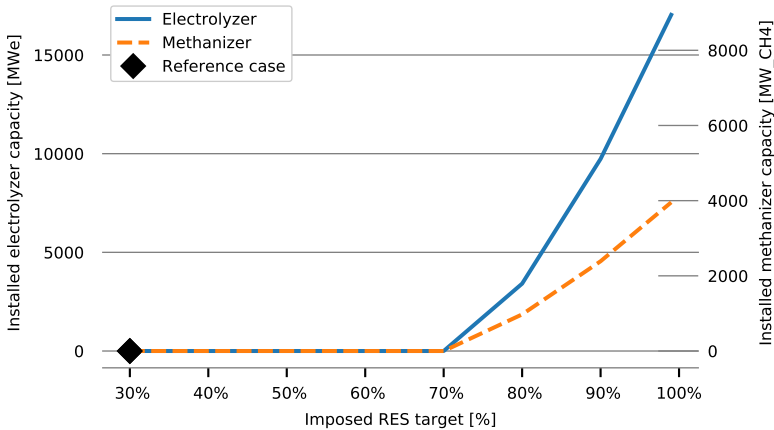


Figure 4.3: Installed electrolyzer capacity (left axis) and methanizer capacity (right axis) for increasing RES target, a CO_2 price of 50 €/ton; no capacity legacy between cases, batteries, CO_2 sequestration and curtailment available, iRES mix as in reference case.

Note that the left axis (electrolyzer capacity) and the right axis (methanizer capacity) of Figure 4.3 have different scales as they are expressed in different units. The electrolyzer capacity is expressed in MW_e , referring to its capacity to consume electricity, while the methanizer capacity is expressed in MW_{CH_4} referring to the flow of methane it can produce. The right axis (methanizer) is scaled such that if the electrolyzer would be connected directly with the methanizer, and no intermediate hydrogen storage would be possible, the curves would coincide on the graph.

Figure 4.3 shows furthermore that it is economically efficient to make use of intermediate hydrogen storage. A greater amount of electrolyzer capacity is installed to capture higher peaks in surplus iRES generation, while the intermediate hydrogen storage would then reduce the amount of required methanizer capacity and hence allow for more operating hours of that lower

installed methanizer capacity. The fully charged hydrogen storage unit could feed the methanizer between 44 hours and 65 hours at full load, the exact size of the storage depending on the case.

4.5.3 Influence of the CO₂ emission price

To investigate the influence of the CO₂ emission price on installed capacities, Figure 4.4 shows the electrolyzer and methanizer capacities for different imposed RES targets and CO₂ emission prices of 50, 100, 500, 1000 and 2000 €/ton. Battery technology, curtailment and CO₂ sequestration remain available as before.

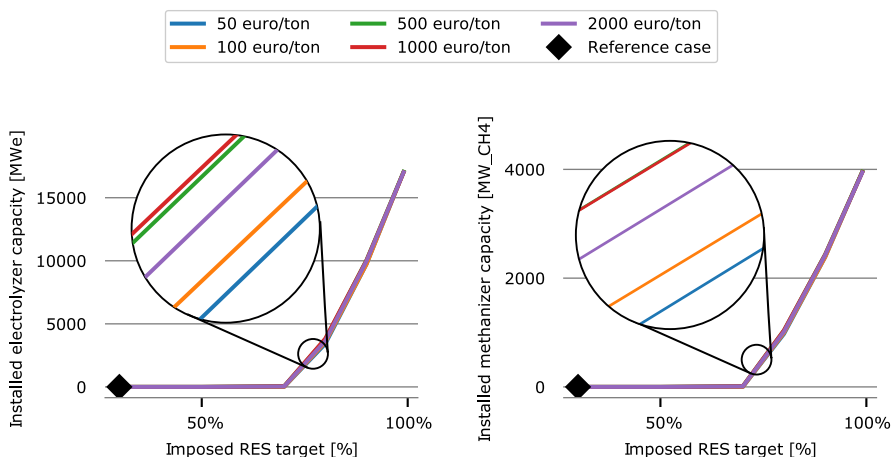


Figure 4.4: Installed electrolyzer capacity (left panel) and methanizer capacity (right panel) for increasing RES target and different CO₂ prices; no capacity legacy between cases; batteries, CO₂ sequestration and curtailment available; iRES mix as in reference case.

Figure 4.4 shows that a change in CO₂ emission price does not really lead to a noticeable change in installed electrolyzer and methanizer capacity. There is an effect, but it is effectively negligible.³ The reason that the CO₂ emission

³Notwithstanding the fact that the effect is very small, it is nevertheless interesting that the effect on electrolyzer and methanizer capacity (Figure 4.4) is not monotonic: higher CO₂ prices do not always lead to more installed capacities. A consequence of using a deterministic cost minimizing model without considering uncertainty is that each variation in cost parameters might trigger a variation in operational schedule and installed capacities, without necessarily having an important underlying physical cause. Therefore, this small change in results is not further elaborated.

price has almost no effect on the electrolyzer and methanizer capacities is that, because the CO₂ sequestration option is available, an increase in CO₂ emission price is not an incentive to install more renewable and storage capacity; a higher CO₂ cost is an incentive to install more carbon capture capacity and sequester more carbon, as shown in Figure 4.5. The slight change in installed P2G capacity that is observed, is predominantly the result of a change in GFPP operation. Indeed, when more GFPPs are equipped with CO₂ capture units and these CO₂ capture units are more frequently used, this leads to a change in operation of the GFPPs, and hence the optimal installed capacity of P2G and battery units.

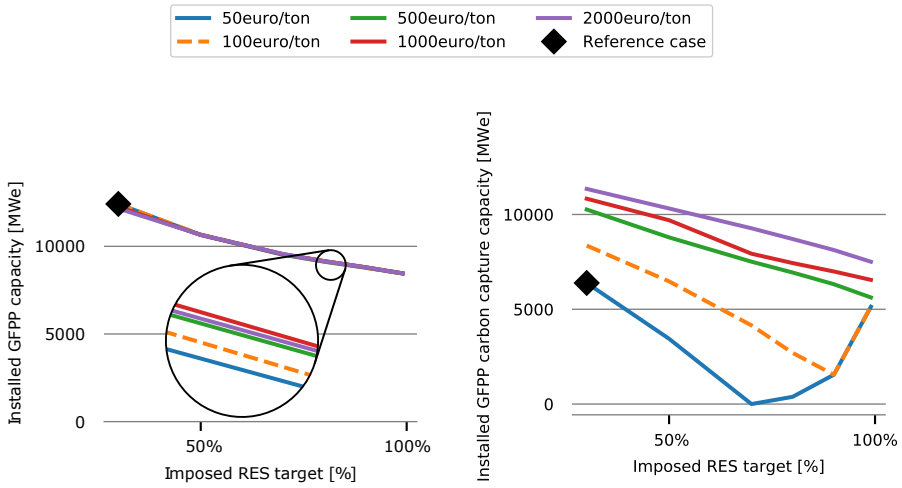


Figure 4.5: Total installed GFPP capacity (left panel) and GFPP capacity with carbon capture (right panel) for increasing RES targets and different CO₂ prices; no capacity legacy between cases; batteries, CO₂ sequestration and curtailment available; iRES mix as in reference case. Note that in the right panel, the 50 €/ton curve and 100 €/ton curve coincide from the 90% RES case onwards.

It is shown in the left panel of Figure 4.5 that an increase in CO₂ emission price has no real effect on the installed GFPP capacity. The right panel, however, shows that it has a significant effect on the installed carbon capture capacity (downstream of the GFPPs).⁴ As mentioned before, if the CO₂ emission price increases, more carbon capture capacity is installed and more CO₂ is captured

⁴It is always the capacity of the GFPPs (with and without CO₂ capture) that is shown. Caution is needed when interpreting the installed capacities of the GFPPs in the two panels shown in Figure 4.5. In the right panel all GFPP capacity shown has post-combustion CO₂ capture installed, in the left panel, showing the capacity of all GFPPs, part of the GFPPs have CO₂ capture whilst the other GFPPs have no CO₂ capture installed. Always gross

and sequestered. The optimally installed carbon capture capacity as a function of the imposed RES share shows two different trends. A first one, which can be observed for all CO₂ emission prices, is a declining carbon capture capacity for an increasing imposed RES share (up to RES share of 70% for 50 €/ton and 90% for 100 €/ton, respectively). Since the imposed RES share constrains the amount of natural gas that can be used, it limits the operating hours of the GFPPs and hence the operating hours of the carbon capture units. This causes the carbon capture unit to be more costly compared to emitting the CO₂ and paying the emission price. A second trend, which only occurs for a CO₂ emission price of 50 €/ton (as of 70% RES share) and 100 €/ton (starting at 90% RES share), is an increasing carbon capture capacity for an increasing RES share. As the share of RES increases, the need for P2G storage increases and consequently the need for carbon to produce synthetic methane increases. The reason this second trend is not observed for higher CO₂ emission prices is that the installed carbon capture capacity is already high due to the high emission price and hence already plenty of CO₂ is available for the methanation unit.

4.5.4 Influence of the CO₂ sequestration option

The influence of CO₂ sequestration availability is investigated next, with installed capacities shown in Figure 4.6 - Figure 4.8.

Figure 4.6 indicates that for a low CO₂ emission price (100 €/ton), the availability of CO₂ sequestration has no influence on the amount of installed electrolyzer (left panel) and methanation (right panel) capacity; both the solid and dashed blue lines coincide (although not quite visible since the green color has priority in the color plotting, it seems). In such case, the CO₂ which would normally be sequestered is now emitted at additional cost but this cost is not high enough to trigger additional investments in iRES or storage. As in Figure 4.4 before, if CO₂ sequestration is available, the installed P2G capacities are almost independent of the CO₂ emission prices and therefore all solid lines almost coincide. However, for higher CO₂ emission prices, the CO₂ sequestration availability has a significant effect. Emitting the normally sequestered CO₂ would be too costly. This cost is avoided partly by using the captured CO₂ in the methanizer unit and partly by reducing the CO₂ production through the use of additional iRES generation, as shown in Figure 4.7. Both effects reinforce

available capacities for the electricity system are shown, i.e. the reported installed capacities indicate the maximum possible GFPP electricity generation, when the attached capture units would not be operated. During time steps when the capture unit is effectively operated, the maximum attainable effective electrical power generation is reduced according to the electrical power sacrificed for own consumption of the capture unit.

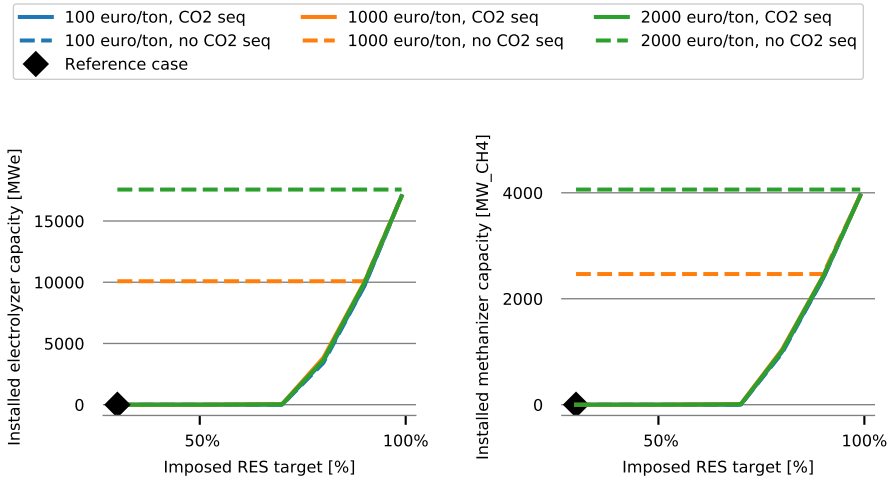


Figure 4.6: Installed electrolyzer capacity (left panel) and methanizer capacity (right panel) for increasing RES targets, with and without sequestration available and different CO₂ prices; no capacity legacy between cases; batteries and curtailment available; iRES mix as in reference case. Note that the curves for the 100 €/ton cases, the 1000 €/ton with sequestration and 2000 €/ton with sequestration cases almost coincide (the green color seems to have priority in the plotting).

each other as additional iRES capacity requires additional storage capacity to operate efficiently.

Figure 4.7 shows the sum of installed iRES power capacities, onshore wind, offshore wind and solar PV, as a function of the (minimally) imposed RES (electrical energy) share. Low CO₂ emission prices do not trigger an investment in additional iRES capacity above the capacity which must be installed to meet the RES target, regardless of the CO₂ sequestration availability (hence the blue solid and dashed lines coincide; albeit that these colors are hidden underneath the green line). As mentioned before, for higher CO₂ emission prices and if no CO₂ sequestration is available, the emission of CO₂ will be reduced both by using captured CO₂ in a methanizer unit and avoiding CO₂ emission by generating more iRES electricity. In such cases, considerably more iRES power capacity is installed than is required to meet the (minimally) imposed RES energy target.

A high CO₂ emission price without the availability to sequester CO₂ leads to a reduction in CO₂ production from GFPPs. As more iRES is installed to avoid

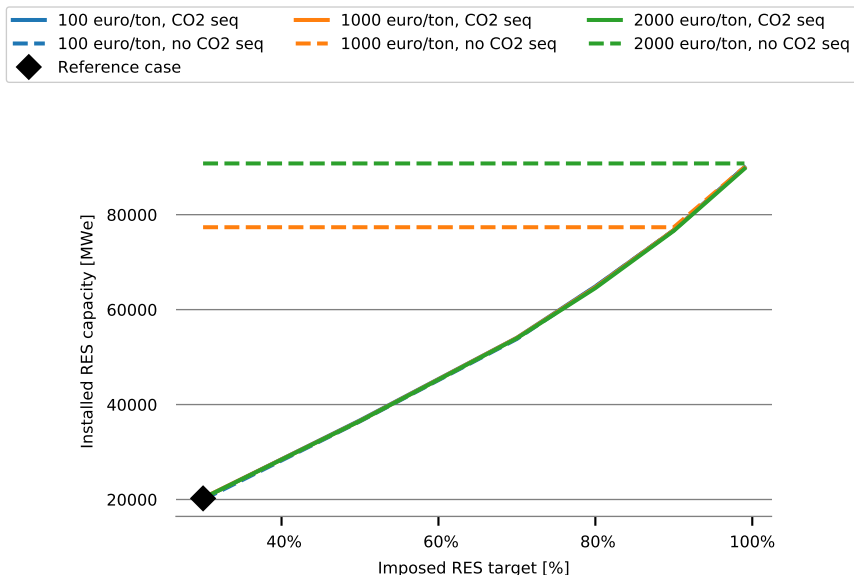


Figure 4.7: Installed iRES capacity (onshore, offshore and solar) for increasing RES targets, with and without sequestration available and different CO₂ prices; no capacity legacy between cases; batteries and curtailment available; iRES mix as in reference case. Note that the curves for the 100 €/ton cases, the 1000 €/ton with sequestration and 2000 €/ton with sequestration cases all coincide (the green color seems to have priority in the plotting).

CO₂ production, less GFPP capacity is required (shown by the dashed lines in the left panel of Figure 4.8) and less carbon capture capacity is required (shown in the right panel of Figure 4.8) compared to cases where CO₂ sequestration is available.⁵ For carbon capture capacity, the same trends as mentioned with respect to Figure 4.5 before can be noticed, i.e., a higher CO₂ emission price leads to higher carbon capture capacities and an increasing RES share leads to lower carbon capture capacities unless for very high RES shares, when massive storage by P2G becomes cost efficient and additional carbon capture capacity is installed to supply the required CO₂ for the methanizer.

⁵The CO₂-sequestration cases shown in Figure 4.8 are identical to those shown in Figure 4.5.

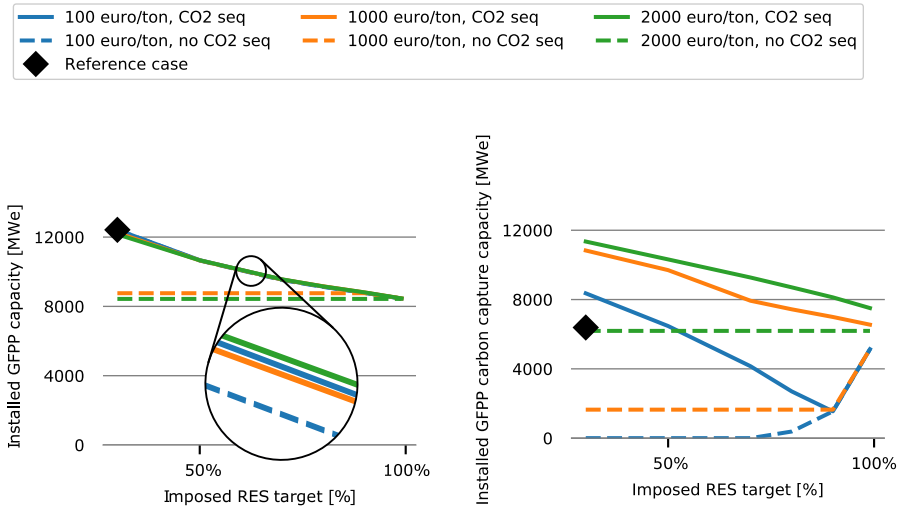


Figure 4.8: Installed GFPP capacity (left panel) and GFPP carbon capture capacity (right panel) for increasing RES targets, with and without sequestration available and different CO₂ prices; no capacity legacy between cases; batteries and curtailment available; iRES mix as in reference case.

4.5.5 Influence of changing the iRES mix

Changing the share of each technology in the iRES mix has an effect on the installed P2G capacity as shown in Figure 4.9.

Although the installed capacities of each iRES technology vary significantly when the imposed mix is changed (see Figure 4.10), the general trend in installed P2G capacity remains the same; a higher imposed RES share leads to a greater need for storage and hence a larger installed electrolyzer and methanizer capacity. The imposed RES target for which P2G technology becomes cost efficient remains above 70%, irrespective of the precise iRES mix.

Figure 4.10 shows the installed iRES capacity per technology for different imposed RES shares and imposed iRES mixes. If no mix is imposed, the iRES capacity mix is optimized based on cost. In that case, no offshore wind is installed, because its cost per MWh generated energy is higher than that of onshore wind and solar PV.

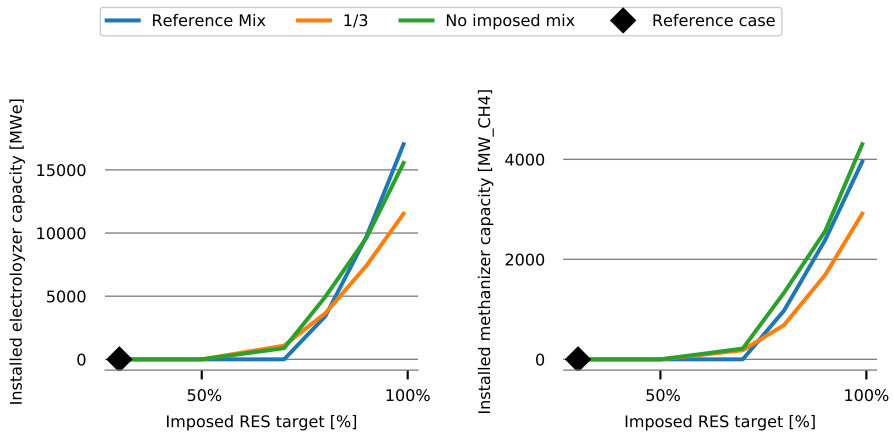


Figure 4.9: Installed electrolyzer capacity (left panel) and methanizer capacity (right panel) for increasing RES targets and three different iRES mixes: the reference mix with 12% onshore wind, 22% offshore wind and 66% solar PV, the 1/3th mix where each iRES technology generates an equal amount of electrical energy and a case with no imposed mix; no capacity legacy between cases; batteries, CO₂ sequestration and curtailment available; CO₂ emission price of 50 €/ton.

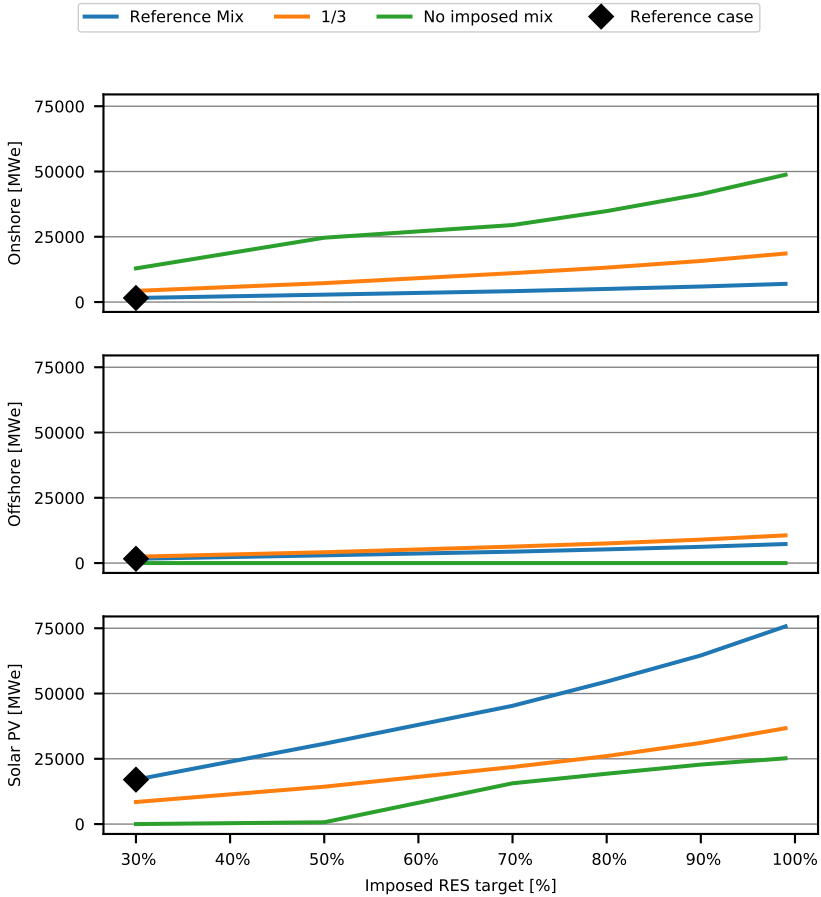


Figure 4.10: Installed onshore wind (upper panel), offshore wind (middle panel) and solar pv (lower panel) capacity for increasing imposed minimum RES targets and three different iRES mixes: the reference mix with 12% onshore wind, 22% offshore wind and 66% solar PV, the 1/3th mix where each each iRES technology generates an equal amount of electrical energy and a case with no imposed mix; no capacity legacy between cases; batteries, CO₂ sequestration and curtailment available; CO₂ emission price of 50 €/ton.

4.5.6 Influence of battery cost

The impact of a variation in battery cost on the installed P2G capacity is shown in Figure 4.11 (separately for the electrolyzer and methanizer capacity), on the battery capacity in Figure 4.12, and on the installed GFPP and carbon capture capacity in Figure 4.13. Recall that the 'reference' battery cost is assumed to be a representative cost for batteries in 2018.

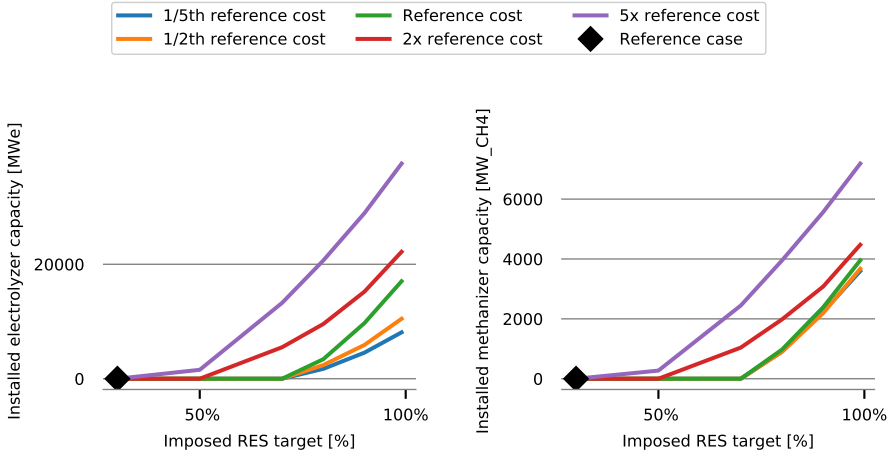


Figure 4.11: Installed electrolyzer capacity (left panel) and methanizer capacity (right panel) for increasing RES targets and five different battery capacity costs: EAC varying from 36.85 (1/5th) – 92.12 (1/2th) – 184.24 (reference) – 368.48 (2x) – 921.20 (5x) €/ (MW_e y); no capacity legacy between cases; CO₂ sequestration and curtailment available; CO₂ emission price of 50 €/ton.

Figure 4.11 in combination with Figure 4.12 shows that for an increasing battery cost, the installed battery capacity decreases while the installed electrolyzer and methanizer capacity increases. This can be expected since both technologies can act as substitutes.

Given the energy system under investigation, a fivefold price increase of batteries would cause no batteries to be installed at all.

An increase in battery cost also triggers an increase in GFPP capacity, since it is used as discharge capacity for the energy stored as synthetic methane, as shown in the left panel of Figure 4.13. The very large increase in GFPP capacity for a fivefold increase in battery cost is due to the fact that GFPPs are now also required to accommodate all peaks in the residual electrical load, whereas otherwise part of these peaks are served by batteries.

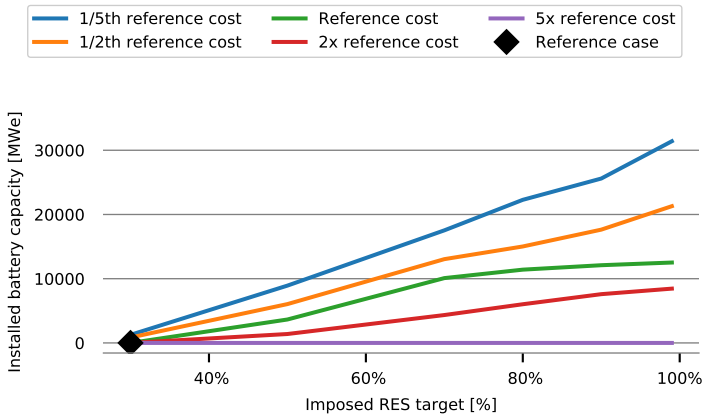


Figure 4.12: Installed battery capacity for increasing RES targets and five different battery capacity costs: EAC varying from 36.85 (1/5th) – 92.12 (1/2th) – 184.24 (reference) – 368.48 (2x) – 921.20 (5x) €/ (MWe y); no capacity legacy between cases; P2G, CO₂ sequestration and curtailment available; CO₂ emission price of 50 €/ton.

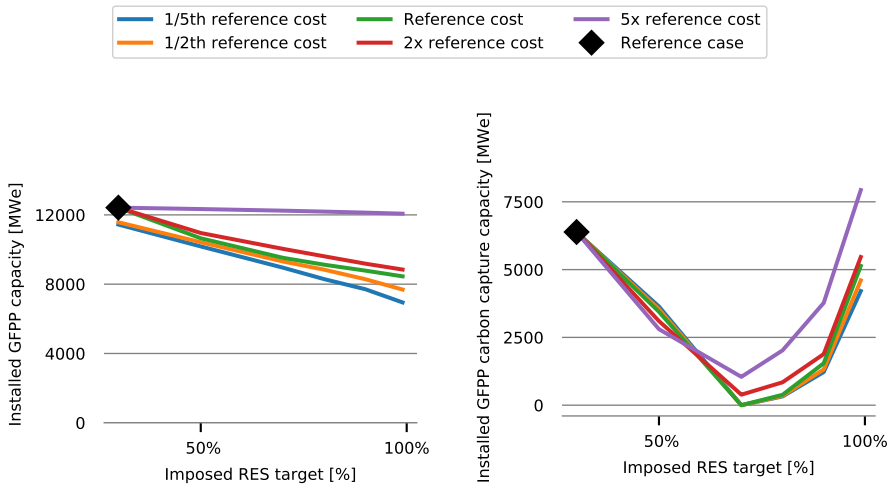


Figure 4.13: Installed GFPP capacity (left panel) and GFPP carbon capture capacity (right panel) for increasing RES targets and five different battery capacity costs: 36.85 (1/5th) – 92.12 (1/2th) – 184.24 (reference) – 368.48 (2x) – 921.20 (5x) €/ (MWe y); No capacity legacy between cases, CO₂ sequestration and curtailment available, CO₂ emission price of 50 €/ton.

4.5.7 Influence of electrolyzer and methanizer cost

Similar but opposite observations can be made when varying the cost of electrolyzer and methanizer capacity. As before, the reference costs, one-fifth, half, double and fivefold increase of the reference cost are used for this analysis. The resulting equivalent annual cost (EAC) for electrolyzer and methanizer capacity are shown in Table 4.8. Again, the 'reference' costs are assumed to be representative in 2018.

Table 4.8: Electrolyzer and methanizer equivalent annual cost (EAC) used in sensitivity analysis.

Equivalent annual cost	Electrolyzer $\text{€}/kW_e y$	Methanizer $\text{€}/kW_{CH_4} y$
1/5 th of reference	12.99	42.51
half of reference	32.48	106.28
Reference	64.95	212.57
2x reference	129.90	425.13
5x reference	324.75	1062.83

Figure 4.14 presents the installed electrolyzer (left panel) and methanizer (right panel) capacities for an increasing P2G cost.

Figure 4.14 in combination with Figure 4.15 shows that an increasing P2G cost leads to a decrease in both electrolyzer and methanizer capacity and an increase in battery capacity. In contrast to the observations made for an increasing battery cost in the previous subsection with regard to battery capacity, there is still some electrolyzer and methanizer capacity installed even when their cost is increased fivefold.

At five times more expensive P2G equipment, the installed battery capacity (see the purple curve in Figure 4.15) only starts to deviate from the reference case (green curve) at a RES share of about 70-80% since that is the share at which P2G starts to enter the picture in the reference case, and it is that which is now replaced by batteries.

Figure 4.16 shows the installed GFPP and carbon capture capacity for different P2G costs.

A change in P2G cost does not have a big effect on the GFPP capacity as the installed GFPP units are still used with conventional natural gas, of which the price remains unchanged.

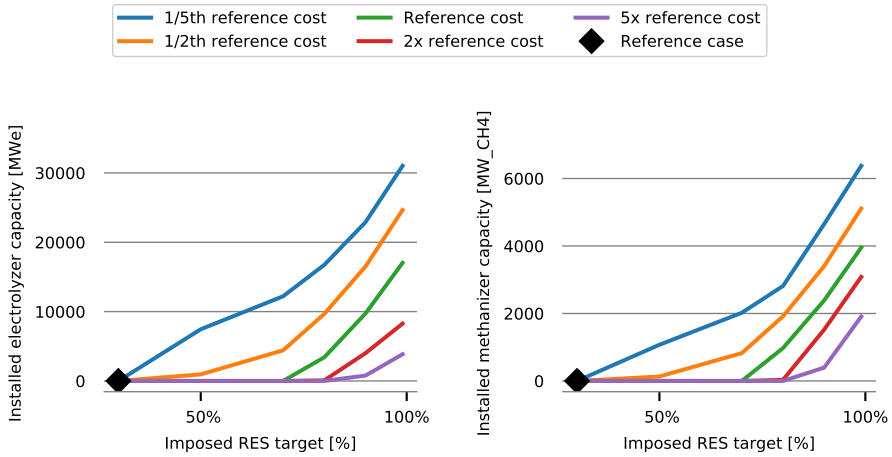


Figure 4.14: Installed electrolyzer capacity (left panel) and methanizer capacity (right panel) for increasing RES targets and five different electrolyzer and methanizer capacity costs: EAC equal to reference cost, 1/5th, half, double and 5 times the reference cost; no capacity legacy between cases; batteries, CO₂ sequestration and curtailment available; CO₂ emission price of 50 €/ton.

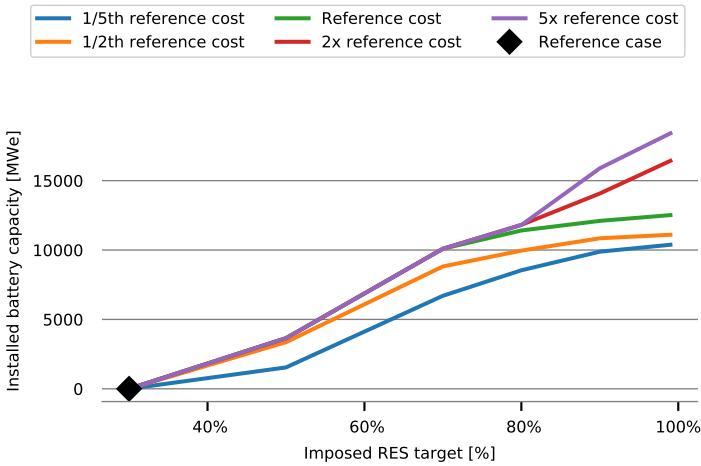


Figure 4.15: Installed battery capacity for increasing RES targets and five different electrolyzer and methanizer capacity costs: EAC equal to reference cost, 1/5th, half, double and 5 times the reference cost; no capacity legacy between case; batteries, CO₂ sequestration and curtailment available; CO₂ emission price of 50 €/ton.

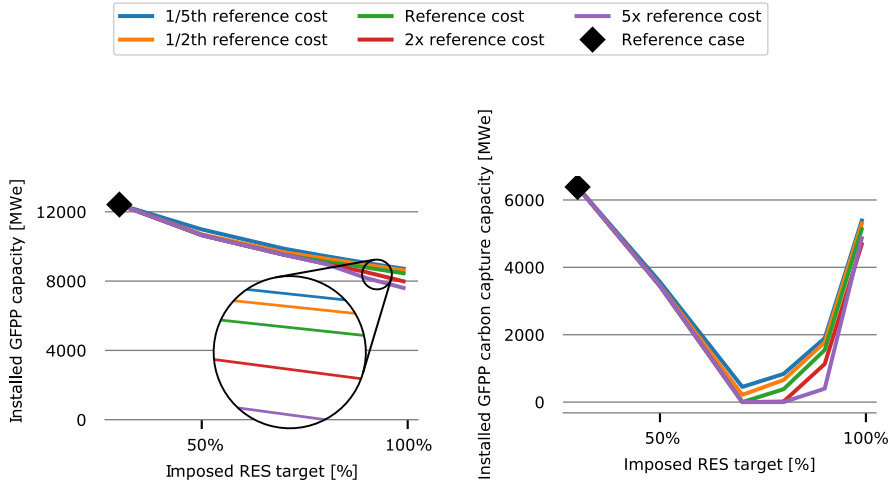


Figure 4.16: Installed GFPP capacity (left panel) and GFPP carbon capture capacity (right panel) for increasing RES targets and five different electrolyzer and methanizer capacity costs: EAC equal to reference cost, 1/5th, half, double and 5 times the reference cost; no capacity legacy between cases; batteries, CO₂ sequestration and curtailment available; CO₂ emission price of 50 €/ton.

4.5.8 Influence of capacity legacy

The following sensitivity analysis starts again from the reference case, i.e. batteries, CO₂ sequestration and curtailment ‘available’, with a CO₂ price of 50 €/ton. However, in this set of ‘legacy’ runs, when increasing the imposed RES target, it is now assumed that capacity which was installed for a lower RES target, remains installed (indicated with the term brownfield). This is in contrast to all previous analyses, where for each optimization point no pre-installed capacity was assumed (indicated with the term greenfield), except for the PHS which is always assumed pre-installed. When capacity legacy is assumed, it applies to all technologies (GFPP, electrolyzer, methanizer and batteries).

Figure 4.17 shows the installed electrolyzer (on the left axis) and methanizer (on the right axis) capacity for an increasing RES share, both when a greenfield and brownfield are assumed.

It is observed that when a brownfield is assumed, slightly more electrolyzer and methanizer capacity is installed, but that the effect on these dedicated P2G

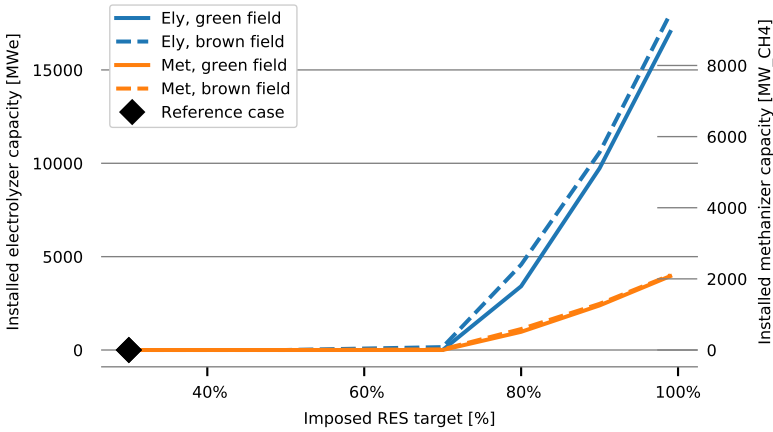


Figure 4.17: Installed electrolyzer capacity (left axis) and methanizer capacity (right axis) for increasing RES targets, without capacity legacy between increasing iRES capacities (greenfield) and with capacity legacy (brownfield); batteries, CO₂ sequestration and curtailment available; CO₂ emission price of 50 €/ton.

technologies is basically negligible. However, the effect on the GFPPs (and their coupled CC units, if applicable) is substantial as shown in Figure 4.18. This can be easily understood since the already built GFPP units needed in the reference case simply remain there. The fact that more discharging capacity (when being fueled by synthetic methane) is present does not lead to more methanizer capacity, and only to a small extra amount of electrolyzer capacity (at least for a CO₂ price of 50 €/ton).

Nevertheless, retaining GFPP capacity does not lead to a significant higher use of it, as shown in Table 4.9.

Table 4.9: GFPP generation (net of consumption by carbon capture unit) for increasing RES targets, without capacity legacy (greenfield) and with capacity legacy (brownfield); batteries, CO₂ sequestration and curtailment available; CO₂ emission price of 50 €/ton.

		30%	50%	70%	80%	90%	99%
Greenfield	[TWhe]	60.63	43.37	26.11	19.24	13.81	10.02
Brownfield	[TWhe]	60.63	43.29	26.03	19.57	13.96	10.17

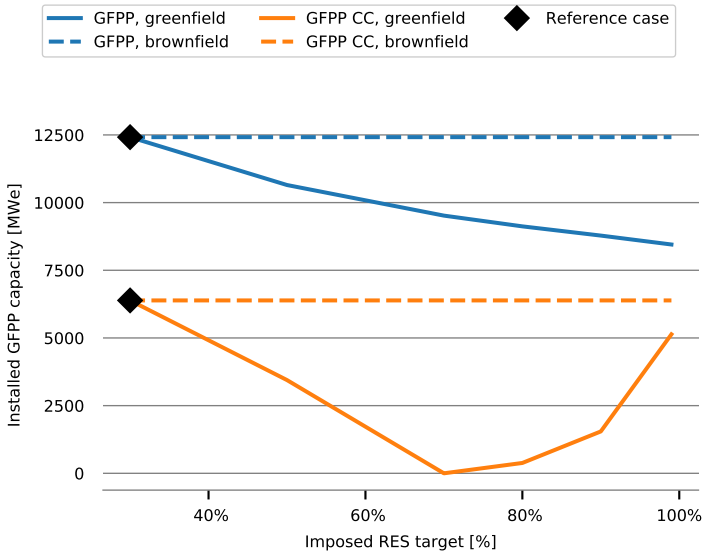


Figure 4.18: Installed GFPP capacity and GFPP carbon capture capacity for increasing RES targets, without capacity legacy between increasing iRES capacities (greenfield) and with capacity legacy (brownfield); batteries, CO₂ sequestration and curtailment available; CO₂ emission price of 50 €/ton.

Figure 4.19 shows the installed battery capacity for cases with assumed greenfield and brownfield.

Also here, it is observed that the greenfield or brownfield assumption has no big impact on the installed battery capacity, similar to the installed electrolyzer and methanizer capacities before. For batteries, however, the brownfield assumption leads to slightly less installed battery capacity (battery and P2G technologies act as substitutes).⁶

⁶The difference in installed capacities between cases assuming a brownfield and a greenfield are discussed for CO₂ emission prices of 50 €/ton. For CO₂ emission prices of 1000 €/ton and 2000 €/ton, results are comparable to the 50 €/ton cases, i.e., a constant GFPP and GFPP CC capacity when assuming a brownfield, a minor increase in electrolyzer and methanizer capacities and a minor decrease in battery capacity when assuming a brownfield compared to a greenfield.

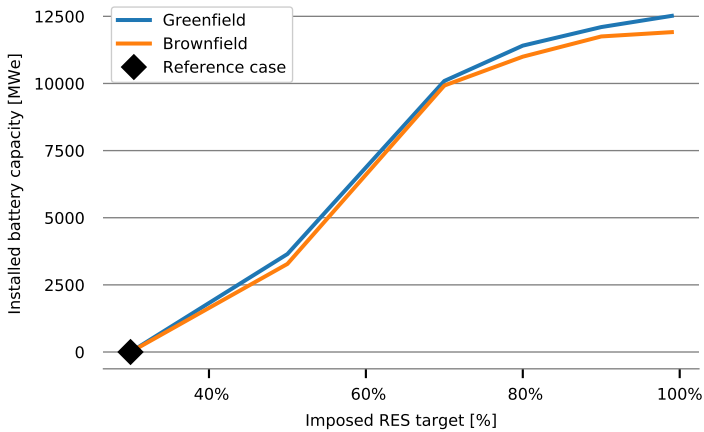


Figure 4.19: Installed battery capacity for increasing RES targets, without capacity legacy between increasing iRES capacities (greenfield) and with capacity legacy (brownfield); CO₂ sequestration and curtailment available; CO₂ emission price of 50 €/ton.

4.5.9 Results for an 'all renewable (99%)' case

Table 4.10 and Table 4.11 show, respectively, the installed capacities per technology and the aggregated energy and carbon quantities in the 99% RES case, if batteries, P2G, curtailment and CO₂ sequestration are 'available', with the reference RES mix, and with a CO₂ emission price of 50 €/ton.

As can be seen from Table 4.10, a total of almost 90 GW_e of iRES capacity is installed, generating almost 120 TWh_e of electricity. An indication on how this RES generation is used, is given in Table 4.12.

From Table 4.12 it is clear that almost half of the iRES generated electricity is serving electrical load directly, while 5% is curtailed and 45% is stored to be used at a later moment. Note, however, that these figures are only indications (opposed to the reported installed capacities). Since not many technical details are accounted for by the model, there is no difference between curtailing electrical energy and simultaneously charging and discharging electricity and hence losing (or thus 'curtailing') electrical energy due to storage inefficiencies. Therefore, the reported storage related numbers can be seen as upper limits, while the reported curtailment and direct load serving numbers can be seen as lower limits. Indeed, simultaneous charging-discharging could substitute curtailment but curtailment could not substitute storing energy.

Table 4.10: Installed capacities in the 99% imposed RES case.

GFPP	8.45	GW_e
GFPP with carbon capture ^a	5.13	GW_e
Onshore wind	6.97	GW_e
Offshore wind	7.29	GW_e
Solar PV	75.73	GW_e
Battery	12.52	GW_e
Electrolyzer	17.03	GW_e
PHS	1	GW_e
Methanizer	3.96	GW_{CH_4}
Methane storage	12.91	TWh_{CH_4}
Hydrogen storage	0.31	TWh_{H_2}

^a 5.13 GW_e of the 8.45 GW_e is equipped with CC capacity. The power rating refers to the nominal output rating of the GFPP, without subtracting any electrical power sacrificed to operate the CC unit.

Table 4.11: Aggregated annual energy and carbon quantities in the 99% imposed RES case.

Electrical energy load	87.03	TWh_e
GFPP net generation ^a	10.02	TWh_e
Onshore wind	14.34	TWh_e
Offshore wind	26.29	TWh_e
Solar PV	78.87	TWh_e
Hydrogen produced	23.91	TWh_{H_2}
SM produced	16.73	TWh_{CH_4}
Natural gas used	1.58	TWh_{CH_4}
CO ₂ emitted	0.32	Mton
CO ₂ sequestered	0	Mton
CO ₂ used	3.35	Mton

^a the 'net' generation refers to the resulting GFPP generation, after subtracting the electrical power sacrificed to operate the CC unit.

Table 4.10 and Table 4.11 show that the size of the methane storage (12.91 TWh_{CH_4}) is only slightly smaller than the yearly amount of produced synthetic methane (SM) (16.74 TWh_{CH_4}), indicating that this storage type has a storage cycle of one year and is thus used for seasonal storage. This is also confirmed by

Table 4.12: Use of iRES generated electricity for the 99% RES case.

Total iRES generation	119.5	TWh_e		
Battery charged	21.82	TWh_e	18.26	% of iRES
PHS charged	1.07	TWh_e	0.90	% of iRES
Electrolyzer consumed	31.88	TWh_e	26.67	% of iRES
Curtailment	6.17	TWh_e	5.17	% of iRES
Direct load serving	58.56	TWh_e	49.0	% of iRES

Figure 4.20 which shows the battery energy storage level (solid line, left axis) and the methane storage level (dashed line, right axis) throughout the year.

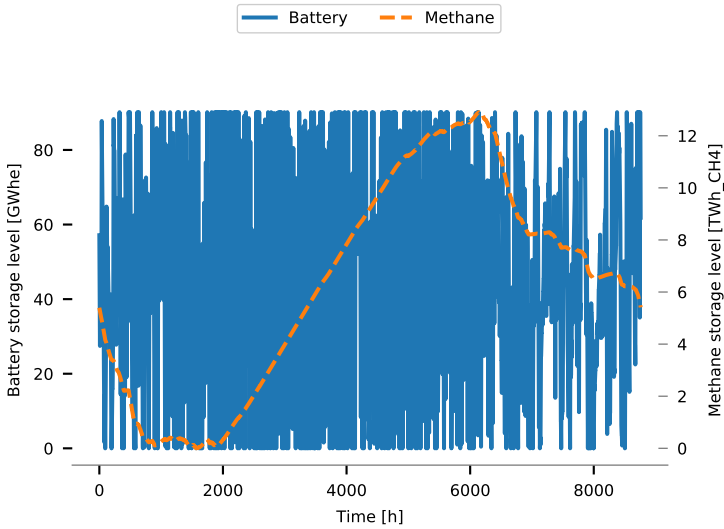


Figure 4.20: Battery energy storage level (left axis) and methane storage level (right axis) through the year; 99% RES share imposed starting from greenfield; CO₂ sequestration and curtailment available; CO₂ emission price of 50 €/ton.

It is clear from Figure 4.20 that the methane storage has roughly one yearly charge-discharge cycle, while the battery storage is used on much shorter term, with e.g. in summer a day-night charge-discharge pattern as shown in more detail on Figure 4.21 for about 4 summer days.

Table 4.11 reports that 10.02 TWh electrical energy is generated by GFPP. The majority of this, 91.4%, is generated with synthetic methane (SM) produced by

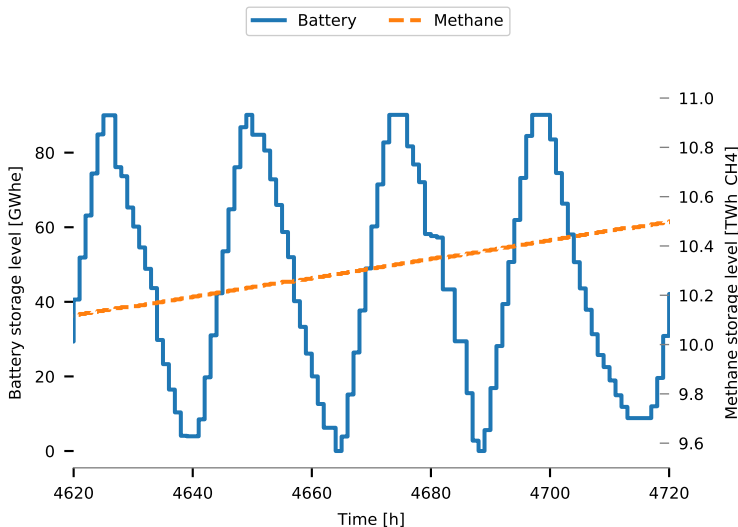


Figure 4.21: Battery storage level (left axis) and methane storage level (right axis) for a few days in summer; 99% RES share imposed starting from greenfield; CO₂ sequestration and curtailment available; CO₂ emission price of 50 €/ton.

P2G while 8.6% comes from fossil natural gas. Note that in a full 100% RES case, no fossil natural gas would be used anymore. Furthermore, it is interesting to look at the load duration curve of the GFPPs, as shown in Figure 4.22.

Figure 4.22 shows the instantaneous electrical power generation of the GFPP technology throughout the year, ordered from high to low. On Figure 4.22 it could seem as if GFPPs have more operating hours in the 80% scenario compared to the 70% scenario. However, note that the total yearly electricity generation by GFPP always decreases with an increasing imposed RES share. For some imposed RES shares, the GFPP load duration curves show a ‘flat’ part; this ‘flat’ part stems from GFPP which is operated as ‘must run’ to use the installed carbon capture capacity in the most economically efficient way. Taking the 99% RES case as example, the flat part has a magnitude of 5.13 GW_e , which is exactly the installed carbon capture capacity. Note that in a truly 100% RES case there would be no ‘flat’ part. This is because no fossil natural gas can be used in a 100% RES case and hence all GFPP capacity should be equipped with CC to fully close the carbon loop. Hence, then there would be no option to optimize the amount of installed CC capacity and no advantage in operating GFPPs as ‘must run’ capacity.

The GFPP operating in base load is further illustrated in Figure 4.23.

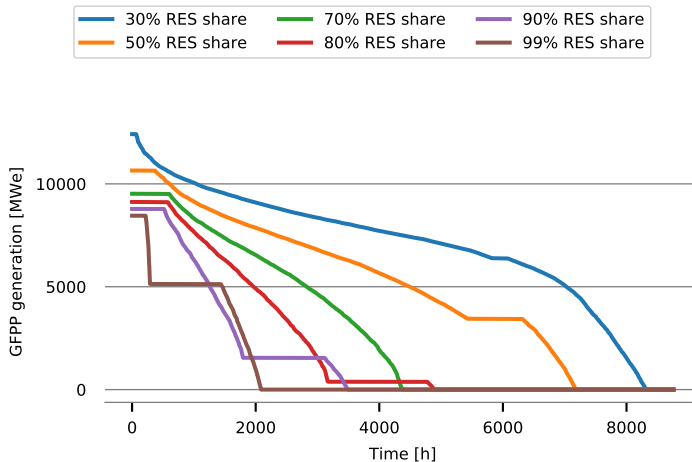


Figure 4.22: Load duration curves of GFPP for different imposed RES shares; no capacity legacy between cases; CO₂ sequestration, batteries, P2G and curtailment available; CO₂ emission price of 50 €/ton.

Figure 4.23 shows that even while (battery and PHS) storage is charged (between the hours 1426 and 1431) the GFPP is operated instead of reducing GFPP output between these hours and increasing the GFPP output on a later moment (e.g. between 1432 hours and 1445 hours), thereby reducing the need for storage discharge. Clearly, a balance has to be found between the cost of storage efficiency losses and the cost of installing additional carbon capture capacity which would be operated during fewer hours. A third option, not installing additional carbon capture capacity, capturing less CO₂ and having a higher CO₂ emission price is also sometimes possible. This behavior is observed for lower imposed RES targets when the sequestration option is not available. For the higher imposed RES targets (above 80%), however, all the captured CO₂ is required as feedstock for the methanizer unit. In such cases, no CO₂ is sequestered even if the option is available; see also the lack of sequestered CO₂ in Table 4.11.

Comment: The recently reported cost decreases of atmospheric carbon capture [69] could alter the cost-efficiency of GFPP and the way GFPPs are operated since this additional source of CO₂ allows for capturing during periods of surplus iRES generation, independent of the GFPP operation. The exact impact of a cheap additional carbon source requires further investigation outside the scope of this study.

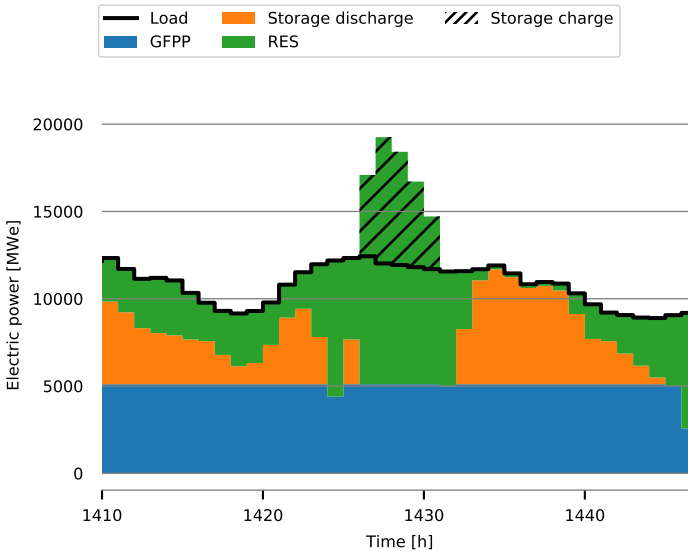


Figure 4.23: Electrical power flows for a 99% imposed RES share starting from greenfield; CO₂ sequestration, batteries, P2G and curtailment available; CO₂ emission price of 50 €/ton. Storage denotes batteries and PHS, no electrolyzer was used in the displayed hours.

4.5.10 Influence of a cold spell

The effect of a cold spell, 14 days in winter without sun or wind generation, on the installed capacities is discussed in this subsection. Two cold spell cases are investigated, one for which it is assumed that a cold spell appears once every three years and one for which a yearly cold spell is considered.

Figure 4.24 shows the installed electrolyzer (left panel) and methanizer (right panel) capacities for each of the cases. The figure shows an increase of both electrolyzer and methanizer capacity when a cold spell is considered. In the most extreme (99% RES case) the magnitude of the increase is however limited to 9% for the electrolyzer capacity and 5% for the methanizer capacity if a cold spell is considered every three years. When a yearly cold spell would occur, the electrolyzer capacity increases with 22% compared to the reference year and the methanizer capacity increases with 15%. Such yearly cold spell is, however, unlikely to occur.

The installed methane storage capacity and the amount of yearly produced synthetic methane are shown in Figure 4.25.

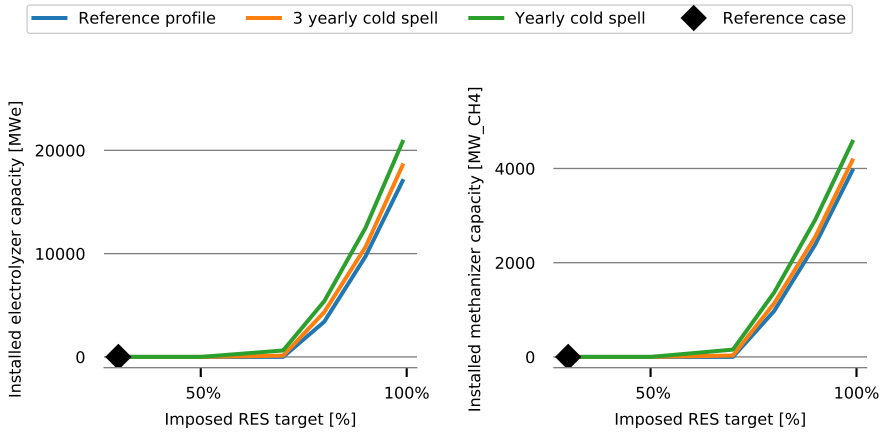


Figure 4.24: Installed electrolyzer capacity (left panel) and methanizer capacity (right panel) for increasing RES targets, with and without yearly and triennial cold spell; CO₂ sequestration available; iRES mix as in reference case and a CO₂ price of 50€/ton.

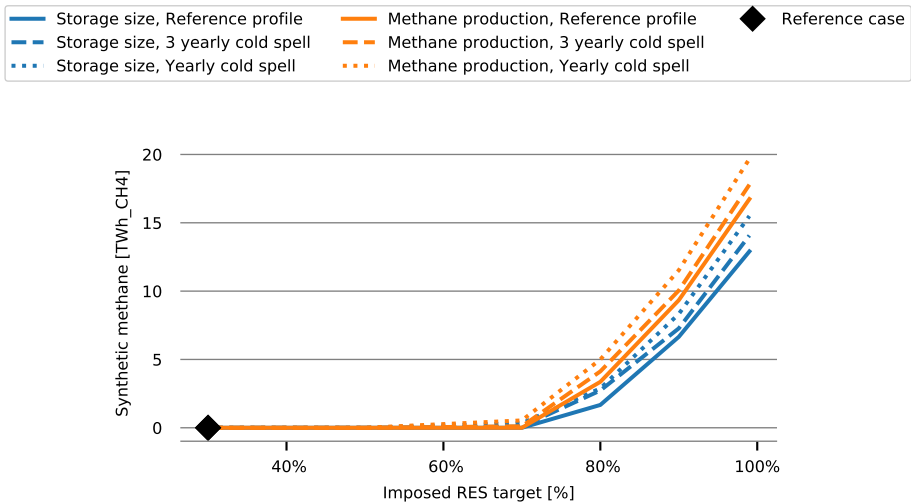


Figure 4.25: Installed methane storage capacity and amount of produced synthetic methane for increasing RES targets, with and without yearly and triennial cold spell; no capacity legacy between cases; CO₂ sequestration available; iRES mix as in reference case and a CO₂ price of 50€/ton.

Similar as to the installed P2G capacity, an increase of around 20% in storage capacity and synthetic methane production is observed if a yearly cold spell would occur for a 99% RES target. If only one cold spell every three years is considered, the increase in storage capacity is limited to 9% and the increase in produced synthetic methane is limited to 6%.

In contrast to the P2G capacity, Figure 4.26 shows that the installed battery capacity is almost constant, irrespective of whether a cold spell is considered or not. More over, the battery capacity even slightly decreases (-2% in the 99% RES cases) since batteries are slightly less used if a cold spell occurs, as more energy is stored via P2G.

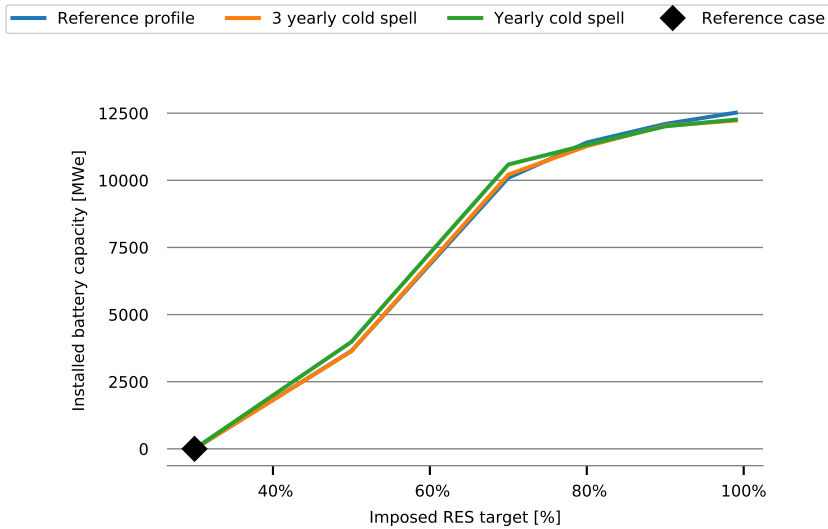


Figure 4.26: Installed battery capacity for increasing RES targets, with and without yearly and triennial cold spell; CO₂ sequestration available; iRES mix as in reference case and a CO₂ price of 50€/ton.

The installed GFPP capacity shown in Figure 4.27 is impacted most if a cold spell is considered, irrespective of the frequency at which such cold spell would occur. The Figure shows a 37% increase in capacity for the 99% RES cases, irrespective of yearly or triennial cold spell is considered (both curves coincide in the left panel). A possible cold spell creates an additional need for discharge capacity which can not be served by batteries as those are predominantly used for shorter term storage. Hence, GFPP which is used as discharge technology for the energy storage via synthetic methane, is additionally installed.

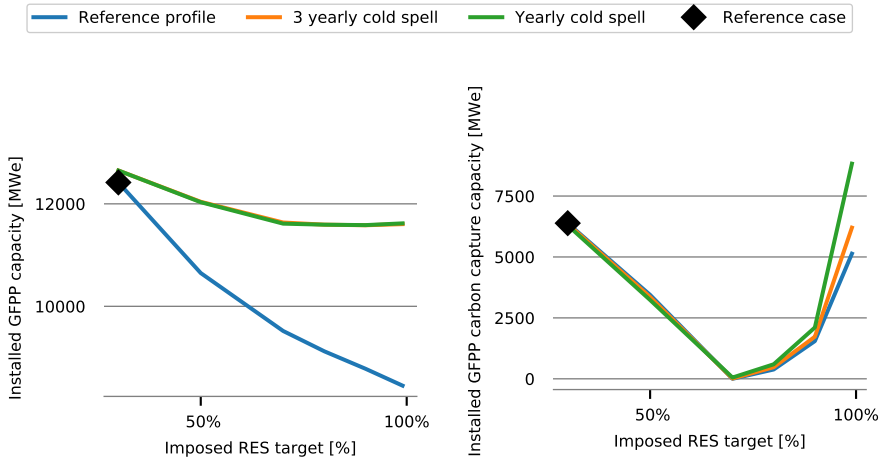


Figure 4.27: Installed GFPP capacity (left panel) and GFPP carbon capture capacity (right panel) for increasing RES targets, with and without yearly and triennial cold spell; CO₂ sequestration available; iRES mix as in reference case and a CO₂ price of 50€/ton.

4.5.11 Influence of battery availability

If batteries are unavailable, more P2G and GFPP capacity is installed to fulfill the storage need. This observation is illustrated in Figures 4.28-4.31 for a CO₂ emission price of 50 €/ton. Although not shown in the figures, this observation is irrespective of the CO₂ emission price.

Figure 4.28 shows the installed electrolyzer capacity in the left panel and installed methanizer capacity in the right panel both if batteries are available and if not. If batteries are unavailable, the electrical load normally served by batteries is now covered both by an increase in iRES capacity (see Figure 4.29) and by using P2G also for shorter term storage.

Figure 4.30 shows the installed GFPP and carbon capture capacity for cases with and without batteries.

As seen from Figure 4.30, the installed GFPP capacity is larger if batteries are not available, compared to the case with batteries. There are two reasons that can be explained as follows. GFPPs are used as discharge technology for energy stored as synthetic methane. Since P2G is more often used in the absence of batteries, also the need for GFPP capacity becomes higher. Besides this, batteries were also used to serve part of the electrical load during peak

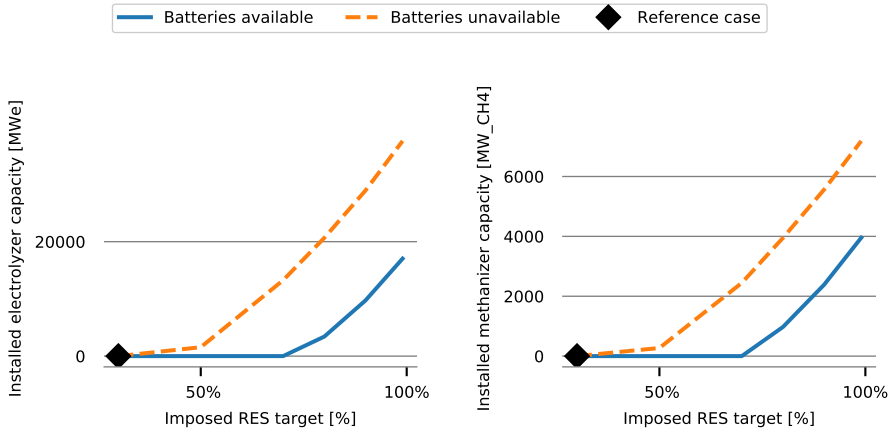


Figure 4.28: Installed electrolyzer capacity (left panel) and methanizer capacity (right panel) for increasing RES targets, with and without batteries available; no capacity legacy between cases; CO₂ sequestration and curtailment available; iRES mix as in reference case and a CO₂ price of 50 €/ton.

consumption. If batteries are unavailable, more of the peak load should be covered with GFPP, requiring a larger installed capacity.

The right panel of Figure 4.30 shows that for high imposed RES shares, a larger amount of carbon capture (CC) capacity is installed to provide more CO₂ for the methanation process if batteries are unavailable, in accordance with the increased methanizer capacity. For lower RES targets, the installed CC capacity depends on the CO₂ emission price. Since the GFPPs are more often used as peak generation in the absence of batteries, capturing the same share of CO₂ as in cases when GFPPs would be used more as base load requires more CC capacity. For a low emission price this would not be economically efficient (as it is cheaper to pay the CO₂ emission penalty) and hence less CC capacity is installed. For high CO₂ emission prices, it is less costly to install additional CC capacity and also capture the produced carbon at moments of peak electricity generation.

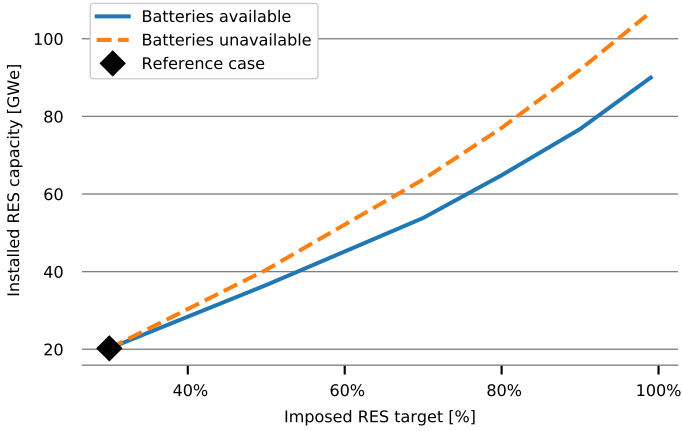


Figure 4.29: Installed iRES capacity for increasing RES targets, with and without batteries available; no capacity legacy between cases; CO₂ sequestration and curtailment available; iRES mix as in reference case and a CO₂ price of 50 €/ton.

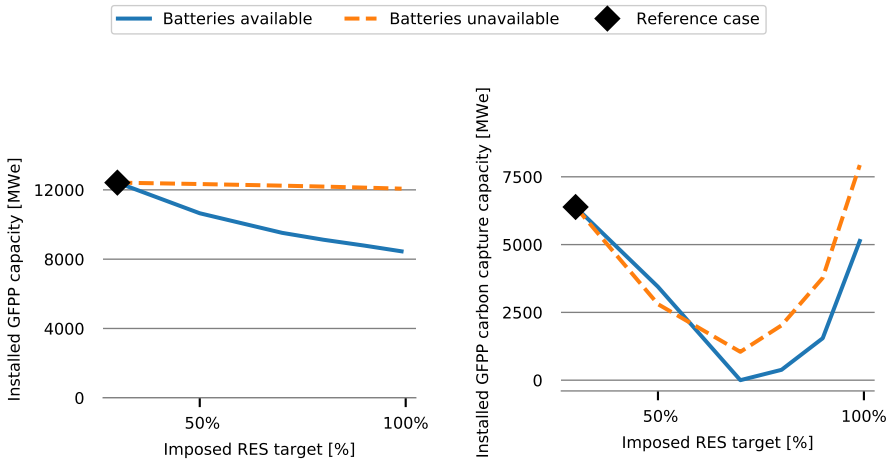


Figure 4.30: Installed GFPP capacity (left panel) and GFPP carbon capture capacity (right panel) for increasing RES targets, with and without batteries available; no capacity legacy between cases; P2G, CO₂ sequestration and curtailment available; iRES mix as in reference case and a CO₂ price of 50 €/ton.

Figure 4.31 shows the installed methane storage size and the yearly produced synthetic methane for different imposed RES shares, with and without battery availability.

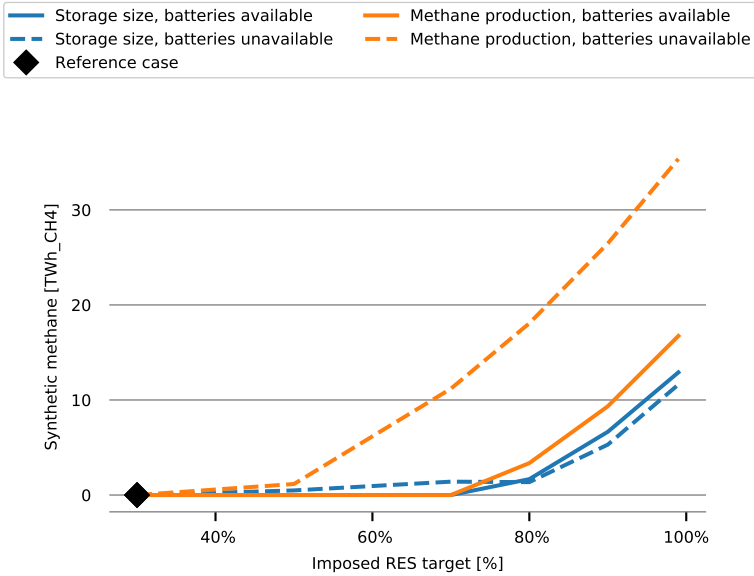


Figure 4.31: Installed methane storage capacity and amount of produced synthetic methane for increasing RES targets, with and without batteries available; no capacity legacy between cases; CO₂ sequestration and curtailment available; iRES mix as in reference case and a CO₂ price of 50 €/ton.

For different CO₂ emission prices, the same trends as displayed in Figure 4.31 would be visible when comparing cases with and without batteries available. If batteries are unavailable, the synthetic methane production is considerably larger compared to cases with batteries available. This happens, as explained before, since the storage needs otherwise fulfilled by batteries are now partly fulfilled by P2G for the case without batteries. However, the methane energy storage size is smaller in cases without battery availability compared to cases where batteries are available. As P2G is more used for short-term storage in cases without batteries available, it is operated with more, but smaller, charge-discharge cycles, leading to a smaller required energy storage capacity.

4.5.12 Influence of P2G availability

The effect of P2G being available or not is investigated next. Note that for a RES target up to 70%, there is no difference between the yes-or-no availability of P2G for all installed technologies since no P2G would be installed anyway below that level (recall Figure 4.3).

Figure 4.32 shows the installed battery capacity for an increasing imposed RES target, both with and without P2G available.

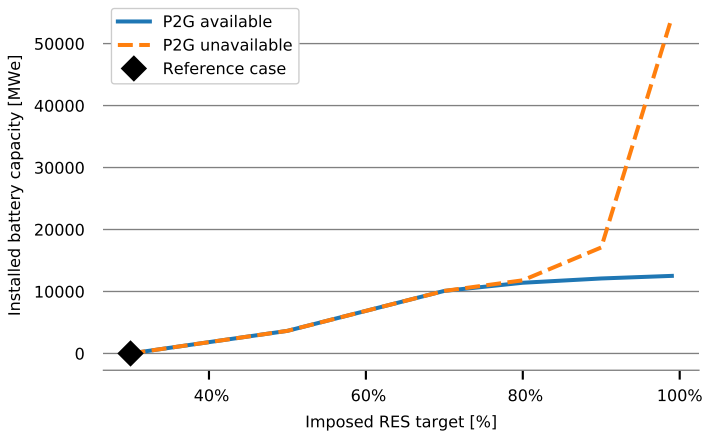


Figure 4.32: Installed battery capacity for increasing RES targets, with and without P2G available; no capacity legacy between cases; CO₂ sequestration and curtailment available; iRES mix as in reference case and a CO₂ price of 50 €/ton.

Similar to the observations made before about batteries and P2G storage, which can be substitute technologies, it is observed that if no P2G is available, the amount of installed battery capacity sharply increases compared to cases where P2G is available. Note that for a truly 100% imposed RES scenario, even more battery capacity would be installed.

Figure 4.33 shows a decrease in GFPP and carbon capture (CC) capacity when P2G is unavailable.

Since GFPPs are used both with conventional natural gas and as discharge technology for P2G, unavailability of P2G makes it economically a less interesting technology to install. Note that for an imposed RES share of 99% still some GFPP capacity is installed, where this would not be the case in a truly 100%

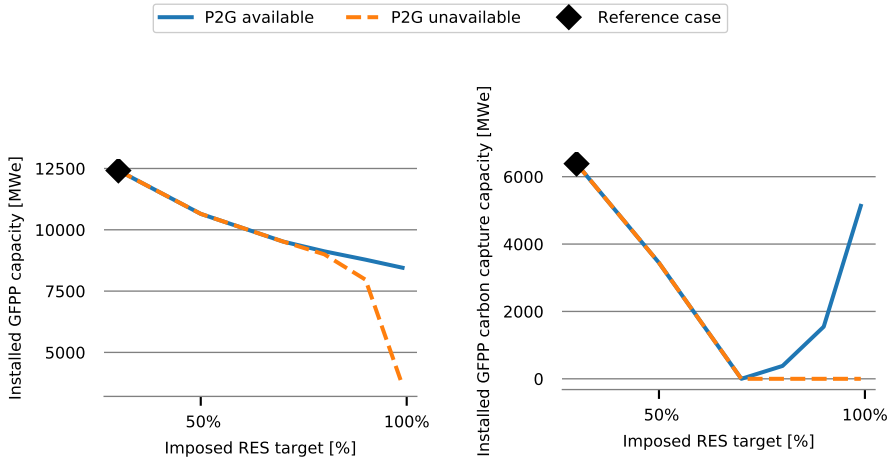


Figure 4.33: Installed GFPP capacity (left panel) and GFPP carbon capture capacity (right panel) for increasing RES targets, with and without P2G available; no capacity legacy between cases; batteries, curtailment and CO₂ sequestration available; iRES mix as in reference case and a CO₂ price of 50 €/ton.

imposed RES case; after all, in a 100% RES case, GFPPs could only be used as discharging capacity in combination with P2G as charging technology. Hence if P2G would be unavailable, there would not be an incentive to install GFPPs.

As explained before (see Figure 4.5), the carbon capture (CC) capacity is installed for two reasons: to avoid CO₂ emission prices and to provide CO₂ feedstock for the P2G process. If no P2G technology is available, the second incentive disappears leaving only the first. Recall however, that an increasing RES share reduces the amount of CO₂ produced by GFPP, making CC technology less economically efficient and resulting in a declining CC capacity for an increasing RES share. For a CO₂ emission price of 50 €/ton, the CC capacity becomes even zero from 70% RES share onward, as shown on the right panel of Figure 4.33.

4.5.13 Influence of curtailment availability

Unavailability or ‘non-permission’ of curtailment leads to a ‘better’ use of iRES generation, by installing slightly less iRES capacity but increasing (expensive) storage capacity to capture all peaks of RES oversupply. Figure 4.34 shows the

installed electrolyzer and methanizer capacity, for an increasing imposed RES share and a 50 €/ton CO₂ emission price.

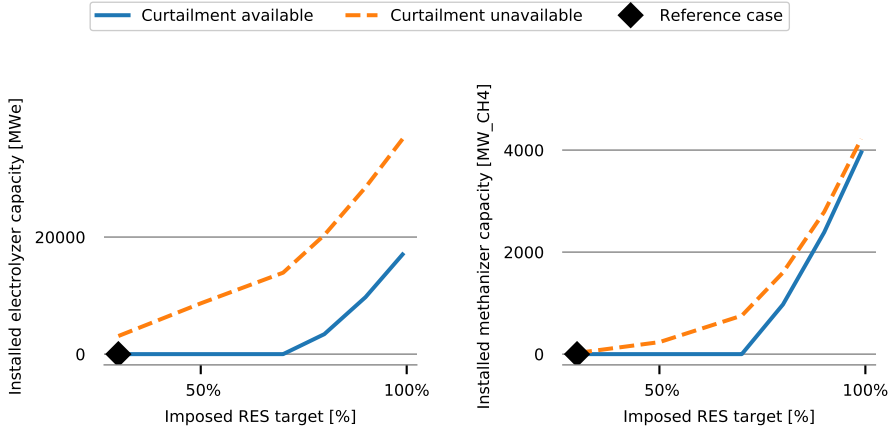


Figure 4.34: Installed electrolyzer capacity (left panel) and methanizer capacity (right panel) for increasing RES targets, with and without curtailment available; no capacity legacy between cases; CO₂ sequestration and batteries available; iRES mix as in reference case and a CO₂ price of 50 €/ton.

The left panel of Figure 4.34 shows a significant increase in installed electrolyzer power capacity when curtailment is not allowed which can be compared to the (smaller) increase in methanizer power capacity, shown in the right panel. Since curtailment is not allowed, more electrolyzer capacity is required to capture the irregular peaks of instantaneous iRES oversupply. Although these peaks have a relative high magnitude, the energy content of them is rather low, resulting in only a small increase in energy stored via P2G and hence, there is no need to greatly increase the methanizer power capacity. To deal with the mismatch between the time of hydrogen production and consumption, a greater amount of hydrogen storage is installed in cases if curtailment is not allowed compared to cases where it is allowed.

Figure 4.35 shows the installed methane storage capacity and the yearly amount of synthetic methane produced, for the cases with and without curtailment.

It is clear from Figure 4.35 that, although P2G becomes economically interesting for lower RES targets if curtailment is not allowed, the amount of produced synthetic methane is not greatly increased compared to cases where curtailment is allowed.

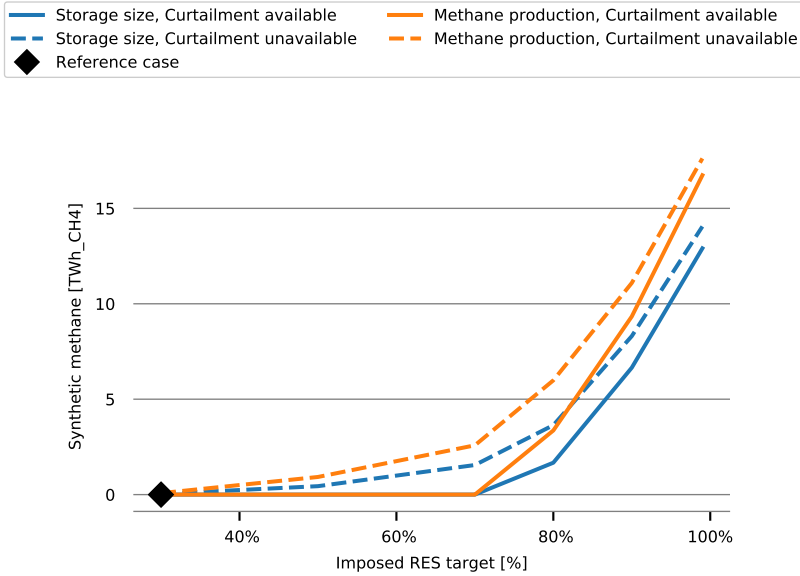


Figure 4.35: Installed methane storage capacity and amount of produced synthetic methane for increasing RES targets, with and without curtailment available; no capacity legacy between cases; CO₂ sequestration and batteries available; iRES mix as in reference case and a CO₂ price of 50 €/ton.

Figure 4.36 shows the installed GFPP and carbon capture capacity both for cases where curtailment is and is not allowed.

The left panel of Figure 4.36 shows a lower GFPP capacity if curtailment is not allowed (for lower iRES penetrations). This may seem counter intuitive since, for the same cases, slightly more synthetic methane is produced. This can be explained however, by the increase in installed battery capacity (to be shown below), which provides extra power capacity to cover the peaks in residual demand and hence provide the opportunity to operate the GFPPs more as base load, generating more energy with less installed power capacity.

The right panel of Figure 4.36 shows a slight increase in carbon capture capacity for cases where curtailment is not allowed. This increase corresponds to the increase in produced synthetic methane as shown on Figure 4.35. Since no CO₂ is sequestered in the cases with increased CC capacity, although sequestration is available, it is clear that the additional capture capacity is used to provide CO₂ feedstock to the methanizer unit.

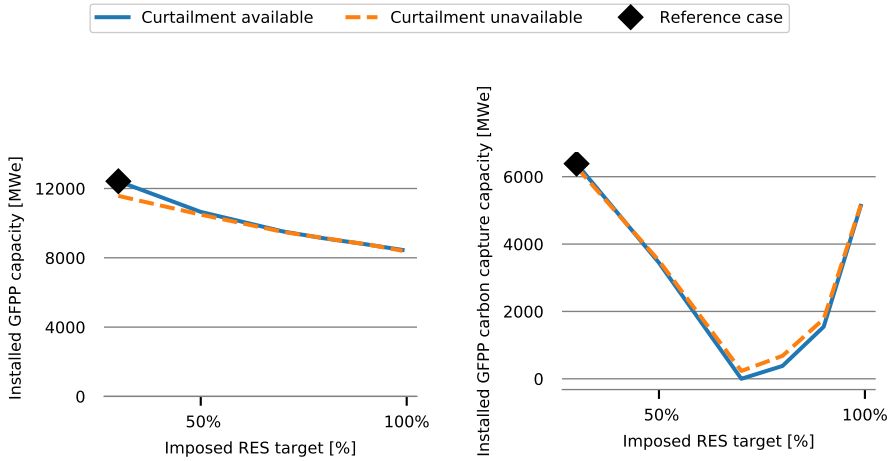


Figure 4.36: Installed GFPP capacity (left panel) and GFPP carbon capture capacity (right panel) for increasing RES targets, with and without curtailment available; no capacity legacy between cases; batteries, P2G and CO₂ sequestration available; iRES mix as in reference case and a CO₂ price of 50 €/ton.

Figure 4.37 shows the installed battery capacity for cases with and without curtailment.

Similar to the installed P2G capacity, an increase in battery capacity is observed if curtailment is not allowed. Since the peaks in iRES generation cannot be curtailed, more storage is needed to store them and hence both battery and P2G capacity increases.

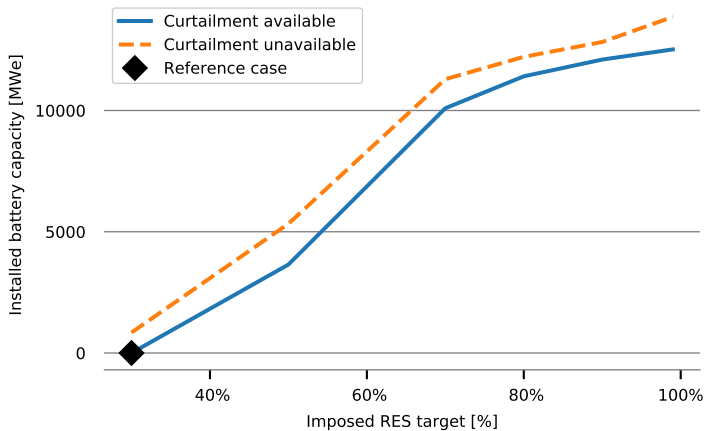


Figure 4.37: Installed battery capacity for increasing RES targets, with and without curtailment available; no capacity legacy between cases; CO₂ sequestration and P2G available; iRES mix as in reference case and a CO₂ price of 50 €/ton.

4.6 Results considering the hydrogen sector

All the parameter influences above discussed in Section 4.5 have the explicit assumption (as indicated in the first paragraph of Section 4.5) that all produced hydrogen would be used for later conversion to synthetic methane via the Sabatier process. No industrial hydrogen demand was accounted for.

The following results will illustrate the effect of optimizing both the electricity and hydrogen sector compared to only optimizing the electricity sector (as was done in the previous subsections). As specified earlier, a flat industrial hydrogen load of 1799 MW_{H₂} is used. This load can be covered by steam methane reformers (SMRs), fueled by methane (both synthetic and fossil), and by electrolyzers. During the following discussion, the hydrogen originating from electrolysis will be termed electric hydrogen (E-H₂). In some of the following cases an additional constraint is imposed, limiting the use of electric hydrogen to serve at most 25% of the instantaneous hydrogen load. In the other cases, this constraint is not imposed.

Note that when the hydrogen sector is accounted for, the iRES (solar PV and wind) share is imposed to both the electricity and hydrogen sector, meaning that a greater amount of renewable electrical energy needs to be generated to

achieve an equal RES share compared to cases without the hydrogen industry taken into account. Similarly, the CO₂ emission price also applies to both the electricity sector and the hydrogen industry.

Figure 4.38 shows the installed electrolyzer and methanizer capacity for an increasing imposed RES share both with and without the hydrogen load accounted for. (The curves for the “No H₂ load” case are identical to those shown in Figure 4.3.)

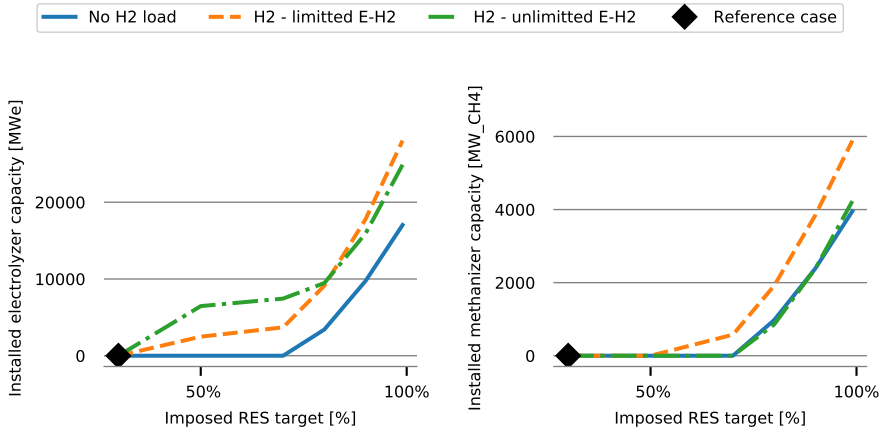


Figure 4.38: Installed electrolyzer capacity (left panel) and methanizer capacity (right panel) for increasing RES targets, with and without hydrogen load accounted for; no capacity legacy between cases; CO₂ sequestration, batteries and curtailment available; iRES mix as in reference case and a CO₂ price of 50€/ton.

From Figure 4.38 we learn that if the hydrogen industry is considered, much more electrolyzer capacity (left panel) is installed, while this is not necessarily the case for methanizer capacity (right panel). Additional electrolyzer power capacity is installed since, for increasing RES targets, it is economically efficient to supply the industrial hydrogen load with electric hydrogen. For cases with an upper limit on the share of electric hydrogen share to be supplied directly to the hydrogen load, the electric hydrogen is first converted to synthetic methane and later converted in the SMRs. This explains the higher installed methanizer capacity for these cases, shown on the right panel of Figure 4.38. If no upper limit is imposed on the direct electric hydrogen supply, then almost no additional methanizer capacity is installed compared to the cases where no hydrogen load is considered.

The increase in produced synthetic methane for cases with a limited direct use of electric hydrogen, is also obvious from Figure 4.39, which shows the synthetic methane production and storage size for increasing imposed RES targets.

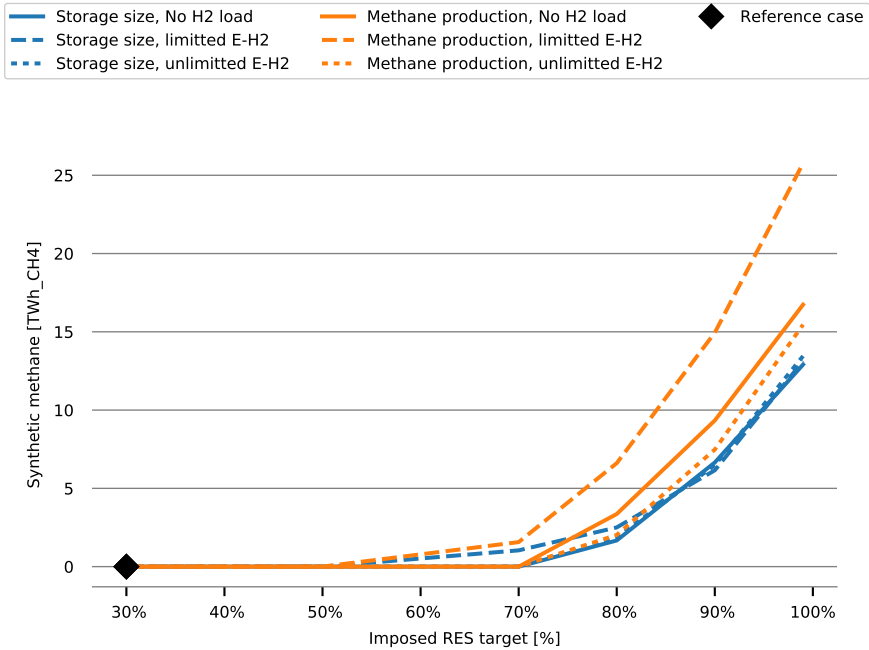


Figure 4.39: Installed methane storage capacity and amount of produced synthetic methane for increasing RES targets, with and without hydrogen load accounted for; no capacity legacy between cases; CO₂ sequestration, batteries and curtailment available; iRES mix as in reference case and a CO₂ price of 50€/ton.

If there is no upper limit on the direct use of electric hydrogen to supply the hydrogen load, even less synthetic methane is produced (the orange dotted curve in Figure 4.39) compared to the cases where no hydrogen load is accounted for (the orange solid curve). This indicates that a larger share of the electricity from iRES can be consumed directly (via H₂ electrolysis), without the need for storage. A similar trend is observed for the use of battery storage.

The size of the methane storage capacity is almost equal for all cases, in contrast to the size of the hydrogen storage (not shown in the figure) which is larger when a hydrogen load is considered, in comparison with cases without hydrogen load.

Figure 4.40 shows the installed GFPP and GFPP carbon capture capacities for cases with and without hydrogen load.

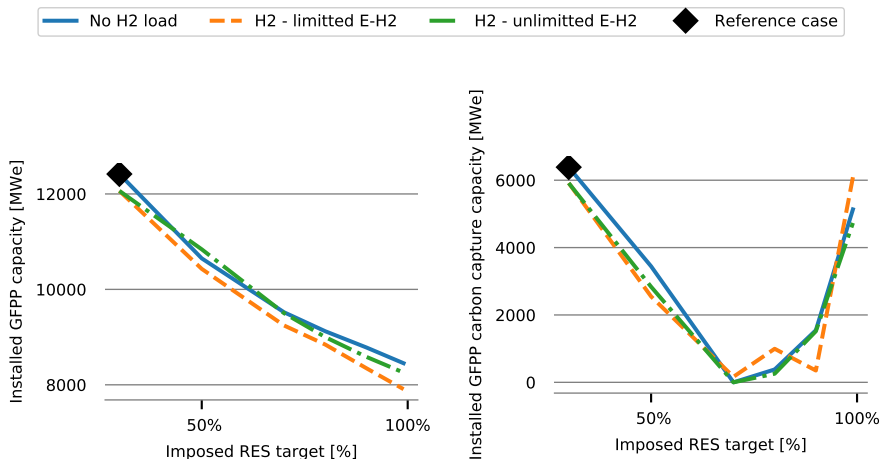


Figure 4.40: Installed GFPP capacity (left panel) and GFPP carbon capture capacity (right panel) for increasing RES targets, with and without hydrogen load accounted for; no capacity legacy between cases; batteries, P2G, curtailment and CO₂ sequestration available; iRES mix as in reference case and a CO₂ price of 50€/ton.

From the left panel of Figure 4.40 it is clear that for most imposed RES targets, the GFPP capacity is slightly lower if a hydrogen load is considered. This is mainly due to the installed iRES capacity which is increased, leading to a slightly lower peak residual demand which should be covered by the GFPP, which is also confirmed by the GFPP load duration curve shown in Figure 4.41.

The GFPP carbon capture capacity differs only slightly between the different cases, except for the case with limited electric hydrogen load, since more carbon capture capacity is required to provide more CO₂ feedstock to the methanizer as significantly more synthetic methane is produced (see right hand side of Figure 4.40). Note that the GFPP carbon capture capacity in the limited E-H₂ case shown in Figure 4.40 is lower than for the other cases for the 90% RES target. Since the required CO₂ can also be captured from the SMRs, in this case the model opts to install more SMR CC instead of GFPP CC. The total amount of capture capacity (for SMRs and for GFPPs combined) installed in the limited electric hydrogen case is, however, always higher than for the other cases.

Figure 4.41 shows the load duration curve of the GFPP for cases with and without hydrogen load accounted for, with an imposed RES target of 80%.

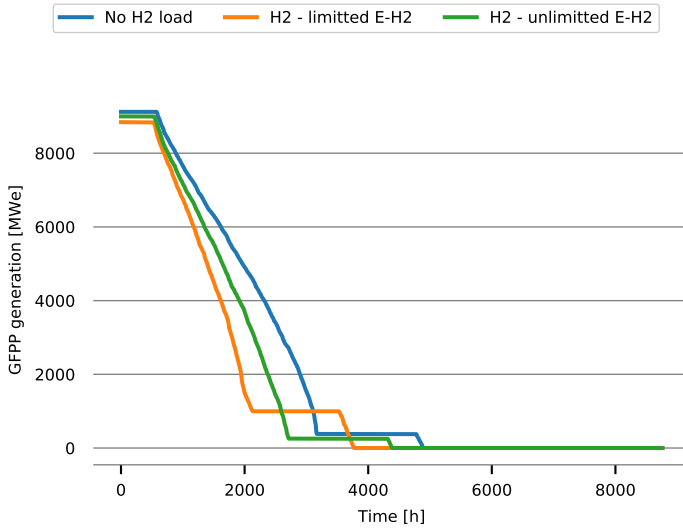


Figure 4.41: Load duration curves of GFPP for cases with and without hydrogen load accounted for, CO₂ sequestration, batteries, P2G and curtailment available, CO₂ emission price of 50€/ton and an imposed RES target of 80% starting from a greenfield.

The peak load served by the GFPPs decreases when the hydrogen load is accounted for, since more iRES capacity is installed which can serve the instantaneous electrical load directly. Furthermore, the ‘flat’ part in the GFPP load duration curves is more pronounced in the limited electric hydrogen case, again referring to the large amount of CO₂ required as feedstock.

4.7 Summary and conclusions

This chapter has presented a study investigating the possible role of power-to-gas (P2G) in future energy systems and the effect of different boundary conditions on the cost-optimal amount of installed P2G capacity. First, the general context of this study was introduced together with a discussion of the sustainability of synthetic fuels when used for energy storage. Next, the energy system investment model was discussed and parameter data for the different cases were presented. This was followed by a thorough discussion of the results.

The results of different case studies, show (given all the assumptions of this

study) that P2G capacity only becomes economic as energy storage technology for high imposed RES shares, above 70%. The installed capacity increasing with an increasing RES target, up to 17 GW_e electrolyzer capacity (relative to 122 GW_e iRES capacity) for a 99% RES target. When no other storage technology would be available or the alternative storage technology would be very expensive, P2G becomes cost-efficient for imposed RES shares of 50%. The specific composition of the iRES portfolio has no significant impact on these observations.

Similar to the P2G capacity, an increase in battery capacity is observed for increasing RES targets, up till 12.5 GW_e for a 99% RES target. If P2G technology is unavailable or very expensive, the installed battery capacity increases quasi exponentially for RES targets above 80%, to more than 54 GW_e for a 99% RES target. In cases where curtailment is not allowed, both battery and P2G capacity increase to make sure all peaks of surplus iRES generation are stored.

Since gas-fired power plants (GFPPs) are both used to serve the residual (peak) demand with conventional natural gas and as discharge technology for energy stored as synthetic methane, it is observed that a decrease in battery capacity usually leads to an increase of GFPP capacity and vice versa, with an increase up to almost 43% GFPP capacity in the 99% case when batteries become 'unavailable'. While an increase in P2G capacity leads to an increase in GFPP capacity and vice versa, there is no GFPP capacity installed in the 99% RES case when P2G is unavailable. This is also observed when capacity legacy is assumed for the subsequent cases with increasing imposed RES shares, where it is seen that a high GFPP capacity legacy is favorable for P2G installation since then more discharge capacity is already available. The increase in P2G is, however, more modest, with an increase of 5% in the 99% RES case.

The effect of CO₂ sequestration availability depends on the CO₂ emission price. If a low CO₂ emission price is imposed, the CO₂ sequestration availability has almost no effect on the installed storage and GFPP capacities since otherwise sequestered CO₂ is now emitted at an (only slightly) increased cost. If, however, a very high CO₂ emission price is imposed (1000 €/ton and above), it is most economic for the electricity system to avoid the emission of additional CO₂ through conventional natural gas, and hence the installed capacities of GFPPs, iRES and storage (battery and P2G), will be similar to those of high imposed RES targets, even if no high (minimal) RES target is imposed. In such cases a large iRES and storage capacities are installed, both battery and P2G.

In conclusion, without industrial hydrogen demand, when multiple storage technologies are available to install, P2G becomes cost-efficient for high imposed RES shares, above 70% or if CO₂ sequestration is not an available option in

combination with very high CO₂ prices, 1000 €/ton and above. P2G and gas-fired power plants (GFPPs) are both required to store energy indirectly via synthetic methane and convert it back to electricity. When GFPP (or P2G) is already available, it is an additional incentive to install P2G (or GFPP) capacity.

If an external hydrogen industry is accounted for (which is subjected to the same imposed RES target as the electricity system), allowing the electrolyzer to (partly) serve the hydrogen load with electrically produced hydrogen, an increase in electrolyzer capacity of 6-7 GW_e is observed, depending on the imposed RES target. The effect on other installed capacities is minor, except for the case where only part of this instantaneous hydrogen load can be served directly by electric hydrogen. In such case, the only way to meet the imposed RES target is to produce additional electric hydrogen which is first converted to synthetic methane to reform this synthetic methane at a later instant to hydrogen using a steam methane reformer (SMR). In such cases, also an increase in methanizer capacity between 550 MW_{CH₄} and almost 2000 MW_{CH₄}, depending on the RES target, is observed.

Chapter 5

Generalization of energy storage sizing: power versus energy requirements

This chapter is mainly based on:

Belderbos, A., Virag, A., Delarue, E. and D'haeseleer, W. *Considerations on the need for electricity storage requirements: Power versus energy.* Energy Conversion and Management 143 (2017), 137-149.

This chapter investigates the link between the cost-efficiency of different storage technologies and the instantaneous electrical power demand and renewable generation profile. The aim of this chapter is to gain understanding of what drives the need for different storage technologies, such as power-to-gas (P2G) and batteries. Compared to the analyses presented in Chapter 4, the current chapter focuses on variations in the demand and iRES generation profiles.

The chapter is organized as follows: a general introduction of the work is presented in Section 5.1. Next, Section 5.2 describes the energy system under consideration, the computation approach, the storage technology characteristics and discusses the general storage principles. In the subsequent sections, the storage portfolio is optimized for different demand and renewable generation profiles. This is done first for methodological block profiles to derive the basic storage principles in Section 5.3. Afterwards more complex methodological sinusoidal profiles are investigated in Section 5.4, followed by real profiles in Section 5.5. Conclusions finalize this chapter in Section 5.6.

5.1 Introduction

Many different electricity storage technologies exist [65, 15], which are divided in two categories in this chapter. A first type of storage technology refers to those where charging power, discharging power and energy rating are coupled, such as most types of batteries. For this type of storage technology, all power and energy ratings are fixed, or locked in, once one of them is determined. In the remainder of this chapter, this storage type is referred to as '*integrated storage*'. For a second type of storage technology, charging power, discharging power and energy rating can be installed (and operated) independently from each other, such as power-to-gas-to-power, compressed air energy storage and redox flow batteries. This storage type is referred to as '*disjoint storage*' in the remainder of the chapter.

5.1.1 Objective

The objective of this chapter is to assess how the temporal variations of a so-called *remaining load profile*¹ impact the cost-optimal installed storage capacity in an optimal storage portfolio. A new metric is presented and introduced to link the optimal installed storage capacity with the shape of the remaining load profile. Special attention is given to the difference between *power* and *energy* ratings of the installed storage capacity.

A welfare optimal generation and storage portfolio can be calculated to serve a given load at the lowest cost. The precise constellation of such optimal portfolio not only depends on numerous factors such as investment cost, operational costs, technical plant characteristics and environmental targets, but it also strongly depends on the time-varying profile of load and intermittent renewable energy sources (RES) generation. It is precisely this relationship between the optimal storage portfolio, both in terms of power and energy, and the specific shape of the remaining load profile that is the subject of the research reported in this chapter. The objective of this chapter is to determine the optimal portfolio for a given set of remaining load profiles, to derive the link between profile and portfolio and to formulate general rules regarding storage investments which are applied to historical load profiles and iRES generation profiles.

¹This remaining load is defined as the difference between the instantaneous electrical power demand and electrical power generation, both renewable and conventional and is thus the profile which should be served by storage. The remaining load differs from the "residual demand", "residual load" or "net load" often used in literature to describe the difference between overall demand and intermittent renewable generation but which does not account for conventional generation.

5.1.2 Related work

Several energy storage sizing studies exist which investigate storage sizing either for a specific scenario or in a general theoretical way. Some studies exist which analyze specific case studies [70, 71]. We consider this as a first category of studies. For example Kaldellis [70] determines the optimal storage size in combination with wind and PV to replace thermal generation in a micro grid. The same author analyzes the required size of a compressed air energy storage system to maximize wind energy contribution on the island of Crete [71]. Our study falls in a second category, i.e., of general theoretical storage sizing studies. Within such studies, the optimal storage size can be determined in combination with PV [72], in combination with wind [73] or in a system containing both conventional and renewable generation [74, 75, 76]. Our study contributes to the limited work of the last category where storage is sized in a general energy system setting. Ru et al. [74] propose an upper bound on storage size to minimize the electricity purchase cost from the grid in a PV battery system. They characterize the exact storage size for a case with ideal PV generation and constant load and show how the optimal storage size changes as a function of a change in constant load level. The energy storage capacity is optimized while the power capacity is assumed to be fixed. Makarov et al. [75] determine the maximum required storage system size, both in terms of power and energy, to balance wind generation and load. They therefore decompose the balancing power signal in four different frequency ranges, corresponding with different technical storage characteristics. Barton and Infield [76] use a probabilistic method to predict the ability of different storage technologies and sizes to increase the penetration of intermittent generation using the frequency spectrum of historic wind profiles. They focus solely on the installed power capacity, however.

5.1.3 Contributions

This chapter presents a contribution to the existing literature [74, 75, 76] by going beyond the state of the art in the following aspects:

- Our study builds further upon the existing literature and optimizes not only storage *power* capacity, but both *energy* and *power* capacity for 'disjoint' storage technology and compares this to 'integrated' storage technology.
- Our study accounts for possible curtailment of intermittent RES generation, which allows storage to be used for temporal arbitrage in general rather than for compensating an imbalance signal.

- In comparison to Barton and Infield [76], our study optimizes the storage size to accommodate a remaining load profile rather than only accounting for a wind generation profile.
- Ru et al. [74] analyze the optimal energy storage capacity for a scenario with constant load and variable PV generation. Our work adds to their analysis as time varying profiles for both load and iRES generation are investigated.

5.2 Input data, assumptions and general principles

In this section, the considered system is presented. The approach to calculate an optimal storage portfolio is given, followed by characteristics of generation and storage technologies. Finally the general storage principles are explained.

5.2.1 System description

This study focuses on the electricity system with the demand and renewable generation profiles as key external parameters, subject to a renewable target and taking into account the characteristics of generation and storage technologies. Different demand and iRES generation profiles are used to determine how different remaining load profiles impact the constellation of the optimal storage portfolio. In a first instance, a flat methodological remaining load profile is used to gain basic insights, followed by a sinusoidal profile to make the link with realistic profiles. Finally, real profiles from the Belgian electricity system [77] are used to apply the presented metric and verify the link between the remaining load profile and the installed storage portfolio which was found by studying methodological flat and sinusoidal profiles. The imposed renewable target is set at 100% of the electrical energy demand for the methodological profiles. 100% implies that all electrical energy is generated from renewable sources, i.e., no electrical energy is generated from fossil fuels. For the real profiles, the renewable target is varied between 60% and 100%.

In a first instance, using a methodological demand and iRES generation profile and imposing a RES target of 100 % provides results which are not directly applicable to realistic scenarios but it simplifies interpretation of the results for explaining the mechanisms determining the optimal storage portfolio.

5.2.2 Computational approach

For complex demand and generation profiles, the optimal portfolio is calculated using the investment model introduced in Chapter 4 and described in Appendix C.

For simplified methodological demand profiles and iRES generation profiles, the optimal generation and storage portfolios are calculated analytically. This allows for a better understanding of the mechanisms determining the optimal amount of storage in a portfolio. Note that these analytical optimizations meet the same constraints as the ones imposed in the investment model. The optimization always starts from a greenfield. The generation and storage portfolios are optimized from a welfare perspective, therefore minimizing the total system cost. The total cost includes the investment cost and fixed operational and maintenance costs. The entire electrical power demand has to be served at all times, either by iRES generation or by discharging stored energy. Curtailment of iRES is allowed. The time resolution of demand and generation profiles is one hour.

5.2.3 Available generation and storage technologies

For all numerical calculations, specific generation and storage technologies are chosen to serve as typical examples. Realistic demand and iRES generation profiles are obtained from the Belgian Transmission System Operator Elia [77] while the methodological profiles are carefully composed and will be explained further on. The cost characteristics of different iRES technologies are given in table 5.1. Note that not all discount rates are equal to reflect different investment risks for different technologies. The iRES cost characteristic are equal to the ones used in the reference case of Chapter 4.

Table 5.1: Cost and operational characteristics of onshore wind, offshore wind and solar PV [65].

	Unit	Onshore	Offshore	Solar PV
CAPEX	[€/kW]	1700	4900	1600
Fixed OPEX	[€/kW/y]	25.5	171.5	16
Lifetime	[y]	20	20	20
Discount rate ^a	[%]	5	7.5	5

^a Discount rates are risk-adjusted

The charging technology for disjoint storage is represented by power-to-gas (P2G), effectively comprehending the electrolyzer and methanizer. Gas-fired power plants (GFPPs) can be used as discharge capacity for the disjoint storage technology and as conventional generation capacity (combined cycle gas turbines (CCGTs) have been used as GFPP-technology). Technical and cost characteristics for the storage and GFPP technologies are presented in table 5.2. When GFPPs are used as discharge capacity, carbon capture (CC) is always used in combination with the GFPPs to have a closed carbon loop (see Chapter 4). It is assumed that the synthetic methane can, in a first instance, be stored in existing natural gas infrastructure and gas storages. Therefore, no additional cost is taken into account for the energy storage capacity of the disjoint technology. The integrated storage is represented by NaS batteries [66]; it is assumed here that the power capacity can be used fully as charge and discharge capacity. The available energy storage capacity is coupled to the charge and discharge capacity by the energy-to-power ratio (EP_i) which ranges between 1 Wh/W and 10 Wh/W for most types of batteries. More specific battery types, like redox flow batteries, could have higher energy-to-power ratios but since their energy storage capacity is sized independently of the charging and discharging power capacity, this storage type is here categorized as disjoint technology.

The techno-economic characteristics shown in Table 5.2 are similar to the ones used in Chapter 4. Note that, different from Chapter 4, the charging technology P2G is modeled as one charging unit comprehending the electrolyzer and methanizer (a hydrogen buffer is not considered). Likewise, for the discharging technology, GFPP and carbon capture unit are combined and modeled as one discharging unit.

Table 5.2: Cost and operational characteristics of different storage technologies [67, 66]. 'Integrated' refers NaS batteries, and 'Disjoint' refers to P2G (electrolyzer and methanizer) for charging and CCGT with CC for discharging.

	Unit	Integrated	Disjoint		
			Charging	Dischar.	Energy
Efficiency (η)	[%]	90 ^a	60	47 ^b	-
CAPEX	[€/kW]	1500	1500	1900	0
Fixed OPEX	[€/kW/y]	15	30	66	0
Lifetime	[y]	12	20	20	-
Discount rate	[%]	5	5	5	-
E/P ratio (EP_i)	[Wh/W]	7.2	-	-	-

^a Single-trip efficiency

^b 55% if CCGT would be used without CC

5.2.4 General storage principles

As mentioned in the introduction, storage technologies are defined by three main operational characteristics: charging power capacity, discharging power capacity and energy storage capacity. Depending on the specific remaining load, each of these characteristics can determine the minimal necessary installed storage capacity.

Power considerations of storage

The chronological remaining load, both positively and negatively, as shown on Figure 5.1a should be taken care of entirely by storage when only iRES generation and storage can be used to serve the electrical energy demand, i.e., a renewable electrical energy target of 100%. A positive remaining load represents an electrical power load which is not served by iRES generation directly. Therefore, the highest positive remaining load determines the necessary discharge power capacity of the storage technology, indicated by c^d in Figure 5.1a. A negative remaining load represents a surplus of iRES generated electrical power, of which the accompanying energy can be stored. If curtailment of iRES generation is not allowed, the most negative remaining load determines the necessary charging capacity. However, if curtailment of iRES generation is allowed, the necessary charging capacity can be less than the most negative remaining load, as long as the charging capacity is high enough to take-up the necessary amount of electrical power. This is shown by the remaining load duration curve, a curve constructed by sorting all remaining load levels in descending order as presented in Figure 5.1b. The required charging capacity is indicated as c^c on Figure 5.1b. It can be seen that the necessary charging capacity is independent of the temporal characteristics of the remaining load.

Energy considerations of storage

The necessary energy storage capacity is determined by the maximum amount of electrical energy that needs to be stored over a given time period, which depends on the temporal characteristics of the remaining load. Indeed, storing a total amount of energy over a certain period requires less installed energy storage capacity if the number of charging-discharging cycles increases.

For disjoint storage technologies, the installed capacities will be determined by the necessary charging, discharging and energy capacity separately. For the integrated storage, the installed capacity is determined by the highest necessary

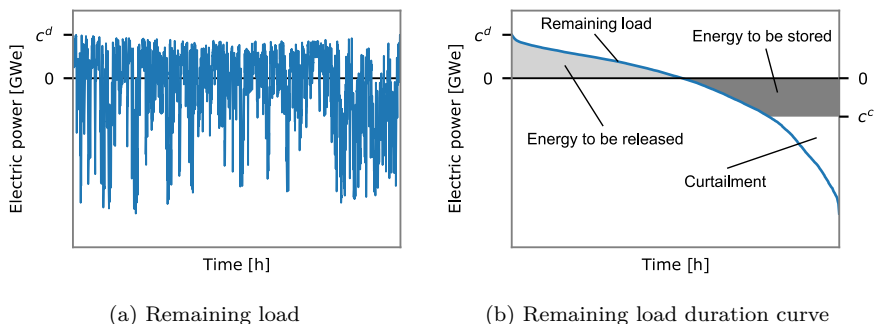


Figure 5.1: Chronological remaining load curve and remaining load duration curve with released and stored energy. The highest positive remaining load determines the required discharge capacity c^d . Surplus iRES generation is given by a negative remaining load. Therefore c^c depicts the required charging capacity.

capacity of the three capacity types. The next section will show how each storage characteristic can determine the installed capacity.

5.3 Methodological case: block profiles

A methodological block profile will be used in this section to analytically calculate the necessary installed storage capacity and optimal storage portfolio. This way, a good understanding of the mechanisms which determine the necessary and optimal capacity can be obtained.

5.3.1 Necessary storage capacity

A block profile is created with a flat load of P_d for the entire time horizon, between $t = 0$ and $t = t_p$. The iRES generation profile is a block profile with a generation power of P_{RES} equal to the amount of installed iRES capacity between $t = 0$ and $t = t_s$ and equal to zero for the remainder of the time horizon ($t_s < t < t_p$). t_s refers to the time with surplus renewable generation and t_p refers to the entire storage period, comprising of a charging and discharging cycle. Both load and iRES generation profiles are shown in Figure 5.2.

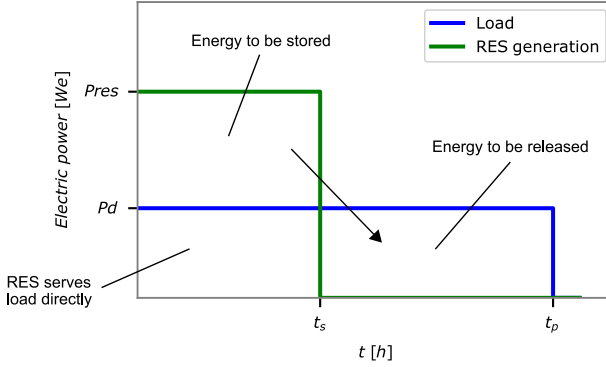


Figure 5.2: Methodological load and iRES generation block profiles with parameters t_s and t_p . The amount of electrical energy to be stored is always higher than the amount of electrical energy to be released if the storage unit has a round-trip efficiency lower than 100%.

For given and fixed values of P_{RES} and P_d , when the entire electrical energy demand needs to be served by renewable electricity, it is clear that there should be a time period with surplus renewable generation, $t_s > 0$, and no storage is needed if $t_s = t_p$. For $0 < t_s < t_p$, the amount of storage capacity depends on both t_s and t_p and should be able to serve the electrical power demand between t_s and t_p . For the flat load and generation profiles presented in Figure 5.2, the necessary charging power, discharging power and energy capacity can be calculated analytically as presented in the equations below. The presented formulation is applicable to both the integrated and the disjoint technology. In these equations c^c , c^d and c^e are the charging power capacity, discharging power capacity and energy storage capacity, respectively. The charging and discharging efficiencies are given by η^c and η^d while Δt is the time step (1h). P_d , t_s and t_p are as shown on Figure 5.2.

$$c^c = \frac{\sum_{t=t_s}^{t_p} (P_d(t) \cdot \Delta t)}{\eta^c \cdot \eta^d} \quad (5.1)$$

$$c^d = \max(P_d) \quad (5.2)$$

$$c^e = \frac{\sum_{t=t_s}^{t_p} (P_d(t) \cdot \Delta t)}{\eta^d} \quad (5.3)$$

The effect of the surplus (t_s) and shortage ($t_p - t_s$) duration

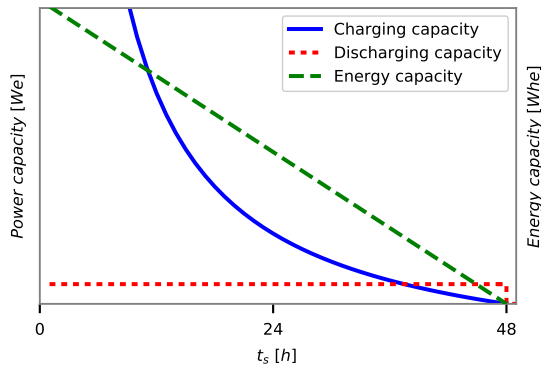
For disjoint storage technologies, charging, discharging and energy capacity are chosen independently. The amount of each capacity type depends on t_p and t_s . Figure 5.3a shows the installed capacity for a block profile of the type shown in Figure 5.2, but with a fixed $t_p = 48h$ and a varying t_s . Note that the horizontal axis shows t_s and thus expresses the number of hours where the demand is directly served by RES.

The necessary installed integrated storage capacity is shown in Figure 5.3b. For integrated storage technologies, it is assumed that both charging and discharging can occur at full installed power capacity. The energy capacity is linked to the power capacity by the energy-to-power ratio (EP_i). This ratio determines the amount of energy that can be stored per installed amount of power capacity, i.e., it reflects the maximum possible charging or discharging duration. The resulting amount of installed capacity is thus equal to the maximum of charging, discharging and energy capacity as given by the following equation:

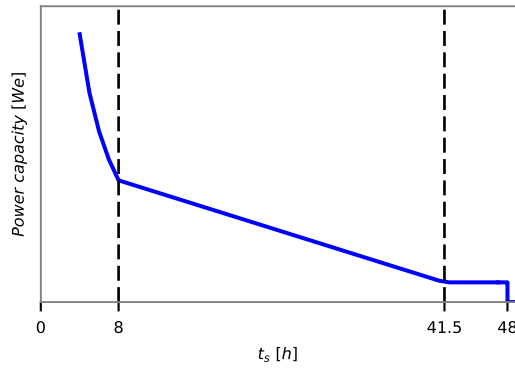
$$c_i = \max(c_i^c, c_i^d, \frac{c^e}{EP_i}) \quad (5.4)$$

The energy-to-power ratio depends on the specific storage technology used and can vary greatly. Although the exact value of the E/P-ratio influences specific results, it has no influence on the general conclusions presented in this work. The E/P-ratio used in this study is 7.2 Wh/W, which is representative for sodium sulfur batteries [66].

Figure 5.3b shows three different zones, characterized by a different capacity constraint that determines the installed capacity. At the uttermost left side of the graph, less than 8 hours of surplus iRES are available while more than 40 hours of the demand need to be served by stored energy ($t_p = 48h$). Therefore, all necessary energy should be stored in a limited number of hours, leading to high charging capacity. In this left interval, the installed storage capacity is thus determined by the necessary charging capacity. At the uttermost right side, more than 42 hours of the demand are served directly by iRES and only a few hours of storage are necessary. In this case the necessary discharging power will determine the installed capacity. In the middle zone of the graph, the amount of energy capacity (per unit time) is bigger than the amount of



(a) Disjoint capacity



(b) Integrated capacity

Figure 5.3: Installed power and energy capacity as a function of the length of the time interval with surplus iRES generation (t_s) for a fixed time horizon (t_p) of 48h. The upper figure shows the installed charging, discharging and energy storage capacity separately. The lower figure shows the installed integrated capacity. Here all integrated capacity is expressed by its power capacity. When the necessary energy capacity determines the installed integrated capacity (in the middle part of the graph), it is converted to power capacity via the energy-to-power ratio.

necessary charging and discharge capacity. Therefore, the energy capacity will determine the installed storage capacity. The precise amount of surplus time t_s which marks the transition point for which each power or energy rating

determines the installed capacity can be expressed by setting c_i^c equal to c_i^e/EP_i and c_i^d equal to c_i^e/EP_i respectively, as given in Eqs. (5.5)-(5.6).

$$c_i^c = \frac{c_i^e}{EP_i} \quad \text{when} \quad t_s = \frac{EP_i}{\eta^c} \tag{5.5}$$

$$c_i^d = \frac{c_i^e}{EP_i} \quad \text{when} \quad t_s = t_p - EP_i \cdot \eta^d \tag{5.6}$$

The effect of varying t_p

Increasing the load duration t_p leads to a relative increase of the interval where energy capacity determines the installed storage capacity in the integrated case, as shown in Figure 5.4. The figure shows that the three zones are visible independent of the duration of t_p , although the precise value of t_s at which a different characteristic becomes constraining depends on the energy-to-power ratio of the storage technology.

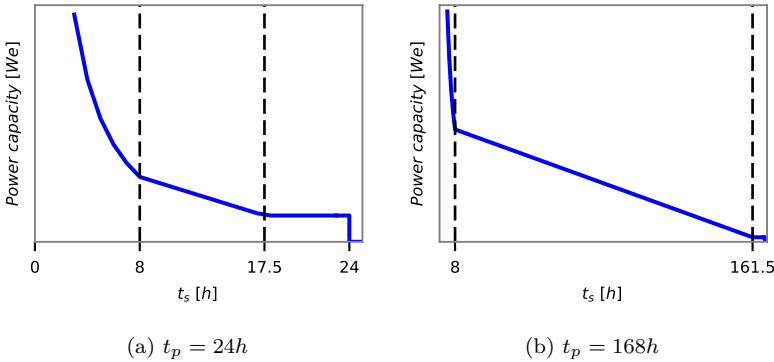


Figure 5.4: Installed integrated storage capacity as a function of t_s for different fixed t_p . In both cases the energy-to-power ratio EP_i is still 7.2 h.

In Figure 5.5, t_p is varied while keeping t_s equal to $\frac{t_p}{2}$. For the disjoint storage technology (Figure 5.5a), discharge power is constant as the demand is flat. The energy storage capacity increases linearly with an increasing t_p as the time interval with a shortage of renewable generation, $\frac{t_p}{2}$, increases linearly with t_p . The necessary charging power is independent of t_p since the increase in energy to be stored is countered by a proportional increase in the time interval

with a surplus of renewable generation. For the integrated storage technology (Figure 5.5b), the installed capacity is determined by the necessary charging power for low values of t_p while for higher values of t_p it is determined by the necessary energy capacity. The precise tipping point between the two zones, here $t_p = 16h$, depends on the energy-to-power ratio of the storage technology (being 7.2 h in the figure shown).

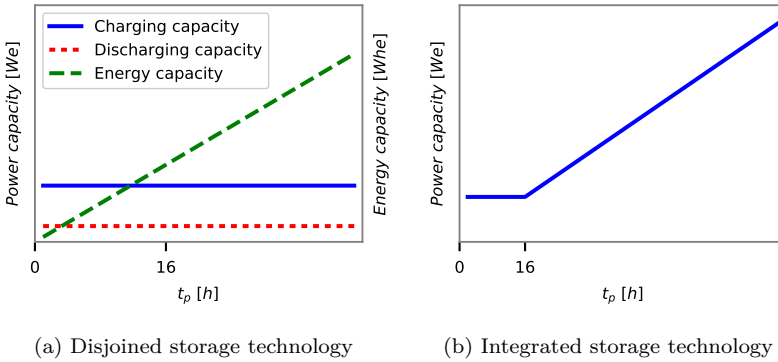


Figure 5.5: Installed storage capacity as a function of t_p with $t_s = \frac{t_p}{2}$, for both types of storage technologies.

A continued series of block profiles

Several single block profiles as used above (Figure 5.2) can be added sequentially together to form a profile of identical block profiles. For a profile consisting of identical block profiles, equations (5.1)-(5.3) can be used to calculate the necessary capacities. It is thus possible to identify the same effects of a varying t_s and t_p as above. The findings for a single storage cycle can thus be generalized for a continued set of storage cycles. We can therefore conclude that a repetitive (continued) set of block profiles can be represented by a single block profile.

5.3.2 Optimal storage portfolio

The total storage cost for block profiles as a function of a varying t_s is shown in Figure 5.6 for $t_p = 168h$. This cost consists of two parts: the investment cost of all installed storage related capacity (charging capacity, discharging capacity and energy storage capacity for the disjoint technology) and the

investment cost of iRES generation capacity necessary to compensate for storage losses. This means that the cost of iRES generation not consumed in storage efficiency losses is not account for in this storage cost. The iRES generation cost includes the investment cost iRES generation which serves the electricity load directly, which is discharged after storing or which is curtailed. The solid line in Figure 5.6 represents the storage cost of the integrated storage technology. In accordance with the results from Figure 5.4, there are again three zones visible, indicating a part where charging capacity determines the installed capacity, a part where energy capacity is determining and a part where discharge capacity is determining. In this example, the disjoint technology is often cheaper to install when the required energy capacity determines the installed integrated capacity.

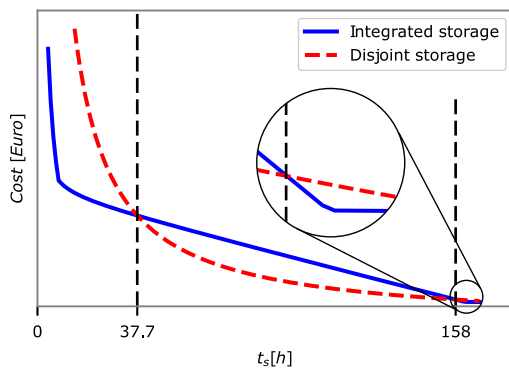


Figure 5.6: Total storage cost for integrated and disjoint technologies as a function of t_s for $t_p = 168h$.

The optimal storage portfolio as a function of a varying t_p is shown in Figure 5.7. For low values of t_p , when the necessary charging capacity determines the amount of installed capacity, integrated storage is preferred. For higher values of t_p , integrated storage is still preferred when little energy storage capacity is necessary. When more energy capacity is necessary, disjoint capacity becomes the preferred technology. Although it is theoretically possible that integrated storage units with any number of energy-to-power (EP) ratio could be developed, most commercial available integrated storage technologies have EP-ratios of maximum 10 hours. Therefore the exact value of t_p which marks the shift from preferred integrated to disjoint technology could vary but the general result effectively stays the same. Note that since a block profile is used where P_{RES} is either equal to the installed iRES capacity or zero, either disjoint or integrated storage will be the most economic option depending on

the surplus time t_s . Hence, for a particular t_s , a portfolio will consist only of either disjoint or integrated capacity, never a combination of the two. This is different compared to other profiles (like sinus-shaped profiles) where it can be optimal to install both storage technologies simultaneously as will be elaborated in the next section.

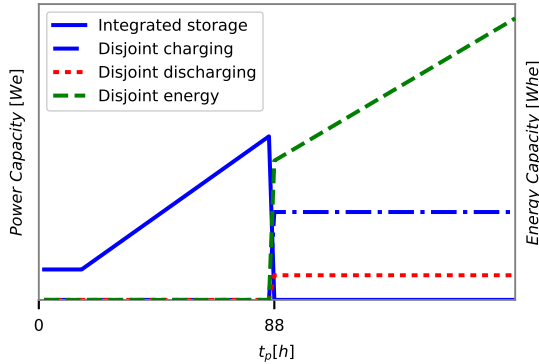


Figure 5.7: Optimal installed storage capacity as a function of t_p with $t_s = \frac{t_p}{2}$.

5.4 Sinusoidal profile

The block-shaped iRES generation profile from the previous section is now replaced by a single-frequency sinusoidal profile², while the load profile is still assumed flat. Sinusoidal profiles with a period of a few hours up to months are used. The calculations are made with a Linear Program (LP) investment model instead of doing them analytically. The LP model is later used for more complex and realistic profiles, but a sinusoidal profile is chosen first to allow easy comparison with the previously discussed block profiles.

5.4.1 Necessary storage capacity

The single-frequency sinusoidal profile, representing the iRES generation, has a period t_p and a magnitude between 0 and P_{RES} (and thus an average of $0.5 \cdot P_{RES}$). The maximum iRES generation P_{RES} is equal to the installed

²Not to be confused with the frequency of the instantaneous electrical AC power (e.g.; 50 or 60 Hz).

iRES capacity, as shown on Figure 5.8. The load profile is still a flat load with magnitude P_d . Note that for sinusoidal profiles, the duration of surplus iRES generation, previously denoted as t_s , is fixed once P_d , P_{RES} and t_p are determined. Furthermore, the duration of surplus will change when the installed iRES generation capacity is varied. This is shown on Figure 5.8 for iRES capacities P_{RES} and P'_{RES}

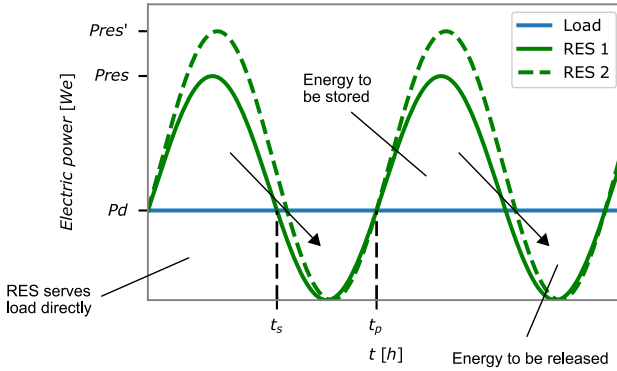


Figure 5.8: Flat load profile and two sinusoidal iRES generation profiles. Both iRES generation profiles have an equal period (t_p) but a different profile amplitude, following from a different amount of installed iRES capacity, leading to a different surplus duration (t_s).

It is again interesting to see the effect of a varying period t_p as was done before. Figure 5.9 shows the installed charging, discharging and energy capacities of the disjoint storage technology and the installed capacity of the integrated storage technology under the pre-specified coupling constraints as a function of the period t_p . Comparing Figure 5.9 to Figure 5.5 shows the same trend for both types installed storage capacity. For low periods t_p , power capacity is dominating the installed capacity for the integrated storage technology. For higher periods t_p , the necessary energy capacity determines the installed capacity. A careful examination of Figure 5.9 shows slight variations in the slope of the integrated capacity, disjoint energy capacity and disjoint charging capacity. These variations were not present in Figure 5.5 and are explained by the nature of the sinusoidal profile. For a sinusoidal iRES profile, the iRES generated electrical power is not necessarily equal to either the installed iRES capacity (P_{RES}) or zero, it also has values in between. Installing more iRES capacity, at a certain cost, has therefore two effects. First, more load will be served directly by renewable generation, reducing the necessary energy storage capacity. Second, the surplus time t_s will increase, reducing the necessary charging capacity. Both

effects are visible on Figure 5.8 when observing the difference between P_{RES} and P'_{RES} . As the linear program optimizes between iRES capacity and necessary storage capacity for each t_p , variations in the installed capacity slopes occur. This is not observed in Figure 5.5 for the block profile since installing more iRES capacity could neither increase the amount of load directly served by renewable generation, nor increase the surplus time t_s .

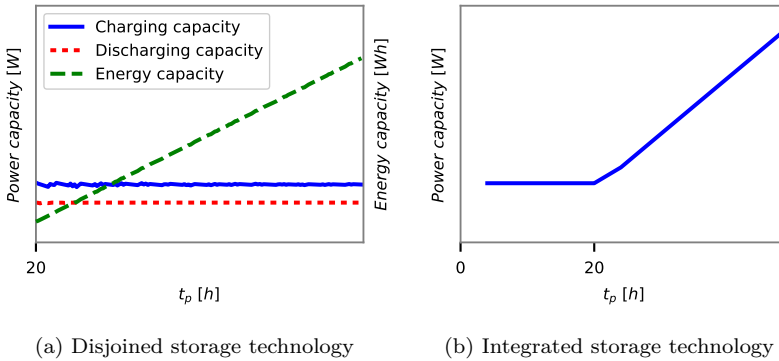


Figure 5.9: Installed storage capacity in function of period t_p .

5.4.2 Interactions between storage technologies

In this section, the optimal storage portfolio is investigated when both integrated and disjoint storage technologies can be installed simultaneously. The exact interactions between the different storage types will depend on their relative cost and technical constraints presented in table 5.2 above, but conclusions can be generalized.

Figure 5.10 shows the installed storage capacity for a flat demand profile and a sinusoidal iRES generation profile with a single varying period t_p . As can be expected, based on the results shown in Figure 5.7, all energy is stored using integrated storage capacity for sinusoidal profiles with short periods (high frequency), corresponding to a large necessary charging power relative to the necessary energy capacity. For sinusoidal profiles with long periods (low frequency), corresponding to a large necessary energy capacity relative to the necessary charging power, almost all energy is stored using disjoint storage technology. For a period $60h < t_p < 200h$, both integrated and disjoint storage technologies are used simultaneously. For profiles with such time period, the necessary energy storage requirements determine the minimum amount of

installed storage capacity. The disjoint technology is preferred to store the bulk of the energy. However, the highest surplus power from renewable generation is only available for a limited time, due to the shape of a sinusoidal profile, i.e., the peak of the profile. To store this part of the surplus iRES generation, it is more economic to install integrated capacity rather than disjoint capacity. Although those sinusoidal profiles are not directly representative for real demand and iRES generation, results from the sinusoidal profile can be generalized towards real profiles by applying them to the frequency spectrum of a real remaining load profile. This is the subject of the next section.

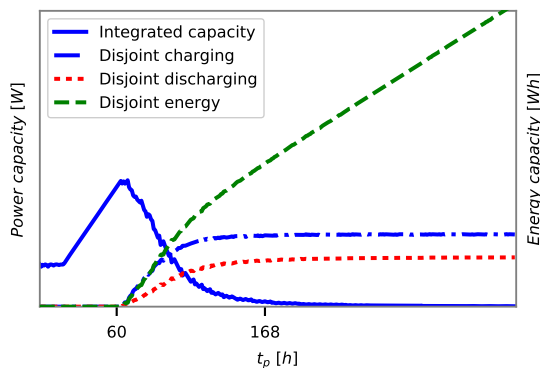


Figure 5.10: Installed integrated capacity and disjoint charging and discharging capacities as a function of a single sinusoidal remaining load with a varying period t_p .

5.5 Real profiles

The load and iRES generation profiles used in this section are based on real profiles from the Belgian electricity system from the period 2013 till 2015. The data are obtained from Elia [77], the Belgian TSO and have a time resolution of 1 hour. The magnitude of the iRES generation profile is scaled in different scenarios to reflect different amounts of installed iRES capacity. The method of Welch [78] is employed to estimate the frequency spectrum of different load and generation profiles. This method provides a robust way to estimate the frequency spectrum as explained by Woods et al. [79]. The method divides the temporal profile in several segments and calculates the discrete Fourier transform for each segment. The resulting Fourier coefficients are then used to calculate the estimated spectral density for each temporal segment. As a final

step, the average of all spectral density estimations is calculated and used as the estimated frequency spectrum of the temporal profile. Figure 5.11 shows an example to illustrate Welch’s method. The left figure shows a time-series which is the summation of two sinusoidal profiles, one with a 24h period and one with a 12h period. The right figure shows the corresponding power spectral density estimate computed using Welch’s method.

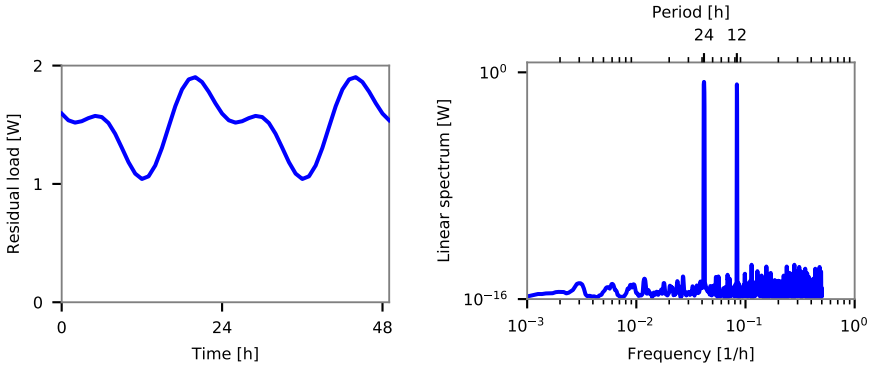


Figure 5.11: Left: brief extract of a time-series which is the summation of two sinusoidal profiles with 24h and 12h period. Right: the corresponding power spectral density estimate computed using Welch’s method.

The estimated frequency spectra of two remaining load profiles, one where onshore wind and one where solar PV is used as RES, are shown in Figure 5.12. These remaining load profiles are created with historic load and iRES generation profiles from the Belgian electricity system [77]. The segment of the frequency spectrum at the left of the dashed line corresponds to sinusoidal profiles with a long period (and low frequency). The low and high frequency segment have a different weight, or importance, depending on the iRES source. This is reflected by the amount of installed capacity of both storage technologies, as shown in table 5.3. A higher relative weight of the low-frequency spectrum corresponds to a higher share of disjoint capacity in the storage portfolio. This is in accordance with the results shown in Figure 5.10, where disjoint storage is preferred for high t_p while integrated storage is preferred for low t_p .

To compare different remaining load profiles and the corresponding storage portfolios, a formal *metric* is developed. To express the relative weight of the low-frequency spectrum, the ratio of the sum of the low-frequency spectrum over the sum of the entire spectrum is chosen. This is expressed in Eq. (5.7) where $P_{spec}(f)$ is the amplitude of the power spectrum of the remaining load

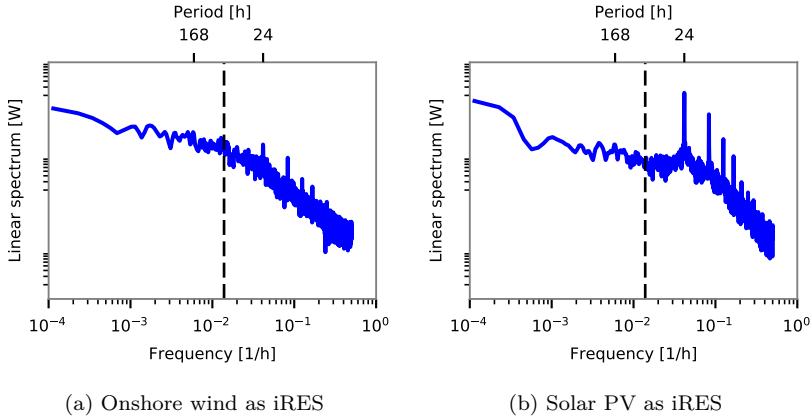


Figure 5.12: Frequency spectrum of remaining load profile when 100% of demand is covered by RES. The dashed line indicates the cut-off frequency f_c , which divides the spectrum in a low and a high-frequency part.

Table 5.3: Installed storage capacity to accommodate the remaining load profile of two 100% RES scenarios shown in Figure 5.12. The storage technology characteristics are presented above in Table 5.2.

Installed capacity	RES source	
	Onshore Wind	Solar PV
Disjoint charging capacity [GW]	25	32
Integrated capacity [GW]	7	31

profile as a function of frequency f , f_c is the cut-off frequency which divides the entire frequency spectrum in a low-frequency and a high-frequency part (the dashed line in Figure 5.12).³ Finally P_{low} is the relative weight of the low-frequency spectrum.

$$P_{low} = \frac{\sum_{f>0}^{f=f_c} P_{spec}(f)}{\sum_{f>0} P_{spec}(f)} \quad (5.7)$$

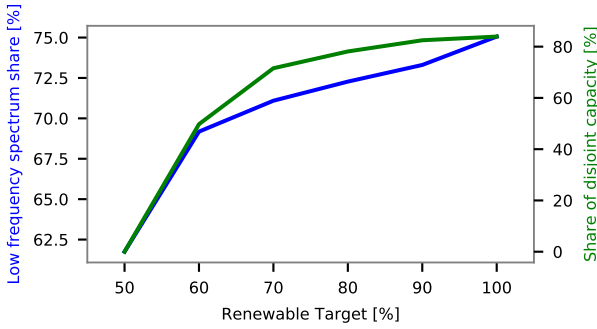
³Note that f_c is here a given frequency to divide the spectrum in two parts, it is not the frequency corresponding to a -3 dB point in the spectrum.

The share of disjoint charging capacity (x_d) in the storage portfolio is expressed as in Eq. (5.8). c_d^c and c_d^d denote the installed disjoint charging and disjoint discharging capacity respectively, c_i denotes the installed integrated capacity.

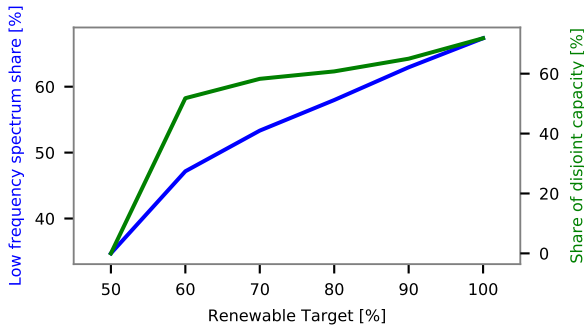
$$x_d = \frac{\frac{c_d^c + c_d^d}{2}}{\frac{c_d^c + c_d^d}{2} + c_i} \quad (5.8)$$

For the share of disjoint capacity, the average of charging and discharging capacity is used. Note that in the presented examples, GFPPs are used as synthetic methane discharging capacity or as conventional generation capacity with common natural gas. Therefore, a distinction is made between GFPPs operated with synthetic methane and conventional natural gas, where only the former is counted as disjoint discharge capacity. The disjoint energy capacity is not taken into account as it is expressed in a different unit than power and thus not directly comparable to the integrated capacity. Nevertheless, results shown in Figure 5.7 and Figure 5.10 indicate that the disjoint power capacity is a good measure for the amount of optimally installed disjoint capacity in general.

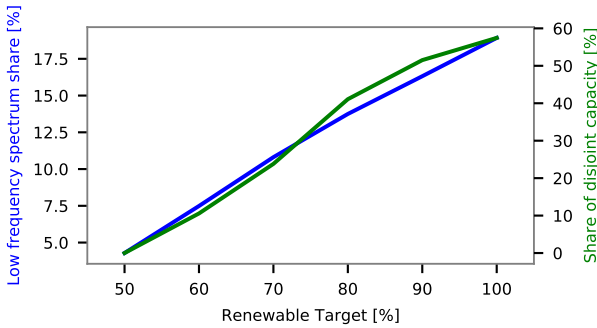
Based on the metrics introduced in Eqs. (5.7) and (5.8) and the results shown in the previous sections, it is expected that an increase in the relative weight of the low-frequency spectrum leads to an increase in the share of disjoint charging capacity in the storage portfolio. One can see that this holds for the sinusoidal profiles investigated earlier. After all, increasing the period of the sinusoidal signal (moving from left to right on the abscissa of Figure 5.10) corresponds to a shift from a high-frequency spectrum to a low-frequency spectrum and results in an increasing share of disjoint capacity in the storage portfolio. The same mechanism is confirmed by the simulation results of real profiles as shown in Figure 5.13. The relative weight of low-frequency spectrum and the share of disjoint charging capacity in the storage portfolio as a function of the renewable energy generation target are shown in this figure. The RES target expresses a minimum percentage of the total energy load that has to be served by RES generation, directly or through storage. It is clear that for most instances both the weight of the low-frequency spectrum and the share of disjoint charging capacity increase simultaneously.



(a) Onshore wind



(b) Offshore wind



(c) Solar PV

Figure 5.13: Relative weight of low-frequency spectrum (P_{low}) and share of disjoint power capacity (x_d) in the storage portfolio as a function of the RES target for different iRES technologies: onshore wind for the upper panel, offshore wind for the middle and solar pv for the lower panel. Note that the ordinate axes are labeled differently.

Next to varying the renewable energy generation target, also different iRES technologies can be compared with each other as presented in Figure 5.14. The figure shows that among different iRES technologies, an increase/decrease in the weight of the low-frequency spectrum (blue bars) leads to an increase/decrease in the share of disjoint charging capacity in the storage portfolio (green bar).

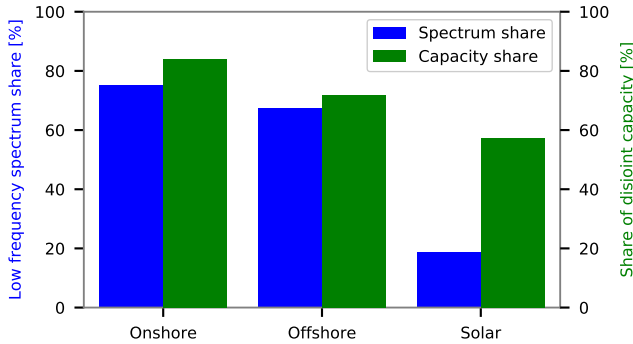
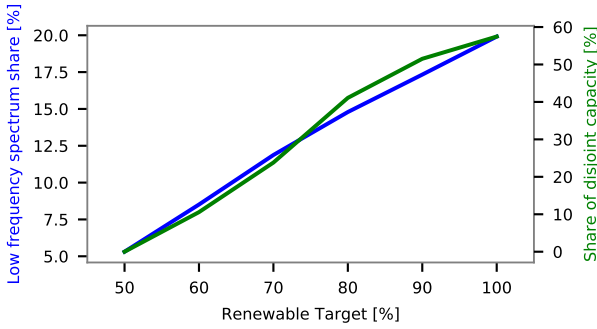


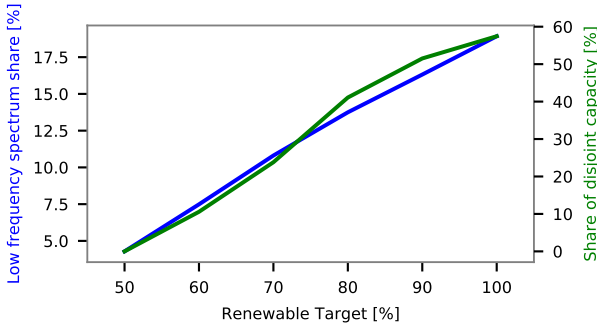
Figure 5.14: Share of low-frequency spectrum (P_{low}) and share of disjoint power capacity (x_d) in the storage portfolio for different remaining load profiles. Each remaining load profile results from using a different iRES technology. The renewable energy target is set at 100% in each case.

Finally, the effect of a change in cut-off frequency is investigated. As this cut-off frequency is arbitrarily chosen, it is important that the results hold for different cut-off frequencies. Figure 5.15 shows the relative weight of the low-frequency spectrum and the share of disjoint charging capacity in the storage portfolio for different cut-off frequencies. It is clear that the results observed and discussed above do not depend on a well chosen cut-off frequency but hold for a wide range of cut-off frequencies.

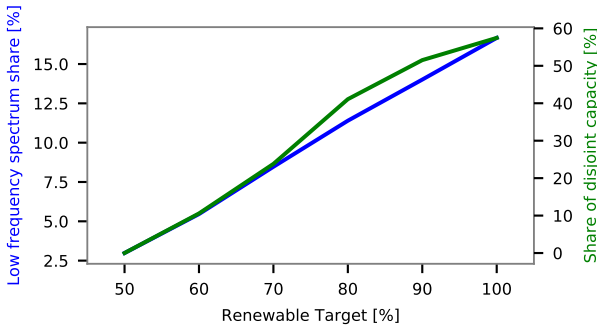
The presented results indicate that the low-frequency components predominantly determine the installed share of disjoint charging capacity in an optimal storage portfolio. The underlying mechanism of this is that the necessary energy storage capacity is high compared to the necessary charging/discharging power capacity. This mechanism was also seen in the results from methodological block profiles and single sinusoidal profiles. In addition, it follows that the high-frequency components determine the share of integrated capacity in the storage portfolio. Note that, although the low-frequency spectrum drives the need to install disjoint storage, once disjoint capacity has been installed, it can be used to accommodate both low and high frequency remaining load. The same holds for integrated storage.



(a) Cut-off frequency: 1/48h



(b) Cut-off frequency: 1/72h



(c) Cut-off frequency: 1/168h

Figure 5.15: Relative weight of low-frequency spectrum (P_{low}) and share of disjoint power capacity (x_d) in the storage portfolio as a function of the iRES target for different cut-off frequencies: 1/48h in the upper panel, 1/72h in the middle and 1/168h in the lower panel.

5.6 Summary and conclusions

This chapter provides a methodological explanation for the relationship between the time-varying shape of a remaining load profile and the optimal storage portfolio, when used for temporal arbitrage. A distinction is made between storage technologies for which installed charging power, discharging power and energy storage can be optimized separately, like power-to-gas-to-power (referred to as a '*disjoint*' storage technology), and storage technologies for which all capacity ratings are physically coupled, like NaS batteries, where the most stringent capacity rating (charging power, discharging power or energy reservoir size) determines the installed capacity (referred to as an '*integrated*' storage technology).

Results show a clear relationship between the share of each storage capacity type and the share of its corresponding range in the frequency spectrum of the '*remaining*' load profile. These results are based on optimal storage portfolio calculations for different methodological and historic load and iRES generation profiles. Results indicate that disjoint storage is predominantly used to serve remaining load profiles with high necessary energy capacity, compared to the necessary power capacity, corresponding to monthly and seasonal cycles. This type of remaining load profiles is expected to occur only when very high shares of intermittent renewable generation (>50%) are installed. Integrated storage is predominantly used to serve remaining load profiles with high necessary power capacity relative to the necessary energy capacity, corresponding to daily and weekly cycles. Residual load profiles with cycles of such duration can occur for lower shares of installed renewable capacity.

The findings from this work are employable in both future generation expansion planning and greenfield investment studies to explain results concerning storage capacity. Moreover, these results are useful to single out the part of storage benefits accountable to temporal arbitrage in broader analyses covering storage for both temporal energy arbitrage and ancillary services like providing reserve capacity.

Chapter 6

Unit commitment model for a combined electricity and gas system

This chapter contains elements from:

Belderbos, A., Bruninx K., Valkaert, T., Delarue, E. and D'haeseleer, W. *Facilitating renewables and power-to-gas via integrated electric power-gas system scheduling*, TME working paper.

Valkaert, T., Belderbos, A. and D'haeseleer, W. *Modeling transient gas flows through uniform pipelines with a focus on line pack and line pack flexibility.*, TME working paper.

This chapter presents a novel operational model comprising a combined electrical power and gas system. This model will be used to investigate extensive case studies on the effect of power-to-gas (P2G) on gas network exploitation, the conventional natural gas production facilities and gas-fired power plants in Chapter 7.

The relevance of such model in energy system operations is discussed together with the novelties of this model compared to the literature in Section 6.1. Section 6.2 provides a qualitative and mathematical description of the model. Section 6.3 presents a verification of the gas part of this model, indicating the model accuracy and its suitability to be used for operational scheduling studies. Different case studies are presented to illustrate the value of the novel model aspects in Section 6.4. Conclusions finalize this chapter in Section 6.5.

6.1 Introduction

The growing share of intermittent renewable energy sources (iRES) requires flexibility in the electric power system which could be provided by a more dynamic operation of conventional (natural) gas-fired power plants (GFPPs). Such increasing flexibility provision will result in an increasingly volatile gas network off-take from GFPPs. If P2G units are installed, an additional coupling between the electrical power grid and the gas network is made which could, depending on the operating profile of the P2G units, lead to a volatile injection into the gas network.¹ Both the increasingly volatile off-take and injection in the gas network could hence transfer a flexibility requirement from the electrical power network to the gas network and warrant further research on the impact of electrical power volatility on the safe and reliable gas network operation.

Some major differences exist between the electrical power grid and the gas network. First, electrical power is transported at the speed of light and hence can be regarded as instantaneous for unit commitment optimization. Natural gas is propelled at much lower velocities resulting in a time-delay between injection and off-take of possibly hours to days, depending on the distance to be covered. Second, in contrast to the electrical power grid, the gas network has some inherent flexibility. Since gas is a compressible fluid, gas can be accumulated in pipelines which allows using the gas network as short-term storage. The amount of gas contained inside a pipeline is termed the *line pack* and depends on the size of the pipeline and the imposed pressure bounds. A higher pressure in a pipeline results in a higher gas density and higher line pack level.

The *line pack flexibility* provides an inherent flexibility for the gas network which could be used to facilitate the integration of iRES in the electric power system by transferring the gas flexibility to the electric power system via gas-fired power plants and P2G, as mentioned in the onset of this chapter.

A gas flow through a pipeline causes a pressure drop between the entry and exit of the pipeline, due to friction losses; this is illustrated by the solid line in Figure 6.1a. The shaded area under the solid pressure line is a metric for the line pack inside the pipeline [80].

The average pressure inside the pipeline can be shifted up or down without impacting the gas flow rate through the pipeline, as long as the pressure drop due to this gas flow does not span the entire allowed pressure range. Figure 6.1b shows two pressure curves for the same gas flow rate as shown in Figure 6.1a, one shifted up reaching the maximum pressure bound and one shifted

¹'Grid' and 'network' are used as synonyms.

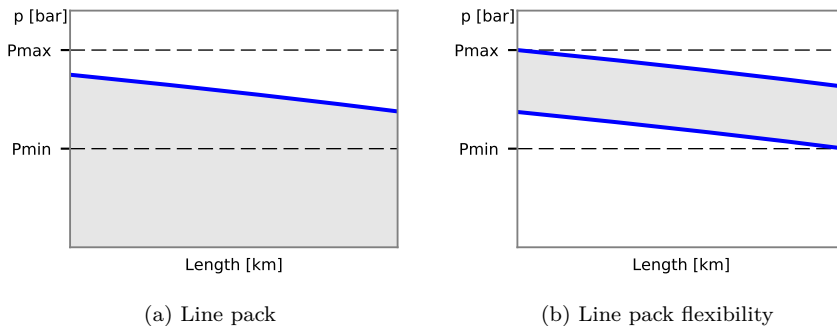


Figure 6.1: Pressure drop due to gas flow indicated by the solid line, with line pack (shaded area under pressure curve in the left-hand panel) and line pack flexibility (shaded area between minimum and maximum pressure curves in right-hand panel). Note that the solid blue curves are not linear in general, but have a concave curvature.

down reaching the minimum pressure bound. The shaded area between the two pressure curves is a metric for the *line pack flexibility*. This line pack flexibility depends on the pressure bounds and on the gas flow rate through the pipeline. When the gas flow rate increases, the pressure drop increases (leading to steeper pressure lines) and the available line pack flexibility decreases.

To study to what extent line pack can provide flexibility to the electric power system and the effect of such flexibility transfer on conventional gas shippers, a multi-carrier energy system (MES) model incorporating both the electric power and gas system is required. Furthermore, it is key to account for gas flows and pressures in this MES model.

Many different MES models are reported in the literature. As for all optimization models, a balance must be struck between the optimization horizon and the level of detail considered in technical, temporal and geographical domain to assure an acceptable computational cost [7]. Depending on the models' purpose, more detail in one or another domain is considered. MES models can roughly be divided into investment models and operational scheduling models. The former typically have a larger optimization horizon at the expense of a reduced level of detail in one or more domains while the latter put more focus on the technical, temporal and/or geographical domain at the expense of a reduced optimization horizon. An extensive overview of the different models is outside the scope of this study, the interested reader is referred to the following literature: [81, 82].

The MES model presented in the following section (6.2) is an operational model comprising an electric power system and a gas system with a high level of technical and geographic detail. Two model characteristics are important when investigating the line pack flexibility in a gas network. First, the assumed 'state' of the gas network is essential; this can be either steady state or transient. Although steady state models of the gas network can provide valuable insights, these models cannot be used to assess variations in line pack levels and line pack flexibility. Since line pack variations require the pipeline inflow to differ from the outflow, it is by definition assumed that the gas flow is not in steady state.

A second characteristic is the strategy employed to determine the optimal MES operating schedule, which could be either the sequential or simultaneous optimization of the electricity system and the gas system. A first group of papers uses sequential optimization. Often the electric power system is optimized first, determining the operational schedule of gas-fired power plants and, if considered, P2G units. Next, the gas system is optimized determining the gas flows and nodal pressures. An iterative algorithm is often employed to assure that the electric power system optimization is re-optimized if it would lead to in-feasibilities in the gas system. However, Zlotnik et al. [83] and Qadrdan et al. [84] show that non-simultaneous optimization of both energy systems often leads to economic non-optimal solutions, especially in high stress situations such as cases with high iRES penetration. Therefore, the electric power system and the gas system are simultaneously optimized in this work.

Table 6.1 provides examples of multi-carrier energy system (MES) models found in the literature with different gas flow representations and optimization strategies as discussed before. The models indicated in the shaded area relate most closely to the model presented in Section 6.2.

Table 6.1: Examples of relevant multi-energy system models found in the literature with respect to their representation of the gas network and optimization strategy

	Steady state	Transient
Sequential	[85]	[86],[87],[88]
Simultaneous	[89],[90]	[83],[91],[92]

Each of the studies listed in Table 6.1 which incorporate a transient gas flow, describe the same physical gas flow problem, although the precise mathematical implementation differs as well as the optimization strategy. The gas system presented in the next section provides an addition to the literature in the following ways:

1. P2G units have been added with a high level of technical detail;
2. the representation of gas production facilities is extended with additional constraints;
3. the mass balance constraints are extended to not only impose nodal mass balances but also zonal mass balances.

The studies from Clegg and Mancarella [85, 86] and He et al. [90] incorporate P2G units as a single, integrated unit. The model presented in this work here extends these formulations by providing a P2G representation with a greater technical detail, modeling the electrolyzer, methanizer and intermediate hydrogen buffer as distinctive units. Increasing the technical detail of the P2G units provides more detailed results on the flexibility P2G can provide to the electrical power system and the flexibility it requires from the natural gas system.

Adding constraints on the natural gas production facilities and modeling zonal mass balances in addition to the nodal mass balances does not necessarily increase the technical detail but it improves the realism of the obtained results. By adding additional constraints to the production facilities, large pressure variations due to large production variations are avoided. Considering zonal loads allows to account for possible flexibility provided by the gas distribution grid [93].

The gas system implementation presented in the following section is based on the implementation described by Correa-Posada [91] and extended with the additions listed before. The electric power system is represented by the LUSYM model taken from Van den Bergh et al. [94],[95] due to its proven solving speed. A DC load flow representation is used for the electrical power grid, while a transient representation is used for the gas network.

6.2 Model description

The model objective is to minimize total system operational cost, while adhering to technical constraints imposed on both the entire energy system and the individual units. The total system cost equals the sum of the operational electric power system cost and the operational gas system cost as follows:

$$\min \quad cost^{elec} + cost^{gas} \quad (6.1)$$

The electric power system cost consists of generation costs, start-up costs, shut-down costs, ramping costs, load curtailment costs, renewables curtailment

costs and reserve allocation costs for load and renewables curtailment:

$$\begin{aligned} cost^{elec} = & \sum_{i,t} (cost_{i,t}^{gen} + cost_{i,t}^{start} + cost_{i,t}^{stop} + cost_{i,t}^{ramp}) \\ & + \sum_{l,t} (cost_{l,t}^{trans}) + \sum_{n,t} (cost_{n,t}^{lc} + cost_{n,t}^{rc} + cost_{n,t}^{rsr}) \end{aligned} \quad (6.2)$$

The operational gas system cost consists of a gas production cost from gas wells, a gas storage cost, a compressor cost and an operational cost from P2G units:

$$cost^{gas} = \sum_t \left[\sum_{gw} cost_{gw,t}^{well} + \sum_{gs} cost_{gs,t}^{stor} + \sum_c cost_{c,t}^{comp} + \sum_e cost_{e,t}^{ptg} \right] \Delta t \quad (6.3)$$

The electrical power and gas system are linked by GFPPs which consume gas from the gas network to generate electrical power (which is injected in the electrical power system) and by P2G units which convert electrical power from the grid to synthetic methane (and inject it in the gas network). Both the electrical power and gas systems are described in the following sections. Both systems are connected to each other via the GFPPs and P2G units.

6.2.1 Electricity system

The model describing the electricity system is taken from Van den Bergh et al. [94],[95], and is added in Appendix D. This model contains technical unit constraints such as generation limits, ramp limits, minimum up times and minimum down times. The electricity network is modeled using a DC power flow representation.

Note that the market clearing constraint is adapted to account for the electricity consumption from P2G units. The adapted market clearing condition reads:

$$\begin{aligned} & \sum_i A_{n,i}^{plant} (z_{i,t} \underline{P}_i + g_{i,t}) + \sum_j A_{n,j}^{stor} (pd_{j,t} - pc_{j,t}) + RES_{n,t} - rc_{n,t} \\ & = D_{n,t} - lc_{n,t} + ls_{n,t} + pi_{n,t} + \sum_e A_{n,e}^{ely} g_{e,t}^{ely} \quad \forall n, t \end{aligned} \quad (6.4)$$

where $A_{n,i}^{plant}$ links each power plant i with a node n in the electrical power grid, $z_{i,t}$ denotes the binary on-off status of each power plant at each time step t , \underline{P}_i is the minimum operating point and $g_{i,t}$ is the electrical power generation above

minimal operating point. $pd_{j,t}$ and $pc_{j,t}$ are respectively de discharging and charging power of each storage unit j at each time step, with $A_{n,j}^{stor}$ a matrix linking each storage to a node in the grid. $RES_{n,t}$ denotes the available iRES generation, $rc_{n,t}$ the iRES curtailment, $D_{n,t}$ is the electricity load, $lc_{n,t}$ the curtailed load, $ls_{n,t}$ the stored load and $pi_{n,t}$ the power injection in the grid at node n . $g_{e,t}^{ely}$ is the electrical energy consumption of electrolyzer e and $A_{n,e}^{ely}$ is a matrix linking each electrolyzer e to a node n .

The main decision variable in the electric power system are the on/off commitment status ($z_{i,t}$), the power plant generation level ($g_{i,t}$), the storage charging ($pc_{j,t}$) or discharging ($pd_{j,t}$) electrical power, the stored load ($ls_{n,t}$) and curtailed load ($lc_{n,t}$), de curtailed renewable energy sources (RES) generation ($rc_{n,t}$) and the electrical power injection in each node ($pi_{n,t}$) from the network.

6.2.2 Gas system

The presented gas system model encompasses a gas network consisting of nodes and arcs. Each node can contain gas wells, storages, loads, P2G units and GFPPs which are respectively modeled by their production limits, injection and withdrawal limits and consumption limits. The arcs connecting the nodes can be either pipelines, compressors or valves. Only the operational cost of the gas system is considered.

Cost

The total operational cost consisting of a gas production cost² from gas wells, a gas storage cost, a compressor cost and an operational cost from P2G units was given in Eq. (6.3) before. The gas well production cost, with C_{gw} the gas production cost per volume of gas for each gas production facility gw and $q_{gw,t}$ the gas production rate at facility gw and time step t , follows from [96]:

$$cost_{gw,t}^{well} = C_{gw} \cdot q_{gw,t} \quad \forall gw, t \quad (6.5)$$

The gas storage cost is modeled as an operational cost per unit of stored gas³:

$$cost_{gs,t}^{stor} = C_{gs} \cdot q_{gs,t} \quad \forall gs, t \quad (6.6)$$

²For countries without domestic gas production, this would become an 'import cost'.

³The operational cost is driven by the cost of mechanical energy required for compression and the cost of thermal energy needed for heating during expansion. Although this energy requirement varies with the storage state-of-charge, an average energy cost is used here to reduce the computational burden [91].

with C_{gs} the storage cost per volume of gas for each storage gs and $q_{gs,t}$ the gas flow to or from each storage at each time step.

The compressor cost is obtained as⁴:

$$cost_{c,t}^{comp} = C_c \cdot q_{c,t} \quad \forall c, t \quad (6.7)$$

with C_c the cost per volume of compressed gas for each compressor c and $q_{c,t}$ the gas flow through each compressor at each time step.

The operational cost of a P2G unit e consists of a variable operation and maintenance (O&M) cost (C_e^{ely}) per unit of consumed electricity ($g_{e,t}^{ely}$) and a variable O&M cost (C_e^{met}) per unit of produced synthetic methane. The amount of produced synthetic methane is equal to on-off status ($z_{e,t}^{met}$) of the methanizer unit e times the production rate at minimal operating point (\underline{F}_e^{met}) summed with the production rate above minimal output ($f_{e,t}^{met}$).

$$cost_{e,t}^{ptg} = C_e^{ely} g_{e,t}^{ely} + C_e^{met} (\underline{F}_e^{met} z_{e,t}^{met} + f_{e,t}^{met}) \quad \forall e, t \quad (6.8)$$

Note that the cost of the consumed electricity itself is not accounted for in this P2G operational cost since the cost of electricity is endogenous to the combined model. Similarly, the earnings for the produced methane are not modeled explicitly as they are endogenous to the model.

Production and generation limits

The production at each gas well gw is constrained by a minimum level (\underline{W}_{gw}) and a maximum level (\overline{W}_{gw}), which can either be set by physical characteristics or contracted amounts:

$$\underline{W}_{gw} \leq q_{gw,t} \leq \overline{W}_{gw} \quad \forall gw, t \quad (6.9)$$

Gas transmission system operators (TSOs) impose maximum upward ramp rates (RU_{gw}) and downward ramp rates (RD_{gw}) on the gas injection from shippers ($q_{gw,t}$) in order to avoid sudden pressure changes in the gas network [93]. These ramp rates follow from:

$$q_{gw,t} \leq q_{gw,t-1} + RU_{gw} \Delta t \quad \forall gw, t \quad (6.10)$$

$$q_{gw,t} \geq q_{gw,t-1} - RD_{gw} \Delta t \quad \forall gw, t \quad (6.11)$$

⁴This cost is driven by the mechanical energy required for compression. Although this energy need increases with increasing pressure ratio, an average compression cost is used to reduce the computational burden [97, 98].

with Δt the duration of a time step.

The natural gas consumption from GFPPs ($q_{ng,t}^{gfpp}$) is linked to their electricity generation (equal to $\underline{P}_i z_{i,t} + g_{i,t}$) by the conversion efficiency⁵ η_i . A conversion factor ζ is used to express the natural gas consumption in Nm³:

$$q_{i,t}^{gfpp} = \frac{1}{\zeta \eta_i} (\underline{P}_i z_{i,t} + g_{i,t}) \quad \forall ng, t \quad (6.12)$$

The gas flow rate injected or withdrawn from storage ($q_{gs,t}$) is limited by a maximum injection rate (IR_{gs}) and maximum withdrawal rate (WR_{gs}):

$$WR_{gs} \leq q_{gs,t} \leq IR_{gs} \quad \forall gs, t \quad (6.13)$$

Analogous to the maximum injection variations from gas wells to avoid large pressure swings in the grid, a maximum upward ramp rate (RU_{gs}) and downward ramp rate (RD_{gs}) is imposed on the gas flow to and from storage ($q_{gs,t}$):

$$q_{gs,t} \leq q_{gs,t-1} + RU_{gs} \Delta t \quad \forall gs, t \quad (6.14)$$

$$q_{gs,t} \geq q_{gs,t-1} - RD_{gs} \Delta t \quad \forall gs, t \quad (6.15)$$

The state of charge of the gas storage ($s_{gs,t}^l$) is bound by its physical limits as follows:

$$\underline{S}_{gs} \leq s_{gs,t}^l \leq \overline{S}_{gs} \quad \forall gs, t \quad (6.16)$$

with \underline{S}_{gs} the minimum gas storage level and \overline{S}_{gs} the maximum storage level.

The correct gas storage state of charge ($s_{gs,t}^l$) is given by Eq. (6.17), note that $q_{gs,t}$ can be both positive, when injecting to storage, and negative, when withdrawing from storage.

$$s_{gs,t}^l = s_{gs,t-1}^l + q_{gs,t} \Delta t \quad \forall gs, t \quad (6.17)$$

Power-to-gas unit

A P2G unit is modeled as three distinct parts: (1) the electrolyzer, converting water to hydrogen and oxygen by using electricity; (2) the methanizer, converting hydrogen and CO₂ to methane; and (3) an intermediate hydrogen storage

⁵Although the efficiency varies with the operation point, a constant efficiency is used for simplicity [91].

to temporarily store the electrically produced hydrogen. The intermediate hydrogen storage allows the electrolyzer to operate very dynamically to capture the surplus generation from iRES while allowing the methanizer, which is less flexible by nature, to operate at a fixed operating point for longer, uninterrupted periods in time.

Electrolyzer

The electrolyzer electricity consumption (g^{ely}) is constrained by its installed capacity (\bar{G}_e^{ely}) as follows:

$$0 \leq g_{e,t}^{ely} \leq \bar{G}_e^{ely} \quad \forall e, t \quad (6.18)$$

The hydrogen produced by an electrolyzer ($h_{e,t}^{ely}$) is given by [85]:⁶

$$h_{e,t}^{ely} = g_{e,t}^{ely} \eta_e^{ely} \quad \forall e, t \quad (6.19)$$

with $g_{e,t}^{ely}$ the electrical energy consumed by the electrolyzer e and η_e^{ely} the conversion efficiency between electrical and hydrogen energy.

Since the electrolyzer technology can be operated very dynamically (with time constants in the order of seconds to minutes [32]), far below the time steps considered in these models (15 minutes - 1 hour), no further technical generation limits are considered.

Methanizer

The amount of synthetic methane produced by a P2G unit can be expressed as:

$$0 \leq q_{e,t}^{met} = \frac{1}{\zeta} (\underline{F}_e^{met} z_{e,t}^{met} + f_{e,t}^{met}) \quad \forall e, t \quad (6.20)$$

with $z_{e,t}^{met}$ the on-off status of the methanizer unit e , \underline{F}_e^{met} the production rate at minimal operating point and $f_{e,t}^{met}$ the production rate above minimal operating point. To express the amount of produced synthetic methane in Nm^3 rather than MWh_{th} , the conversion factor ζ is used.

The hydrogen consumption for synthetic methane production is given by [85]:

$$\underline{F}_e^{met} z_{e,t}^{met} + f_{e,t}^{met} = h_{e,t}^{met} \eta_e^{met} \quad \forall e, t \quad (6.21)$$

⁶The efficiency could be varied depending on the operating point. This would, however, substantially increase run times while only slightly increasing accuracy [27].

with $h_{e,t}^{met}$ the hydrogen consumption of methanizer e and η_e^{met} the conversion efficiency from hydrogen to methane.

In analogy to the power plant generation limits [95], the maximum methane production from methanizers, above \underline{F}^{met} follows from (given that the $MUT^{met} > 2$):

$$\begin{aligned} f_{e,t}^{met} \leq & \left(\overline{F}_e^{met} - \underline{F}_e^{met} \right) z_{e,t}^{met} - \left(\overline{F}_e^{met} - SU_e^{met} \right) v_{e,t}^{met} \\ & - \left(\overline{F}_e^{met} - SD_e^{met} \right) w_{e,t-1}^{met} \quad \forall e, t \end{aligned} \quad (6.22)$$

where \overline{F}_e^{met} is the maximum methane production rate of methanizer e , SU_e^{met} is the start-up rate, SD_e^{met} is the shut-down rate, $v_{e,t}^{met}$ is the start-up status of methanizer e and $w_{e,t}^{met}$ is the shut-down status. Both $v_{e,t}^{met}$ and $w_{e,t}^{met}$ are binary variable which become '1' on the time step at which the methanizer, respectively, starts up and shuts down.

Given that reactor temperature control puts a limitation on the dynamic operation flexibility of methanizers [31], ramp rates are imposed as follows:

$$\begin{aligned} f_{e,t}^{met} - f_{e,t-1}^{met} \leq & RU_e^{met} z_{e,t}^{met} \\ & + \left(SU_e^{met} - \underline{F}_e^{met} - RU_e^{met} \right) v_{e,t}^{met} \quad \forall e, t \end{aligned} \quad (6.23)$$

$$\begin{aligned} f_{e,t-1}^{met} - f_{e,t}^{met} \leq & RD_e^{met} z_{e,t-1}^{met} \\ & + \left(SD_e^{met} - \underline{F}_e^{met} - RD_e^{met} \right) w_{e,t}^{met} \quad \forall e, t \end{aligned} \quad (6.24)$$

with RU_e^{met} and RD_e^{met} the ramp-up rate and ramp-down rate, respectively.

The minimum up-time (MUT_e^{met}) and down-time (MDT_e^{met}) are, respectively, enforced by:

$$z_{e,t}^{met} \geq \sum_{t'=t+1-MUT_e^{met}}^t v_{e,t'}^{met} \quad \forall e, t \quad (6.25)$$

$$1 - z_{e,t}^{met} \geq \sum_{t'=t+1-MDT_e^{met}}^t w_{e,t'}^{met} \quad \forall e, t \quad (6.26)$$

In addition to the constraints above, the following logic relation between the different methanizer unit statuses is needed:

$$z_{e,t-1}^{met} - z_{e,t}^{met} + v_{e,t}^{met} - w_{e,t}^{met} = 0 \quad \forall e, t \quad (6.27)$$

Hydrogen storage

The energy balance of the intermediate hydrogen storage ($s_{e,t}^h$) is given by:

$$s_{e,t}^h = s_{e,t-1}^h + h_{e,t}^{ely} - h_{e,t}^{met} \quad \forall e, t \quad (6.28)$$

with $h_{e,t}^{ely}$ the hydrogen production from the electrolyzer and $h_{e,t}^{met}$ the hydrogen consumption from the methanizer.

The storage injection and withdrawal are limited by the electrolyzer and methanizer capacity, respectively. Limits on the hydrogen storage level are imposed explicitly as follows:

$$\underline{S}_e^h \leq s_{e,t}^h \leq \overline{S}_e^h \quad \forall e, t \quad (6.29)$$

where \underline{S}_e^h is the minimum storage level and \overline{S}_e^h is the maximum storage level of hydrogen storage e .

Network

The gas network is modeled as a graph consisting of nodes and arcs. The arcs can be either passive, i.e., pipelines, or active, such as compressors and valves. Each node can connect multiple pipelines and can contain gas wells, storages, methanizers, gas-fired power plants and gas loads.

Nodes

A minimum pressure bound (\underline{p}_{ng}) and maximum pressure bound (\overline{p}_{ng}) is imposed in each node (ng) to assure the safe operation of the gas grid:

$$\underline{p}_{ng} \leq p_{ng,t} \leq \overline{p}_{ng} \quad \forall ng, t \quad (6.30)$$

Market clearing

Since mass accumulation is not possible within a node, each node requires a balance between the inflow and outflow of gas. The gas load served through nodes can originate from GFPPs, industrial gas use and residential gas use, the GFPP and industrial gas load is linked to individual nodes in the network. The residential gas use, however, is linked to 'gas zones'. Since the residential gas load is served through the distribution network, which is coupled with

the transmission network in multiple nodes, it is not possible to assign the residential gas load to unique nodes; instead, this load is assigned to 'gas zones'.

The nodal balance requires the gas in- and outflow of each node to be equal. However, since it is not possible to assign the residential gas load to a specific node a-priori, the nodal balance constraint is relaxed and an additional zonal balance constraint is imposed. The adapted (relaxed) nodal balance requires that the net inflow of gas (inflow minus outflow) should at least cover the industrial gas load and GFPP consumption. The inflow is allowed to be higher, in order to serve a possible residential gas load:

$$\begin{aligned}
& \sum_{pl} (Ia_{ng,pl}^{out} q_{pl,t}^{out} - Ia_{ng,pl}^{in} q_{pl,t}^{in}) + \sum_c (Ic_{ng,c}^{out} q_{c,t} - Ic_{ng,c}^{in} q_{c,t}) \\
& + \sum_v (Iv_{ng,v}^{out} q_{v,t} - Iv_{ng,v}^{in} q_{v,t}) - q_{gs,t} + q_{gw,t} + \sum_e A_{ng,e}^{met} q_{e,t}^{met} \\
& \geq L_{ng,t}^g + \sum_i A_{ng,i}^{gfpp} q_{i,t}^{gfpp} \quad \forall ng, t \quad (6.31)
\end{aligned}$$

with $q_{pl,t}^{in}$ and $q_{pl,t}^{out}$, respectively, the inflow and outflow of pipelines connected to node ng , $Ia_{pl,ng}^{in}$ and $Ia_{pl,ng}^{out}$ are matrices linking the entry and the exit nodes, respectively, to the pipelines. $q_{c,t}$ is the flow through compressor c , linked to its entry and exit node via $Ic_{c,ng}^{in}$ and $Ic_{c,ng}^{out}$, respectively. Analogously, $q_{v,t}$ denotes the flow through valve v and is linked to its entry and its exit nodes via matrices $Iv_{v,ng}^{in}$ and $Iv_{v,ng}^{out}$. $q_{gs,t}$ is the storage injection rate, $q_{gw,t}$ the gas production rate, $q_{ng,t}^{met}$ the methanizer production rate and $A_{ng,e}^{met}$ a matrix linking each methanizer to a node in the gas network. $L_{ng,t}^g$ denotes the nodal gas load in node ng at time step t and $q_{ng,t}^{gfpp}$ is the gas load from GFPPs, with $A_{ng,i}^{gfpp}$ linking each GFPP to a node in the gas network.

Within a gas zone, the sum of nodal gas inflows and outflows should be exactly equal at all time steps:

$$\begin{aligned}
& \sum_{ng} Iz_{zg,ng} \left(\sum_{pl} (Ia_{ng,pl}^{out} q_{pl,t}^{out} - Ia_{ng,pl}^{in} q_{pl,t}^{in}) + \sum_c (Ic_{ng,c}^{out} q_{c,t} - Ic_{ng,c}^{in} q_{c,t}) \right. \\
& \quad \left. + \sum_v (Iv_{ng,v}^{out} q_{v,t} - Iv_{ng,v}^{in} q_{v,t}) - q_{gs,t} + q_{gw,t} + \sum_e A_{ng,e}^{met} q_{e,t}^{met} \right) \\
& = \sum_{ng} \left(L_{ng,t}^g + \sum_i A_{ng,i}^{gfpp} q_{i,t}^{gfpp} \right) + L_{zg,t}^g \quad \forall zg, t \quad (6.32)
\end{aligned}$$

where $Iz_{zg,ng}$ is a matrix linking gas nodes to gas zones and $L_{zg,t}^g$ is the zonal gas load in each zone zg .

Note that if no residential gas load is considered, Eqs. (6.31)-(6.32) imply a mass balance at each node; i.e., in Eq. (6.31), the equality in " \geq " becomes strictly binding. Furthermore, Eq. (6.32) imposes an overall gas balance on the nodes within a zone. It is, however, still allowed to accumulate gas in the pipelines connecting nodes within one zone and in pipelines between different zones, thereby using the line pack flexibility available in pipelines as storage.

Pipelines

The gas flow through a pipeline is governed by three conservation laws: conservation of mass, momentum and energy, described by partial differential equations [99, 100]. Solving these equations to optimize the gas flows in a given transmission network is very computationally demanding. It is therefore standard practice to assume an isothermal flow, allowing to neglect the conservation of energy and to use a coarse discretization of the remaining conservation equations (mass and momentum) [101]. In this model, the formulation as presented by Correa-Posada [91] is used.

Conservation of mass

The amount of gas contained in a pipeline ($m_{pl,t}$), also termed the line pack, is tracked through time as follows:

$$m_{pl,t} = m_{pl,t-1} + q_{pl,t}^{in}\Delta t - q_{pl,t}^{out}\Delta t \quad \forall pl, t \quad (6.33)$$

with $q_{pl,t}^{in}$ and $q_{pl,t}^{out}$, respectively, the pipeline inlet flow and outlet flow.

This line pack mass is proportional to the average pressure (\bar{p}) inside the pipeline as given by:⁷

$$m_{pl,t} = K_{pl}^m \bar{p}_{pl,t} \quad \forall pl, t \quad (6.34)$$

$$\bar{p}_{pl,t} = \frac{\sum_{ng} I a_{pl,ng}^{in} p_{ng,t} + \sum_{ng} I a_{pl,ng}^{out} p_{ng,t}}{2} \quad \forall pl, t \quad (6.35)$$

⁷The average pressure inside the pipeline is given by $\bar{p}_{ab} = \frac{2}{3} \frac{p_a^3 - p_b^3}{p_a^2 - p_b^2}$ due to the non-linear pressure drop along the length of a pipeline [80]. Using this average would introduce additional non-linearities to the model which demand great computational effort to solve, therefore, the arithmetic mean pressure is used [91].

where K_{pl}^m denotes the proportionality factor and matrices $Ia_{pl,ng}^{in}$ and $Ia_{pl,ng}^{out}$ link the pipeline to their entry and exit nodes.

The proportionality factor K_{pl}^m in Eq. (6.34) depends on the pipeline and gas flow characteristics and is given in Eq. (6.36), with L the pipeline length, D the pipeline diameter, T the temperature which is assumed constant, Z the compressibility factor, T_0 and p_0 the temperature and pressure at standard conditions respectively and C_m^{te} a constant depending on the units in which pressure and line pack mass are expressed.

$$K_{pl}^m = C_m^{te} \frac{\pi}{4} \frac{LD^2 T_0}{p_0 T Z} \quad (6.36)$$

Conservation of momentum

Assuming horizontal pipelines and neglecting inertia en kinetic energy effects on the gas flow, the pressure drop over the pipeline due to the gas flow through the pipeline can be written as [91]:

$$\tilde{q}_{pl,t} |\tilde{q}_{pl,t}| = K_{pl}^q \sum_{ng} (Ia_{pl,ng}^{in} p_{ng,t}^2 - Ia_{pl,ng}^{out} p_{ng,t}^2) \quad \forall pl, t \quad (6.37)$$

with K_{pl}^q a proportionality factor relating the flow rate through a pipeline to the pressure drop over the pipeline and \tilde{q} the arithmetic mean of pipeline in- and outflow:

$$\tilde{q}_{pl,t} = \frac{q_{pl,t}^{in} + q_{pl,t}^{out}}{2} \quad \forall pl, t \quad (6.38)$$

Note that in Eq. (6.37) the square of the gas flow is expressed as the product of the gas flow and its absolute value, since the gas flow can be both positive and negative, depending on its flow direction. The constant K_{pl}^q depends again on the pipeline and gas flow characteristics and is given by:

$$K_{pl}^q = C_q^{te} \left(\frac{\pi}{4}\right)^2 \frac{D^5 T_0}{p_0 T Z L f \rho_0} \quad (6.39)$$

In Eq. (6.39), ρ_0 is the gas density at standard conditions, f is the Darcy friction factor and C_q^{te} is a constant which depends on the units in which the gas flow and pressure are expressed.

The friction factor is dependent upon the gas flow regime and the wall roughness of the pipeline. For highly turbulent gas flows, however, this friction factor is

only a function of pipeline roughness [102] as defined in Eq. (6.40) [103, 104]:

$$\frac{1}{\sqrt{f}} = 2 \log_{10} \left(3.7 \frac{D}{e} \right) \quad (6.40)$$

with D the pipeline diameter and e the roughness.

Compressors

Compressors are modeled as frictionless, short pipelines which increase the pressure. Hence the exit pressure should at least equal the inlet pressure and can be as high as the inlet pressure times a certain pressure ratio G_c :

$$\sum_{ng} I_{c,ng}^{out} p_{ng,t} \leq G_c \sum_{ng} I_{c,ng}^{in} p_{ng,t} \quad \forall c, t \quad (6.41)$$

$$\sum_{ng} I_{c,ng}^{out} p_{ng,t} \geq \sum_{ng} I_{c,ng}^{in} p_{ng,t} \quad \forall c, t \quad (6.42)$$

Valves

Valves are used for pressure reduction, the outlet pressure is hence constrained by a minimum equal to the inlet pressure times a pressure ratio G_v and a maximum equal to the inlet pressure itself:

$$\sum_{ng} I_{v,ng}^{out} p_{ng,t} \geq G_v \sum_{ng} I_{v,ng}^{in} p_{ng,t} \quad \forall v, t \quad (6.43)$$

$$\sum_{ng} I_{v,ng}^{out} p_{ng,t} \leq \sum_{ng} I_{v,ng}^{in} p_{ng,t} \quad \forall v, t \quad (6.44)$$

Piecewise linear implementation

The conservation of momentum (Eq. (6.37)) introduces two non-linearities to the model. Both $\tilde{q}|\tilde{q}|$ and p^2 are non-linear and the former term is even non-convex since the flow \tilde{q} can be both positive and negative. To keep reasonable model run times, these non-linear terms are approximated with piece-wise linear curves.

There are several strategies to formulate piece-wise linear models. In this work, the incremental method is used due to its superior solving speed [91].

In the incremental method, the non-linear function is approximated by a sum of incremental quantities. Auxiliary binary variables are used to assure the segments are summed in the correct order, this will be illustrated next.

Figure 7.5 shows the piece-wise linear approximation of the quadratic pressure. At discrete pressures $D_{x=1..4}^p$ the quadratic pressure is calculated as $H_{x=1..4}^p$, in between these discrete pressure points, the quadratic pressure is calculated as the linear interpolation between H_x^p and H_{x+1}^p .

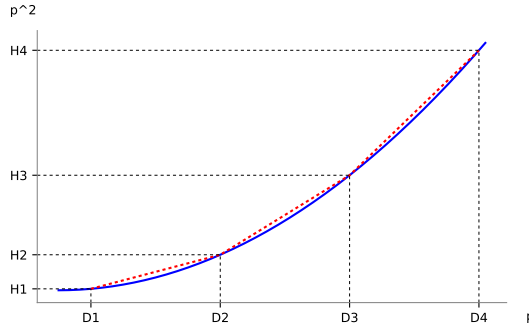


Figure 6.2: Piece-wise linear approximation of quadratic pressure

The pressure and its square are both calculated as the sum of incremental segments:

$$p_{ng,t} = D_1^p + \sum_x (D_{x+1}^p - D_x^p) \delta_{ng,t,x}^p \quad \forall ng, t \quad (6.45)$$

$$p_{ng,t}^2 = H_1^p + \sum_x (H_{x+1}^p - H_x^p) \delta_{ng,t,x}^p \quad \forall ng, t \quad (6.46)$$

δ^p and γ^p are both auxiliary variables to assure the piece-wise linear segments are used in the correct order. With $\delta^p \in [0, 1]$ and $\gamma^p \in \{0, 1\}$:

$$\delta_{ng,t,x+1}^p \leq \gamma_{ng,t,x}^p \quad \forall ng, t, x \quad (6.47)$$

$$\delta_{ng,t,x}^p \geq \gamma_{ng,t,x}^p \quad \forall ng, t, x \quad (6.48)$$

The quadratic flow $\tilde{q}_{pl,t}|\tilde{q}_{pl,t}|$ is approximated in the same manner:

$$\tilde{q}_{pl,t} = D_1^q + \sum_{x2} (D_{x2+1}^q - D_{x2}^q) \delta_{pl,t,x2}^q \quad \forall pl, t \quad (6.49)$$

$$\tilde{q}_{pl,t}|\tilde{q}_{pl,t}| = H_1^q + \sum_{x2} (H_{x2+1}^q - H_{x2}^q) \delta_{pl,t,x2}^q \quad \forall pl, t \quad (6.50)$$

With δ^q and γ^q again auxiliary variables:

$$\delta_{pl,t,x2+1}^q \leq \gamma_{pl,t,x2}^q \quad \forall pl, t, x2 \quad (6.51)$$

$$\delta_{pl,t,x2}^q \geq \gamma_{pl,t,x2}^q \quad \forall pl, t, x2 \quad (6.52)$$

6.3 Model verification

The electric power system model was taken from Van den Bergh et al. who present a verification of the model in [95]. Hence, no further verification is given here. The gas flow formulation presented before was taken from [91], where the formulation is derived from the gas dynamics governing equations using an implicit discretization method of finite differences. The author from [91] points out that the discretization step, both in time and space, should be sufficiently small to guarantee sufficient accuracy. However, since small discretization steps are not practical for optimization purposes, a coarser discretization with time steps ranging from 15 minutes to 2 hours and spatial steps going up to 80 km are used [91]. The resulting formulation is hence termed a 'dynamic model' rather than a 'transient model' to indicate the coarse time discretization [91]. A verification of the accuracy of such coarse discretization is not provided in [91] and hence will be done here.

To gain insight in the accuracy of the dynamic model formulation, a transient gas flow is applied to a pipeline resulting in a varying pressure in the pipeline. This pressure is calculated in two different ways, (1) using the dynamic gas model from [91] as presented in Section 6.2, and (2) using a transient gas model which is modeled using a fine discretization of the gas dynamics governing equations as presented in the next section.

6.3.1 Gas dynamics governing equations

Transient, compressible gas flows can be described by the conservation equations of mass, momentum and energy. For simplicity, the gas flow is assumed to be one dimensional and the pipeline itself is assumed to have a constant diameter and no differences in height. In that case, the conservation equations take the following form [99, 100]:

Conservation of mass:

$$\frac{\partial \rho}{\partial t} + \frac{\partial(\rho u)}{\partial x} = 0 \quad (6.53)$$

Conservation of momentum:

$$\rho \frac{\partial u}{\partial t} + \rho u \frac{\partial u}{\partial x} + \frac{\partial p}{\partial x} + \frac{f}{2D} \rho u^2 = 0 \quad (6.54)$$

Conservation of energy:

$$\rho C_v \left(\frac{\partial T}{\partial t} + u \frac{\partial T}{\partial x} \right) + T \left(\frac{\partial p}{\partial T} \right)_\rho \frac{\partial u}{\partial x} - \frac{f}{2D} \rho u^3 + \frac{4U}{D} (T - T_a) = 0 \quad (6.55)$$

The energy equation can be expressed in different equivalent ways. It is opted here to express it in terms of temperature, rather than in terms of enthalpy. In the above equations ρ represents the gas density, u the gas velocity, p the local gas pressure and T the gas temperature. The heat capacity of natural gas is represented by C_v and the heat transfer coefficient U gives an indication of the amount of heat transfer between the gas and its surroundings at a temperature T_a . The diameter of the pipeline is indicated by parameter D . Viscous flow effects are captured by Darcy's friction factor, represented by f . Recall that for turbulent gas flows, this friction factor is only a function of pipeline roughness.

The conservation Eqs. (6.53) - (6.55) contain four unknowns (pressure p , density ρ , temperature T and velocity u) for only three equations. An additional equation is needed to complement the above set of equations. This additional relation is the equation of state for real gases:

$$p = zrT\rho, \quad (6.56)$$

where z and r represent respectively the compressibility factor and the specific gas constant. The compressibility factor z is a correction for the ideal gas law and is not a constant for each gas — as is the specific gas constant r — but is temperature and pressure dependent. By definition, this factor equals the ratio of the volume taken up by a real gas at a certain temperature and pressure compared to the volume an ideal gas would take up at identical conditions [105]:

$$z(p, T) = \frac{V_{realgas}(p, T)}{V_{idealgas}(p, T)} \quad (6.57)$$

In most cases the volume taken up by a real gas is less than the volume taken up by an ideal gas, such that the compressibility factor is less than unity. An overview of different methods to calculate this compressibility coefficient can be found in [106]. This work calculates the factor by linear interpolation in between determined values of temperature and pressure, based on [107].

The Eqs. (6.53) - (6.55) are expressed in terms of density, velocity and temperature. To be able to apply boundary conditions of pressure and mass flow in case studies, the conservation equations might be expressed in terms of pressure, mass flow and temperature as well. The derivation and final expression of these equations can be found in [108].

To solve the system (6.53) - (6.55), complemented with the equation of state (6.56) subjected to certain boundary conditions in a numerical way, there exist multiple solution techniques. An overview of the possible methods can be found in the review paper of Thorley and Tiley [109]. Here, a second order spatial discretization scheme has been employed using central differences for all internal points, and forward/backward differences on the left/right boundaries (note that we model the pipeline as a 1D system as shown in the next section). An explicit fourth order Runge-Kutta method is employed for time integration.

6.3.2 Verification set-up

The accuracy of the momentum conservation equation in the dynamic model is verified on one single pipeline, modeled as a one-dimensional system. Since the conservation of momentum is imposed on each pipeline individually, a verification on one pipeline can be generalized to the entire network.

The 'benchmark' pipeline, gas and environment characteristics are given in Table 6.2. The pipeline is assumed to run horizontal and to have a constant diameter D over the entire pipeline length.

The compressibility factor⁸ Z is assumed constant and equal to 0,8 in the dynamic model run. For the transient model, the compressibility factor is calculated as a function of the pressure and temperature as presented in Eq. (6.57).

The discretization parameters for the two different models are provided in Table 6.3.

A constant inflow of $300 \text{ Nm}^3/\text{s}$ and a continuously varying outflow are applied to the pipeline. Since the dynamic formulation works with larger time steps, an hourly average outflow is applied in the dynamic model, as shown in Figure 6.3.

⁸Note that a capital Z is adopted if a constant compressibility factor is used, while a lower case $z(p, T)$ is adopted if a compressibility factor as a function of pressure and temperature is used.

Table 6.2: Parameters used for dynamic model verification

Parameter		Value	source
Length L	[km]	100	
Diameter D	[m]	1	
Roughness e	[m]	$5 \cdot 10^{-5}$	[101]
Thermal conductivity k	$[\frac{W}{mK}]$	25	[101]
Heat transfer coefficient U	$[\frac{W}{m^2K}]$	7.96	
Heat capacity C_v	$[\frac{J}{kgK}]$	1759	[101]
Specific gas constant r	$[\frac{J}{kgK}]$	518.8	[101]
Friction factor f	[-]	0.00806	
Gas density at standard conditions ρ_0	$[\frac{kg}{m^3}]$	0.7156	
Temperature at standard conditions T_0	[K]	288.15	
Pressure at standard conditions p_0	[bar]	1.013	
Ambient temperature T_a	[K]	285.15	[101]

Table 6.3: Discretization parameters for verifications

Domain	Step size	
	Transient	Dynamic
Spatial	500 m	100 km
Temporal	0.82 s	3600 s

6.3.3 Results and discussion

Figure 6.4 presents the inlet pressure (left panel) and outlet pressure (right panel) calculated with the dynamic and transient model for the imposed constant inlet flow and varying outlet flow presented before. It is clear that there is a difference in calculated pressures, due to the difference in discretization and the difference in the compressibility factor Z used. Figure 6.4 shows however that the dynamic model, with very coarse time steps, is able to follow the pressure trends.

The hourly calculated pressure values and the relative difference between the results from both models are reported in Table 6.4. The average reported error is 1.23% with a maximum error up to 1.92%.

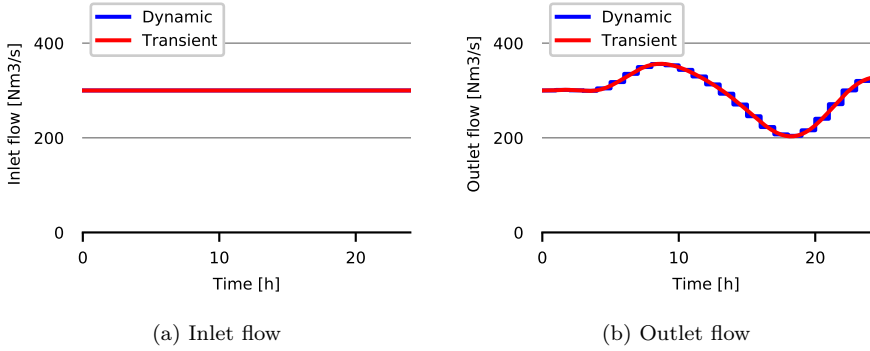


Figure 6.3: Constant inlet flow, continuously varying outlet flow and its hourly average used for the dynamic model verification. Note that both dynamic and transient curves exactly coincide, since they are exogenously imposed, hence only one curve is visible.

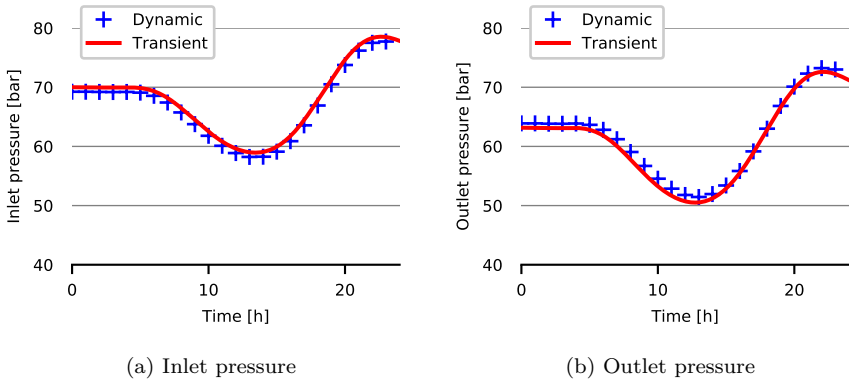


Figure 6.4: Inlet and outlet pressure resulting from the transient and dynamic model when isothermal conditions are assumed

Table 6.4: Inlet and outlet pressure values and the relative difference between the transient and dynamic model formulation when assuming isothermal flow.

Hour	Inlet pressure			Outlet pressure		
	Transient	Dynamic	Error	Transient	Dynamic	Error
1	70.00	69.24	1.08%	64.71	63.89	1.26%
2	70.00	69.24	1.08%	64.71	63.89	1.26%
3	69.96	69.21	1.08%	64.65	63.84	1.25%
4	69.94	69.19	1.08%	64.66	63.83	1.28%
5	69.97	69.21	1.09%	64.68	63.87	1.25%
6	69.86	69.09	1.10%	64.39	63.65	1.15%
7	69.29	68.55	1.06%	63.46	62.81	1.03%
8	68.09	67.42	0.98%	61.80	61.22	0.95%
9	66.33	65.74	0.89%	59.61	59.06	0.93%
10	64.29	63.76	0.82%	57.27	56.70	1.00%
11	62.29	61.80	0.80%	55.17	54.54	1.13%
12	60.61	60.11	0.84%	53.55	52.86	1.30%
13	59.42	58.88	0.92%	52.56	51.79	1.47%
14	58.83	58.22	1.03%	52.31	51.45	1.63%
15	58.94	58.26	1.16%	52.89	51.95	1.79%
16	59.88	59.11	1.28%	54.43	53.40	1.90%
17	61.75	60.89	1.40%	56.94	55.84	1.92%
18	64.51	63.56	1.47%	60.26	59.16	1.84%
19	67.93	66.91	1.49%	64.07	63.00	1.68%
20	71.55	70.50	1.47%	67.85	66.84	1.49%
21	74.80	73.76	1.39%	71.03	70.10	1.31%
22	77.19	76.19	1.30%	73.15	72.31	1.15%
23	78.44	77.51	1.18%	73.99	73.23	1.03%
24	78.56	77.73	1.06%	73.71	73.00	0.96%

In the previous verification, the flow through the pipeline was assumed isothermal in order to simplify the gas dynamics governing equations by disregarding the conservation of energy. It is, however, interesting to explore the error introduced by this simplification. In the following example, the pressures calculated using the dynamic model assume again isothermal flow conditions. For the pressure calculated with the transient model, the conservation of energy equation is now taken into account, considering the actual gas temperature due to compression and heat transfer to its surroundings. Furthermore, an inlet temperature of 42°C is assumed [101]. Figure 6.5 presents the calculated inlet and outlet pressures resulting from the imposed inlet and outlet flows.

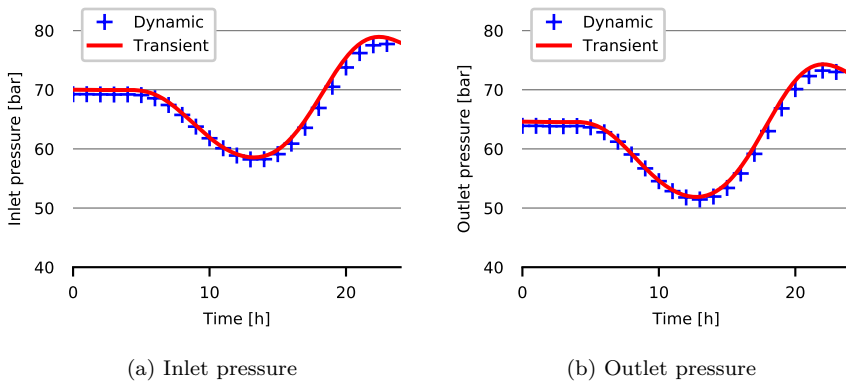


Figure 6.5: Inlet and outlet pressure resulting from the transient and dynamic model. Isothermal conditions are assumed for the dynamic model while non-isothermal conditions are assumed for the transient model.

The hourly calculated pressure values and the relative difference between the results from both models are reported in Table 6.5. The maximum and average error are now, respectively, 2.29% and 1.14%. Since the parameters values found in the literature for the cost and technical characteristics used in the unit commitment model have a larger variation than the average error of 1.14% , it is found that the dynamic gas flow formulation is sufficiently accurate for the unit commitment model.

Table 6.5: Inlet and outlet pressure values and the relative difference between the transient and dynamic model formulation when assuming isothermal flow for the dynamic model and non-isothermal flow for the transient model.

Hour	Inlet pressure			Outlet pressure		
	Transient	Dynamic	Error	Transient	Dynamic	Error
1	70.00	69.24	1.08%	64.60	63.89	1.09%
2	70.00	69.24	1.08%	64.60	63.89	1.09%
3	69.96	69.21	1.07%	64.53	63.84	1.08%
4	69.94	69.19	1.07%	64.54	63.83	1.11%
5	69.97	69.21	1.10%	64.57	63.87	1.08%
6	69.83	69.09	1.06%	64.25	63.65	0.94%
7	69.19	68.55	0.92%	63.25	62.81	0.70%
8	67.88	67.42	0.68%	61.47	61.22	0.42%
9	66.02	65.74	0.42%	59.17	59.06	0.20%
10	63.91	63.76	0.23%	56.77	56.70	0.12%
11	61.89	61.80	0.16%	54.64	54.54	0.17%
12	60.24	60.11	0.22%	53.03	52.86	0.34%
13	59.10	58.88	0.37%	52.09	51.79	0.57%
14	58.57	58.22	0.60%	51.90	51.45	0.86%
15	58.78	58.26	0.88%	52.58	51.95	1.21%
16	59.84	59.11	1.22%	54.25	53.40	1.58%
17	61.87	60.89	1.59%	56.93	55.84	1.91%
18	64.82	63.56	1.94%	60.45	59.16	2.14%
19	68.41	66.91	2.19%	64.44	63.00	2.25%
20	72.15	70.50	2.29%	68.35	66.84	2.22%
21	75.44	73.76	2.23%	71.57	70.10	2.05%
22	77.75	76.19	2.01%	73.61	72.31	1.77%
23	78.84	77.51	1.68%	74.29	73.23	1.43%
24	78.78	77.73	1.33%	73.83	73.00	1.12%

6.4 Illustrative case studies

Four cases are presented in this section to illustrate the value of incorporating gas production ramp rates, zonal loads and a detailed P2G representation in the integrated electricity and gas model. Results show that incorporating these additional constraints might have only a small effect on the total operational cost, but has a significant impact on the pressure swings observed in the network and on operation schedules of gas production and P2G units.

All technical and cost characteristics used in the reference case are given first,

after which the different cases are explained. The case study results are presented and discussed next.

6.4.1 Reference case parameter data

Except for the topology of the electrical power grid and the natural gas network, the energy system used is inspired by the Belgian electricity and gas systems. All power plant and storage unit characteristics are based on existing technologies. Load and generation profiles are based on real profiles from 2015. To determine the amount of installed power generation and storage capacity, results from an 80% RES case⁹ presented in chapter 4 are used. An 80% RES case is chosen since it was shown in chapter 4 that P2G only becomes desirable for such high RES shares. To limit the computational run times, the system and its installed capacities are scaled down to $1/10^{th}$ of its size reported in chapter 4.

Gas network topology

The gas network topology used in the different case studies is shown in Figure 6.6, consisting of 7 nodes connected with 6 pipelines (solid lines) and divided in 2 load zones (dashed lines). A simple, fictitious, topology is used consisting of pipelines with characteristics based on pipelines in the Belgian gas network [104].

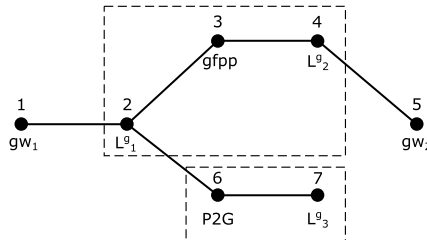


Figure 6.6: Gas network topology used in the illustrative case studies consisting of 7 nodes connected with 6 pipelines (solid lines) and divided in 2 zones (dashed lines).

Two gas production facilities (*gw*) are placed in node 1 and 5, a GFPP (gas consumption) is placed in node 3 and a P2G unit (gas production) in node 6.

⁹The precise case used has an 80% RES target, all storage, curtailment and sequestration allowed and a CO₂ emission cost of 50 €/ton. RES technology shares of 66% solar, 22% offshore wind and 12% onshore wind are imposed and costs for all storage technologies are as in the reference case of chapter 4.

Nodes 2, 4 and 7 contain gas loads (residential and industrial) with gas loads in nodes 2 and 4 belonging to the same gas zone and the gas load in node 7 belonging to another gas zone. The characteristics of each load, conversion unit and gas production facility will be discussed in the following sections.

The gas pipeline characteristics are listed in Table 6.6, with L de pipeline length, e the absolute roughness, D the pipeline diameter and f the resulting friction factor, calculated following Eq. (6.40). For simplicity, all pipelines have equal length and absolute roughness. Although this gas network topology is not a representation of the Belgian gas network, the characteristics of individual pipelines are representative for real pipelines.

Table 6.6: Gas pipeline characteristics used in the illustrative case studies.

From node	1	2	2	3	4	6
To node	2	3	6	4	5	7
L [km]	30	30	30	30	30	30
e [mm]	0.05	0.05	0.05	0.05	0.05	0.05
D [m]	0.89	0.89	0.59	0.59	0.59	0.59
f [—]	0.0108	0.0108	0.0116	0.0116	0.0116	0.0116

The gas and environment characteristics are listed in Table 6.7 and are equal to the characteristics used for the model verification (Table 6.2).

Table 6.7: Gas and environment characteristics used in the illustrative case studies.

Parameter	Unit	Value
Gas temperature T	[K]	285.15
Gas density at standard conditions ρ_0	[kg/m ³]	0.7156
Gas compressibility factor at standard conditions Z	[—]	0.8
Pressure at standard conditions p_0	[bar]	1.013
Temperature at standard conditions T_0	[K]	288.15

Since all novel model additions are made in the gas part of our integrated model, the illustrative cases only focus on the gas part. The electric power system is hence simplified to a one node system which contains an electrical load, RES generation, a battery storage unit, a GFPP and a P2G unit (both connected to the gas system).

Load profiles

Belgian electrical power and gas load data from 2015 are used in the illustrative cases. A one day period at the end of January 2015 is chosen as example to optimize. The hourly electrical power load (as seen by the TSO) is obtained from Elia, the Belgian TSO [77]. The minimum, maximum and average electrical power load are reported in Table 6.8 for this one day period, corresponding to $1/10^{th}$ of the Belgian electrical power load reported by Elia.

Table 6.8: Gas and electrical power load characteristics used in the illustrative case studies.

	Unit	Load		
		Minimum	Maximum	Average
Electrical	MW_e	1017	1360	1210
Gas	MW_{CH_4}	1717	4639	3207

The Belgian hourly gas load on the same winter day in 2015 is used and obtained from Synergrid [110]. The minimum, maximum and average load are listed in Table 6.8; note that these are also scaled to $1/10^{th}$ of the load reported by Synergrid. Both the electrical power and natural gas load are shown in Figure 6.7.

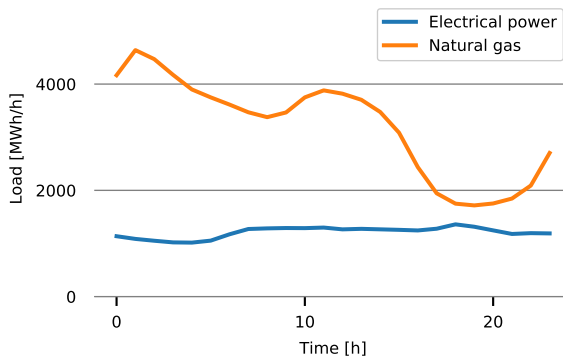


Figure 6.7: Electricity and gas load during the studied 24h period. Electricity load expressed in MWh_e/h and gas load expressed in MWh_{CH_4}/h .

The total reported gas load is broken down in an industrial gas load, accounting for 33% of the total gas load (excluding the GFPP load), and a residential

gas load, accounting for 67% of the total. These loads per type are further assigned to the different nodes in the gas network as reported in Table 6.9. Note that Table 6.9 reports the residential load per node which is strictly only the case when no load zones are considered. In most cases, load zones are used as presented in Figure 6.6 and hence the residential load from nodes 2 and 4 are accumulated to one zonal load and the residential load of node 7 is assigned to another zonal load.

Table 6.9: Gas load characteristics detailed per load type and node. The residential loads from nodes 2 and 4 are accumulated to the load of 1 zone when gas zones are used, the residential load of node 7 is assigned to a separate zone.

	Node		
	2	4	7
Industrial	-	50%	50%
Residential	10%	75%	15%

Renewable generation profiles

The installed RES generation capacities (onshore wind, offshore wind and solar PV) are shown in Table 6.10 (scaled to $1/10^{th}$ of the size reported in Chapter 4). The instantaneous renewable generation profile is based on the Belgian RES generation occurring on a winter day at the end of January 2015, the same day is used as for the load profiles. The RES generation profiles are obtained from Elia [77] and scaled according to the installed capacities. The resulting hourly minimum, maximum and average RES generation is also shown in Table 6.10.

Table 6.10: Renewable capacities and resulting generation used in the illustrative case studies.

RES capacity [MW_e]			Total RES generation [MW_e]		
Onshore	Offshore	Solar PV	Minimum	Maximum	Average
502	525	5457	18	1419	360

Gas-fired power plant

A modern combined cycle gas turbine (CCGT) with characteristics shown in Table 7.5 is used as GFPP technology in the following cases. The characteristics are based on the CCGT technology reported by Van den Bergh [95].

Table 6.11: Gas-fired power plant characteristics.

Parameter	Unit	Value
Maximum power output	$[MW_e]$	1000
Minimum power output	$[MW_e]$	280
Ramp-up/-down rate	$[\%/Pmax/t]$	100
Minimum up/down-time	$[h]$	3
Efficiency	$[\%]$	58
Variable O&M	$[\text{€}/MWh_e]$	12.8
Start-up cost	$[\text{€}]$	26200

The maximum power output is equal to the installed capacity which is taken from Chapter 4 (912 MW_e) and rounded-up to 1000 MW_e . Since more technical constraints are considered in the current operational model compared to the investment model, using exactly 912 MW_e could lead to infeasibilities if the technical constraints become limiting, hence the installed GFPP is rounded-up.

Battery storage

Sodium-sulfur (NaS) battery characteristics are used since they are suitable for grid-scale battery storage [66]. The installed power and energy capacities are shown in Table 6.12.

Table 6.12: Battery characteristics.

Parameter	Unit	Value
Maximum charging power	$[MW_e]$	1141
Maximum discharging power	$[MW_e]$	1141
Energy storage capacity	$[MWh_e]$	8215
Single-trip efficiency	$[\%]$	90

Power-to-gas

The power-to-gas (P2G) plant is modeled as three consecutive units, the electrolyzer, hydrogen storage and methanation unit.

The electrolyzer characteristics are given in Table 6.13. The maximum electrical power consumption is equal to the installed capacity reported in Chapter 4

(scaled-down by a factor 10). The technical characteristics are based on the literature review presented in Chapter 2.

Table 6.13: Electrolyzer characteristics.

Parameter	Unit	Value
Maximum electrical power consumption	$[MW_e]$	341.4
Efficiency	$[\%]$	75
Variable O&M	$[\text{€}/MWh_e]$	2

The methanation unit has dynamic operation characteristics which are slower than the hourly time step used in this model. The characteristics used are based on the review presented in chapter 2 and given in Table 6.14.

Table 6.14: Methanizer characteristics.

Parameter	Unit	Value
Maximum production	$[MW_{CH_4}]$	179.24
Minimum production	$[MW_{CH_4}]$	65
Ramp-up/-down rate	$[\%/Pmax/t]$	10
Start-up/shut-down rate	$[\%/Pmax/t]$	50
Minimum up-time	$[h]$	6
Minimum down-time	$[h]$	6
Efficiency	$[\%]$	70
Variable O&M	$[\text{€}/MWh_{CH_4}]$	5

No minimum up-times or down-times have been reported in the literature, most likely because there is no technical limit which requires such minimum up- or down-time. However, since only high-level characteristics of the methanation plant are used and hence the cost of a start-up and shut-down or the possibly reduced life-time due to rapid switching between on and off state are not explicitly accounted for, a minimum up- and down-time imposed on the methanation reactor could serve as a proxy for these cost aspects as it forces the dispatch schedule to start a methanation reactor only when it is worthwhile for several hours, which would also be the expected behavior of a real methanation plant operator. This is similar to the scheduling problem of conventional generation units [111].

The hydrogen buffer between the methanation unit is modeled in a succinct way, considering only the minimum and maximum state-of-charge as given in Table 6.15. The assumption is made that the charging and discharging capacity of the hydrogen buffer is sized to accommodate the maximum electrolyzer

production rate and methanation consumption rate and should hence not be modeled explicitly. The buffer size (maximum state-of-charge) has been taken corresponding to the average hydrogen buffer size observed in the different cases presented in Chapter 4.

Table 6.15: Hydrogen buffer characteristics.

Parameter	Unit	Value
Maximum state-of-charge	$[MWh_{H_2}]$	6165
Minimum state-of-charge	$[MWh_{H_2}]$	200

Gas production facilities

Two gas production facilities with equal operational characteristics have been incorporated in the case study. Only the cost at which both facilities produce differs whereby production facility 1 is a mainstream facility with a cost of 0.22 €/Nm^3 ($\sim 20.3 \text{ €/MWh}_p$) and facility 2 represents a more expensive facility with a cost which is threefold that of facility 1.

The ramp rates imposed on the different production facilities are chosen based on information received from Fluxys, the Belgian gas TSO [93]. Although production facilities are technically capable of higher ramping rates, they are not desirable to avoid large pressure swings in the gas network.

Table 6.16: Gas production facility characteristics.

Parameter	Unit	Facility 1	Facility 2
Maximum production	$[\text{Nm}^3/h]$	700 000	700 000
Minimum production	$[\text{Nm}^3/h]$	0	0
Ramp-up/down rate	$[\%/\overline{W}_{gw}/t]$	10	10
Production cost	$[\text{€/Nm}^3]$	0.22	0.66

6.4.2 Case set-up

Four different cases are presented to illustrate the value of incorporating gas production ramp rates, zonal loads and a detailed P2G representation in the integrated electricity and gas model. A first case is the reference case, in which all novel model aspects are incorporated. In each of the other three cases, one

of the novel model aspects will be neglected and the results will be compared to the reference case.

In the *reference* case, all novel model aspects are considered. The parameters as given in Tables 6.6-6.16 are used. For the residential gas loads (presented in Table 6.9), zonal loads are considered, meaning that residential loads in node 2 and 4 are taken together as one zonal load which can be served through nodes 2, 3 and 4, assuming that in these nodes, the high pressure gas grid is coupled with the low pressure gas distribution grid to serve the residential demand.

In the *single unit P2G* case, the P2G unit consisting of electrolyzer and methanizer is regarded as one, integrated, unit by removing the hydrogen buffer.

In the *no ramp rates* case, no ramp rates for the gas production facilities are accounted for. Allowing these production facilities to vary their production levels each hour between minimum and maximum.

In the *no zonal load* case, the residential gas loads are assigned to a specific node rather than to a 'load zone', effectively assuming that gas distribution networks can only be coupled to the gas transmission network in one node. The load division as presented in Table 6.9 is used in this case.

6.4.3 Results and discussion

The effect of including a detailed P2G model, ramp rates for gas production facilities and load zones is illustrated by discussing the total operation cost, the pressure in the gas network, the methane production from P2G plants and the gas production from gas facilities. Note that the presented results serve as an illustration of possible effects of including a detailed P2G model, ramp rates and load zones. However, this does not mean that each effect illustrated here will always be observed in any system, since the possible effect becomes only clear when a constraint is limiting, which depends on the specific case.

P2G operational detail

First the effect of including a detailed P2G model is investigated by looking at the methane production from P2G units shown in Table 6.17. It is clear that modeling a P2G unit as a single, integrated unit rather than as distinctive electrolyzer, methanizer and hydrogen buffer can lead to an underestimation of the P2G unit operation.

Table 6.17: Methane production form P2G.

Case	Production [MNm ³]	Relative difference
Reference	0.1163	
Single-unit P2G	0	-100%
No ramp rates	0.1163	0%
No zonal loads	0.1163	0%

When the P2G unit is modeled as a single unit without intermediate hydrogen buffer, the electrolyzer and methanizer are directly coupled. Hence, the dynamic constraints of the methanizer unit also apply to the electrolyzer unit, since the electrolyzer can only produce hydrogen at times that it can be consumed instantaneous by the methanizer. The reduced methane production shown in Table 6.17 can be understood since the integrated P2G unit might be operated too slowly to take advantage of short periods of surplus iRES generation.

More surprisingly, relaxing the dynamic operational constraints of the methanizer, thereby making the integrated unit effectively as dynamic as the electrolyzer, could also yield a lower methane production (not shown in Table 6.17). This can be understood as the P2G operation not only depends on the availability of surplus electrical power, but also on the possibility to inject the produced methane in the gas network. Disregarding the intermediate hydrogen buffer hence reduces the flexibility of the P2G unit and forces it to operate only when there is a simultaneous availability of electrical power and possibility to inject methane in the gas grid. This could lead to an underestimation of the possible P2G operation compared to cases where a hydrogen buffer is considered.

Note that whether or not ramp rates for conventional gas production facilities and zonal gas load are considered, does not have an effect on the synthetic methane production in this illustrative case.

Gas production ramp rates

Next, the effect of including ramp rates for the gas production facilities is discussed. Note that these ramp rates do not represent technical production limits but are rather imposed by the gas TSO to avoid large pressure swings in the gas network. Hence the hourly pressure variations, i.e., the difference in nodal pressure between two consecutive hours, are shown in Table 6.18. For each of the four cases, the mean and median pressure variation is given, together with the relative difference with the pressure variations in the reference case.

Table 6.18: Hourly pressure variations

Case	Hourly pressure difference [bar]			
	Average	Rel. diff.	Median	Rel. diff.
Reference	1.886		1.840	
Single-unit P2G	1.821	-3.5%	1.860	+1.1%
No ramp rates	2.446	+29.7%	2.680	+45.7%
No zonal loads	1.858	-1.5%	1.975	+7.4%

The increase pressure variability is also illustrated in Figure 6.8 which shows that imposing ramp rates on the gas production facilities leads to smoother variations in the pressure profile.

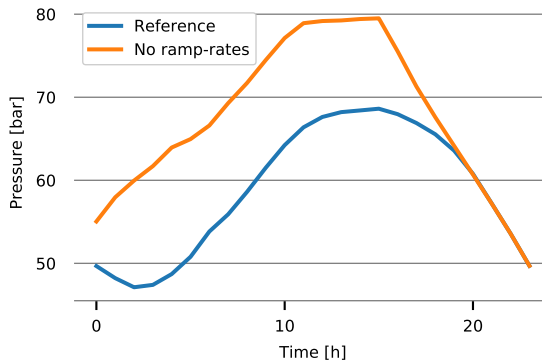


Figure 6.8: Pressure profile in node 2 for the reference case and for the case without ramp rates imposed.

Not including ramp rates for gas production facilities provides additional operational freedom that could lead to a more optimal operation of the gas network. However, it could also result in increased pressure variations, as shown in Table 6.18, which could be undesirable for the gas network operator and would hence not be realistic in gas network operations.

Gas load zones

Incorporating gas load zones can provide additional flexibility to the gas network. By assuming that the gas distribution network is coupled to the transmission

network in multiple nodes, the residential gas load is allowed to be served through these multiple nodes in the transmission network. Not modeling these gas load zones could lead to less optimal operational schedules as shown in Tables 6.19 and 6.20.

Table 6.19 presents the total gas production of each gas production facility in each case. For most cases, only gas production facility 1 (at lower cost) is required to serve the different gas loads. When no gas load zones are considered to serve the residential gas load, the pipeline between node 4 and 5 becomes a bottleneck in the network and gas production facility 2 (at higher cost) is required to serve part of the load in node 5.

Table 6.19: Natural gas production from different production facilities.

Case	Natural gas production [MNm ³]	
	gw ₁	gw ₂
Reference	10.263	0.0
Single-unit P2G	10.388	0.0
No ramp rates	10.255	0.0
No zonal loads	10.219	0.160

The necessary use of the more expensive gas production facility is also reflected by the higher total operational cost shown in Table 6.20. All cases are optimized with a optimality gap of 0.1%, since the cost difference between all cases are larger than this optimality gap, they result from the difference in modeling constraints which are considered.

Table 6.20: Total operational system cost, resulting from optimization with a 0.1% optimality gap.

Case	Cost [M€]	Rel. Diff.
Reference	2.899	
Single-unit P2G	2.922	+0.78%
No ramp rates	2.896	-0.12%
No zonal loads	3.000	+3.47%

Table 6.20 shows that excluding the ramp rates of gas production facilities provides more freedom for optimization and could lower the total cost, while modeling the P2G unit as a single integrated unit removes optimization freedom resulting in an increased total cost.

6.5 Summary and conclusions

This chapter started with a discussion on the increasing need for flexibility in the electric power system which could be transferred to the natural gas system due to the interconnection of both systems via gas-fired power plants (GFPPs) and P2G units. The concept of line pack and line pack flexibility was introduced next, together with an explanation of how the line pack flexibility can serve as a short-term gas storage inherent to the gas transmission network. Further in the introduction, it is explained that line pack and line pack flexibility can only be adequately modeled if both pressures and flows are explicitly calculated in the gas network. Hence it is key for operational models to incorporate this.

An overview and high-level categorization of existing multi-carrier energy system (MES) models is provided and the integrated electric power and gas model introduced in Section 6.2 is situated in this categorization. Next, three novel model elements are introduced together with a description of the model:

1. P2G units are modeled with a higher level of technical detail than currently found in the literature;
2. the representation of gas production facilities found in the current literature is extended with ramp rates to model a more realistic gas production profile;
3. the nodal mass balance constraint found in the current literature is extended to include a zonal mass balance constraint which allows to consider possible flexibility provided by the gas distribution network, without explicitly modeling this gas distribution network.

The relevance of each of these novel model elements has been illustrated with different case studies. These case studies show that a less-detailed representation of P2G units could lead to an underestimation of the P2G unit operation. Since the detailed P2G model considers the electrolyzer, methanizer and intermediate hydrogen buffer as three distinctive units, the hydrogen buffer can effectively decouple the electrolyzer and methanizer operation for a short period of time. Not considering this decoupling requires a simultaneous surplus of electrical power (for the electrolyzer to consume) and availability of transport capacity in the gas network (for the methanizer to be able to inject the produced methane). Hence, modeling the P2G unit as a single integrated unit requires favorable conditions for synthetic methane production in the electric power and gas system simultaneously. This could lead to an underestimation of P2G unit operation if a single unit model is used compared to a detailed model. The case studies show furthermore that this lower synthetic methane production is independent of

whether the integrated P2G unit is modeled with or without dynamic operating constraints such as ramp rates, minimum operating level and minimum up- and down-times.

A case study evaluating the impact of imposed ramp rates on gas production facilities shows that these ramp rates lead to more realistic gas production profiles. Although these ramp rates do not follow from any technical constraints, they are imposed by gas transmission system operators (TSOs) to avoid large pressure swings in the pipeline which could endanger a safe operation of the gas network. Case studies show indeed that neglecting such ramp rates could result in an increased intra-hourly pressure variation in the gas network, up to almost 30% on average.

A case study evaluating the impact of incorporating zonal gas loads shows that including such zonal loads, and thereby assuming a gas distribution network which could provide some flexibility to the gas system, could result in a more optimal operation of the entire gas system. When no zonal loads are considered and hence the possible flexibility from the gas distribution system is not accounted for, the gas transmission network is more constrained which could lead to a less optimally operated gas network. In this case study, this results in an increase of the operating cost by almost 3.5%.

Besides case studies illustrating the value of novel model elements, also a verification of the flow-pressure relation is given. This relation is used to calculate the pressure drop corresponding to given a gas flow in a certain pipeline and results from a simplification of the gas flow governing equations. These governing equations, comprising the conservation of mass, momentum and energy, are strongly simplified to reduce their computational complexity. In this simplification, isothermal gas flow is assumed and a coarse temporal and spacial discretization is used. Although this relation and its implementation is found in the literature [91], an empirical verification of such model was not yet available and has therefore been presented in this chapter. In the verification, the pressure drop resulting from a gas flow through a pipeline is calculated with two different models. The first model being the integrated operational scheduling model and a second model which considers all governing equations without simplifications. The second model also uses a much finer discretization, allowing to account for all transient effects in the gas flow. The pressure drops calculated with both models show that the integrated (simplified) model can calculate pressure drops with a maximum relative error of 2.29% and an average relative error of 1.14% compared to the detailed model. Hence the integrated model is found suitable for realistic modeling of gas flows in a scheduling problem.

Chapter 7

Operational impact of P2G on the energy system

This chapter contains elements from:

Belderbos, A., Bruninx K., Valkaert, T., Delarue, E. and D'haeseleer, W. *Facilitating renewables and power-to-gas via integrated electric power-gas system scheduling*, TME working paper.

In this chapter, the operational impact of power-to-gas (P2G) on an interconnected electric power system and natural gas system is analyzed. The model presented in Chapter 6 will be used in combination with a simplified representation of the Belgian energy system which serves as example.

Since P2G will produce synthetic methane when surplus iRES generation is available, a possible volatile injection profile in the gas grid can occur for which gas network flexibility should be available in order to assure reliable operation of the network. Investigating the impact of P2G on the available gas flexibility is the subject of this chapter.

This chapter starts with a general introduction in Section 7.1, followed by an outline of the employed methodology in Section 7.2. The input parameters and an overview of the different case studies is provided in Sections 7.3 and 7.4. Results of the different case studies are presented and discussed next in Section 7.5. The chapter concludes with a summary and conclusions in Section 7.6.

7.1 Introduction

The increasing share of iRES capacity in the electric power system could transfer flexibility requirements from the electric power system to the natural gas system via an increasingly volatile gas off-take by gas-fired power plants and a volatile injection of synthetic methane by P2G units. To study the impact of such possible flexibility transfer on the natural gas network, different case studies are presented in this chapter, investigating the economic optimal operation of an integrated electrical power network and natural gas grid in different circumstances.

The objective of this chapter is two-fold. First, it is to evaluate to what extent the natural gas network can cope with the additional, possibly volatile, injection from P2G units. If the available gas network flexibility would not be sufficient to accommodate such additional injection of synthetic methane, it could limit the conversion and storage of surplus iRES generation via P2G or would require additional infrastructure investments at additional cost.

Second, it must be investigated to what extent the integration of P2G impacts the flexibility available for conventional gas production facilities. Even if the gas network has abundant inherent flexibility to accommodate the volatile injection of synthetic methane, such additional injection will reduce the flexibility available to conventional gas production facilities. This could result in additional costs for conventional production facilities to align their production profile with the gas load profile and should, if necessary, be considered in modeling the gas system.

A comparable study is presented by Clegg and Mancarella in which the operational impact of P2G on the Great Britain electrical power and natural gas networks is investigated [86]. For a British energy system which contains wind generation capacity amounting to 40% of the overall generation portfolio (on an installed power capacity basis), the authors conclude that energy transport capacities of the Great Britain gas network far exceeds the energy generation capacity of the installed wind turbines. Hence no issues would arise from converting surplus wind generation to gas via P2G and injecting it in the gas network. The same authors investigated the injection of electrically produced hydrogen in the gas grid in a later paper where they find that such hydrogen injection leads to larger pressure swings in the gas network [85]. They hereby explain that, due to the lower energy density of hydrogen, gas flow rates should increase to serve a given energy-flux demand. These higher flow rates lead to higher pressure drops in the gas network. Although an increase in flow rate and pressure drop in the gas network reduces the available flexibility, the authors point out that the networks still operates safely within imposed pressure bounds,

even for high shares of installed iRES capacity resulting in high injection rates of hydrogen.

Vandewalle et al. have presented a study on the impact of large-scale P2G on the electric power, gas and CO₂ sectors, using the Belgian energy system as an example [60]. The study concludes that P2G can significantly increase the demand for flexibility in the gas network. The consequence of this increased flexibility demand on the gas network operation has, however, not been investigated as the study did not explicitly model the network itself.

The current study reaches similar findings for the Belgian energy system as Clegg and Mancarella for the British system [86]. It is observed that for gas networks resembling the Belgian gas network, the integration of P2G capacity is not limited by a lack of flexibility in the natural gas network. Although the integration of P2G could lead to an increased flexibility demand in the gas network, no effect on the operation of conventional gas producers has been found.

7.2 Methodology

The integrated electric power and natural gas model presented in Chapter 6 is used to investigate the operational impact of P2G. A simplified model of the Belgian electrical power grid and natural gas network is implemented based on information provided by the Belgian electrical power transmission system operator (TSO) [112] and the gas TSO [93]. The CO₂ system is not explicitly modeled in this system, hence implicitly assuming that adequate infrastructure is in place to transport and temporarily store captured CO₂ from gas-fired power plants to be used in the P2G process. If insufficient CO₂-infrastructure would be available, this could limit the synthetic methane production which would in turn limit the possibly injection from P2G in the gas network, thereby reducing the demand for flexibility from the gas network.

The electrical power demand and natural gas demand together with the iRES generation profiles from 2015 are used. Installed iRES, conventional generation, battery and P2G capacities are obtained from the energy system investment study presented in Chapter 4. Two investment cases will be used as input, one with an imposed RES target of 80% and one with a target of 99%. The selected investment cases use the reference construction costs listed in Chapter 4, a CO₂ price of 50 €/ton, allow for CO₂-sequestration and iRES curtailment and assume that all storage technologies (pumped hydro storage (PHS), batteries and P2G) are available.

A description of all the input parameters is provided in the following Section. An overview of the different operational case studies covered in this Chapter is given in Section 7.4.

7.3 Input parameters

An overview of both the high-voltage electrical power grid and high-pressure gas network in Belgium is presented in Figure 7.1. Each of the systems will be discussed in more detail throughout this section.



Figure 7.1: The high-voltage Belgian electrical power grid (black) and high-pressure gas network (gray). Note that the indicated connections do not represent the actual physical line paths.

7.3.1 Natural gas system

Network topology

The gas network used in this chapter is inspired on the Belgian high-pressure gas transmission network. The geographic topology is presented in Figure 7.2.

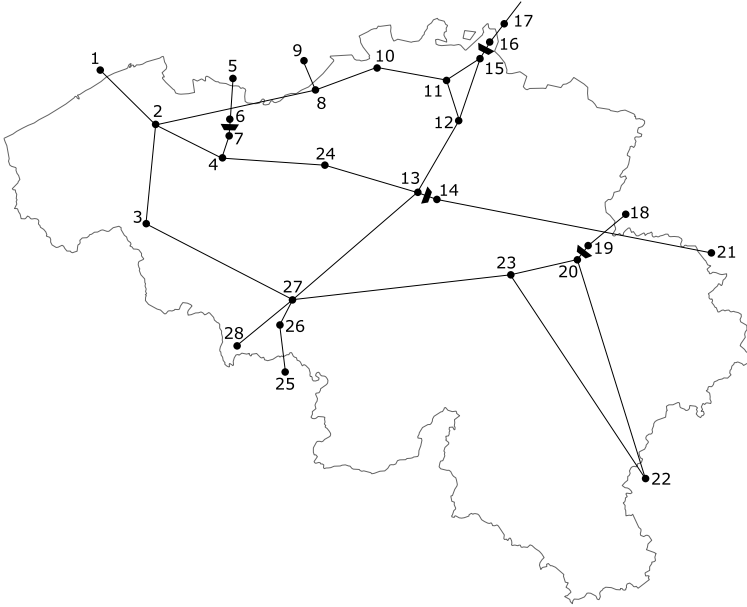


Figure 7.2: Simplification of the Belgian gas transmission network. Note that the indicated connections do not represent the actual physical pipeline paths.

No difference is made between the current Belgian high-calorific and low-calorific gas networks; both are modeled as high-calorific (since a conversion to high-calorific is to take place over the coming years). The actual Belgian gas transmission network is obtained from Fluxys, the Belgian high-pressure transmission system operator [93], and simplified to assure reasonable computation times: multiple parallel pipelines between two nodes are aggregated into one pipeline, pipelines which have a varying pipeline section along the length of the pipeline are simplified to a pipeline with one average section along its entire length and compressor stations which can compress gas in both flow directions are simplified with single-direction compressors in the direction which is most often used.

Pipelines

The pipeline constants K_{pl}^q and K_{pl}^m , used in the pressure-flow relation (Eq. (6.37)) and pressure-line-pack relation (Eq. (6.34)), respectively, are shown in Table 7.1. The constants K_{pl}^q and K_{pl}^m are calculated expressing the flow in million Nm^3/h and the pressure in bar.

Table 7.1: Pipeline specifications inspired by the Belgian gas network.

From node	To node	K_{pl}^q [$(\text{MNm}^3/(\text{bar}\cdot\text{h}))^2$]	K_{pl}^m [MNm^3/bar]
1	2	$1.44\cdot 10^{-1}$	$1.68\cdot 10^{-1}$
2	6	$8.27\cdot 10^{-2}$	$3.49\cdot 10^{-2}$
2	4	$8.27\cdot 10^{-2}$	$3.49\cdot 10^{-2}$
9	8	$3.12\cdot 10^{-3}$	$1.06\cdot 10^{-3}$
8	10	$2.60\cdot 10^{-4}$	$1.27\cdot 10^{-2}$
10	11	$9.36\cdot 10^{-4}$	$3.53\cdot 10^{-3}$
11	15	$3.47\cdot 10^{-4}$	$9.52\cdot 10^{-3}$
17	16	$1.15\cdot 10^{-1}$	$6.35\cdot 10^{-3}$
15	12	$1.49\cdot 10^{-2}$	$4.92\cdot 10^{-2}$
11	12	$4.07\cdot 10^{-4}$	$8.11\cdot 10^{-3}$
12	13	$1.40\cdot 10^{-2}$	$5.24\cdot 10^{-2}$
13	27	$6.49\cdot 10^{-3}$	$1.13\cdot 10^{-1}$
18	19	$3.05\cdot 10^{-2}$	$3.80\cdot 10^{-3}$
20	23	$2.84\cdot 10^{-3}$	$4.08\cdot 10^{-2}$
20	22	$9.65\cdot 10^{-5}$	$3.42\cdot 10^{-2}$
23	22	$6.41\cdot 10^{-5}$	$5.15\cdot 10^{-2}$
23	27	$8.41\cdot 10^{-4}$	$7.22\cdot 10^{-2}$
26	25	$5.12\cdot 10^{-2}$	$1.43\cdot 10^{-2}$
27	26	$1.01\cdot 10^{-1}$	$3.09\cdot 10^{-2}$
27	28	$6.01\cdot 10^{-3}$	$2.15\cdot 10^{-2}$
27	3	$7.67\cdot 10^{-2}$	$1.42\cdot 10^{-2}$
2	3	$7.39\cdot 10^{-3}$	$1.47\cdot 10^{-1}$
5	6	$1.32\cdot 10^{-1}$	$4.50\cdot 10^{-3}$
7	4	$1.20\cdot 10^{-1}$	$1.98\cdot 10^{-2}$
4	24	$3.00\cdot 10^{-3}$	$4.31\cdot 10^{-2}$
24	13	$2.09\cdot 10^{-2}$	$7.44\cdot 10^{-2}$
14	19	$7.94\cdot 10^{-3}$	$1.96\cdot 10^{-1}$

The gas and environmental characteristics used to calculate the pipeline constants K_{pl}^q and K_{pl}^m are equal for all pipelines and are given in Table 7.2.

Table 7.2: Gas and environment characteristics used to calculate the pipeline constants K_{pl}^q and K_{pl}^m .

Parameter	Unit	Value
Gas temperature T	[K]	285.15
Gas density at standard conditions ρ_0	[kg/m ³]	0.7156
Gas compressibility factor at standard conditions Z	[-]	0.8
Pressure at standard conditions p_0	[bar]	1.013
Temperature at standard conditions T_0	[K]	288.15

Compressors

Four compressor stations have been incorporated in the network as shown in Figure 7.2. All compressors have been modeled equal, with a maximum compression ratio of 1.5 [93].

Gas production facilities

Since Belgium has no domestic conventional natural gas production, all production facilities are import 'injection' facilities placed at the Belgian border (although they will still be called 'production facilities' in the remainder of this work). The location and technical characteristics are shown in Table 7.3. The maximum production rate is based on the maximum occurring import flow at each node in 2015, which is obtained from the ENTSOG Transparency platform [113]. The maximum production rate is rounded up to assure feasibility. The exact production (i.e., 'injection') profile is not taken as in 2015, but is left to be optimized in the different cases.

The ramp rates imposed on the different production facilities are chosen based on information received from Fluxys [93].

Gas storage

Two gas storage facilities are considered: a large underground storage facility in Loenhout (node 10) and a smaller facility in Zeebrugge (node 1).

Since the modeling optimization horizon is small compared to the size of the gas storage facilities, the storage facilities can hold more gas than could be used to serve the load within one optimization horizon. As a result, the model *sees* no value for the gas that remains in storage at the end of the optimization horizon

Table 7.3: Gas production facility characteristics. With \overline{W}_{gw} the maximum production rate. Note that although node 22 and 25 make a connection to neighboring countries, no gas is imported via these connections and they are hence omitted from the Table.

Parameter	Unit	Facility					
Node	$[-]$	1	5	9	17	18	21
Minimum production	$[\text{MNm}^3/\text{h}]$	5	1	0.5	2.2	1.5	1
Maximum production	$[\text{MNm}^3/\text{h}]$	0	0	0	0	0	0
Ramp up/down rate	$[\% \overline{W}_{gw}/\text{h}]$	10	10	10	10	10	10

Table 7.4: Gas storage facility characteristics in the 80% RES case [93, 110].

		Loenhout	Zeebrugge
Node	$[-]$	10	1
Gas storage cost	$[\text{€}/\text{MNm}^3]$	6800 ^a	6800 ^a
Maximum storage capacity	$[\text{MNm}^3]$	785	228
Maximum injection/withdrawal rate	$[\text{MNm}^3/\text{h}]$	0.625	1.70
Maximum ramp up/down rate	$[\text{MNm}^3/\text{h}]$	0.188	0.51

^a For simplicity, both storage units have been given an equal storage cost. In reality, however, the storage in Zeebrugge will be more costly since it stores gas as a liquid compared to the storage in Loenhout where gas is stored in compressed form.

and hence would never be incentivized to store additional gas for a moment in time after the optimization horizon. To avoid such situations, which could lead to suboptimal results due to modeling limitations, the model works with an initial and final storage level in each gas storage facility. The storage levels in all intermediate hours are determined during the optimization.

The imposed storage level in the Loenhout storage facility are obtained from the ENTSOG Transparency platform [113]. The storage levels for the storage in Zeebrugge are taken from the 80% RES case from Chapter 4. In the 99% RES case, more methane storage is required, hence the storage size in Zeebrugge is increased, as will be discussed in Section 7.4.

Gas load profiles

Three types of gas loads are considered, two of which are exogenous to the model: residential and industrial. The third gas load, originating from GFPPs is endogenous to the model. Next to the different gas loads, gas transit flows

through the Belgian pipelines towards neighboring countries are considered. Each of the loads per node and the residential load zones are indicated on Figure 7.3.

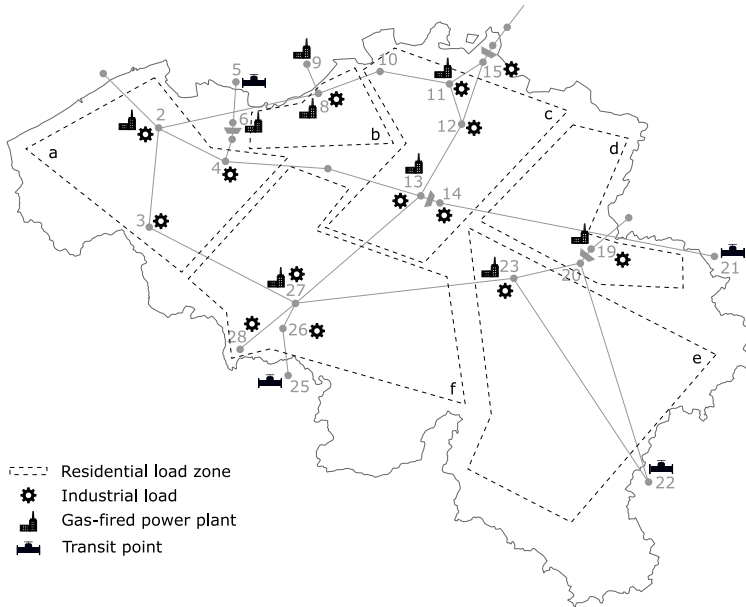


Figure 7.3: Nodal loads (from industry, GFPP and transit) and residential load zones which are used to distribute the residential gas load.

The hourly **residential load** is taken from the ENTSOG Transparency platform [113] and divided over load zones according to information received from Fluxys [93]. Residential load data from 2015 are used.

For the **industrial load** also 2015 data are used. Hourly values are obtained from the ENTSOG Transparency platform [113] and distributed over nodes according to information received from Fluxys [93].

The **transit load** at interconnection points to neighboring countries are also obtained from the ENTSOG Transparency platform [113] (2015 data). Note that in some interconnection points, physical flows both to and from Belgium occur. Only the flows from Belgium to neighboring countries are imposed as certain transit loads. Flows towards Belgium are modeled as a production facility, for these production facilities, the hourly gas production is optimized by the model within imposed bounds as explained before.

The hourly **gas-fired power plant** load is determined endogenously by the model in order to serve the residual electrical power load.

7.3.2 Conversion units

Gas-fired power plants

The gas-fired power plants are placed on nodes with currently existing GFPPs. In addition to these existing plants, two major GFPPs are placed in Doel (connected to gas-node 8) and Tihange (connected to gas-node 23) since there is a major connection to the electric power system (to connect the current nuclear power plants, which are assumed to be phased-out in this study) and these locations are close to existing natural gas pipelines.

An overview of the different GFPPs and their characteristics is given in Table 7.5 [114]. All gas-fired power plants are assumed to be combined cycle gas turbines, except for the last plant which is an existing open cycle gas turbine. The ramp rates (both up and down) and start-up and shut-down rates are for all units 100% of P_{\max}/h , assuming very flexible units. The minimum operating point is equal to 28% of the maximum generation capacity. To close the carbon loop through P2G, it is assumed that all units are equipped with a carbon capture unit (see Chapter 4, Section 4.2). These capture units lead to an efficiency loss of 15% of the GFPPs rated efficiency, which amounts to an average efficiency loss of 8.4%pt for each unit. A variable cost of 12.8 €/MWh_e is considered and equal for all GFPPs.

Table 7.5: Gas-fired power plant characteristics [114]. E-node and G-node indicate the node to which the GFPP is connected in respectively the electrical power grid and gas network, Pmax = maximum generation capacity, MUT = minimum up-time, MDT = minimum down-time.

E-Node	G-Node	Pmax [MW_e]	Efficiency ^a [%]	Start-up cost [$EUR/start$]	MUT/MDT [h]
29	19	188	46.84	4926	3
42	6	663	46.92	17371	3
24	23	451	47.01	11816	3
10	13	513	47.09	13441	3
11	2	465	47.18	12183	3
1	23	350	47.26	9170	3
36	9	384	47.35	10061	3
35	27	405	47.43	10611	3
17	11	422	47.52	11056	3
9	8	500	49.30	13100	3
9	8	500	49.30	13100	3
9	8	500	49.30	13100	3
9	8	500	49.30	13100	3
9	8	500	49.30	13100	3
9	8	500	49.30	13100	3
37	23	500	49.22	13100	3
37	23	500	49.22	13100	3
38	23	500	49.13	13100	3
38	23	500	49.13	13100	3
39	23	500	49.05	13100	3
39	23	500	49.05	13100	3
40	19	86	34.00	2253	1

^a Including efficiency loss due to capture unit.

Power-to-gas units

Two equally sized P2G units are considered in the different cases which each have an electrolyzer capacity of 1750 MW_e and methanizer capacity of 500 MW_{CH_4} connected via an intermediate hydrogen storage unit with a maximum storage capacity of 15.75 GWh_{H_2} . Both P2G units are modeled equal with characteristics given in Table 7.6. These characteristics are based on the literature review presented in Chapter 2.

The P2G units are placed in nodes 11 and 12 in the electrical power network near

Table 7.6: Power-to-gas characteristics of an individual P2G plant in the 80% RES case.

	Electrolyzer	Methanizer	
Pmax	1750 MW _e	500 MW _{CH₄}	
Pmin	0 %Pmax	40 %Pmax	[31]
Efficiency	75 %	70 %	[26, 28, 29]
Marginal Cost	2 €/MWh _e	5 €/MWh _{CH₄}	
Ramp up/down rate	100 %Pmax/h	10 %Pmax/h	[25, 32]
Start-up/shut-down rate	100 %Pmax/h	40 %Pmax/h	[25, 32]
Min up/down time	0 h	6 h	[28]

Eeklo Noord, where an electrical connection is made with the offshore wind farms and near Gramme, which connects only a small amount of intermittent renewable energy sources (iRES) but has a strong existing electrical interconnection due to the vicinity of the nuclear generators in Tihange, which are replaced by GFPPs in the model. In the gas network, the P2G are connected in nodes 2 and 23.

7.3.3 Electric power system

Network topology

The Belgian high voltage electrical power network obtained from the Belgian transmission system operator [112] is used for the different case studies. The geographic topology is presented in Figure 7.4. Both the 380 kV and 220 kV electrical power lines are considered.

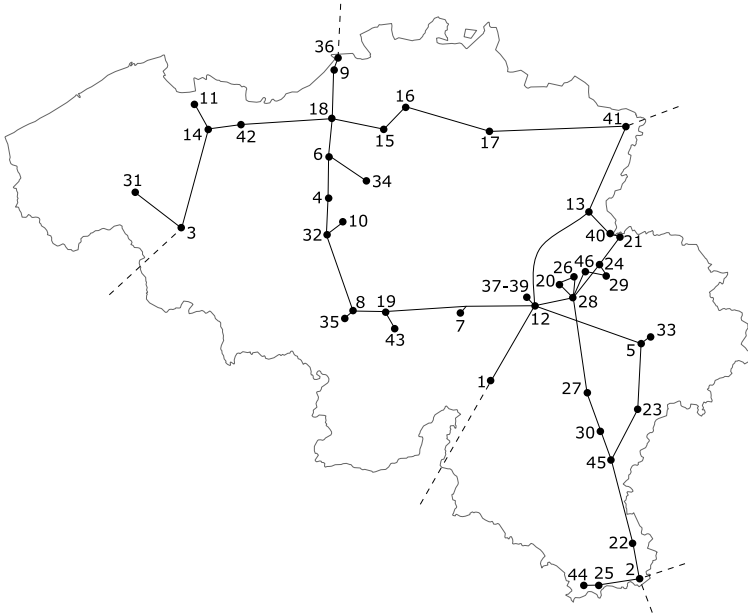


Figure 7.4: The high-voltage Belgian electrical power grid. Note that the indicated connections do not represent the actual physical line paths.

Electrical power lines

The total reactance and power carrying capacity of each line is obtained from the Belgian TSO [112]. A DC load flow approximation of the electric power system is used. An overview of the line characteristics is given in Table 7.7.

Table 7.7: Characteristics of the different electrical power lines. Reactance denotes the total reactance, PCC denotes the power carrying capacity of each line.

From node	To node	Reactance [p.u.]	PCC [MW_e]	From node	To node	Reactance [p.u.]	PCC [MW_e]
1	12	0.121	1184.7	12	37	0.010	1184.4
2	5	0.313	1295.1	12	38	0.009	1295.1
3	31	0.075	1295.1	12	39	0.011	1295.1
3	31	0.075	1295.1	13	40	0.034	1295.1
3	14	0.130	1184.4	13	41	0.139	1184.4
3	14	0.130	1295.1	14	42	0.046	1295.1
4	6	0.051	1184.4	15	16	0.046	1296.9
4	6	0.053	1295.1	15	18	0.069	1295.1
4	8	0.155	1295.1	15	18	0.069	1295.1
4	32	0.046	1184.4	16	17	0.107	1295.1
5	33	0.007	1184.4	16	18	0.115	1295.1
5	33	0.007	1184.4	17	41	0.189	1295.1
5	12	0.145	1184.4	18	42	0.112	1184.4
5	12	0.145	1373.4	19	43	0.025	1295.1
6	18	0.051	1295.1	2	22	0.044	364.5
6	18	0.050	1184.4	2	25	0.062	305.1
6	34	0.071	1295.1	2	44	0.084	305.1
6	34	0.069	1373.4	2	45	0.142	364.5
7	8	0.145	1295.1	20	26	0.026	374.4
7	12	0.106	1295.1	20	28	0.031	334.8
8	35	0.006	1295.1	21	24	0.033	610.2
8	35	0.006	1184.4	21	40	0.010	480.6
8	32	0.110	1184.4	5	23	0.081	426.6
8	19	0.041	1184.4	22	45	0.097	364.5
9	18	0.075	1184.4	23	45	0.075	426.6
9	18	0.068	1295.1	24	28	0.089	374.4
9	18	0.075	1184.4	24	29	0.022	270.0
9	36	0.024	1184.4	25	44	0.022	305.1
9	14	0.226	1184.4	26	28	0.053	334.8
10	32	0.034	1295.1	27	28	0.113	364.5
11	14	0.039	1295.1	27	30	0.080	364.5
12	13	0.140	1184.4	28	46	0.046	355.5
12	28	0.048	1184.4	29	46	0.058	355.5
12	19	0.185	1184.4	30	45	0.021	364.5
12	37	0.010	1184.4				

Electrical load profile

The Belgian electrical load from 2015 as seen by Elia on the high-voltage grid is used as load in this Chapter [64]. During 2015, the minimum and maximum electrical load was 5776.75 MW_e and 13670.25 MW_e, respectively, with an average of 9934.82 MW_e. The total yearly electrical energy load was 87 TWh_e. The electrical load is assigned to the different nodes in the electric power system according to the rated capacity of the transformer feeding each node; a similar methodology was adopted in [115].

Table 7.8: Electrical load division among different nodes.

Node	Share [%]	Node	Share [%]	Node	Share [%]
2	3.70	17	5.21	34	5.39
3	5.39	18	5.39	35	8.04
4	4.82	20	2.87	36	5.65
5	2.68	22	0.48	37	2.97
1	2.73	16	2.41	31	5.09
7	2.36	23	0.32	40	4.82
10	2.68	24	2.47	42	2.41
11	2.41	27	0.46	43	3.38
12	2.41	28	5.68	45	0.94
15	4.82	29	0.68	46	1.34

iRES generation profile

The Belgian iRES generation profiles from 2015 are used in this Chapter [64]. Separate profiles for wind onshore, wind offshore and solar PV are used and scaled according to the installed capacities obtained from the 80% RES case from Chapter 4. An overview of the installed capacities and capacity factor of each iRES technology in 2015 is given in Table 7.9.

Table 7.9: iRES capacity and generation characteristics in the 80% RES case.

	Onshore wind	Offshore wind	Solar PV
Capacity [GW _e]	5.02	5.25	54.6
Capacity factor	23.5%	41.2 %	11.9%

The offshore wind capacity is all placed near the Belgian shore, connected to the electrical power network in node 11 (Eeklo Noord). The onshore wind and solar

photovoltaic (PV) capacity is distributed over the different nodes according to the distribution made in [115].

Electrical energy storage

Pumped hydro storage (PHS) and battery storage are used as electrical energy storage technologies. The existing PHS unit in Coo is modeled together with Sodium-sulfur (NaS) batteries since they are suitable for grid-scale battery storage [66]. The installed power and energy capacities of both technologies are shown in Table 7.10.

Table 7.10: Electrical energy storage characteristics in the 80% RES case.

Parameter	Unit	Nas Battery	PHS
Maximum charging power	$[GW_e]$	11.41	1.14
Maximum discharging power	$[GW_e]$	11.41	1.14
Energy storage capacity	$[GWh_e]$	82.15	8.22
Single-trip efficiency	$[\%]$	90	85

The PHS storage is placed at its actual location in Coo (node 33). The battery capacity is distributed over different nodes in the electrical power network according to the share of installed solar PV capacity at each node.

7.3.4 Assumptions

Linearizations

To compute the pressure-flow relation at each time step and in each pipeline of the gas network, a quadratic pressure and gas flow is calculated. This is done by a linearization of the quadratic functions as shown in Section 6.2.2. For the quadratic pressure, two intervals are used, between 45 and 65 bar and between 65 and 85 bar. The linearization is illustrated in Figure 7.5.

The maximum linearization error occurs in the middle of the linearization interval. For the pressure linearization, the largest relative error is at 55 bar, where the linearization differs 3.31% from the actual quadratic pressure. Note that this error is no measure for the average linearization error in the entire network. Since there will be different pressures at different nodes and at different time steps, the average error will always be lower.

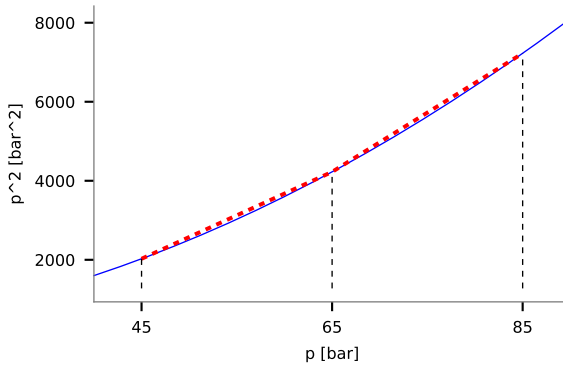


Figure 7.5: Piecewise linearization of the quadratic pressure using two linearization intervals between 45 and 65 bar and between 65 and 85 bar.

The quadratic flow is linearized using 15 intervals between -7 and $7 \text{ MNm}^3/\text{h}$ as shown in Figure 7.6.

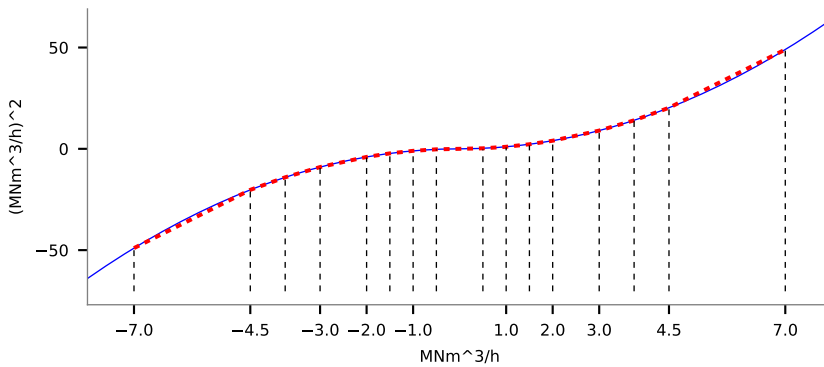


Figure 7.6: Piecewise linearization of the quadratic flow using 15 linearization intervals between -7 and $7 \text{ MNm}^3/\text{h}$.

Expressing a relative linearization error for the flow is more difficult since flow rates could be very low or zero. For flow rates reaching zero, even very small linearization errors could become very large relative errors. The largest absolute error occurs at -5.75 and $5.75 \text{ MNm}^3/\text{h}$, where the linearization differs 4.7% from the real quadratic flow rate. Although this difference is significant, it

should be noted that this is the maximum linearization error while the average error is expected to be much less, since smaller flows are more common and more linearization intervals are used in this region.

Optimality gap

An optimality gap of 1% is used as stopping tolerance during the different mixed integer program (MIP) optimizations. The optimality gap is defined as the relative difference between the best solution found so far and the best possible solution, which is calculated by relaxing the integer problem. The optimality gap triggers the solver to stop the solution process and return the best solution found so far.

7.4 Case studies

Several case studies are presented to analyze the impact of P2G on the gas network and the operation of conventional gas production facilities. Two sets of installed generation and storage capacities are analyzed, corresponding to the optimally installed capacities for an imposed RES target of 80% and 99%. Four days of energy system operation are optimized. For each of these days, the ramp rates of conventional production facilities and the imposed bounds on nodal pressures are varied in each case study. An overview of the different cases is provided in Table 7.11.

Table 7.11: Overview of parameter variations in different cases. With \overline{W}_{gw} the maximum production rate.

Parameter	Unit	Values
Day of year		100, 160, 200, 250
Environmental constraint	$[\%RES]$	80, 99
Maximum ramp rate	$[\%\overline{W}_{gw}/h]$	0%, 5%, 10%, 15%, 20%, 25%
Pressure bounds	$[bar]$	45-75, 50-70, 55-65

Days 100, 200 and 250 are respectively Friday 10th of April, Sunday 19th of July and Monday 7th of September 2015, providing a mix of week and weekend days to serve as example. Day 160 is Tuesday 9th of June and is interesting to investigate as it is the day with highest iRES generation. The days with the largest electrical power demand and natural gas demand have been investigated but are not reported in the results subsection since they fall in winter and have

almost no surplus iRES generation and hence no synthetic methane is produced during those days.

The case studies with an imposed RES target of 80% and 99% have the same input parameters as given before in Section 7.3, except for the installed iRES, P2G and battery capacities as shown in Table 7.12. The division of generation and storage capacity between different nodes in the electric power and natural gas system is as explained in Section 7.3 before.

Table 7.12: Overview of the installed generation and storage capacities for scenarios with imposed RES targets of 80% and 99%.

Technology	Unit	80% RES	99% RES
Onshore wind	$[GW_e]$	5.02	6.97
Offshore wind	$[GW_e]$	5.25	7.29
Solar PV	$[GW_e]$	54.57	75.73
Battery	$[GW_e]$	11.41	12.91
Electrolyzer	$[GW_e]$	3.5	17.3
Methanizer	$[GW_{CH_4}]$	1.0	4.0
Methane storage	$[MNm^3]$	1013	1195
GFPP	$[GW_e]$	9.93	9.93

The ramp rates of conventional gas production facilities, which express their flexibility, are varied between 0% and 25% of their maximum production rate per hour. If ramp rates of conventional natural gas production facilities are very low, the inherent flexibility from gas networks needs to be used to match the imbalance between gas production and consumption. Hence less flexibility will be left for P2G to inject and store synthetic methane, which could have a negative effect on the P2G operation.

The imposed bounds on nodal pressure are tightened, reducing the allowed pressure range in the gas network and consequently reducing the amount of available line pack flexibility. Although technical pressure bounds are well known to the gas network operator, he could chose to operate the gas network within a more narrow pressure range to assure reliable operation of the gas network under uncertainty. Examples of such uncertainty could be the limitedly predictable natural gas load.

7.5 Results and discussion

First an illustration of the gas network flexibility will be given by presenting results from a single case. Afterwards, the impact of P2G on the gas network is analyzed by discussing the total operational cost and pressure levels in the gas network for different cases.

7.5.1 Illustration of gas network flexibility

Friday 10th of April 2015 (day 100) is used for this illustration in an energy system with 80% imposed RES target when conventional gas production facilities have a constant production (ramp rate 0%). The sum of production, both conventional gas and synthetic methane, the sum of gas storage and the sum of consumption per hour is shown in Figure 7.7. It is clear from Figure 7.7 that, since conventional gas production is constant, the difference in gas production and gas demand which is not covered by storage, should be taken care of by the flexibility available in the network. In addition, the figure shows that the volume of conventional gas production is much larger than the volume of synthetic methane production. On this day, synthetic methane production is on average at 30% of its own nominal capacity.

The total line pack present in the network at every hour is shown in Figure 7.8. Comparing Figures 7.7 and 7.8 shows that the line pack varies to compensate for mismatches between gas production and demand, illustrating the flexibility available in the network.

7.5.2 Operational impact of P2G

Operational cost

A first result which is used to analyze the impact of P2G on the gas network is the total operation cost for different days in the 80% RES case, shown in Table 7.13. The cost is calculated for different days and for different cases, which differ in the imposed pressure bounds on gas nodes and in the magnitude of the ramp rate allowed for conventional gas production facilities. It is expected that when the allowed ramp rate is reduced, operational costs would increase. After all, if conventional shippers can only slowly vary their production rate, they need to rely on flexibility from the gas network to match production and demand. Decreasing the allowed production ramp rates would thus increase the flexibility required by conventional shippers and would hence reduce the

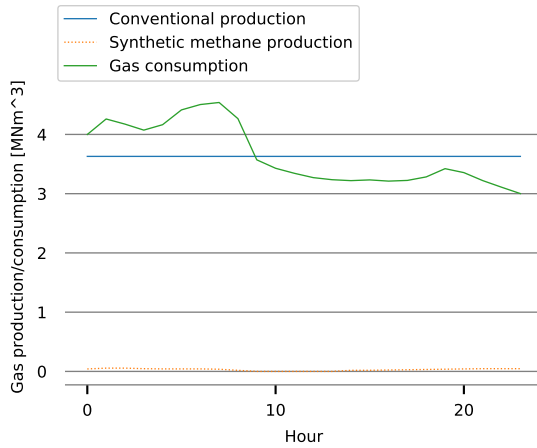


Figure 7.7: The hourly consumption of gas, the production of conventional natural gas and synthetic methane and the gas storage injection and withdrawal. For a natural gas load, an electrical energy load and iRES generation as seen on Friday 10th of April 2015, for an 80% imposed RES case without ramping flexibility available to conventional gas production facilities.

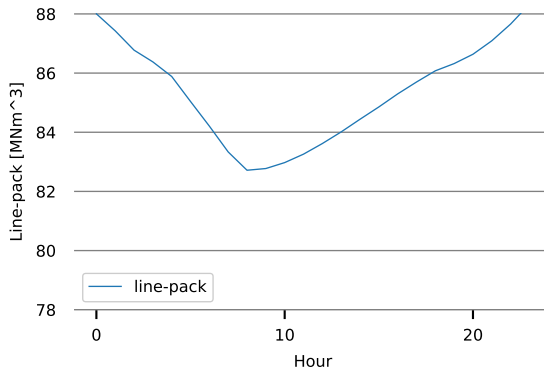


Figure 7.8: The total line pack present in the gas network at each hour. For a natural gas load, an electrical energy load and iRES generation as seen on Friday 10th of April 2015, for an 80% imposed RES case without ramping flexibility available to conventional gas production facilities.

remaining flexibility to accommodate P2G. Limiting possible P2G injection

would reduce the amount of produced synthetic methane, which should be replaced by conventional natural gas, at a higher cost than synthetic methane.¹ Hence lowering the allowed ramp rates could increase the total operational cost.

Table 7.13 shows, however, that for most cases the cost remains equal apart from random variations within the optimality gap of 1%. Since these variations in costs are smaller in magnitude than the 1% optimality gap, they have no economic meaning. Hence, a reduction in allowed ramp rate does not lead to a clear increase in operational cost. Only for day 250, an increase in operational cost is observed in the cases with most stringent imposed ramp rates (0%). The cost increase is, however, limited to 1.34% (or 0.34% above the optimality gap) and does not follow from a restriction in the gas network as will be shown when looking at the pressure levels in the network in the next section.

Note that Table 7.13 does not present a cost for the 0% ramp rate case with imposed pressure bound between 50 bar and 70 bar since an optimal solution (subjected to the 1% optimality gap) could not be found for this case within the allowed optimization run-time of 24 hours.

The results presented in Table 7.13 indicate that there is no shortage for gas flexibility which would trigger a reduction in synthetic methane injection at an increased cost for the production of additional conventional natural gas. This observation is confirmed by investigating the pressure occurring in the gas network over the entire optimization horizon.

¹The marginal cost of synthetic methane production is lower than the cost of conventional natural gas since all investment costs are considered 'sunk costs' in this operational optimization.

Table 7.13: Total operational cost for different allowed ramp rates (RR) of conventional gas production facilities. Cases with an 80% RES target are shown (Ref = reference case to which all other cases of the same day are compared).

Day 100				Day 160			
Pressure limits				Pressure limits			
RR	45-75	50-70	55-65	RR	45-75	50-70	55-65
25%	Ref %	-0.32%	-0.78%	25%	Ref %	-0.46%	-0.49%
20%	-0.08%	-0.74%	-0.79%	20%	0.10%	-0.55%	-0.79%
15%	0.16%	-0.64%	0.11%	15%	0.16%	-0.25%	-0.79%
10%	-0.63%	-0.38%	-0.77%	10%	0.16%	0.18%	-0.79%
5%	-0.06%	0.14%	-0.78%	5%	0.17%	-0.43%	-0.79%
0%	0.25%	0.62%	0.56%	0%	0.57%	0.29%	0.08%
Day 200				Day 250			
Pressure limits				Pressure limits			
RR	45-75	50-70	55-65	RR	45-75	50-70	55-65
25%	Ref	0.18%	-0.68%	25%	Ref	-0.02%	0.41%
20%	0.10%	-0.02%	-0.68%	20%	0.69%	0.18%	0.69%
15%	0.27%	-0.24%	-0.68%	15%	0.14%	-0.16%	0.10%
10%	-0.11%	0.31%	0.02%	10%	0.57%	0.07%	-0.20%
5%	0.06%	0.00%	-0.68%	5%	0.44%	0.36%	-0.07%
0%	0.13%	-0.13%	-0.23%	0%	1.34%	-	1.22%

Pressure levels

Table 7.14 shows minimum and maximum pressure levels occurring over the optimization horizon for different cases. The pressure range (maximum - minimum pressure) which is used during the gas network operation is compared to the allowed pressure range in the network.

If the used pressure range during operation is smaller than the allowed pressure range, this provides an indication that more gas network flexibility is available than is useful during gas network operation. After all, if economic gains could be made by relying more on the flexibility from the gas network (e.g., by depleting the line pack during a certain period in order to replenish the line pack at a later, more convenient, moment), a larger pressure range would be used.

Note that the opposite reasoning does not hold. Since no explicit cost is assigned to the pressure levels occurring in the gas network, the model sees no cost for

using more flexibility than is strictly required to operate the gas network in an optimal way. I.e., even when the full allowed pressure range is used during operation, it could be that an equivalent solution exists which uses a smaller pressure range. Hence it is not possible to conclude that the used pressure ranges (and their corresponding flexibility) indicated in Table 7.14 are required to operate the gas network in a cost optimal way, but it is possible to conclude that if the used pressure range is smaller than the allowed pressure ranges, more flexibility is available than useful.²

Table 7.14: Allowed pressure range and used pressure range per case indicating an abundance of flexibility in the gas network for most cases. Cases with an 80% RES target without ramp rates for conventional gas production facilities are shown (RR = 0%).

Day	Allowed pressure range	Occuring pressure		Pressure range used
		Pmin	Pmax	
100	45-75	56.4	75.0	62%
	50-70	58.4	70.0	58%
	55-65	55.0	65.0	100%
160	45-75	64.6	75.0	35%
	50-70	62.4	70.0	38%
	55-65	57.4	65.0	76%
200	45-75	62.7	75.0	41%
	50-70	63.3	70.0	34%
	55-65	58.8	65.0	62%
250	45-75	62.7	75.0	41%
	50-70	62.1	70.0	40%
	55-65	55.0	65.0	100%

Only cases which do not allow ramping of the conventional gas production facilities (ramp rate at 0%) are shown in Table 7.14 since they rely more on the gas network flexibility compared to cases where ramping is allowed. Even in those cases where gas network flexibility is most heavily used by the conventional gas production facilities, Table 7.14 shows that more flexibility is available in the network than required during optimal operation.

²Note that minimizing the pressure range by penalizing the absolute pressure levels could distort the results if the cost exceeds the gains from synthetic methane production. Reducing the penalty cost to an order of magnitude lower than possible gains from synthetic methane would diminish its effect since the cost would fall within the 1% optimality gap.

Both the total operational cost and the used pressure ranges shown before indicate that more flexibility is available in the gas network than is necessary during operation. Hence the gas network does not form a constraint for the integration of P2G in an integrated electric power system and gas system resembling the Belgian situation. The reason for this is first that the Belgian gas network has more capacity than strictly required to serve the gas load; second, the production of synthetic methane is small compared to the production of conventional natural gas. For day 160, which has the largest iRES surplus and on which day all P2G capacity operates at full load during the entire day, the total synthetic methane production during this period only amounts to 2.9% of the total gas production.

99% RES case

Since a relatively small amount of P2G capacity is installed in the 80% RES case, also the 99% RES case is investigated to study the impact of a larger P2G integration on the gas network. The installed methanizer capacity in the 99% RES case is fourfold the capacity of the 80% RES case. The total operational cost for different days, under different imposed pressure bounds and different allowed ramp rates for conventional gas production facilities, is shown in Table 7.15.

For the 99% RES case, the same observations can be made as for the 80% RES case. Although the synthetic methane production now amounts to maximum 10.1% of the total gas production, it has again no impact on the cost to operate the gas network. The results thereby indicate that even for very high-RES scenarios with a large P2G penetration, abundant flexibility is available in the gas network to accommodate both conventional gas production and more volatile synthetic methane production. These findings are in line with the results reported by Clegg and Mancarella for the British system [86].

Table 7.15: Total operational cost for different allowed ramp rates (RR) of conventional gas production facilities. For different days in the year and different imposed pressure bounds as specified in Table 7.11, for cases with 99% imposed RES share. (Ref = reference case to which all other cases of the same day are compared.)

Day 100				Day 160			
	Pressure limits				Pressure limits		
RR	45-75	50-70	55-65	RR	45-75	50-70	55-65
25%	Ref	-0.30%	-0.55%	25%	Ref	0.41%	-0.27%
20%	0.09%	0.35%	-0.36%	20%	0.56%	0.38%	-0.27%
15%	-0.02%	-0.54%	-0.34%	15%	0.52%	0.61%	-0.27%
10%	0.44%	0.45%	-0.55%	10%	0.54%	0.61%	-0.27%
5%	0.29%	0.45%	-0.55%	5%	0.18%	0.48%	-0.27%
0%	0.45%	0.31%	-0.47%	0%	0.66%	0.61%	0.00%
Day 200				Day 250			
	Pressure limits				Pressure limits		
RR	45-75	50-70	55-65	RR	45-75	50-70	55-65
25%	Ref	0.18%	-0.44%	25%	Ref	-0.29%	-0.15%
20%	0.50%	0.18%	-0.39%	20%	0.06%	-0.68%	-0.88%
15%	0.51%	-0.06%	-0.44%	15%	0.03%	0.02%	-0.13%
10%	0.01%	0.52%	-0.42%	10%	0.05%	-0.12%	0.11%
5%	0.46%	0.20%	-0.39%	5%	0.08%	-0.40%	-0.63%
0%	0.51%	0.46%	-0.40%	0%	-	0.15%	-0.36%

7.6 Summary and conclusions

The main objectives of this chapter were to evaluate (i) in how far the natural gas network can cope with the methane injection from P2G units and (ii) to what extent the integration of P2G impacts the flexibility available for conventional gas production facilities. The integrated electric power and natural gas model presented in Chapter 6 is used in combination with a representation of the Belgian electric power system and natural gas system to answer these research questions. The input parameters of each network, together with the technical and economic parameters of each generation and storage unit were presented next. The amount of installed electrical power generation, electrical energy storage capacity and P2G capacity is taken from results presented in Chapter 4. Two different sets of installed capacities are used, one resulting from an imposed

RES target of 80% and one resulting from a 99% RES target.

Different case studies are presented in which the combined electricity and gas system operation is optimized for four different days. For each of these days, a sensitivity analysis is performed on two parameters. First, the inherent flexibility of the gas network is varied by imposing different allowed pressure ranges on the nodes in the gas network. The minimum and maximum nodal pressures in the reference case are set at 45 bar and 75 bar. This range is tightened in subsequent cases to 50-70 bar and 55-65 bar. Second, the flexibility of conventional gas production facilities is varied by imposing different ramp rates on them. The imposed ramp rates range from 0% to 25% of nominal production capacity per hour.

Results of each case study indicated that for gas networks similar to the Belgian gas network, abundant flexibility is inherently available to accommodate conventional gas production in combination with the integration of P2G even though it possibly causes volatile injections of synthetic methane.

Chapter 8

Summary, conclusions and suggestions for further research

This work has explored the role of power-to-gas for energy storage in future energy systems with high shares of intermittent renewables. A first focus has been on developing cost metrics to express the economic viability of storage units. Second, the amount of power-to-gas (P2G) capacity in a cost optimal energy system under different (environmental) constraints has been analyzed. In addition, the relationship between the need for different storage technologies and the shape of both the electrical power demand and the intermittent renewable generation profile is investigated. Third, assuming a setting where P2G capacity has been installed, its operational impact on an interconnected electric power and gas system has been investigated.

This chapter summarizes the work presented in this dissertation, draws the main conclusions and specifies the contributions. In addition, suggestions for further research are provided. Detailed conclusions can be found at the end of each chapter.

8.1 Summary and conclusions

8.1.1 Overview of the power-to-gas production process

The production of synthetic methane via P2G occurs in two phases. First, hydrogen is produced from water using electrical power in an electrolyzer, after which this hydrogen is allowed to react with CO₂ to form methane via the so-called Sabatier reaction. Three different types of electrolyzers have been discussed based on their technical and economic characteristics: alkaline electrolyzers (AELs), polymer electrolyte membrane (PEM) and solid oxide electrolysis cells (SOECs). It has been found that both alkaline and PEM electrolyzers are capable of following the volatile production profile of electrical power producing intermittent renewables. For SOECs it is currently unclear whether they can handle dynamic operation due to their high operating temperatures, which lead to high thermal inertia.

During the discussion of the methanation process, the difference between catalytic and biochemical methanation has been highlighted. The catalytic process is more controllable, but it is highly sensitive to impurities in the reactant stream. Impurities form a lesser problem for biological methanation but the methane production rate per reactor volume is significantly lower compared to catalytic methanation reactors. Biological methanation is hence less suitable for large-scale units and was not further considered in this work. Both the electrolyzer and methanation characteristics presented in Chapter 2 have been used as input parameters for studies presented in the following chapters.

8.1.2 Assessing the value of electricity storage for an investor in a given electricity market

Conclusion 1: *The economic viability of different storage technologies can be analyzed by three newly developed levelized cost metrics applied to storage, as compared to the LCOE for conventional electrical power generation. It has been found that the energy reservoir size has a big impact when using the different levelized cost metrics, since storage units which have only a small energy storage reservoir could be only dispatchable to a limited extent.*

Chapter 3 investigated simple economic tools inspired by the well-known *levelized cost of electricity (LCOE)* to assess whether an investment in a certain storage technology is worthwhile in a particular market. Given that for storage, the input energy (charged electricity or ‘fuel’) and the generated energy (discharged electricity) are both the same commodity, provides the opportunity to create

improved and more transparent cost metrics rather than simply trying a one-on-one translation of the LCOE to storage. These metrics are expressed as the *required average discharge price*, the *required average price spread* and the *required average operational profit* and differ in the share of variable costs that is accounted for.

It has been shown that a limited energy storage capacity can limit the storage operator to capture the full possible arbitrage profit of a certain price profile. In fact, the influence of this limited energy capacity is hard to evaluate without extensive calculation since it impedes estimating the total number of operating hours, the average electricity price during charging and the average electricity price during discharging. Therefore, it is recommended to use a leveled cost metric in combination with an analysis of an entire representative price profile. This methodology has been illustrated on real historical price profiles occurring in Belgium during different years.

8.1.3 Identification of the circumstances which require electricity storage via P2G

Conclusion 2: *Investments in P2G are triggered by a requirement for large energy storage capacities which is typically related to long-term seasonal storage of surplus iRES generation. Once P2G is installed, it can also be used for short-term storage cycles and deliver auxiliary services to the electrical power grid.*

Chapter 4 presents an investment study analyzing the possible role of power-to-gas (P2G) in a cost-optimal, high-RES energy system. First, a discussion on the sustainability of synthetic fuels when used for energy storage has been presented. It is postulated that if P2G is used to store surplus iRES generation with the intention to reconvert this produced methane to electrical power using gas-fired power plants (GFPPs), the CO₂ used during methane synthesis should be part of a closed carbon loop if the energy discharged from storage is still to be regarded as environmentally sustainable. Closing the carbon loop could be realized by capturing CO₂ emissions from GFPPs or by capturing CO₂ from the atmosphere via so-called atmospheric carbon capture or via carbon extraction from biomass.

Next, an energy system investment model is introduced which is used to determine the cost optimal electrical power generation and storage portfolio, including P2G, for an electric power system subject to different boundary conditions. Via different case studies the imposed RES-target, the iRES mix and CO₂ emission cost have been varied, together with the availability of

CO₂ sequestration and the possibility for iRES curtailment. Other sensitivity analyses include the effect of battery and P2G availability, a variation in cost of each storage technology, the effect of electrical power generation and storage capacity legacy and impact of including a hydrogen load from industry, where pure hydrogen is used as chemical feedstock.

Results show that P2G as storage option becomes a cost efficient technology for energy systems with a high iRES penetration, starting from 70% RES shares. The optimally installed amount of P2G capacity increases for an increasing imposed RES share. In addition, the amount of installed capacity depends only to a limited extent on the specific composition of the iRES portfolio.

If a low or no RES target is imposed, the main incentive to install P2G disappears. In such cases it is only economic to install P2G if no CO₂-sequestration is allowed in combination with very high CO₂ emission costs (1000€/ton and above). A high emission cost makes it uneconomic to use conventional GFPPs and emit CO₂. The lack of sequestration availability, however, prohibits capturing and sequestering CO₂ from GFPPs. In such situation, installing iRES capacity in combination with storage is the most economic option and will hence also lead to investments in P2G.

If an external hydrogen industry is accounted for (which is subjected to the same imposed RES target as the electricity system), allowing the electrolyzer to (partly) serve the hydrogen load with electrically produced hydrogen leads to an increase in installed electrolyzer capacity. The effect on other installed capacities (such as the methanizer) is minor in most cases.

These findings from Chapter 4 are confirmed and generalized in Chapter 5, which explored the relation between the optimally installed storage capacity and the time-varying shape of a demand and iRES profile. In Chapter 5, a distinction is made between storage technologies for which installed charging power, discharging power and energy storage can be optimized separately, like power-to-gas-to-power, and storage technologies for which all capacity ratings are physically coupled, like NaS batteries.

The study first looks at methodological, block-shaped, demand and iRES generation profiles. The study investigates the relation between the optimally installed storage capacity of each technology and the magnitude of surplus generation (impacting charging capacity), the magnitude of the remaining demand (impacting the discharging capacity) and the amount of energy required to serve the residual demand (impacting the energy storage capacity). After block profiles, a study was performed on sinusoidal-shaped demand and iRES profiles and finally on real historical profiles. The study shows a clear link between the shape of the demand and iRES profiles and the cost-efficiency of

certain storage technologies. If the residual demand has more low-frequency components, a preference for storage with low cost energy storage capacity (e.g., via P2G) is observed. If the residual demand has more high-frequency components, the cost optimal storage portfolio will favor storage technologies with low cost charge and discharge capacity (e.g., NaS batteries).

8.1.4 The operational impact of P2G units on the electrical power and gas networks

Conclusion 3: *Model results indicate that the current Belgian gas network contains ample amounts of inherent flexibility to accommodate P2G integration in high RES settings, up to 99% imposed RES targets.*

Chapter 6 presents a unit commitment model for the integrated electricity and gas system which is used to study the impact of P2G on energy system operation in Chapter 7. The chapter starts with an explanation of line-pack and the flexibility it inherently provides to the gas network. This is followed by an overview of existing models comprising both the electric power and natural gas system and a discussion on the novel model aspects presented in this work, which are as follows:

1. P2G units have been added with a higher level of technical detail than currently found in the literature;
2. the representation of gas production facilities found in the literature is extended with ramp rates;
3. next to the nodal mass balance constraints found in the literature, zonal mass balances are introduced to give a better representation of gas loads served through the gas distribution system at low pressure, which is typically connected to more than one node in the high pressure transmission network.

A description of the model is provided together with the implementation details. A verification of the model is given, confirming its suitability to study the gas network operation. Chapter 6 ends with different case studies to illustrate the relevance of the novel model aspects.

Chapter 7 evaluates in how far the natural gas network can cope with the methane injection from P2G units and to what extent the integration of P2G impacts the flexibility available for conventional gas production facilities. A simplified representation of the Belgian electric power and natural gas systems has been used in combination with the model presented in Chapter 6.

Optimization results show that if P2G is installed in a Belgian context, it is expected that integration of this P2G capacity will not be hindered by the gas network since an abundant amount of flexibility is available in the gas network to accommodate, possibly volatile, injection of synthetic methane. In addition, results indicate that conventional gas production facilities will experience no negative effects on the flexibility available to them when P2G is deployed, even in 99% RES scenarios with the largest amount of installed P2G capacity. The reason for this is twofold. First, the Belgian gas network has more capacity than strictly required to serve the gas load. Second, the production of synthetic methane is small compared to the production of conventional natural gas. Even for a day when all P2G capacity operates at full load during the entire day, the total synthetic methane production during this day only amounts to 9.3% of the total gas production.

8.2 Suggestions for further research

8.2.1 Levelized cost metrics for storage

The levelized cost metrics presented in Chapter 3 of this thesis have been compared to representative price profiles to determine the economic viability of possible storage technologies. When doing so, only arbitrage revenues were considered when analyzing those price profiles without considering possible revenue for providing additional services, e.g., ancillary services. This means that the obtained results give a pessimistic outlook of possible profits as it is expected that technically suitable storage units will participate in providing ancillary services and hence increase their profit. Accounting for this extra revenue is possible by adding the profit from such services to the available average operational profit.

When the possible arbitrage revenues were analyzed for different price profiles, the effect of the storage unit operation on the electricity price was not considered. However, depending on the specific storage unit and the electric power system, the storage unit could influence the electricity price, thereby reducing the possible arbitrage profit. Since the current calculation of the available average operational profit could indicate both too optimistic or too pessimistic results, a further elaboration of the available average operational profit calculation is advised to assess the economic viability of storage units in different electricity markets.

8.2.2 Analyzing the need for energy storage via synthetic fuels

The study presented in Chapter 4 focuses on the need for long-term storage via P2G in future energy systems. However, many different synthetic fuels exist, as outlined in Chapter 2, which could all potentially be used as storage technologies. Although the existence of a well developed natural gas infrastructure and GFPPs led this research to be focused on P2G, it would be interesting to analyze the roles of other synthetic fuels in cost optimal generation and storage portfolios.

In addition to looking at other synthetic fuels, it would be interesting to investigate the effect of different carbon sources like atmospheric carbon capture and biomass. Recently reported costs for atmospheric carbon capture in the literature suggest CO₂ capture costs only slightly higher than the carbon capture from gas fired power plants [69]. Especially for high-RES cases it could be possible that the production of synthetic fuels is limited by the availability of carbon feedstock. Decoupling the availability of carbon from the use of GFPPs could hence lead to additional insights regarding synthetic fuels.

The chemical industry, using large amounts of hydrogen feedstock, has been considered in some case studies presented in Chapter 4. Results show that the impact on the cost-optimal installed amount of installed electrolyzer capacity is significant. In the same fashion, it would be interesting to investigate the joint optimization of additional sectors such as transportation, heating, steel and cement to analyze possible mutually beneficial synergies in reaching imposed environmental targets.

8.2.3 Operational impact of P2G on the integrated electrical power and natural gas network

In Chapters 6 and 7 a first step has been made to model and analyze the operational impact of P2G on the electric power and natural gas systems. A first aim in this study was to verify the effect of P2G on the availability of inherent gas network flexibility, which is also used by conventional gas production facilities. However, since the model is deterministic and assumes perfect foresight, no short-term uncertainty was considered. Coping with short-term uncertainty in the gas network will require flexibility to assure reliable operation of the gas network. In addition, also uncertainty in the electric power system could propagate to the gas system when relying on GFPPs to provide ancillary services in the electric power system. Hence, requiring additional flexibility in the gas network. Explicitly considering uncertainty in both networks/systems would refine the results presented in Chapter 7.

In this thesis, only power-to-methane is considered as energy storage technology. Considering the possibility of injecting hydrogen in the gas network could be a first step for the adaptation of P2G as storage technology. Since hydrogen is less energy dense and more volatile than methane, it could have a more significant operational impact on the gas network. First, because it is generally assumed that concentrations of hydrogen should be limited to assure reliable operation of all gas-consuming devices. Second, since hydrogen is less energy dense, more volume will need to be injected in the gas network in order to store a certain amount of energy, which could lead to a higher impact on pressure swings. Extending the model presented in Chapter 6 to allow for direct hydrogen injection could provide interesting insights.

During the case studies presented in Chapter 7, energy systems with a RES target of 80% and 99% are considered. Although the GFPP and iRES generation capacity is determined as a function of the RES target (Chapter 4), historical demand profiles from 2015 have been used (both electrical power and natural gas). In the future, further environmental targets in other sectors could lead to electrification, resulting in more electricity consumption and less natural gas consumption. Such change in demand could put additional stress on the gas network, if increased electrification would lead to more (volatile) P2G injection and GFPP off-take, or could relax the flexibility requirements from the gas network, if less capacity is required for gas transport leaving more capacity for flexibility.

For all further research towards the operational aspects of the gas network, improving the computational performance of the presented gas network is most likely necessary to assure reasonable computation run times and would hence also be desirable as future work.

Appendix A

Levelized cost metrics including income tax

Following the example set by Reichelstein and Yorston [58], the levelized cost metrics for storage are now extended to account for corporate income tax. The corporate income affect the levelized cost of storage through a direct tax on the cash flow, depreciation and debt tax shields and a possible investment tax credit. The debt related tax shield is assumed to be accounted for in the calculation of the Weighted Average Cost of Capital, which is represented in the levelized cost of storage through the discount rate r . To incorporate the other tax factors, following variables are used:

i	= Investment tax credit (in %)
α	= Effective corporate income tax rate (in %)
T^0	= Useful plant life for tax purposes (in years)
d_t	= Allowable tax depreciation charge in year t (in %)

Similar to Reichelstein and Yorston [58], a tax factor Δ is defined as in Eq. (A.1) to incorporate corporate income tax following US tax arrangements. In contrast to Reichelstein and Yorston [58], the asset value reduction factor for tax purposes is left out in our formulation as it is only applicable in specific situations.

$$\Delta = \frac{1 - i - \alpha \cdot (1 - i) \cdot \sum_t (1 + r)^{-t}}{1 - \alpha} \quad (\text{A.1})$$

In the following metric formulation, the overnight construction cost is assumed to be invested entirely during year $t = 0$. If the construction period would span multiple years, different depreciation charges would be introduced corresponding to each year of construction and applying to the share of the construction cost invested during that year. Furthermore, for completeness, a term for the variable operational and maintenance cost (VOM_t) is incorporated. Any variable cost different from the charging cost is represented by this term, like e.g. a carbon tax.

Proposition 1. The *required average discharge price (RADP)* is defined as in Eq. (A.2).

$$RADP = \frac{OCC \cdot \Delta + \sum_t (FOM_t + VOM_t + TCC_t) \cdot (1+r)^{-t}}{\sum_t MWh_t^d (1+r)^{-t}} \quad (\text{A.2})$$

To proof that the RADP as defined in Eq. (A.2) is indeed equal to the verbal definition of *Required Average Discharge Price* for the investor to break even on his investment, let us define the taxable income I_t in period t as in Eq. (A.3) with p the sales price during discharging.

$$I_t = MWh_t^d \cdot p - TCC_t - FOM_t - VOM_t - OCC \cdot (1-i) \cdot d_t \quad (\text{A.3})$$

Assuming the firm pays a share α of its taxable income as corporate income tax, the annual after-tax cash-flow CFL_t becomes:

$$CFL_t = MWh_t^d \cdot p - TCC_t - FOM_t - VOM_t - \alpha \cdot I_t \quad (\text{A.4})$$

In accordance with conventional Net-Present Value calculations, the investor will break even on his investment when the price p during discharging is such that the present value of his investment is zero:

$$0 = -OCC \cdot (1-i) + \sum_t CFL_t \cdot (1+r)^{-t} \quad (\text{A.5})$$

Solving Eq. (A.5) for p yields Eq. (A.6). The numerator in Eq. (A.6) equals the present value of all cash outflows per unit installed capacity. The last term represents the depreciation tax shield. The denominator equals the total value of electricity output, multiplied by the factor $(1-\alpha)$.

$$\begin{aligned} p &= \frac{(1-i) \cdot OCC + (1+\alpha) \cdot \sum_t [TCC_t + FOM_t + VOM_t] \cdot (1+r)^{-t}}{(1-\alpha) \cdot \sum_t MWh_t^d (1+r)^{-t}} \\ &= \frac{-\alpha \cdot \sum_t [OCC \cdot (1-i) \cdot d_t] \cdot (1+r)^{-t}}{(1-\alpha) \cdot \sum_t MWh_t^d (1+r)^{-t}} \end{aligned} \quad (\text{A.6})$$

Using the tax factor Δ as defined in Eq. (A.1), Eq. (A.6) can be rewritten as Eq. (A.7) which is precisely the RADP as defined in Eq. (A.2).

$$p = \frac{OCC \cdot \Delta + \sum_t [TCC_t + FOM_t + VOM_t] \cdot (1 + r)^{-t}}{\sum_t MWh_t^d (1 + r)^{-t}} \tag{A.7}$$

Similar to the LCOE interpretation of Reichelstein and Yorston [58], The RADP can be interpreted as the lifetime cost of the storage plant over the lifetime electricity discharged (Eq. (A.6)) or as the sum of the initial investment cost, adapted with a tax factor, and the lifetime operating costs, over the lifetime electricity discharged (Eq. (A.7)).

In analogy to the RADP, an adapted definition of the required average price spread (RAPS) and the required average operational profit (RAOP) is given in Eqs. (A.8)-(A.9).

Proposition 2. The *required average price spread (RAPS)* is defined as in Eq. (A.8).

$$RAPS = \frac{OCC \cdot \Delta + \sum_t (FOM_t + VOM_t + (1 - \eta_{RT}) TCC_t) \cdot (1 + r)^{-t}}{\sum_t MWh_t^d (1 + r)^{-t}} \tag{A.8}$$

To prove that the RAPS as defined in Eq. (A.8) is indeed equal to the verbal definition of Required Average Price Spread for the investor to break even on his investment, Eq. (A.5) is solved for $(p - ACC)$. Doing so yields precisely the definition as given in Eq. (A.8).

Proposition 3. The *required average operational profit (RAOP)* is defined as in Eq. (A.9).

$$RAOP = \frac{OCC \cdot \Delta + \sum_t FOM_t \cdot (1 + r)^{-t}}{\sum_t MWh_t^d (1 + r)^{-t}} \tag{A.9}$$

To prove that the RAPS as defined in Eq. (A.9) is indeed equal to the verbal definition of Required Average Operational Profit for the investor to break even on his investment, Eq. (A.5) is solved for:

$$p - \frac{\sum_{t=1}^T TCC_t \cdot (1 + r)^{-t}}{\sum_{t=1}^T MWh_t^d \cdot (1 + r)^{-t}} = p - \frac{ACC}{\eta_{RT}} \tag{A.10}$$

Appendix B

Arbitrage model formulation

Nomenclature

Sets

$t \in \mathcal{T}$ set of time steps t

Parameters

η_c charging efficiency of storage unit
 η_d discharging efficiency of storage unit
 ϕ_t electricity price during time step t
 \bar{C} maximum charging capacity
 \bar{D} maximum discharging capacity
 \bar{S} maximum energy storage capacity

Decision Variables

Π total profit
 c_t amount of charged electricity within time step t
 d_t amount of discharged electricity within time step t
 s_t storage level at time t

Model description

The objective of the storage operator is to maximize the profit Π by optimizing the charging and discharging actions.

$$\Pi = \sum_t \phi_t (d_t - c_t) \quad (\text{B.1})$$

The storage level at time step t is determined by the storage level from the previous time step and the charging and discharging actions during time step t .

$$s_t = s_{t-1} + \eta_c \cdot c_t - \frac{d_t}{\eta_d} \quad \forall t \quad (\text{B.2})$$

The charging and discharging actions are limited by a maximum charging capacity, discharging capacity and energy storage capacity.

$$c_t \leq \bar{C} \quad \forall t \quad (\text{B.3})$$

$$d_t \leq \bar{D} \quad \forall t \quad (\text{B.4})$$

$$s_t \leq \bar{S} \quad \forall t \quad (\text{B.5})$$

Appendix C

Investment model

Nomenclature

Sets

$i \in \mathcal{I}$	set of renewable energy technologies i
$t \in \mathcal{T}$	set of time steps t

Parameters

C_{NG}	natural gas cost	$[\text{€}/\text{MWh}_{CH_4}]$
C_{bat}	battery cost	$[\text{€}/(\text{MW}_e \text{ y})]$
C_{ely}	electrolyzer cost	$[\text{€}/(\text{MW}_e \text{ y})]$
$C_{CO_2}^{em}$	CO ₂ emission cost	$[\text{€}/\text{ton}]$
C_{gs}	gas storage cost	$[\text{€}/(\text{MW}_{CH_4} \text{ y})]$
C_{hs}	hydrogen storage cost	$[\text{€}/(\text{MW}_{H_2} \text{ y})]$
C_{met}	methanizer cost	$[\text{€}/(\text{MW}_{CH_4} \text{ y})]$
C_{pp}	gas fired power plant cost	$[\text{€}/(\text{MW}_e \text{ y})]$
C_{cc}^{pp}	gas fired power plant carbon capture unit cost	$[\text{€}/(\text{MW}_e \text{ y})]$
C_i^{res}	iRES cost	$[\text{€}/(\text{MW}_e \text{ y})]$
$C_{CO_2}^{seq}$	CO ₂ sequestration cost	$[\text{€}/\text{ton}]$
C_{smr}	steam methane reformer cost	$[\text{€}/(\text{MW}_{CH_4} \text{ y})]$
C_{cc}^{smr}	steam methane reformer carbon capture unit cost	$[\text{€}/(\text{MW}_{CH_4} \text{ y})]$
EP_{bat}	battery energy-to-power ratio	$[\text{MWh}/\text{MW}]$

\dot{E}_t^l	electricity load	$[MWh_e/h]$
E_{phs}	pumped hydro storage reservoir size	$[MWh_e]$
\dot{H}_t^l	hydrogen load	$[MWh_{H_2}/h]$
\bar{K}	maximum capture rate	
$R\%$	renewable share in consumed end-energy	
$\alpha_{CH_4 \rightarrow CO_2}^{pp}$	carbon content per MWh methane released in GFPP	$[ton/MWh_{CH_4}]$
$\alpha_{CH_4 \rightarrow CO_2}^{smr}$	carbon content per MWh methane released in SMR	$[ton/MWh_{CH_4}]$
η_{bat}^c	battery charging efficiency	
η_{phs}^c	pumped hydro storage charging efficiency	
η_{bat}^d	battery discharging efficiency	
η_{phs}^d	pumped hydro storage discharging efficiency	
η_{ely}	electrolyzer efficiency	
η_{met}	methanizer efficiency	
η_{pp}	gas fired power plant efficiency	
η_{smr}	steam methane reformer efficiency	
Π_i^{RES}	iRES generation profile	
χ_{cc}^{pp}	electricity given up to capture 1 ton of CO ₂ from GFPP exhaust	$[MWh_e/ton]$
χ_{cc}^{smr}	methane given up to capture 1 ton of CO ₂ from SMR	$[MWh_{CH_4}/ton]$

Decision Variables

\bar{e}_{hs}	hydrogen storage capacity	$[MWh_{H_2}]$
\bar{e}_{SM}	synthetic methane storage capacity	$[MWh_{CH_4}]$
e_t^{bat}	battery storage level	$[MWh_e]$
$\dot{e}_t^{c,bat}$	battery instantaneous charging electric power	$[MW_e]$
$\dot{e}_t^{c,phs}$	pumped hydro storage instantaneous charging electric power	$[MW_e]$
\dot{e}_t^{cu}	instantaneous curtailed electric power	$[MW_e]$
$\dot{e}_t^{d,bat}$	battery instantaneous discharging electric power	$[MW_e]$
$\dot{e}_t^{d,phs}$	pumped hydro storage instantaneous discharging electric power	$[MW_e]$

e_t^{ely}	electrolyzer instantaneous electric power consumption	$[MW_e]$
e_t^{hs}	hydrogen storage level	$[MWh_{H_2}]$
$e_t^{net,pp}$	gas fired power plant instantaneous net electric power generation	$[MW_e]$
$e_t^{p,hs}$	pumped hydro storage reservoir level	$[MWh_e]$
e_t^{pp}	gas fired power plant instantaneous electric power generation	$[MW_e]$
$e_t^{pp,cc}$	gas fire power plant instantaneous electric power consumption by cc unit	$[MW_e]$
e_t^{SM}	synthetic methane storage level	$[MWh_{CH_4}]$
$\dot{j}_t^{met,sm}$	methanizer instantaneous methane production	$[MW_{CH_4}]$
$\dot{j}_t^{pp,NG}$	gas fired power plant instantaneous fossil fuel consumption	$[MW_{CH_4}]$
\dot{j}_t^{pp}	gas fired power plant total instantaneous fuel consumption	$[MW_{CH_4}]$
$\dot{j}_t^{pp,SM}$	gas fired power plant instantaneous synthetic methane consumption	$[MW_{CH_4}]$
$\dot{j}_t^{smr,cc}$	steam methane reformer carbon capture unit instantaneous fuel consumption	$[MW_{CH_4}]$
$\dot{j}_t^{smr,NG}$	steam methane reformer instantaneous fossil fuel consumption	$[MW_{CH_4}]$
$\dot{j}_t^{smr,SM}$	steam methane reformer instantaneous synthetic methane consumption	$[MW_{CH_4}]$
\dot{h}_t^c	hydrogen storage instantaneous hydrogen charging	$[MW_{H_2}]$
\dot{h}_t^d	hydrogen storage instantaneous hydrogen discharging	$[MW_{H_2}]$
\dot{h}_t^{ely}	electrolyzer instantaneous hydrogen production	$[MW_{H_2}]$
\dot{h}_t^{met}	methanizer instantaneous hydrogen consumption	$[MW_{H_2}]$
\dot{h}_t^{smr}	steam methane reformer instantaneous hydrogen production	$[MW_{H_2}]$
\dot{k}_t^{em}	CO ₂ emission rate	$[ton/h]$
\dot{k}_t^{met}	CO ₂ consumption rate in methanizer	$[ton/h]$
$\dot{k}_t^{pp,capt}$	CO ₂ capture rate from gas fired power plant	$[ton/h]$

$\dot{k}_t^{pp,prod}$	CO ₂ production rate by gas fired power plant	[ton/h]
k_t^s	CO ₂ storage level	[ton]
\dot{k}_t^{seq}	CO ₂ sequestration rate	[ton/h]
$\dot{k}_t^{smr,capt}$	CO ₂ capture rate from steam methane reformer	[ton/h]
$\dot{k}_t^{smr,prod}$	CO ₂ production rate by steam methane reformer	[ton/h]
\bar{p}_{bat}	battery capacity	[MW _e]
\bar{p}_{ely}	electrolyzer capacity	[MW _e]
\bar{p}_{met}	methanizer capacity	[MW _{CH₄}]
\bar{p}_{phs}	pumped hydro storage capacity	[MW _e]
\bar{p}_{pp}	gas fired power plant capacity	[MW _e]
\bar{p}_{cc}^{pp}	gas fired power plant carbon capture capacity	[MW _e]
\bar{p}_i^{res}	iRES capacity	[MW _e]
\bar{p}_{smr}	steam methane reformer capacity	[MW _{CH₄}]
\bar{p}_{cc}^{smr}	steam methane reformer carbon capture capacity	[MW _{CH₄}]
q_{NG}	total amount of consumed fossil natural gas	[MWh _{CH₄}]

Model description

The objective function is given in Eq. (C.1), with C the cost per technology and \bar{p} the installed capacity per technology. RES denotes renewable technologies, PP conventional power plants, CC carbon capture technology, ely electrolyzer capacity, met stands for methanizer, SMR for steam methane reformer, BAT for battery, NG for natural gas, with q_{NG} the total amount of consumed natural gas, gs stands for gas storage with \bar{e} the installed storage size. hs stands for hydrogen storage, CO₂ for carbon dioxide, em for emission and seq for sequestration with \dot{k} the total amount of CO₂.

$$\begin{aligned}
 Cost = & \sum_i C_i^{res} \bar{p}_i^{res} + C_{pp} \bar{p}_{pp} + C_{cc}^{pp} \bar{p}_{cc}^{pp} + C_{ely} \bar{p}_{ely} + C_{met} \bar{p}_{met} + C_{smr} \bar{p}_{smr} \\
 & + C_{cc}^{smr} \bar{p}_{cc}^{smr} + C_{bat} \bar{p}_{bat} + C_{NG} q_{NG} + C_{gs} \bar{e}_{SM} + C_{hs} \bar{e}_{hs} \\
 & + C_{CO_2}^{em} \sum_t \dot{k}_t^{em} + C_{CO_2}^{seq} \sum_t \dot{k}_t^{seq}
 \end{aligned} \tag{C.1}$$

Electricity system

The load should equal the sum of all generation at each time interval t as expressed in Eq. (C.2) with \dot{E}_t^l the instantaneous electricity load, Π_i^{RES} the normalized renewable generation profile (which has values between 0 and 1) and \dot{e} the instantaneous generation from conventional power plants (pp), discharge from storage (d), charging of storage (c), consumption from the electrolyzer (ely) or curtailment (cu).

$$\dot{E}_t^l = \sum_i (\Pi_i^{RES} \bar{p}_i^{res}) + \dot{e}_t^{net,pp} + \dot{e}_t^{d,bat} + \dot{e}_t^{d,phs} - \dot{e}_t^{ely} - \dot{e}_t^{c,bat} - \dot{e}_t^{c,phs} - \dot{e}_t^{cu} \quad \forall t \quad (C.2)$$

The net amount of electricity generated by gas fired power plants is equal to the gross amount of electricity generated, minus the share of electricity used for carbon capture.

$$\dot{e}_t^{net,pp} = \dot{e}_t^{pp} - \dot{e}_t^{pp,cc} \quad \forall t \quad (C.3)$$

Eqs. (C.4) to (C.7) limit respectively the electricity generation by the gas fired power plant (Eq. (C.4)), the instantaneous electricity consumption of the carbon capture unit attached to the gas fired power plant (Eq. (C.5)), the installed carbon capture capacity (Eq. (C.6)) and the electricity consumption of the electrolyzer (Eq. (C.7)).

$$\dot{e}_t^{pp} \leq \bar{p}_{pp} \quad \forall t \quad (C.4)$$

$$\dot{e}_t^{pp,cc} \leq \dot{e}_t^{pp} \quad \forall t \quad (C.5)$$

$$\bar{p}_{cc}^{pp} \leq \bar{p}_{pp} \quad \forall t \quad (C.6)$$

$$\dot{e}_t^{ely} \leq \bar{p}_{ely} \quad \forall t \quad (C.7)$$

The sum of instantaneous charging and discharging of batteries and pumped hydro storage is also limited to the installed capacity. Note that the formulation in Eqs. (C.8)-(C.9) does not exclude simultaneous charging and discharging of the storage unit, which is physically impossible with one unit (although it would be possible if a distinction between multiple units was made). However, simultaneous charging and discharging can be seen as curtailment and does not influence the objective value or the amount of installed capacity of each

technology.

$$\dot{e}_t^{c,bat} + \dot{e}_t^{d,bat} \leq \bar{p}_{bat} \quad \forall t \quad (\text{C.8})$$

$$\dot{e}_t^{c,phs} + \dot{e}_t^{d,phs} \leq \bar{p}_{phs} \quad \forall t \quad (\text{C.9})$$

The battery and pumped hydro storage state of charge at each time interval is determined by the state of charge at the previous time interval and the amount of electricity charged or discharged in the current time interval, corrected for the efficiency. These constraints are circular implemented, forcing the state of charge at the beginning of the optimization period to be equal to the state of charge at the end of the optimization period.

$$e_t^{bat} = e_{t-1}^{bat} + \dot{e}_t^{c,bat} \eta_{bat}^c - \frac{\dot{e}_t^{d,bat}}{\eta_{bat}^d} \quad \forall t \quad (\text{C.10})$$

$$e_t^{phs} = e_{t-1}^{phs} + \dot{e}_t^{c,phs} \eta_{phs}^c - \frac{\dot{e}_t^{d,phs}}{\eta_{phs}^d} \quad \forall t \quad (\text{C.11})$$

The battery storage capacity is limited by the installed capacity and the energy-to-power ratio of the battery technology. The energy storage capacity of the pumped hydro storage unit is limited by its installed energy capacity (Eq. (C.13)).

$$e_t^{bat} \leq \bar{p}_{bat} EP_{bat} \quad \forall t \quad (\text{C.12})$$

$$e_t^{phs} \leq E_{phs} \quad \forall t \quad (\text{C.13})$$

Coupling between the electricity and the natural gas system

The electricity and gas system are coupled through the gas fired power plant. The instantaneous electricity generation is, through the efficiency, coupled with the instantaneous fuel consumption.

$$\dot{f}_t^{pp} \eta_{pp} = \dot{e}_t^{pp} \quad \forall t \quad (\text{C.14})$$

Coupling between the electricity and the hydrogen system

The electricity and hydrogen system are coupled through the electrolyzer.

$$\dot{h}_t^{ely} = \dot{e}_t^{ely} \eta_{ely} \quad \forall t \quad (\text{C.15})$$

Coupling between the natural gas and the hydrogen system

The coupling between the natural gas and hydrogen system is twofold. Methane can be produced from hydrogen through the methanizer unit (Eq. (C.16)) and hydrogen could be produced from natural gas or synthetic methane through the steam methane reformer (Eq. (C.17)). Note in Eq. (C.17) that, if SMR carbon capture technology is used, not all methane consumed by the SMR unit is converted to hydrogen as part of it is used to fuel the carbon capture unit.

$$\dot{f}_t^{met,sm} = \dot{h}_t^{met} \eta_{met} \quad \forall t \quad (C.16)$$

$$\dot{h}_t^{smr} = \left(\dot{f}_t^{smr,NG} + \dot{f}_t^{smr,SM} - \dot{f}_t^{smr,cc} \right) \eta_{smr} \quad \forall t \quad (C.17)$$

Natural gas system

The gas consumption of the gas fired power plants is equal to the sum of natural gas consumption and synthetic methane consumption.

$$\dot{f}_t^{pp} = \dot{f}_t^{pp,NG} + \dot{f}_t^{pp,SM} \quad \forall t \quad (C.18)$$

The total natural gas consumption during the entire optimization horizon is equal to the sum of the natural gas consumption during each time interval.

$$q_{NG} = \sum_t \dot{f}_t^{pp,NG} + \sum_t \dot{f}_t^{smr,NG} \quad \forall t \quad (C.19)$$

The fuel consumption of the respectively the methanizer and steam methane reformer is limited to their installed capacity (Eqs. (C.20)-(C.21)).

$$\dot{f}_t^{met,sm} \leq \bar{p}_{met} \quad \forall t \quad (C.20)$$

$$\dot{f}_t^{smr,NG} + \dot{f}_t^{smr,SM} \leq \bar{p}_{smr} \quad \forall t \quad (C.21)$$

Eq. (C.22) limits the instantaneous consumption of the carbon capture unit attached to the steam methane reformer and Eq. (C.23) limits the installed SMR capacity.

$$\dot{f}_t^{smr,cc} \leq \dot{f}_t^{smr,NG} + \dot{f}_t^{smr,SM} \quad \forall t \quad (C.22)$$

$$\bar{p}_{cc}^{smr} \leq \bar{p}_{smr} \quad \forall t \quad (C.23)$$

Similar to batteries and PHS, the state of charge of a gas reservoir is determined by its previous state of charge, the synthetic methane produced by methanizer units and the synthetic methane used in GFPP. Also Eq. (C.24) is implemented circular. The non-renewable natural gas used by GFPP or SMR is assumed to be bought when needed, so storage of fossil natural gas is not included.

$$e_t^{SM} = e_{t-1}^{SM} + \dot{f}_t^{met,sm} - \dot{f}_t^{pp,SM} - \dot{f}_t^{smr,SM} \quad \forall t \quad (C.24)$$

The amount of synthetic methane that can be stored is limited by the size of the gas reservoir.

$$e_t^{SM} \leq \bar{e}_{SM} \quad \forall t \quad (C.25)$$

Hydrogen system

The amount of hydrogen that can be stored is limited to the installed hydrogen storage capacity.

$$e_t^{hs} \leq \bar{e}_{hs} \quad \forall t \quad (C.26)$$

The state of charge of the hydrogen storage is determined by the state of charge on the previous time step, the current hydrogen injection and off-take. The state of charge constraint is again circular implemented to make sure the state of charge at the end of the optimization horizon is equal to the state of charge at the beginning of the optimization.

$$e_t^{hs} = e_{t-1}^{hs} + \dot{h}_t^c - \dot{h}_t^d \quad \forall t \quad (C.27)$$

The hydrogen demand from industry, the hydrogen demand from the methanizer unit and charging of the storage should, at each time step, be covered by the hydrogen production from the electrolyzer, SMR or discharging the hydrogen storage.

$$\dot{H}_t^l = \dot{h}_t^{ely} + \dot{h}_t^{smr} - \dot{h}_t^{met} - \dot{h}_t^c + \dot{h}_t^d \quad \forall t \quad (C.28)$$

Coupling between the natural gas and the carbon system

The amount of CO₂ used in the methanizer unit is equal to the CO₂ content of the produced synthetic methane.

$$\dot{k}_t^{met} \alpha_{CH_4 \rightarrow CO_2}^{pp} = \dot{f}_t^{met,sm} \quad \forall t \quad (C.29)$$

The amount of CO₂ produced in the gas fired power plant is equal to the CO₂ content of the natural gas which is released during combustion.

$$\dot{k}_t^{pp,prod} = \dot{f}_t^{pp} \alpha_{CH_4 \rightarrow CO_2}^{pp} \quad \forall t \quad (C.30)$$

Similarly, the CO₂ produced by the SMR is equal to the CO₂ content released during the reforming process.

$$\dot{k}_t^{smr,prod} = \left(\dot{f}_t^{smr,NG} + \dot{f}_t^{smr,SM} \right) \alpha_{CH_4 \rightarrow CO_2}^{smr} \quad \forall t \quad (C.31)$$

The amount of fuel used by the SMR carbon capture unit is linked to the amount of CO₂ effectively captured.

$$\dot{f}_t^{smr,cc} = \chi_{cc}^{smr} \dot{k}_t^{smr,capt} \quad \forall t \quad (C.32)$$

Coupling between the electricity and the carbon system

The amount of electric power used by the carbon capture plant is equal to the amount of carbon captured multiplied by the required energy to capture a ton of CO₂.

$$\dot{e}_t^{pp,cc} = \chi_{cc}^{pp} \dot{k}_t^{pp,capt} \quad \forall t \quad (C.33)$$

The carbon system

The amount of captured CO₂ is limited by the capacity of the installed capture plant (Eq. (C.34)) and by the instantaneous amount of produced CO₂ from the gas fired power plant (Eq. (C.36)). Analog constraints are formulated for the steam methane reformer (Eqs. (C.35) and (C.37)).

$$\frac{\dot{k}_t^{pp,capt} \eta_{pp}}{\bar{K} \alpha_{CH_4 \rightarrow CO_2}^{pp}} \leq \bar{p}_{cc}^{pp} \quad \forall t \quad (C.34)$$

$$\frac{\dot{k}_t^{smr,capt} \eta_{smr}}{\bar{K} \alpha_{CH_4 \rightarrow CO_2}^{smr}} \leq \bar{p}_{cc}^{smr} \quad \forall t \quad (C.35)$$

$$\dot{k}_t^{pp,capt} \leq \bar{K} \dot{k}_t^{pp,prod} \quad \forall t \quad (C.36)$$

$$\dot{k}_t^{smr,capt} \leq \bar{K} \dot{k}_t^{smr,prod} \quad \forall t \quad (C.37)$$

The part of the produced CO₂ that is not captured by carbon capture plants, is emitted into the atmosphere.

$$\dot{k}_t^{em} = \dot{k}_t^{pp,prod} + \dot{k}_t^{smr,prod} - \dot{k}_t^{pp,capt} - \dot{k}_t^{smr,capt} \quad \forall t \quad (C.38)$$

A difference is made between temporary storage and final sequestration of CO₂. Eq. C.39 ensures that all captured CO₂ is either used in a methanizer plant or sequestered.

$$k_t^s = k_{t-1}^s + \dot{k}_t^{pp,capt} + \dot{k}_t^{smr,capt} - \dot{k}_t^{met} - \dot{k}_t^{seq} \quad \forall t \quad (C.39)$$

Environmental constraint

Depending on the case under investigation an imposed minimum share of the end-electricity and hydrogen consumption should originate from renewables. In order to exclude efficiency losses from the share of useful renewable energy, the environmental constraint is expressed as maximum share of the electricity and hydrogen which may originate from fossil sources. When the hydrogen industry is not taken into account, the hydrogen load is set to zero and the environmental constraint only applies to the electricity sector. When a hydrogen load is accounted for, the environmental constraint applies to both the electricity and hydrogen sector, allowing the system to use more renewables in one sector to compensate for a higher fossil use in another sector, depending on the economic optimum.

$$\sum_t \dot{f}_t^{pp,NG} + \dot{f}_t^{smr,NG} \leq (1 - R\%) \sum_t \left(\frac{\dot{E}_t^l}{\eta_{pp}} + \frac{\dot{H}_t^l}{\eta_{smr}} \right) \quad \forall t \quad (C.40)$$

Appendix D

Leuven University System Model (LUSYM)

The MIP UC formulation presented in this appendix is taken from Van den Bergh et al. [94],[95].

Nomenclature

Sets

$j \in \mathcal{J}$	set of storage units j
$l \in \mathcal{L}$	set of lines l
$lac \in \mathcal{L}^{ac}$	set of AC transmission lines lac
$ldc \in \mathcal{L}^{dc}$	set of DC transmission lines ldc
$lpst \in \mathcal{L}^{pst}$	set of AC transmission lines with PST $lpst$
$m \in \mathcal{M}$	set of must-run groups m
$n \in \mathcal{N}$	set of nodes n
$s \in \mathcal{S}$	set of reserve zones s
$t \in \mathcal{T}$	set of time steps t

Parameters

$AV_{i,t}$	availability of power plant i at time step t	$\{0,1\}$
$A_{l,n}$	element of incidence matrix of the grid	$\{-1,0,1\}$

$A_{m,i}^{must}$	element linking power plant i to must-run group m	$\{0,1\}$
$A_{n,i}^{plant}$	element linking power plant i to node n	$\{0,1\}$
$A_{s,n}^{rsr}$	element linking node n to reserve zone s	$\{0,1\}$
$A_{s,i}^{rsr}$	element linking power plant i to reserve zone s	$\{0,1\}$
$A_{n,j}^{stor}$	element linking storage unit j to node n	$\{0,1\}$
CC	CO ₂ emission cost	$[\text{€}/\text{ton}]$
$DCDF_{lac,ldc}$	DC line distribution factors	
$D_{n,t}$	electricity load at node n at time step t	$[MW]$
EF_i	CO ₂ emission factor of power plant i	$[\Delta t \text{ ton}/MWh_{th}]$
F_{lac}^0	zero-imbalance flow through AC line l	$[MW]$
FC_i	fuel cost of power plant i	$[\Delta t \text{ €}/MWh_{th}]$
\bar{F}_l	maximum power flow through AC or DC line l	$[MW]$
\underline{F}_l	minimum power flow through AC or DC line l	$[MW]$
LCC_n	load curtailment cost at node n	$[\Delta t \text{ €}/MWh]$
$\overline{LSE}_{n,t}$	maximum storable load energy at node n at time step t	$[MWh]$
$\underline{LSE}_{n,t}$	minimum storable load energy at node n at time step t	$[MWh]$
$\overline{LS}_{n,t}$	maximum storable load at node n at time step t	$[MW]$
MC_i	marginal generation cost of power plant i	$[\Delta t \text{ €}/MWh]$
MDT_i	minimum down time of power plant i	$[\Delta t]$
MRM_m	must-run requirement of group of power plants m	
MRP_i	must-run requirement of power plant i	
MUT_i	minimum up time of power plant i	$[\Delta t]$
NC_i	generation cost at minimum output of power plant i	$[\text{€}/\Delta t]$
OP_i	required planned outages of power plant i	$[\Delta t]$
PC_j	maximum charging power of storage unit j	$[MW]$
PD_j	maximum discharging power of storage unit j	$[MW]$

\overline{PE}_j	maximum energy content of storage unit j	[MWh]
\underline{PE}_j	minimum energy content of storage unit j	[MWh]
$PSDF_{lac,lpst}$	phase shifter distribution factors	
\overline{P}_i	maximum power output of power plant i	[MW]
\underline{P}_i	minimum power output of power plant i	[MW]
RAC^{tot}	reserve allocation cost for load curtailment	$[\Delta t \text{ €/MW}]$
RAC^{cur}	reserve allocation cost for renewables curtailment	$[\Delta t \text{ €/MW}]$
RC_i	ramping cost of power plant i	$[\text{€/MW}]$
RCC_n	renewables curtailment cost at node n	$[\Delta t \text{ €/MWh}]$
RD_i	maximum ramp-down rate of power plant i	$[MW/\Delta t]$
$RES_{n,t}$	available renewable generation at node n at time step t	[MW]
RU_i	maximum ramp-up rate of power plant i	$[MW/\Delta t]$
SD_i	maximum shut-down rate of power plant i	$[MW/\Delta t]$
SDC_i	shut-down cost of power plant i	$[\text{€/shut-down}]$
SEC_n	simultaneous export capacity of node n	[MW]
SIC_n	simultaneous import capacity of node n	[MW]
$SR_{s,t}^-$	downward spinning reserve in reserve zone s at time step t	[MW]
$SR_{s,t}^+$	upward spinning reserve in reserve zone s at time step t	[MW]
SU_i	maximum start-up rate of power plant i	$[MW/\Delta t]$
SUC_i	start-up cost of power plant i	$[\text{€/start-up}]$
TC_l	transmission cost for line l	$[\Delta t \text{ €/MWh}]$
VOM_i	variable O&M cost of power plant i	$[\Delta t \text{ €/MWh}]$
$\overline{\alpha}_{lpst}$	maximum phase shifter angle at line $lpst$	$[\text{°}]$
Δt	length of one time step in hours	[h]
η_j^c	charging efficiency of storage unit j	[-]
η_j^d	discharging efficiency of storage unit j	[-]
η_i	rated efficiency of power plant i	[-]

Decision Variables

$\alpha_{lpst,t}$	phase shifter angle at line $lpst$ at time step t	$[\circ]$
$cost_{c,t}^{comp}$	operation cost of compressor c at time step t	$[\text{€}/\Delta t]$
$cost^{gas}$	total operational cost of gas system	$[\text{€}]$
$cost_{i,t}^{gen}$	generation cost of power plant i at time step t	$[\text{€}/\Delta t]$
$cost_{gs,t}^{stor}$	operation cost of gas storage gs at time step t	$[\text{€}/\Delta t]$
$cost_{n,t}^{lc}$	load curtailment cost at node n at time step t	$[\text{€}/\Delta t]$
$cost_{gw,t}^{well}$	operation cost of gas well gw at time step t	$[\text{€}/\Delta t]$
$cost_{i,t}^{ramp}$	ramping cost of power plant i at time step t	$[\text{€}/\Delta t]$
$cost_{n,t}^{rc}$	renewables curtailment cost at node n at time step t	$[\text{€}/\Delta t]$
$cost_{n,t}^{rsr}$	reserve allocation cost for load and renewables curtailment at node n at timestep t	$[\text{€}/\Delta t]$
$cost_{i,t}^{start}$	start-up cost of power plant i at time step t	$[\text{€}/\Delta t]$
$cost_{i,t}^{stop}$	shut-down cost of power plant i at time step t	$[\text{€}/\Delta t]$
$cost_{l,t}^{trans}$	transmission cost of line l at time step t	$[\text{€}/\Delta t]$
$f_{l,t}$	power flow through AC or DC line l at time step t	$[MW]$
$g_{i,t}$	power generation of power plant i above minimum output at time step t	$[MW]$
$g_{i,t}$	power generation of power plant i at time step t	$[MW]$
$lc_{n,t}$	load curtailment at node n at time step t	$[MW]$
$ls_{n,t}$	storable load at node n at time step t	$[MW]$
$lse_{n,t}$	storable load energy at node n at time step t	$[MWh]$
$of_{i,t}$	forced outage of power plant i at time step t	$\{0, 1\}$
$op_{i,t}$	planned outage of power plant i at time step t	$\{0, 1\}$

$pc_{j,t}$	charging power of storage unit j at time step t	[MW]
$pd_{j,t}$	discharging power of storage unit j at time step t	[MW]
$pe_{j,t}$	energy level of storage unit j at time step t	[MWh]
$pi_{n,t}$	power injection in the grid at node n at time step t	[MW]
$r_{n,t}^{lol}$	scheduled reserve from load curtailment at node n at time step t	[MW]
$rc_{n,t}$	renewables curtailment at node n at time step t	[MW]
$r_{i,t}^-$	scheduled downward spinning reserve from power plant i at time step t	[MW]
$r_{i,t}^+$	scheduled upward spinning reserve from power plant i at time step t	[MW]
$r_{n,t}^{cur}$	scheduled reserve from renewables curtailment at node n at time step t	[MW]
$v_{i,t}$	start-up status of power plant i at time step t	{0, 1}
$w_{i,t}$	shut-down status of power plant i at time step t	{0, 1}
$z_{i,t}$	on/off-status of power plant i at time step t	{0, 1}

Model description

Objective function

The objective function of the UC model is to minimize total operational system cost, consisting of generation costs, start-up costs, shut-down costs, ramping costs, load curtailment costs, renewables curtailment costs and reserve allocation costs for load and renewables curtailment:

$$\begin{aligned}
 cost^{elec} = & \sum_{i,t} (cost_{i,t}^{gen} + cost_{i,t}^{start} + cost_{i,t}^{stop} + cost_{i,t}^{ramp}) \\
 & + \sum_{l,t} (cost_{l,t}^{trans}) + \sum_{n,t} (cost_{n,t}^{lc} + cost_{n,t}^{rc} + cost_{n,t}^{rsr})
 \end{aligned} \tag{D.1}$$

The generation costs include fuel costs, CO₂ emission costs and variable operations and maintenance costs. The generation cost of a power plant is

time depending (due to changing fuel and CO₂ emission prices) and output depending (due to the output-dependent generation efficiency). The non-linear cost curve is linearized and time-averaged as follows:¹

$$cost_{i,t}^{gen} = NC_i z_{i,t} + MC_i g_{i,t} \quad \forall i, \forall t \quad (D.2)$$

The start-up and shut-down costs follow from, respectively:²

$$cost_{i,t}^{start} = SUC_i v_{i,t} \quad \forall i, \forall t \quad (D.3)$$

$$cost_{i,t}^{stop} = SDC_i w_{i,t} \quad \forall i, \forall t \quad (D.4)$$

The ramping cost follows from:

$$0 \leq cost_{i,t}^{ramp} \geq RC_i (g_{i,t} - g_{i,t-1}) \quad (D.5)$$

$$0 \leq cost_{i,t}^{ramp} \geq RC_i (g_{i,t-1} - g_{i,t}) \quad (D.6)$$

The transmission cost follows from:

$$0 \leq cost_{l,t}^{trans} \geq TC_l f_{l,t} \quad \forall l, \forall t \quad (D.7)$$

$$0 \leq cost_{l,t}^{trans} \geq -TC_l f_{l,t} \quad \forall l, \forall t \quad (D.8)$$

The load curtailment cost follows from:

$$cost_{n,t}^{lc} = LCC_n lc_{n,t} \quad \forall n, \forall t \quad (D.9)$$

The renewables curtailment cost follows from:

$$cost_{n,t}^{rc} = RCC_n rc_{n,t} \quad \forall n, \forall t \quad (D.10)$$

The reserve allocation cost for load and renewables curtailment follows from:

$$cost_{n,t}^{rsr} = RAC^{lol} r_{n,t}^{lol} + RAC^{cur} r_{n,t}^{cur} \quad \forall n, \forall t \quad (D.11)$$

Note that the reserve allocation cost for spinning reserves from conventional units is implicitly taken into account in the generation cost.

¹The cost curve can be approximated with multiple linear intervals, but this increases run times drastically while accuracy only increases slightly [116, 117]. Moreover, time-dependent cost parameters $NC_{i,t}$ and $MC_{i,t}$ can be imposed to the unit commitment model.

²A more advanced formulation of the start-up cost takes account of the off-line time of the power plant and distinguishes between hot starts, warm start and cold starts [116, 118].

Market clearing

The market clearing constraint imposes the supply-demand balance at each node for each time step. The supply-demand balance consists of generation from conventional units, (dis)charging from storage units, generation from renewables, the (flexible) electricity load and injections in the electricity grid:

$$\sum_i A_{n,i}^{plant} (z_{i,t} \underline{P}_i + g_{i,t}) + \sum_j A_{n,j}^{stor} (pd_{j,t} - pc_{j,t}) + RES_{n,t} - rc_{n,t} =$$

$$D_{n,t} - lc_{n,t} + ls_{n,t} + p_{n,t} + \sum_e A_{n,e}^{ely} g_{e,t}^{ely} \quad \forall n, \forall t \quad (\text{D.12})$$

Renewables and load curtailment

Electricity generation from renewables (and cogeneration units) is mainly driven by other factors than the electricity demand (e.g., weather conditions, subsidies) and is therefore only to a limited extent dispatchable. Renewable generation can be curtailed in the energy market or scheduled as reserves, but renewables curtailment is limited by the available renewable generation:³

$$0 \leq rc_{n,t} + r_{n,t}^{cur} \leq RES_{n,t} \quad \forall n, \forall t \quad (\text{D.13})$$

Renewables curtailment is non-negative:

$$rc_{n,t}, r_{n,t}^{cur} \geq 0 \quad \forall n, \forall t \quad (\text{D.14})$$

³In today's electricity markets, most of the renewable generation has priority access to the grid, meaning that renewable generators have an incentive to generate as much electricity as possible, regardless of any electricity market signal. As such, generation of renewable electricity sources can be modeled as negative load, resulting in a residual load (i.e., original load minus renewables generation) to be met by centralized and dispatchable units. However, renewable electricity generators are becoming increasingly integrated in the electricity market operation. As such, renewable generation units can be modeled in a similar way as conventional generation units, with the difference that renewable generation units have zero marginal generation costs (or even negative marginal generation costs if subsidized) and time-variable maximum power outputs (depending on the meteorological conditions). In the LUSYM model, renewable generation time series are imposed to the model with the possibility to curtail renewables at a certain cost. A high renewables curtailment cost corresponds to today's electricity markets with priority access for renewables, whereas a zero (or low) renewables curtailment cost corresponds to future electricity markets with active participation of renewables.

Flexible load and load curtailment

Load curtailment (or load shedding) can be scheduled in the energy market or as reserve, and is limited by the load:

$$0 \leq lc_{n,t} + r_{n,t}^{lol} \leq D_{n,t} \quad \forall n, \forall t \quad (\text{D.15})$$

Load curtailment is non-negative:

$$lc_{n,t}, r_{n,t}^{lol} \geq 0 \quad \forall n, \forall t \quad (\text{D.16})$$

Storable load is characterized by an energy limit, a power limit and an energy balance equation, respectively:

$$\underline{LSE}_{n,t} \leq lse_{n,t} \leq \overline{LSE}_{n,t} \quad \forall k, \forall t \quad (\text{D.17})$$

$$0 \leq ls_{n,t} \leq \overline{LS}_{n,t} \quad \forall n, \forall t \quad (\text{D.18})$$

$$lse_{n,t} = lse_{n,t-1} + \Delta t ls_{n,t} \quad \forall n, \forall t \quad (\text{D.19})$$

Power plant generation limits

A power plant can only generate power within a certain power range. It is important to highlight that the power plant output is defined as $gen_{i,t} = z_{i,t} \underline{P}_i + g_{i,t}$. The lower limit for the power output above the minimum power output is:

$$0 \leq g_{i,t} - r_{i,t}^- \quad \forall i, \forall t \quad (\text{D.20})$$

The upper generation limit for power plants with $MUT_i \geq 2$ is given by:

$$g_{i,t} + r_{i,t}^+ \leq (\overline{P}_i - \underline{P}_i) z_{i,t} - (\overline{P}_i - SU_i) v_{i,t} - (\overline{P}_i - SD_i) w_{i,t+1} \quad (\text{D.21})$$

$$\forall i \in MUT_i \geq 2, \forall t$$

If $MUT_i = 1$, Eq. (D.21) is replaced by:

$$g_{i,t} + r_{i,t}^+ \leq (\overline{P}_i - \underline{P}_i) z_{i,t} - (\overline{P}_i - SU_i) v_{i,t} - \max(SU_i - SD_i, 0) w_{i,t+1}$$

$$\forall i \in MUT_i = 1, \forall t$$

(D.22)

$$g_{i,t} + r_{i,t}^+ \leq (\overline{P}_i - \underline{P}_i) z_{i,t} - (\overline{P}_i - SD_i) w_{i,t+1} - \max(SD_i - SU_i, 0) v_{i,t}$$

$$\forall i \in MUT_i = 1, \forall t$$

(D.23)

Eqs. (D.20)-(D.23) describe the convex hull of the power plant generation limits [119].

Additional generation limit constraints can be imposed by considering multiple time steps [120], however it is not sure that these constraints result in a speed-up given that they make the formulation tighter but less compact. These additional constraints are:

$$g_{i,t} + r_{i,t}^+ \leq (\bar{P}_i - \underline{P}_i) z_{i,t+K_i} + \sum_{k=1}^{K_i} (SD_i - \underline{P}_i + (k-1) RD_i) w_{i,t+k} \quad (D.24)$$

$$- \sum_{k=1}^{K_i} (\bar{P}_i - \underline{P}_i) v_{i,t+k} \quad \forall i, \forall t = 1, \dots, T - K$$

with $K_i = \min\{MUT_i; (\bar{P}_i - SD_i)/RD_i + 1; T - t\}$. Eq. (D.24) is only tightening Eq. (D.21) if $K \geq 2$.

Finally, generation and reserve scheduling variables are non-negative or binary.

$$gen_{i,t}, g_{i,t}, r_{i,t}^+, r_{i,t}^- \geq 0 \quad \forall i, \forall t \quad (D.25)$$

$$z_{i,t}, v_{i,t}, w_{i,t} \in \{0, 1\} \quad \forall i, \forall t \quad (D.26)$$

Power plant ramping limits

The basic ramping-up and ramping-down constraints are, respectively:

$$g_{i,t} + r_{i,t}^+ - g_{i,t-1} \leq RU_i z_{i,t} + (SU_i - \underline{P}_i - RU_i) v_{i,t} \quad \forall i, \forall t \quad (D.27)$$

$$g_{i,t-1} - g_{i,t} + r_{i,t}^- \leq RD_i z_{i,t-1} + (SD_i - \underline{P}_i - RD_i) w_{i,t} \quad \forall i, \forall t \quad (D.28)$$

Additional ramping constraints can be imposed by considering more time steps [120], however it is again not sure that these additional constraints result in a speed-up as they make the formulation tighter but also less compact. Additional ramping-up constraints are:

$$g_{i,t} + r_{i,t}^+ - g_{i,t-1} \leq RU_i z_{i,t} - (RU_i - SD_i + \underline{P}_i) w_{i,t+1} \quad (D.29)$$

$$+ (SU_i - \underline{P}_i - RU_i) v_{i,t} \quad \forall t, \forall i \in RU_i > SD_i - \underline{P}_i \ \& \ MUT_i \geq 2$$

$$g_{i,t} + r_{i,t}^+ - g_{i,t-2} \leq 2 RU_i z_{i,t} + (SU_i - \underline{P}_i - RU_i) v_{i,t-1} \quad (D.30)$$

$$+ (SU_i - \underline{P}_i - 2 RU_i) v_{i,t} \quad \forall t, \forall i \in MUT_i \geq 2 \ \& \ MDT_i \geq 2$$

Analogously, additional ramping-down constraints are:

$$g_{i,t-1} - g_{i,t} + r_{i,t}^- \leq RD_i z_{i,t} + (SD_i - \underline{P}_i) w_{i,t} - RD_i v_{i,t} \quad (D.31)$$

$$-(RD_i - SU_i + \underline{P}_i) v_{i,t-1} \quad \forall t, \forall i \in RD_i > SU_i - \underline{P}_i \ \& \ MUT_i \geq 2$$

$$g_{i,t-2} - g_{i,t} + r_{i,t}^- \leq 2RD_i z_{i,t} + (SD_i - \underline{P}_i) w_{i,t-1} - 2RD_i (v_{i,t-1} + v_{i,t})$$

$$+(SD_i - \underline{P}_i + RD_i) w_{i,t} \quad \forall t, \forall i \in MUT_i \geq 2 \ \& \ MDT_i \geq 2 \quad (D.32)$$

Power plant minimum up and down times

The minimum down time and up time constraints are given by, respectively:

$$1 - z_{i,t} \geq \sum_{t'=t+1-MDT_i}^t w_{i,t'} \quad \forall i, \forall t \quad (D.33)$$

$$z_{i,t} \geq \sum_{t'=t+1-MUT_i}^t v_{i,t'} \quad \forall i, \forall t \quad (D.34)$$

In addition to the above constraints, the following logic relationship between the different power plant statuses is needed:

$$z_{i,t-1} - z_{i,t} + v_{i,t} - w_{i,t} = 0 \quad \forall i, \forall t \quad (D.35)$$

Eqs. (D.33)-(D.35) describe the convex hull of the minimum up and down time constraints [121].

Must-run constraints

Must-run constraints can be imposed to a subset of power plants:

$$\sum_i A_{m,i}^{must} (z_{i,t} \underline{P}_i + g_{i,t}) \geq MRM_m \sum_i A_{m,i}^{must} AV_{i,t} \bar{P}_i \quad \forall m, \forall t \quad (D.36)$$

A must-run constraint can also be imposed to a single power plant:

$$z_{i,t} \underline{P}_i + g_{i,t} \geq MRP_i AV_{i,t} \bar{P}_i \quad \forall i, \forall t \quad (D.37)$$

Note that the must-run constraint can be overruled by power plant outages.

Spinning reserve constraints

Spinning reserve constraints can be imposed to reserve zones, consisting of one or multiple nodes. Upward spinning reserves can be delivered by online power plants, load curtailment and curtailed renewable generation. Downward spinning reserves can be delivered by online power plants and renewables curtailment. Upward and downward spinning reserve requirements are given by, respectively:

$$\sum_i A_{s,i}^{rsr} r_{i,t}^+ + \sum_n A_{s,n}^{rsr} (r_{n,t}^{lol} + rc_{n,t}) \geq SR_{s,t}^+ \quad \forall s, \forall t \quad (D.38)$$

$$\sum_i A_{s,i}^{rsr} r_{i,t}^- + \sum_n A_{s,n}^{rsr} r_{n,t}^{cur} \geq SR_{s,t}^- \quad \forall s, \forall t \quad (D.39)$$

Storage unit constraints

Different storage technologies, such as pumped hydro storage and electric batteries, can be implemented in the unit commitment model by the same set of constraints. The energy balance of a storage unit is given by:

$$pe_{j,t} = pe_{j,t-1} + \Delta t pc_{j,t} \eta_j^c - \frac{\Delta t pd_{j,t}}{\eta_j^d} \quad \forall j, \forall t \quad (D.40)$$

The energy level of a storage unit and its charging and discharging power rates are limited:

$$0 \leq pc_{j,t} \leq PC_j \quad \forall j, \forall t \quad (D.41)$$

$$0 \leq pd_{j,t} \leq PD_j \quad \forall j, \forall t \quad (D.42)$$

$$\underline{PE}_j \leq pe_{j,t} \leq \overline{PE}_j \quad \forall j, \forall t \quad (D.43)$$

Grid constraints

A DC power flow representation of the electricity grid is implemented, including HVDC lines, phase shifting transformers (PSTs) and the possibility to add a zero-imbalance flow to the line flows. The DC power flow is a linearized description of the electricity grid characteristics, respecting Kirchhoff's voltage and current laws. Injection shift factors (ISFs) or power transfer distribution factors (PTDFs) give the linear relationship between power injections in the

grid and flows through transmission lines.⁴

$$f_{lac,t} = \sum_n PTDF_{lac,n} p_{n,t} + \sum_{lpst} PSDF_{lac,lpst} \alpha_{lpst,t} + \sum_{l^{dc}} DCDF_{lac,l^{dc}} f_{l^{dc},t} + F_{lac}^0 \quad \forall l, \forall t \quad (D.44)$$

$$\sum_n p_{n,t} = 0 \quad \forall t \quad (D.45)$$

$$-\bar{\alpha}_{lpst} \leq \alpha_{lpst,t} \leq \bar{\alpha}_{lpst} \quad \forall lpst, \forall t \quad (D.46)$$

$$\underline{F}_{lac} \leq f_{lac,t} \leq \bar{F}_{lac} \quad \forall l^{ac}, \forall t \quad (D.47)$$

$$\underline{F}_{l^{dc}} \leq f_{l^{dc},t} \leq \bar{F}_{l^{dc}} \quad \forall l^{dc}, \forall t \quad (D.48)$$

Alternatively, a trade-based grid representation can be used. In a trade-based grid representation, only Kirchhoff's current law is respected. If the trade-based grid representation is used, Eqs. (D.44)-(D.48) are replaced by:

$$p_{n,t} = \sum_l A_{l,n} f_{l,t} \quad \forall n, \forall t \quad (D.49)$$

$$\underline{F}_l \leq f_{l,t} \leq \bar{F}_l \quad \forall l, \forall t \quad (D.50)$$

In a trade based grid model, an additional constraint can be imposed on the gross import or export in a node (in order to compensate for the lower accuracy of a trade based grid model compared to a DC power flow grid model):

$$\sum_{l \in L_n^{imp}} |A_{l,n} f_{l,t}| \leq SIC_n \quad \forall n, \forall t \quad (D.51)$$

$$\sum_{l \in L_n^{exp}} |A_{l,n} f_{l,t}| \leq SEC_n \quad \forall n, \forall t \quad (D.52)$$

with L_n^{imp} and L_n^{exp} the lines connected to node n that import and export electricity, respectively.

⁴Given the properties of linearity and superposition, the sensitivity of line flows to power injections in a node with another node as sink (not the reference node) can be written as a linear combination of ISF-elements, composing a PTDF. As such, ISFs depend on the chosen reference node, PTDFs do not.

References

- [1] UNFCCC, COP21, “Paris agreement.” [Online] Available at https://unfccc.int/sites/default/files/english_paris_agreement.pdf, 2015.
- [2] European Commission, “2020 climate and energy package.” Available at ec.europa.eu/clima/policies/strategies/2020, 2009.
- [3] European Commission, “2030 climate and energy package.” Available at ec.europa.eu/clima/policies/strategies/2030_en, 2016.
- [4] European Commission, “Press release: Commission welcomes European Parliament adoption of key files of the Clean Energy for All Europeans package.” Available at europa.eu/rapid/press-release_IP-18-6383_en.htm, 2018.
- [5] European Commission, “Directive 2009/28/EC of the European Parliament and of the Council of 23 April 2009 on the promotion of the use of energy from renewable sources,” 2009.
- [6] European Commission, “Energy roadmap 2050.” Available at ec.europa.eu/energy/sites/ener/files/documents/2012_energy_roadmap_2050_en_0.pdf, 2018.
- [7] K. Poncet, *Long-term energy-system optimization models: Capturing the challenges of integrating intermittent renewable energy sources and assessing the suitability for descriptive scenario analyses*. PhD thesis, University of Leuven, 2018.
- [8] International Energy Agency (IEA), “World Energy Outlook,” 2015. Paris.
- [9] International Energy Agency (IEA), “Key world energy statistics,” 2018. Paris.

- [10] K. Hedegaard and P. Meibom, “Wind power impacts and electricity storage – A time scale perspective,” *Renewable Energy*, vol. 37, pp. 318–324, Jan. 2012.
- [11] H. Sharman, B. Leyland, and M. Livermore, *Renewable energy: vision or mirage?* Cambridge: The Scientific Alliance, 2011. ISBN 1 902737 81 4.
- [12] F. Steinke, P. Wolfrum, and C. Hoffmann, “Grid vs. storage in a 100% renewable europe,” *Renewable Energy*, vol. 50, pp. 826–832, 2013.
- [13] S. Ruester, J. Vasconcelos, X. HE, E. Chong, and J.-M. Glachant, “Electricity storage: how to facilitate its deployment and operation in the eu,” tech. rep., EU, Florence, 2012. Think Topic 8, ISBN: 978-92-9084-087-9.
- [14] D. Anderson and M. Leach, “Harvesting and redistributing renewable energy: on the role of gas and electricity grids to overcome intermittency through the generation and storage of hydrogen,” *Energy policy*, vol. 32, no. 14, pp. 1603–1614, 2004.
- [15] H. Ibrahim, A. Ilinca, and J. Perron, “Energy storage systems—characteristics and comparisons,” *Renewable and Sustainable Energy Reviews*, vol. 12, no. 5, pp. 1221 – 1250, 2008.
- [16] M. Specht, J. Brellochs, V. Frick, B. Stürmer, U. Zuberbühler, M. Sterner, and G. Waldstein, “Speicherung von bioenergie und erneuerbarem strom im erdgasnetz,” Tech. Rep. 10, ForschungsVerbund Erneuerbare Energien, 2009.
- [17] F. Ess, L. Haefke, J. Hobohm, F. Peter, and M. Wunsch, “The significance of international hydropower storage for the energy transition,” tech. rep., Prognos, 2012.
- [18] M. Gimeno-Gutiérrez and R. Lacal-Arantequi, “Assessment of the european potential for pumped hydropower energy storage,” tech. rep., Joint Research Center, 2013.
- [19] P. Gardner, F. Jones, M. Rowe, A. Nouri, and H. van de Vegte, “E-storage: Shifting from cost to value: Wind and solar applications,” tech. rep., World Energy Council (WEC), London, UK, 2016.
- [20] P. D. Lund, J. Lindgren, J. Mikkola, and J. Salpakari, “Review of energy system flexibility measures to enable high levels of variable renewable electricity,” *Renewable and Sustainable Energy Reviews*, vol. 45, pp. 785–807, 2015.

- [21] M. Sterner, *Bioenergy and renewable power methane in integrated 100% renewable energy systems*. PhD thesis, Univ. of Kassel, Kassel, 2009.
- [22] G. Centi and S. Perathoner, “Opportunities and prospects in the chemical recycling of carbon dioxide to fuels,” *Catalysis Today*, vol. 148, no. 3-4, pp. 191–205, 2009.
- [23] G. Benjaminsson, J. Benjaminsson, and R. B. Rudberg, “Power-to-Gas – A technical review,” tech. rep., Svenskt Gastekniskt Center AB, Malmö, 2013.
- [24] M. Lehner, R. Tichler, H. Steinmüller, and M. Koppe, *Power-to-Gas: Technology and Business Models*. Springer, 2014.
- [25] A. Buttler and H. Spliethoff, “Current status of water electrolysis for energy storage, grid balancing and sector coupling via power-to-gas and power-to-liquids: A review,” *Renewable and Sustainable Energy Reviews*, vol. 82, 2018.
- [26] E. Frank, J. Gorre, F. Ruoss, and M. J. Friedl, “Calculation and analysis of efficiencies and annual performances of Power-to-Gas systems,” *Applied Energy*, vol. 218, pp. 217 – 231, 2018.
- [27] O. Atlam and M. Kolhe, “Equivalent electrical model for a proton exchange membrane (PEM) electrolyser,” *Energy Conversion and management*, vol. 52, no. 8-9, pp. 2952–2957, 2011.
- [28] L. Grond, P. Schulze, and J. Holstein, “Systems Analysis Power to Gas. Final report, deliverable 1: technology review,” tech. rep., DNV Kema Energy & Sustainability, Groningen, 2013.
- [29] G. Müller-Syring, M. Henel, W. Köppel, H. Mlaker, M. Sterner, and T. Höcher, “Entwicklung von modularen Konzepten zur Erzeugung, Speicherung und Einspeisung von Wasserstoff und Methan ins Erdgasnetz,” tech. rep., Deutscher Verein des Gas- und Wasserfaches e.V. (DVGW), Bonn, 2013.
- [30] C. Schug, “Operational characteristics of high-pressure, high-efficiency water-hydrogen-electrolysis,” *International Journal of Hydrogen Energy*, vol. 23, no. 12, pp. 1113 – 1120, 1998.
- [31] M. Götz, J. Lefebvre, F. Mörs, A. M. Koch, F. Graf, S. Bajohr, R. Reimert, and T. Kolb, “Renewable power-to-gas: A technological and economic review,” *Renewable energy*, vol. 85, pp. 1371–1390, 2016.

- [32] J. Eichman, K. W. Harrison, and M. Peters, “Novel electrolyzer applications: providing more than just hydrogen,” tech. rep., National Renewable Energy Laboratory, Golden, CO, 2014.
- [33] D. Parra, X. Zhang, C. Bauer, and M. K. Patel, “An integrated techno-economic and life cycle environmental assessment of power-to-gas systems,” *Applied Energy*, vol. 193, pp. 440 – 454, 2017.
- [34] J. Lefebvre, M. Götz, S. Bajohr, R. Reimert, and T. Kolb, “Improvement of three-phase methanation reactor performance for steady-state and transient operation,” *Fuel Processing Technology*, vol. 132, pp. 83 – 90, 2015.
- [35] T. Schaaf, J. Grünig, M. R. Schuster, T. Rothenfluh, and A. Orth, “Methanation of CO₂ - storage of renewable energy in a gas distribution system,” *Energy, Sustainability and Society*, vol. 4, p. 2, Dec 2014.
- [36] K. Ghaib and F.-Z. Ben-Fares, “Power-to-methane: A state-of-the-art review,” *Renewable and Sustainable Energy Reviews*, vol. 81, pp. 433 – 446, 2018.
- [37] G. Leonzio, “State of art and perspectives about the production of methanol, dimethyl ether and syngas by carbon dioxide hydrogenation,” *Journal of CO₂ Utilization*, vol. 27, pp. 326–354, 2018.
- [38] M. Pérez-Fortes, J. C. Schöneberger, A. Boulamanti, and E. Tzimas, “Methanol synthesis using captured CO₂ as raw material: Techno-economic and environmental assessment,” *Applied Energy*, vol. 161, pp. 718–732, 2016.
- [39] G. A. Olah, A. Goepfert, and G. S. Prakash, “Chemical recycling of carbon dioxide to methanol and dimethyl ether: from greenhouse gas to renewable, environmentally carbon neutral fuels and synthetic hydrocarbons,” *The Journal of organic chemistry*, vol. 74, no. 2, pp. 487–498, 2008.
- [40] K. Atsonios, K. D. Panopoulos, and E. Kakaras, “Thermocatalytic CO₂ hydrogenation for methanol and ethanol production: Process improvements,” *international journal of hydrogen energy*, vol. 41, no. 2, pp. 792–806, 2016.
- [41] V. Subramani and S. K. Gangwal, “A review of recent literature to search for an efficient catalytic process for the conversion of syngas to ethanol,” *Energy & Fuels*, vol. 22, no. 2, pp. 814–839, 2008.
- [42] T. A. Semelsberger, R. L. Borup, and H. L. Greene, “Dimethyl ether (dme) as an alternative fuel,” *Journal of Power Sources*, vol. 156, no. 2, pp. 497–511, 2006.

- [43] L. Jamshidi, C. Barbosa, L. Nascimento, and J. Rodbari, "Catalytic dehydration of methanol to dimethyl ether (dme) using the al62, 2cu25, 3fe12, 5 quasicrystalline alloy," *J Chem Eng Process Technol*, vol. 4, pp. 1–8, 2013.
- [44] W. Schakel, G. Oreggioni, B. Singh, A. Strømman, and A. Ramírez, "Assessing the techno-environmental performance of co2 utilization via dry reforming of methane for the production of dimethyl ether," *Journal of CO2 Utilization*, vol. 16, pp. 138–149, 2016.
- [45] R. Lan, J. T. Irvine, and S. Tao, "Ammonia and related chemicals as potential indirect hydrogen storage materials," *International Journal of Hydrogen Energy*, vol. 37, no. 2, pp. 1482 – 1494, 2012. 10th International Conference on Clean Energy 2010.
- [46] A. Skodra and M. Stoukides, "Electrocatalytic synthesis of ammonia from steam and nitrogen at atmospheric pressure," *Solid State Ionics*, vol. 180, no. 23, pp. 1332 – 1336, 2009.
- [47] R. J. Pearson, M. D. Eisaman, J. W. Turner, P. P. Edwards, Z. Jiang, V. L. Kuznetsov, K. A. Littau, L. Di Marco, and S. G. Taylor, "Energy storage via carbon-neutral fuels made from co2, water, and renewable energy," *Proceedings of the IEEE*, vol. 100, no. 2, pp. 440–460, 2012.
- [48] International Energy Agency (IEA) & Nuclear Energy Agency (NEA), "Projected Costs of Generating Electricity," 2015. Paris.
- [49] P. L. Joskow, "Comparing the costs of intermittent and dispatchable electricity generating technologies," *American Economic Review*, vol. 101, no. 3, pp. 238–41, 2011.
- [50] S. Reichelstein and A. Sahoo, "Time of day pricing and the levelized cost of intermittent power generation," *Energy Economics*, vol. 48, pp. 97–108, 2015.
- [51] DOE/EPRI, *Electricity storage handbook in collaboration with NRECA*. Albuquerque: DOE, 2006.
- [52] V. Jülch, "Comparison of electricity storage options using levelized cost of storage (LCOS) method," *Applied energy*, vol. 183, pp. 1594–1606, 2016.
- [53] B. Zakeri and S. Syri, "Electrical energy storage systems: A comparative life cycle cost analysis," *Renewable and Sustainable Energy Reviews*, vol. 42, pp. 569–596, 2015.

- [54] I. Pawel, “The cost of storage—how to calculate the levelized cost of stored energy (LCOE) and applications to renewable energy generation,” *Energy Procedia*, vol. 46, pp. 68–77, 2014.
- [55] C. S. Lai and M. D. McCulloch, “Levelized cost of energy for PV and grid scale energy storage systems,” *arXiv preprint arXiv:1609.06000*, 2016.
- [56] P. Poonpun and W. T. Jewell, “Analysis of the cost per kilowatt hour to store electricity,” *IEEE Transactions on energy conversion*, vol. 23, no. 2, pp. 529–534, 2008.
- [57] IRENA, *Battery storage for renewables: Market status and technology outlook*. Abu Dhabi: International Renewable Energy Agency, 2015.
- [58] S. Reichelstein and M. Yorston, “The prospects for cost competitive solar PV power,” *Energy Policy*, vol. 55, pp. 117–127, 2013.
- [59] Belpex, “Belpex spot market prices.” [Online] Available at <https://www.belpex.be/market-results/the-market-today/dashboard/>, 2016.
- [60] J. Vandewalle, K. Bruninx, and W. D’haeseleer, “Effects of large-scale power to gas conversion on the power, gas and carbon sectors and their interactions,” *Energy Conversion and Management*, vol. 94, pp. 28 – 39, 2015.
- [61] M. Jentsch, T. Trost, and M. Sterner, “Optimal use of power-to-gas energy storage systems in an 85% renewable energy scenario,” *Energy Procedia*, vol. 46, pp. 254–261, 2014.
- [62] A. van Stiphout, *Short-Term Operational Flexibility in Long-Term Generation Expansion Planning*. PhD thesis, University of Leuven, 2017.
- [63] H. Blanco, W. Nijs, J. Ruf, and A. Faaij, “Potential of power-to-methane in the eu energy transition to a low carbon system using cost optimization,” *Applied Energy*, vol. 232, pp. 323–340, 2018.
- [64] Elia, “Grid data.” Available at www.elia.be/en/grid-data/data-download, 2015.
- [65] International Energy Agency (IEA), “Energy Technology Perspectives,” 2014. Paris.
- [66] F. Geth, *Battery Energy Storage Systems and Distribution Grid Support*. PhD thesis, Univ. of Leuven, Leuven, September 2014.

- [67] J. Vandewalle, *Natural Gas in the Energy Transition - Technical challenges and opportunities of natural gas and its infrastructure as a flexibility-providing resource*. PhD thesis, Univ. of Leuven, Leuven, November 2014.
- [68] International Energy Agency (IEA) & Nuclear Energy Agency (NEA), "Projected Costs of Generating Electricity," 2010. Paris.
- [69] D. W. Keith, G. Holmes, D. S. Angelo, and K. Heidel, "A process for capturing CO_2 from the atmosphere," *Joule*, vol. 2, no. 8, pp. 1573–1594, 2018.
- [70] J. K. Kaldellis, "Integrated electrification solution for autonomous electrical networks on the basis of RES and energy storage configurations," *Energy Conversion and Management*, vol. 49, no. 12, pp. 3708 – 3720, 2008.
- [71] D. Zafirakis and J. Kaldellis, "Autonomous dual-mode CAES systems for maximum wind energy contribution in remote island networks," *Energy Conversion and Management*, vol. 51, no. 11, pp. 2150–2161, 2010.
- [72] T. Khatib, I. A. Ibrahim, and A. Mohamed, "A review on sizing methodologies of photovoltaic array and storage battery in a standalone photovoltaic system," *Energy Conversion and Management*, vol. 120, pp. 430–448, 2016.
- [73] Y. Luo, L. Shi, and G. Tu, "Optimal sizing and control strategy of isolated grid with wind power and energy storage system," *Energy Conversion and Management*, vol. 80, pp. 407–415, 2014.
- [74] Y. Ru, J. Kleissl, and S. Martinez, "Exact sizing of battery capacity for photovoltaic systems," *European Journal of Control*, vol. 20, no. 1, pp. 24–37, 2014.
- [75] Y. V. Makarov, P. Du, M. C. Kintner-Meyer, C. Jin, and H. F. Illian, "Sizing energy storage to accommodate high penetration of variable energy resources," *IEEE Transactions on Sustainable Energy*, vol. 3, no. 1, pp. 34–40, 2012.
- [76] J. P. Barton and D. G. Infield, "Energy storage and its use with intermittent renewable energy," *IEEE transactions on energy conversion*, vol. 19, no. 2, pp. 441–448, 2004.
- [77] ELIA, "Grid data - Elia." Online, accessed: 2016-01-08.

- [78] P. D. Welch, "The use of fast fourier transform for the estimation of power spectra: A method based on time averaging over short, modified periodograms," *IEEE Transactions on audio and electroacoustics*, vol. 15, no. 2, pp. 70–73, 1967.
- [79] M. J. Woods, R. J. Davy, C. J. Russell, and P. A. Coppin, "Cross-spectrum of wind speed for meso-gamma scales in the upper surface layer over south-eastern australia," *Boundary-layer meteorology*, vol. 141, no. 1, pp. 93–116, 2011.
- [80] N. Keyaerts, *Gas Balancing and Line-pack Flexibility. Concepts and Methodologies for Organizing and Regulating Gas Balancing in Liberalized and Integrated EU Gas Markets*. PhD thesis, University of Leuven, 2012.
- [81] D. Connolly, H. Lund, B. V. Mathiesen, and M. Leahy, "A review of computer tools for analysing the integration of renewable energy into various energy systems," *Applied energy*, vol. 87, no. 4, pp. 1059–1082, 2010.
- [82] P. Mancarella, "MES (multi-energy systems): An overview of concepts and evaluation models," *Energy*, vol. 65, pp. 1–17, 2014.
- [83] A. Zlotnik, L. Roald, S. Backhaus, M. Chertkov, and G. Andersson, "Coordinated scheduling for interdependent electric power and natural gas infrastructures," *IEEE Transactions on Power Systems*, vol. 32, no. 1, pp. 600–610, 2017.
- [84] M. Qadrdan, J. Wu, N. Jenkins, and J. Ekanayake, "Operating strategies for a gb integrated gas and electricity network considering the uncertainty in wind power forecasts," *IEEE Transactions on Sustainable Energy*, vol. 5, no. 1, pp. 128–138, 2014.
- [85] S. Clegg and P. Mancarella, "Storing renewables in the gas network: modeling of power-to-gas seasonal storage flexibility in low-carbon power systems," *IET Generation, Transmission & Distribution*, vol. 10, no. 3, pp. 566–575, 2016.
- [86] S. Clegg and P. Mancarella, "Integrated modeling and assessment of the operational impact of power-to-gas (p2g) on electrical and gas transmission networks," *IEEE Transactions on Sustainable Energy*, vol. 6, no. 4, pp. 1234–1244, 2015.
- [87] C. Liu, M. Shahidepour, Y. Fu, and Z. Li, "Security-constrained unit commitment with natural gas transmission constraints," *IEEE Trans. Power Syst.*, vol. 24, no. 3, pp. 1523–1536, 2009.

- [88] C. Liu, M. Shahidehpour, and J. Wang, "Coordinated scheduling of electricity and natural gas infrastructures with a transient model for natural gas flow," *Chaos: An Interdisciplinary Journal of Nonlinear Science*, vol. 21, no. 2, p. 025102, 2011.
- [89] Y. He, M. Yan, M. Shahidehpour, Z. Li, C. Guo, L. Wu, and Y. Ding, "Decentralized optimization of multi-area electricity-natural gas flows based on cone reformulation," *IEEE Transactions on Power Systems*, vol. 33, no. 4, 2018.
- [90] C. He, T. Liu, L. Wu, and M. Shahidehpour, "Robust coordination of interdependent electricity and natural gas systems in day-ahead scheduling for facilitating volatile renewable generations via power-to-gas technology," *Journal of Modern Power Systems and Clean Energy*, vol. 5, no. 3, p. 375, 2017.
- [91] C. M. Correa Posada, *Optimal security-constrained model for the integrated power and natural-gas system*. PhD thesis, Universidad Pontificia Comillas, 2015.
- [92] M. Chaudry, N. Jenkins, and G. Strbac, "Multi-time period combined gas and electricity network optimisation," *Electric power systems Research*, vol. 78, no. 7, pp. 1265–1279, 2008.
- [93] Fluxys, "Personal correspondence," 2018.
- [94] K. Van den Bergh, K. Bruninx, E. Delarue, and W. D'haeseleer, "LUSYM: a unit commitment model formulated as a mixed-integer linear program." Available at www.mech.kuleuven.be/en/tme/research/energy_environment/Pdf/wpen2014-07-2.pdf, 2015.
- [95] K. Van den Bergh, *Impact of energy and climate policies on electricity generation: analysis based on large-scale unit commitment modeling*. PhD thesis, University of Leuven, 2016.
- [96] C. M. Correa-Posada and P. Sánchez-Martín, "Integrated power and natural gas model for energy adequacy in short-term operation," *IEEE Transactions on Power Systems*, vol. 30, pp. 3347–3355, Nov 2015.
- [97] C. Wang, W. Wei, J. Wang, L. Bai, and Y. Liang, "Distributed optimal gas-power flow using convex optimization and ADMM." [Online] Available at arxiv.org/abs/1610.04681, 2016.
- [98] S. Wu, R. Z. Rios-Mercado, E. A. Boyd, and L. R. Scott, "Model relaxations for the fuel cost minimization of steady-state gas pipeline networks," *Mathematical and Computer Modelling*, vol. 31, no. 2-3, pp. 197–220, 2000.

- [99] A. H. Shapiro, *The Dynamics and Thermodynamics of Compressible Fluid Flow: In Two Volumes*. John Wiley & Sons, 1953.
- [100] J. F. Helgaker and T. Ytrehus, "Coupling between continuity/momentum and energy equation in 1d gas flow," *Energy Procedia*, vol. 26, pp. 82–89, 2012.
- [101] A. J. Osiadacz and M. Chaczykowski, "Comparison of isothermal and non-isothermal pipeline gas flow models," *Chemical Engineering Journal*, vol. 81, no. 1-3, pp. 41–51, 2001.
- [102] R. W. Fox, A. T. McDonald, and P. J. Pritchard, *Introduction to fluid dynamics*. John Wiley & Sons, 2004.
- [103] P. M. Coelho and C. Pinho, "Considerations about equations for steady state flow in natural gas pipelines," *Journal of the Brazilian Society of Mechanical Sciences and Engineering*, vol. 29, no. 3, pp. 262–273, 2007.
- [104] D. De Wolf and Y. Smeers, "The gas transmission problem solved by an extension of the simplex algorithm," *Management Science*, vol. 46, no. 11, pp. 1454–1465, 2000.
- [105] S. Mokhatab and W. A. Poe, *Handbook of natural gas transmission and processing*. Oxford, UK: Gulf professional publishing, 2006.
- [106] R. Z. Ríos-Mercado and C. Borraz-Sánchez, "Optimization problems in natural gas transportation systems: A state-of-the-art review," *Applied Energy*, vol. 147, pp. 536–555, 2015.
- [107] Checalc, "Natural gas compressibility factor." [Online] Available at <http://checalc.com/solved/naturalgasZ.html>, 2015.
- [108] M. Chaczykowski, "Transient flow in natural gas pipeline—the effect of pipeline thermal model," *Applied Mathematical Modelling*, vol. 34, no. 4, pp. 1051–1067, 2010.
- [109] A. Thorley and C. Tiley, "Unsteady and transient flow of compressible fluids in pipelines—a review of theoretical and some experimental studies," *International journal of heat and fluid flow*, vol. 8, no. 1, pp. 3–15, 1987.
- [110] Synergrid, "Grid statistics." Online, accessed: 2018-09-03, www.synergrid.be/index.cfm?PageID=16898, 2015.
- [111] K. Van den Bergh and E. Delarue, "Cycling of conventional power plants: technical limits and actual costs," *Energy Conversion and Management*, vol. 97, pp. 70–77, 2015.

- [112] Elia, “Grid technical data.” Available at www.elia.be/nl/grid-data/Grid-Technical-Data, 2015.
- [113] Europan network of tranmission system operators for gas (entsog), “entsog Transparency platform.” [Online] Available at <https://transparency.entsog.eu/>, 2018.
- [114] A. Schröder, F. Kunz, J. Meiss, R. Mendelevitch, and C. Von Hirschhausen, “Current and prospective costs of electricity generation until 2050,” tech. rep., DIW Berlin - Data Documentation 68, 2013.
- [115] K. Bruninx, E. Delarue, H. Ergun, K. May, K. Van den Bergh, and D. Van Hertem, “Determining the impact of renewable energy on balancing costs, back up costs, grid costs and subsidies.” Available at www.creg.info/pdf/ARCC/161019-KULeuven.pdf, 2016. AR-CC/013/15 2015/02/210815, Final report.
- [116] J. Arroyo and A. Conejo, “Optimal response of a thermal unit to an electricity spot market,” *IEEE Transactions on Power Systems*, vol. 15, no. 3, pp. 1098–1104, 2000.
- [117] A. Frangioni, C. Gentile, and F. Lacalandra, “Tighter approximated MILP formulations for unit commitment problems,” *IEEE Transactions on Power Systems*, vol. 24, no. 1, pp. 105–113, 2009.
- [118] G. Morales-España, J. Latorre, and A. Ramos, “Tight and compact MILP formulation of start-up and shut-down ramping in unit commitment,” *IEEE Transactions on Power Systems*, vol. 28, no. 2, pp. 1288–1296, 2013.
- [119] G. Morales-España, *Unit commitment - computational performance, system representation and wind uncertainty management*. PhD thesis, Universidad Pontificia Comillas, 2014.
- [120] J. Ostrowski, M. Anjos, and A. Vannelli, “Tight mixed integer linear programming formulations for the unit commitment problem,” *IEEE Transactions on Power Systems*, vol. 27, no. 1, pp. 39–46, 2012.
- [121] D. Rajan and S. Takriti, “Minimum up/down polytopes of the unit commitment problem with start-up costs,” *IBM Research Report*, 2005.

Short curriculum

Andreas Belderbos

Born in Leuven (Belgium) on November 7, 1989.

Education:

- since 2014 PhD student in Mechanical Engineering, KU Leuven.
- 2011-2013 Master of Science in Engineering: Energy, KU Leuven.
Cum Laude.
- 2008-2011 Bachelor of Science in Engineering: Mechanical Engineering,
KU Leuven.

Work:

- 2013-2014 Advanced Process Control Engineer, IPCOS.

List of publications

Publications are available at https://www.mech.kuleuven.be/en/tme/research/energy_environment

Articles published in peer-reviewed academic journals

Belderbos, A., Delarue, E., Kessels, K., D'haeseleer, W. (2017). Levelized cost of storage - Introducing novel metrics. *Energy Economics*, 67, 287–299

Belderbos A., Virag A., D'haeseleer W., Delarue E. (2017). Considerations on the need for electricity storage requirements: Power versus energy. *Energy Conversion and Management*, 143, 137-149

Belderbos, A., Delarue, E. (2015). Accounting for flexibility in power system planning with renewables. *International Journal of Electrical Power & Energy Systems*, 71, 33-41

Articles submitted to peer-reviewed academic journals

Belderbos, A., Delarue, E., D'haeseleer, W. Critical factors shaping the need for long-term energy storage via power-to-gas. Submitted to *Energy Conversion and Management*

Belderbos, A., Bruninx, K., Valkaert, T., Delarue, E., D'haeseleer, W. Facilitating renewables and power-to-gas via integrated electrical power-gas system scheduling. Submitted to *IEEE Transactions on Power systems*

Papers at international scientific conferences, published in full proceedings

Belderbos, A., Delarue, E., D'haeseleer, W. (2016). Methodological considerations on the need for electricity storage: power versus energy. IEEE International Energy Conference. IEEE International Energy Conference. Leuven, 4-8 April 2016 IEEE Xplore.

Belderbos, A., Delarue, E., D'haeseleer, W. (2015). Possible role of Power-to-Gas in future energy systems. 12th International Conference on the European Energy Market (EEM), 2015. European Energy Markets. Lisbon, 19-22 May 2015 (pp. 1-5) IEEE.

Presentations at international scientific conferences

Belderbos A., Delarue E., Kessels K., D'haeseleer W. (2018). Levelised Cost of Storage – Novel Metrics. Energy Storage Global Conference. Brussels, October 2018.

Belderbos A., Delarue E., D'haeseleer W. (2018). Justification for the use of a dynamic gas flow formulation. European Conference on Operational Research. Valencia, July 9th 2018.

Belderbos A., Delarue E., D'haeseleer W. (2017). Overview of optimization models for gas network operation with a focus on physical network constraints and line-pack tracking. Benelux Association for Energy Economics. Leuven, November 10th 2017.

Belderbos A., Delarue E., Kessels K., D'haeseleer W. (2017). Impact of storage efficiency and charging costs on storage profitability in the electricity market. IAEE European Conference. Vienna, September 2017.

Belderbos A., Delarue E., D'haeseleer W. (2016). Considerations on the Levelized Cost of Storage. BAEE Research Workshop on Energy Economics. Delft, 4 November 2016.

Belderbos A., Delarue E., D'haeseleer W. (2016). Calculating the Levelized Cost of Electricity Storage?: vol. 494. International Association for Energy Economists (IAEE) International Conference. Bergen, Norway, 19-22 June 2016.

Belderbos A., Delarue E., D'haeseleer W. (2015). Influence of external factors on the share of Power-to-Gas in an optimal storage portfolio. European Gas Technology Conference (EGATEC). Vienna, 25-26 November 2015

Belderbos A., Delarue E., D'haeseleer W. (2015). Methodological considerations on the need for electricity storage: power versus energy. Young Energy Economists and Engineers Seminar (YEEES). Madrid, 2-4 November 2015.

FACULTY OF ENGINEERING SCIENCE
DEPARTMENT OF MECHANICAL ENGINEERING
TME DIVISION, ENERGY & ENVIRONMENT GROUP
Celestijnenlaan 300 box 2421
B-3001 Leuven
<http://www.mech.kuleuven.be/en/tme>

